Title
Exploration of Ln(II) Reactivity with Isolated and In-Situ Generated [LnII(NR2)3]1− (R = SiMe3)

Permalink
https://escholarship.org/uc/item/4wg7336s

Author
Chung, Amanda B

Publication Date
2022

Peer reviewed|Thesis/dissertation

UNIVERSITY OF CALIFORNIA,
IRVINE

Exploration of Ln(II) Reactivity with Isolated and In-Situ Generated
$[Ln^{II}(NR_2)_3]^{1-}$ (R = SiMe_3)

DISSERTATION

submitted in partial satisfaction of the requirements
for the degree of

DOCTOR OF PHILOSOPHY

in Chemistry

by

Amanda B. Chung

Dissertation Committee:
Professor William J. Evans, Chair
Professor Jenny Y. Yang
Professor Andy S. Borovik

2022

DEDICATION

This dissertation is dedicated to my parents, Lisa and Robert,

and to my sister, Sasha.

Thank you for your love and support.

Science is magic that works.
Kurt Vonnegut
Cat's Cradle

and

All time is all time. It does not change. It does not lend itself to warnings or explanations. It simply is. Take it moment by moment, and you will find that we are all, as I've said before, bugs in amber.
Kurt Vonnegut
Slaughterhouse-Five

TABLE OF CONTENTS

LIST OF FIGURES

drawn at the 50% probability level. Hydrogen atoms were omitted for clarity.

vi

LIST OF TABLES

xiii

ACKNOWLEDGEMENTS

<div align="center">

VITA

Amanda B. Chung

</div>

EDUCATION

Ph.D. University of California, Irvine, 2022

Principal Investigator: Prof. William J. Evans

B.S. Nova Southeastern University, 2018

Principal Investigator: Prof. Dimitrios Giarikos

PUBLICATIONS

1. **Chung, A. B**.; Rappoport, D.; Ziller, J. W.; Cramer, R. E.; Furche, F.; Evans, W. J. *J. Am. Chem. Soc.* **2022**, in revision.

2. **Chung, A. B**.; Fang, M.; Ziller, J. W.; Evans, W. J. **2022**. In preparation.

3. **Chung, A. B**.; Moyle, A. B.; Nyansa, M. M. S.; Powell, J. A. *ACS Chem. Health and Safety*. **2022**, *29* (3), 240-241.

4. **Chung, A. B**.; Ryan, A. J.; Fang, M.; Ziller, J. W.; Evans, W. J. *Inorg. Chem.* **2021**, *60* (20), 15635–15645.

5. **Chung, A. B**.; Ziller, J. W.; Evans, W. J. *Acta Crystallogr. Sect. E Crystallogr. Commun.* **2020**, *76*, 1047–1050.

6. **Chung, A. B**.; Huh, D. N.; Ziller, J. W.; Evans, W. J. *Inorg. Chem. Front.* **2020**, *7* (22), 4445–4451.

ORAL PRESENTATIONS

1. **Chung, A.B**. Solid state end-on to side-on isomerization of $(N=N)^{2-}$ in the $\{[(R_2N)_3Nd]_2N_2\}^{2-}$ complex (R = SiMe$_3$). University of California Chemical Symposium, Virtual, March 26th, 2022.

2. **Chung, A.B**. Solid state end-on to side-on isomerization of $(N=N)^{2-}$ in the $\{[(R_2N)_3Nd]_2N_2\}^{2-}$ complex (R = SiMe$_3$). American Chemical Society (ACS) National Meeting, San Diego, March 24th, 2022.

WORK EXPERIENCE

Reviewer, *ACS Essentials of Lab Safety for Organic Chemistry*   2022

Graduate Teaching Assistant, *University of California, Irvine*   2018 – 2021

General Chemistry Laboratory (CHEM 1LD), Organic Chemistry Laboratory (CHEM 51LB, CHEM 51LC, CHEM 51LD), Organometallic Chemistry (CHEM 216)

Laboratory Assistant, *Nova Southeastern University*   2017 – 2018

General Chemistry Laboratory (CHEM 1300, CHEM 1310), Inorganic Chemistry Laboratory (CHEM 4010), Physical Chemistry Laboratory (CHEM 3700, CHEM 3710), Quantitative Analysis Laboratory (CHEM 3460), Chemical Instrumentation Laboratory (CHEM 4150).

FELLOWSHIPS AND AWARDS

Graduate Student Scholar Recognition for Promotion of Research Safety,   2022
American Chemical Society

Chemistry Safety Fellowship, *University of California, Irvine*   2021 – 2022

Division of Teaching Excellence and Innovation Graduate   2020
Fellowship, *University of California, Irvine*

Department of Chemistry Honoree, *University of California, Irvine*   2020

Presidential Scholarship, *Nova Southeastern University*   2018

SoFL-ACS Student Travel Award, *Nova Southeastern University*   2018

Chemistry Major of the Year, *Nova Southeastern University*   2018

OUTREACH

Graduate Safety Team, *University of California, Irvine*   2018 – 2022

     Students dedicated to improving laboratory safety and safety culture at UCI.

Facilitator and Moderator, *Empowering Academic Researchers to*   2022

Strengthen Safety Culture, *ACS Chemical Health and Safety Peer*

Led Workshop

Guest Editor, *ACS Chemical Health and Safety Journal*   2022

President, Chemistry Club, *Nova Southeastern University*   2016 – 2017

Make a Meal, *Nova Southeastern University*   2016 – 2018

     Nonprofit organization that works to raise awareness and funds for those unable

     to have a proper meal on a regular basis.

ABSTRACT OF THE DISSERTATION

Exploration of Ln(II) Reactivity with Isolated and In-Situ Generated
$[Ln^{II}(NR_2)_3]^{1-}$ (R = SiMe$_3$)

by

Amanda B. Chung

Doctor of Philosophy in Chemistry

University of California, Irvine, 2022

Professor William J. Evans, Chair

This dissertation describes the Ln(II) reduction reactivity of both isolated Ln(II) complexes containing $(NR_2)^{1-}$ (R = SiMe$_3$) amide ligands and *in situ* Ln(NR$_2$)$_3$/M reactions. The results show the diversity of products obtained by amide-based Ln(II) reduction due to subtle changes in reaction conditions. Chapter 1 outlines the reactions of isolated $[Gd^{II}(NR_2)_3]^{1-}$ with N,N-dicyclohexylcarbodiimide, CS$_2$, S$_8$, pyridine, (2,2,6,6-tetramethylpiperidin-1-yl)oxyl (TEMPO), MeCN, BiPh$_3$, and SnPh$_4$ in order to determine if the $4f^7 5d^1$ configuration in Gd(II) in an isolated compound could reveal new reaction pathways. Chapter 2 outlines solvent decomposition reactions by Ln(NR$_2$)$_3$/K reactions with the smaller rare earth metals, Ln = Y, Ho, Er, and Lu. This Chapter provides more information on solvent reactivity in these reductive systems by describing a series of C–O cleavage products isolated from Ln(NR$_2$)$_3$/K reactions with ethers. Chapter 3 outlines the investigation of the reductive chemistry of cerium with *in-situ* Ce(NR$_2$)$_3$/M/N$_2$ reactions. In this Chapter it is shown that crypt can function as a bidentate ligand to rare-earth ions. Chapter 4 outlines the reductive chemistry of neodymium with *in-situ* Nd(NR$_2$)$_3$/M/N$_2$ reactions. Examination of the in-situ reduction of Nd(NR$_2$)$_3$ at low temperature in Et$_2$O in the presence of 18-crown-6 provides a crystal system that demonstrates a solid-state isomerization of

an end-on bound $(N=N)^{2-}$ moiety to side-on. This Chapter also describes a possible connection between the $Ln(NR_2)_3/M$ reductions of N_2 and reductions by isolated $Ln(II)$ complexes.

INTRODUCTION

The Rare Earth Elements. The rare earth elements, the metals Y and Sc coupled with the metals in the lanthanide series (La to Lu), were not named because they are rare in abundance, but simply because their metal oxides were among the last to be discovered. Initially, these elements were believed to have very limited chemistry compared to the transition metals because of the limited radial extension of the 4f orbitals compared to the d orbitals.[1–4] Unlike their "rare earth" name, these elements have become common in many modern life applications such as lighting, batteries, and MRI imaging.[5] Even in the age of information, these elements have found a place as single molecule magnets (SMMs).[6] The lanthanide ions' intrinsically large magnetic moments, and the limited radial extension of the f orbitals, which contributes to preservation of orbital angular momentum, makes them beneficial for SMMs.[6]

Oxidation States. The +3 oxidation state can be found for all the lanthanides in the series, and for many years the reductive chemistry was centered on just six ions in the +2 oxidation state: Eu^{2+}, Yb^{2+}, Sm^{2+}, Tm^{2+}, Dy^{2+}, and Nd^{2+}.[2,7–9] It was believed that these were the only Ln(II) ions available in isolable molecular complexes. Given the proper tris(cyclopentadienyl) coordination environment, it was discovered that molecular complexes of Ln(II) ions for all lanthanides could be isolated using an LnA_3/M reaction, where Ln is a rare earth metal (Sc, Y, lanthanides), A is an anionic ligand, and M is an alkali metal. The complexes of the new Ln(II) ions (Ln = Y, La, Ce, Pr, Nd, Sm, Gd, Tb, Dy, Ho, Er, Tm, Lu) were discovered with the ligands $C_5H_3(SiMe_3)_2$ (Cp″) and $C_5H_4SiMe_3$, (Cp′).[9–14] Four of the six Ln(II) ions, Ln = Eu, Yb, Sm, and Tm, were found to have $4f^{n+1}$ electron configurations compared to their $4f^n$ Ln(III) precursors and are known as the "traditional" lanthanides.[15–18] The new Ln(II) ions, for Ln = La, Ce, Pr, Gd, Tb, Ho, Er, and Lu, were found to have a $4f^n5d^1$ electron configuration, and a $4d^1$ electron configuration for yttrium,

based on structural, spectroscopic, and magnetic data.[9–12,19] The new Ln(II) ions that adopt this $4f^n5d^1$ electron configuration are the "non-traditional" lanthanides, where the electron is added into the 5d orbital. Nd(II) and Dy(II) have been shown to be "crossover" ions, meaning these metals could adopt either electronic configuration based on the coordination environment.[19] The LnA_3/M reaction scheme for these species is shown in eq 0.1.

R = SiMe$_3$; M = La, Ce

R = H; M = Y, La, Ce, Pr, Nd, Sm, Gd, Tb, Dy, Ho, Er, Tm, Lu
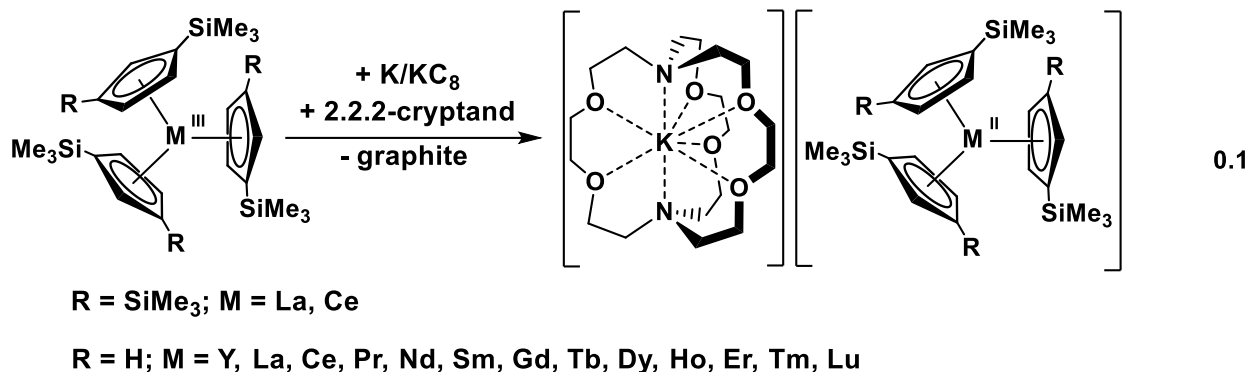
Small Molecule Activation with Sm(II). The discovery of the traditional Sm(II) complex, $(C_5Me_5)_2Sm(THF)_2$,[20] eq 0.2, led to an extensive array of reactions with small molecules like CO and CO_2 that resulted in unusual complexes.[21,22] A specific example of the unusual reactivity with $(C_5Me_5)_2Sm(THF)_2$ is shown in eq 0.3, where three CO molecules are reductively coupled.[21]

$$4\ (C_5Me_5)_2Sm(THF)_2 \ + \ 6\ CO \longrightarrow \qquad 0.3$$
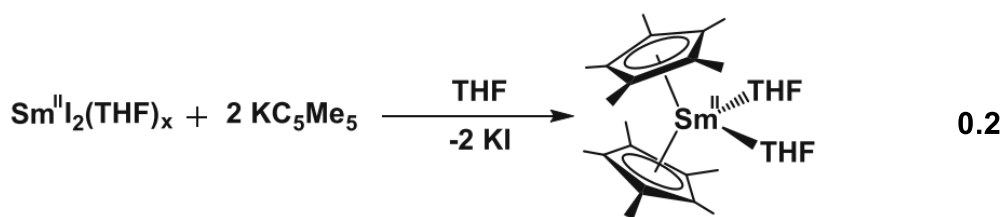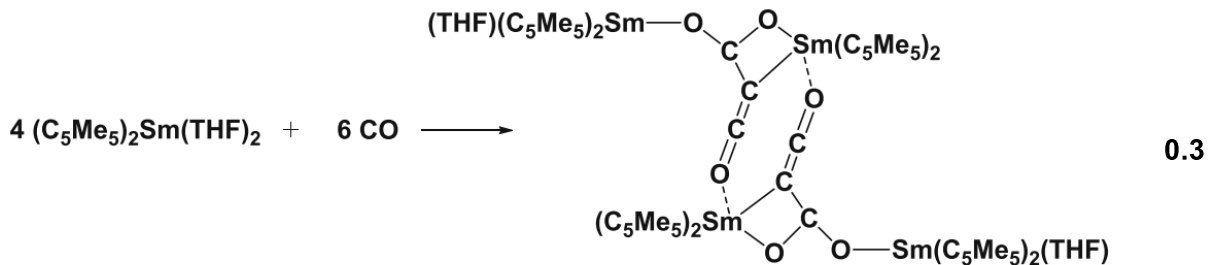
It was later discovered that the unsolvated derivative, $(C_5Me_5)_2Sm$,[23] could be generated leading to even more unusual reactivity with polycyclic aromatic hydrocarbons, aromatic nitrogen heterocycles, butadiene, isoprene, and N_2.[24–28] In particular, $(C_5Me_5)_2Sm$ reduced N_2 to make the first reduced-dinitrogen complex containing a rare-earth metal, $[(C_5Me_5)_2Sm]_2[\mu\text{-}\eta^2\text{:}\eta^2\text{-}N_2]$. This complex was also the first example of any metal containing an $M_2(\mu\text{-}\eta^2\text{:}\eta^2\text{-}N_2)$ unit with a planar geometry, eq 0.4.[24] This abundance of reactivity from $(C_5Me_5)_2Sm(THF)_2$ and $(C_5Me_5)_2Sm$ prompted further exploration of reactivity with other Ln(II) complexes.

$$2\ \ Sm^{II} \ + \ N_2 \ \underset{\text{toluene}}{\rightleftharpoons} \qquad 0.4$$
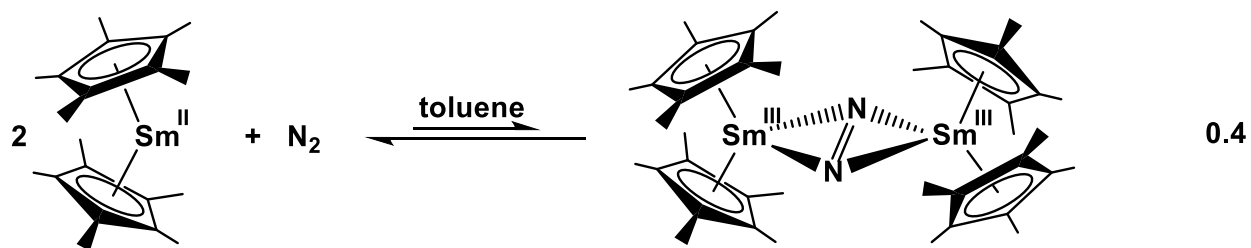
Dinitrogen Reduction with Other Rare Earth Metals. After the initial discovery of $[(C_5Me_5)_2Sm]_2[\mu\text{-}\eta^2\text{:}\eta^2\text{-}N_2]$, the Ln(II) complexes, NdI_2, DyI_2, and TmI_2, were found to react with KNR_2 (R = $SiMe_3$), under dinitrogen to generate the $(N=N)^{2-}$ complexes, $[(THF)(R_2N)_2Ln]_2[\mu\text{-}\eta^2\text{:}\eta^2\text{-}N_2]$, eq 0.5.[29–31] Subsequently, these $(N=N)^{2-}$ complexes were synthesized from Ln(III) precursors by LnA_3/M reactions, eq 0.6.[32–34] These complexes were neutral with a reduced dinitrogen unit, $(N=N)^{2-}$, that is bound side-on to each Ln center with a coordinated THF molecule.

$$2\ \text{Ln}^{\text{II}}\text{I}_2\ +\ 4\ \text{MA}\ \xrightarrow[-\ 4\ \text{MI}]{\underset{\text{THF}}{\overset{\text{N}_2}{}}}$$

0.5
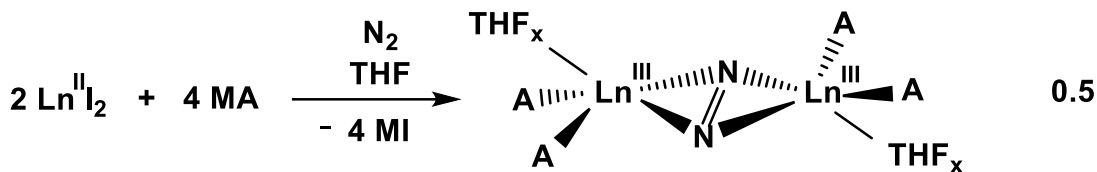
Ln = Nd, Dy, Tm

A = N(SiMe₃)₂

M = K, KC₈, Na; x = 0-2

$$2\ \text{Ln}^{\text{III}}\text{A}_3\ +\ 2\ \text{K}\ \xrightarrow{\text{THF}}\ \begin{bmatrix} 2\ "\text{Ln}^{\text{II}}\text{A}_2"\ +\ 2\ \text{MA} \\ \text{or} \\ 2\ "\text{MLn}^{\text{II}}\text{A}_3" \end{bmatrix}\ \xrightarrow[-\ 2\ \text{KA}]{\text{N}_2}$$

0.6
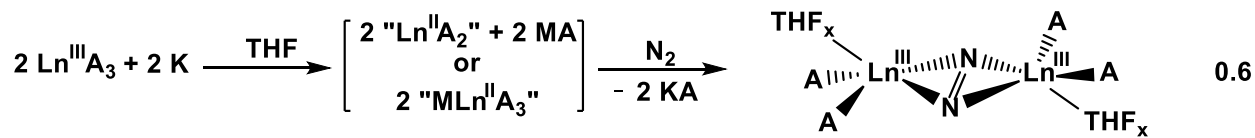
Ln = Sc, Y, La, Ce, Pr, Nd, Gd, Tb, Dy, Ho, Er, Tm, Lu

A = N(SiMe₃)₂

x = 1, 2

These dinitrogen reduction studies also led to the isolation of the first complexes of the radical trianion $(N_2)^{3-}$ which was later discovered to make outstanding single molecule magnets.[35–38] It was also discovered that the $(N_2)^{3-}$ complex with Y reacts with NO to form the first complex of with the radical dianion, $(NO)^{2-}$.[39]

The LnA₃/M reactions were expected to involve Ln(II) intermediates (shown in eq 0.6) to form the dinitrogen complexes since the complexes were originally isolated via Ln(II) complexes, LnI₂.[32] However, the same LnA₃/M reactions performed under an argon atmosphere only gave the Ln(III) starting materials following work-up rather than Ln(II) complexes.[9,10]

Isolated Divalent Rare Earth Amide Complexes. In 2013, new Ln(II) ions were discovered across the lanthanide series using the cyclopentadienyl ligand set, eq 0.1, but not with the amide ligands that gave the dinitrogen complexes. However, in 2018, it was discovered that the new $4f^n5d^1$ Ln(II) ions could be isolated in the amide-ligated anions $[\text{Ln}(NR_2)_3]^{1-}$, eq 0.7 and

0.8, providing a ligand set different from the cyclopentadienyls for investigating Ln(II) reactivity.[40,41]

$$Ln^{III}(NR_2)_3 + 2\ 18\text{-crown-6} \xrightarrow{K/KC_8} [\ \ ][\ R_2N\text{-}Ln^{II}(NR_2)_2\ ]\quad 0.7$$

Ln = Gd, Tb, Dy, Ho, Er, Y
R = SiMe$_3$

$$Ln^{III}(NR_2)_3 + 2.2.2\text{-cryptand} \xrightarrow{K/KC_8} [\ \ ][\ R_2N\text{-}Ln^{II}(NR_2)_2\ ]\quad 0.8$$

Ln = Gd, Tb, Dy, Sc
R = SiMe$_3$
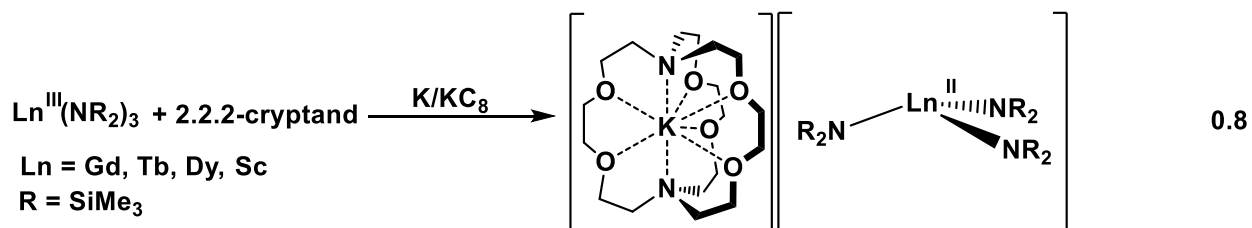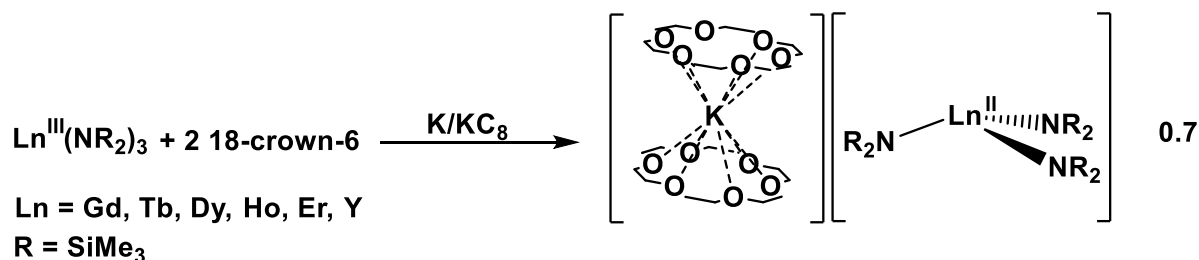
Although the tris(amide) ligand set proved to be more favorable than the tris(cyclopentadienyl) complexes for small molecule reactivity studies, it has not provided Ln(II) complexes across the series. Crystallographically characterized $[Ln(NR_2)_3]^{1-}$ complexes are known only for Nd, Sm, Eu, Gd, Tb, Dy, Ho, Er, Tm, Yb, Y, and Sc, and some of these examples are challenging to synthesize and have limited stability in solution.[40-44] So far, reactions of these isolated $[Ln(NR_2)_3]^{1-}$ Ln(II) complexes with CO and N_2 showed the amide ligand set to be advantageous in the isolation of reduced small molecules.[41,42,45,46]

End-On Bound Dianionic Dinitrogen Complexes. Exposure of dinitrogen to $[Ln(NR_2)_3]^{1-}$ complexes (Ln = Sc, Gd, Tb) at low temperatures in Et$_2$O, with either 18-c-6 or crypt, produced the first end-on bound reduced dinitrogen complexes of the Ln metals, $[\{(R_2N)_3Ln\}_2(\mu\text{-}\eta^1{:}\eta^1\text{-}N_2)]^{2-}$, eq 0.9.[45,46]

$$2\,[\text{Ln}^{II}(\text{NR}_2)_3]^{1-} \quad \underset{\substack{h\nu \\ -\,\text{N}_2}}{\overset{\substack{+\,\text{N}_2 \\ \text{Et}_2\text{O} \\ -\,35\,°\text{C}}}{\rightleftharpoons}} \quad \left[\begin{array}{c} \text{R}_2\text{N}\,\,\,\,\,\,\,\text{R}_2\text{N} \\ \text{R}_2\text{N}\diagdown\,\,\,\,\,\text{Ln}^{III}\!\!-\!\text{N}\!\!=\!\!\text{N}\!\!-\!\text{Ln}^{III}\!\!-\!\text{NR}_2 \\ \text{R}_2\text{N}\,\,\,\,\,\,\,\text{NR}_2 \end{array} \right]^{2-} \qquad 0.9$$

Ln = Sc, Tb
R = SiMe$_3$
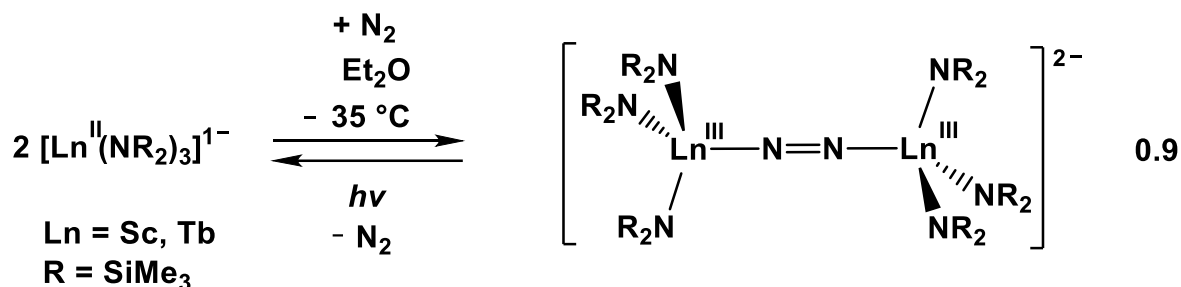
In contrast to the previously isolated neutral complexes with two amide ligands per metal, these complexes were dianionic, with three $(\text{NR}_2)^{1-}$ ligands per metal. The reactions that formed the end-on complexes, $[\{(\text{R}_2\text{N})_3\text{Ln}\}_2(\mu\text{-}\eta^1{:}\eta^1\text{-N}_2)]^{2-}$, eq 0.9, were performed at $-35\,°\text{C}$ in Et$_2$O and in the presence of a chelating agent. In comparison, the reactions that formed the side-on complexes, $[(\text{THF})(\text{R}_2\text{N})_2\text{Ln}]_2[\mu\text{-}\eta^2{:}\eta^2\text{-N}_2]$, were performed at room temperature in THF without the presence of a chelating agent.

Although the Sc and Tb complexes had the end-on structure, $[\{(\text{R}_2\text{N})_3\text{Ln}\}_2(\mu\text{-}\eta^1{:}\eta^1\text{-N}_2)]^{2-}$, the X-ray crystallographic evidence of the Gd complex showed that it was comprised of a mixture of side-on and end-on bound $(\text{N=N})^{2-}$ units, $[\{(\text{R}_2\text{N})_3\text{Gd}\}_2(\mu\text{-}\eta^x{:}\eta^x\text{-N}_2)]^{2-}$ (x = 1, 2), eq 0.10.[46] The end-on $(\text{N=N})^{2-}$ ions in these complexes, $[\{(\text{R}_2\text{N})_3\text{Ln}\}_2(\mu\text{-}\eta^1{:}\eta^1\text{-N}_2)]^{2-}$ (Ln = Sc, Tb) and $[\{(\text{R}_2\text{N})_3\text{Gd}\}_2(\mu\text{-}\eta^x{:}\eta^x\text{-N}_2)]^{2-}$, are potent reductants and can revert back to the highly reactive Ln(II) complexes, $[\text{Ln}(\text{NR}_2)_3]^{1-}$, also shown in eq 0.9 and eq 0.10.[45,46] This has not been observed for the side-on species.

$$2\,[\text{Gd}^{II}(\text{NR}_2)_3]^{1-} \quad \underset{\substack{\Delta \\ -\,\text{N}_2}}{\overset{\substack{+\,\text{N}_2 \\ \text{Et}_2\text{O} \\ -\,35\,°\text{C}}}{\rightleftharpoons}} \quad \left[\begin{array}{c} \text{R}_2\text{N}\,\,\,\,\,\text{N}\,\,\,\,\text{NR}_2 \\ \text{R}_2\text{N}\diagdown\,\,\,\text{Gd}^{III}\!\!-\!\text{N}\!\!=\!\!\!=\!\!\text{N}\!\!-\!\text{Gd}^{III}\!\!-\!\text{NR}_2 \\ \text{R}_2\text{N}\,\,\,\,\,\text{N}\,\,\,\,\text{NR}_2 \end{array} \right]^{2-} \qquad 0.10$$

R = SiMe$_3$
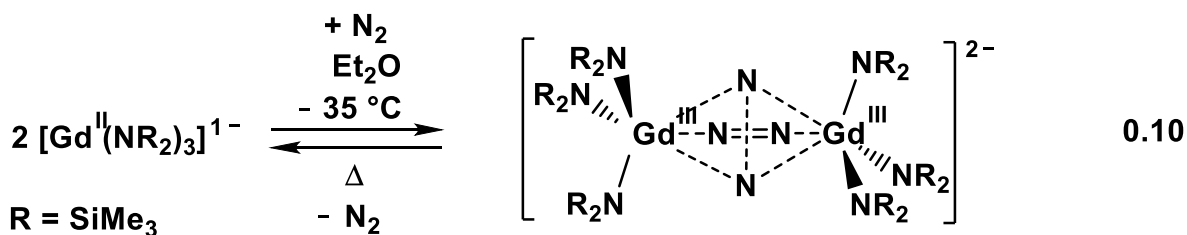
Dissertation Outline. The research presented in this dissertation is focused on Ln(II) reduction reactivity with $(NR_2)^{1-}$ ligands. The results show the diversity of products obtained by amide-based Ln(II) reduction due to subtle changes in reaction conditions.

Chapter 1 outlines the reactions of isolated $[Gd^{II}(NR_2)_3]^{1-}$ with N,N-dicyclohexylcarbodiimide, CS_2, S_8, pyridine, (2,2,6,6-tetramethylpiperidin-1-yl)oxyl (TEMPO), MeCN, $BiPh_3$, and $SnPh_4$ in order to determine if the $4f^75d^1$ configuration in Gd(II) in an isolated compound could reveal new reaction pathways.[47,48] These Ln(II) reactivity studies focus on the gadolinium complex, $[Gd(NR_2)_3]^{1-}$, because it is the most thermally stable non-traditional lanthanide ion isolated with the tris amide ligand set.[40]

Chapter 2 outlines solvent decomposition reactions by $Ln(NR_2)_3/K$ reactions with the smaller rare earth metals, Ln = Y, Ho, Er, and Lu. This Chapter provides more information on solvent reactivity in these reductive systems by describing a series of C–O cleavage products isolated from $Ln(NR_2)_3/K$ reactions with ethers.

Chapter 3 outlines the investigation of the reductive chemistry of cerium with *in-situ* $Ce(NR_2)_3/M/N_2$ reactions. A new coordination mode for crypt with rare-earth metal ions was discovered that is an intermediate between the 8-coordinate mode with the rare-earth metal ion inside crypt and the situation in which crypt is not coordinating the rare-earth metal ion at all.[49] In this Chapter it is shown that crypt can function as a bidentate ligand to rare-earth ions.

Chapter 4 outlines the reductive chemistry of neodymium with *in-situ* $Nd(NR_2)_3/M/N_2$ reactions. Examination of the in-situ reduction of $Nd(NR_2)_3$ at low temperature in Et_2O in the presence of 18-crown-6 provides a crystal system that demonstrates a solid-state isomerization of an end-on bound $(N=N)^{2-}$ moiety to the side-on structure found in most of the previously reported

rare-earth metal complexes of reduced dinitrogen ligands. This Chapter also describes a possible

connection between the LnA_3/M reductions of N_2 and the Ln(II) reductions.

References

(1)   Freeman, A. J.; Watson, R. E. *Phys. Rev.* **1962**, *127* (6), 2058–2075.
(2)   Evans, W. J. *Polyhedron* **1987**, *6* (5), 803–835.
(3)   Evans, W. J. *Inorg. Chem.* **2007**, *46* (9), 3435–3449.
(4)   Schumann, H.; Meese-Marktscheffel, J. A.; Esser, L. *Chem. Rev.* **1995**, *95* (4), 865–986.
(5)   Atwood, D. A. John Wiley & Sons, 2013.
(6)   Woodruff, D. N.; Winpenny, R. E. P.; Layfield, R. A. *Chem. Rev.* **2013**, *113* (7), 5110–5148.
(7)   Morss, L. R. *Chem. Rev.* **1975**, *76* (6), 827–841.
(8)   Mikheev, N. B., A. N. K. *Coord. Chem. Rev.* **1991**, *109*, 1–59.
(9)   Evans, W. J. *Organometallics* **2016**, *35*, 3088–3100.
(10)   Woen, D. H.; Evans, W. J. In *Handbook on the Physics and Chemistry of Rare Earths*; Elsevier B.V., 2016; pp 1–57.
(11)   MacDonald, M. R.; Bates, J. E.; Fieser, M. E.; Ziller, J. W.; Furche, F.; Evans, W. J. *J. Am. Chem. Soc.* **2012**, *134* (20), 8420–8423.
(12)   Macdonald, M. R.; Bates, E.; Ziller, J. W.; Furche, F.; Evans, W. J. *J. Am. Chem. Soc.* **2013**, *135*, 9857–9868.
(13)   MacDonald, M. R.; Ziller, J. W.; Evans, W. J. *J. Am. Chem. Soc.* **2011**, *133* (40), 15914–15917.
(14)   Hitchcock, P. B.; Lappert, M. F.; Maron, L.; Protchenko, A. V. *Angew. Chem. Int. Ed.* **2008**, No. 47, 1488–1491.
(15)   Meyer, G. *Z. Anorg. Allg. Chem.* **2007**, *633* (15), 2537–2552.
(16)   Meyer, G. *Chem. Rev.* **1988**, *88* (1), 93–107.
(17)   Klemm, W.; Bommer, H. *Z. Anorg. Allg. Chem.* **1937**, *231* (1-2), 138–171.
(18)   Jantsch, G.; Grubitsch, H.; Hoffmann, F.; Alber, H. *Z. Anorg. Allg. Chem.* **1929**, *185* (1), 49–64.
(19)   Fieser, M. E.; Macdonald, M. R.; Krull, B. T.; Bates, J. E.; Ziller, J. W.; Furche, F.; Evans, W. J. *J. Am. Chem. Soc.* **2015**, *137* (1), 369–382.
(20)   Evans, W. J.; Bloom, I.; Hunter, W. E.; Atwood, J. L. *J. Am. Chem. Soc.* **1981**, *103*, 6508–6510.
(21)   Evans, W. J.; Grate, J. W.; Hughes, L. A.; Zhang, H.; Atwood, J. L. *J. Am. Chem. Soc.* **1985**, *107* (12), 3728–3730.
(22)   Evans, W. J.; Hughes, L. A.; Drummond, D. K.; Zhang, H.; Atwood, J. L. *J. Am. Chem. Soc.* **1986**, *108*, 1722–1723.
(23)   Evans, W. J.; Hughes, L. A.; Hanusa, T. P. *J. Am. Chem. Soc.* **1984**, *106* (15), 4270–4272.
(24)   Evans, W. J.; Ulibarri, T. A.; Ziller, J. W. *J. Am. Chem. Soc.* **1988**, *110* (20), 6877–6879.
(25)   Evans, W. J.; Gonzales, S. L.; Ziller, J. W. *J. Am. Chem. Soc.* **1994**, *116* (6), 2600–2608.
(26)   Evans, W. J.; Drummond, D. K. *J. Am. Chem. Soc.* **1989**, *111* (9), 3329–3335.
(27)   Kaita, S.; Hou, Z.; Wakatsuki, Y.; Mao, C. T.; Vcl, C. *Macromolecules* **1999**, *32*, 9078–

9079.

(28) Hou, Z.; Zhang, Y.; Nishiura, M.; Wakatsuki, Y. *Organometallics* **2003**, *22* (1), 129–135.

(29) Evans, W. J.; Allen, N. T.; Ziller, J. W. *J. Am. Chem. Soc.* **2001**, *123* (32), 7927–7928.

(30) Evans, W. J.; Allen, N. T.; Ziller, J. W. *Angew. Chem. Int. Ed.* **2002**, *41* (2), 359–361.

(31) Evans, W. J.; Zucchi, G.; Ziller, J. W. *J. Am. Chem. Soc.* **2003**, *125* (1), 10–11.

(32) Evans, W. J.; Lee, D. S.; Lie, C.; Ziller, J. W. *Angew. Chem. Int. Ed.* **2004**, *43* (41), 5517–5519.

(33) Evans, W. J.; Lee, D. S.; Ziller, J. W. *J. Am. Chem. Soc.* **2004**, *126*, 454–455.

(34) Evans, W. J.; Lee, D. S.; Rego, D. B.; Perotti, J. M.; Kozimor, S. A.; Moore, E. K.; Ziller, J. W. *J. Am. Chem. Soc.* **2004**, *126* (44), 14574–14582.

(35) Demir, S.; Gonzalez, M. I.; Darago, L. E.; Evans, W. J.; Long, J. R. *Nat. Commun.* **2017**, *8*, 1–9.

(36) Fang, M.; Lee, D. S.; Ziller, J. W.; Doedens, R. J.; Bates, J. E.; Furche, F.; Evans, W. J. *J. Am. Chem. Soc.* **2011**, *133* (11), 3784–3787.

(37) Rinehart, D.; Fang, M.; Evans, W. J.; Long, R. *J. Am. Chem. Soc.* **2011**, *133*, 14236–14239.

(38) Chilton, N. F.; Goodwin, C. A. P.; Mills, D. P.; Winpenny, R. E. P. *Chem. Commun.* **2015**, *51* (1), 101–103.

(39) Evans, W. J.; Fang, M.; Bates, J. E.; Furche, F.; Ziller, J. W.; Kiesz, M. D.; Zink, J. I. *Nat. Chem.* **2010**, *2*, 644–647.

(40) Ryan, A. J.; Darago, L. E.; Balasubramani, G.; Chen, G. P.; Ziller, J. W.; Furche, F.; Long, J. R.; Evans, W. J. *Chem. Eur. J.* **2018**, No. 2, 7702–7709.

(41) Woen, D. H.; Chen, G. P.; Ziller, J. W.; Boyle, T. J.; Furche, F.; Evans, W. J. *Angew. Chem. Int. Ed.* **2017**, *129*, 2082–2085.

(42) Ryan, A. J.; Ziller, J. W.; Evans, W. J. *Chem. Sci.* **2020**, No. 11, 2006–2014.

(43) Tilley, T. D.; Andersen, R. A.; Zalkin, A. *Inorg. Chem.* **1984**, *23* (15), 2271–2276.

(44) Evans, W. J.; Johnston, M. A.; Clark, R. D.; Anwander, R.; Ziller, J. W. *Polyhedron* **2001**, *20* (19), 2483–2490.

(45) Woen, D. H.; Chen, G. P.; Ziller, J. W.; Boyle, T. J.; Furche, F.; Evans, W. J. *J. Am. Chem. Soc.* **2017**, *139*, 14861–14864.

(46) Ryan, A. J.; Balasubramani, S. ganesh; Ziller, J. W.; Furche, F.; Evans, W. J. *J. Am. Chem. Soc.* **2020**, *142* (20), 9302–9313.

(47) Chung, A. B.; Ziller, J. W.; Evans, W. J. *Acta Crystallogr. Sect. E Crystallogr. Commun.* **2020**, *76*, 1047–1050.

(48) Chung, A. B.; Ryan, A. J.; Fang, M.; Ziller, J. W.; Evans, W. J. *Inorg. Chem.* **2021**, *60* (20), 15635–15645.

(49) Chung, A. B.; Huh, D. N.; Ziller, J. W.; Evans, W. J. *Inorg. Chem. Front.* **2020**, *7* (22), 4445–4451.

Chapter 1

Reductive Reactivity of the $4f^7 5d^1$ Gd(II) Ion in $\{Gd^{II}[N(SiMe_3)_2]_3\}^{1-}$; Structural Characterization of Products of Coupling, Bond Cleavage, Insertion, and Radical Reactions

Introduction*

This Chapter describes the reactivity of the $[Gd^{II}(NR_2)_3]^{1-}$ complex (R = SiMe₃) with a series of reagents in order to explore Ln(II) reductive reactivity with an isolated Ln(II) amide complex to contrast with *in situ* reactions. As outlined in the Introduction, the discovery that the new $4f^n 5d^1$ Ln(II) ions could be isolated with the bis(trimethylsilyl) amide ligand, $(NR_2)^{1-}$, provided a different ligand set for investigating Ln(II) reactivity.[1,2] Although, Ln(II) ions could be isolated across the lanthanide series from La to Lu as well as for Y, in $(Cp'_3Ln)^{1-}$ complexes $(Cp' = C_5H_4SiMe_3)$,[3–8] the tris-cyclopentadienyl ligand set was not ideal for isolating products of reactions with small molecules. Recently, reactions of these isolated $[Ln(NR_2)_3]^{1-}$ complexes, with CO and N_2 showed the amide ligand set to be advantageous in the isolation of reduced small molecules.[2,9–11]

Since only a handful of crystallographically characterized $[Ln(NR_2)_3]^{1-}$ complexes are known and some of these examples are challenging to synthesize and have limited stability in solution,[1,2,11–13] the $[Gd(NR_2)_3]^{1-}$ anion was chosen for this study because it is the member of the $4f^n 5d^1$ Ln(II) amide series most readily isolated as a crystalline solid and the most thermally stable non-traditional lanthanide ion isolated with the tris amide ligand set.

$[Gd(NR_2)_3]^{1-}$ has been crystallographically characterized as both $[K(crypt)]^{1+}$ and $[K(18\text{-}c\text{-}6)_2]^{1+}$ salts[1] (crypt = 2.2.2-cryptand; 18-c-6 = 18-crown-6) and both salts were investigated since previous studies have shown that the identity of the cation can be crucial to successful isolation of reaction products.[1,11]

A wide variety of reagents were looked at with both $[K(18\text{-}c\text{-}6)_2][Gd(NR_2)_3]$, **1**, and $[K(crypt)][Gd(NR_2)_3]$, **2**, to survey the many reaction pathways available to this ion. It should be noted that since the Gd(III) products of these reactions are complexes of $4f^7$ Gd(III) which has a 7.9 μ_B magnetic moment, X-ray crystallography was necessary to identify the products of these reactions. As discussed in previous papers,[11,14] the products isolated from these reactions reflect the least soluble products of the reaction that are most prone to crystallize in a form analyzable by X-ray crystallography. Hence, the reaction products are representative of the types of reactions that can occur with Gd(II), but they should not be used to infer reaction mechanisms or even main reaction pathways.

Results and Discussion

N,N′-di-tert-butylcarbodiimide. N,N′-di-tert-butylcarbodiimide was chosen as a reagent due to the reduction of carbodiimides with Sm(II) bis(trimethylsilyl)amides known to form oxalamidinates and amidinates.[15] It was of interest to identify if $[Gd(NR_2)_3]^{1-}$ could reduce carbodiimides to form amidinates and coordinate to the Gd center since Gd(II) is known to be more reducing than Sm(II).

A crystal containing two different potassium 18-c-6 salts of tert-butylcyanamide anions, $(Me_3CNCN)^{1-}$, and one equivalent of 1,3-di-tert-butyl urea, Figure 1.1, was isolated during the reduction of incompletely dried N,N′-di-tert-butylcarbodiimide with $[K(18\text{-}c\text{-}6)_2][Gd(NR_2)_3]$, **1**. A reductive N–C bond cleavage evidently occurred to remove a tert-butyl group from the starting

11

carbodiimide forming the $(Me_3CNCN)^{1-}$ anions, a reaction that could be attributed to the highly reducing Gd(II) ion present.[1,11] The urea component of the crystal is a formal hydrolysis product of di-tert-butylcarbodiimide. The presence of water in this reaction system is evident from the fact that one of the 18-c-6 counter-cations is aquated.
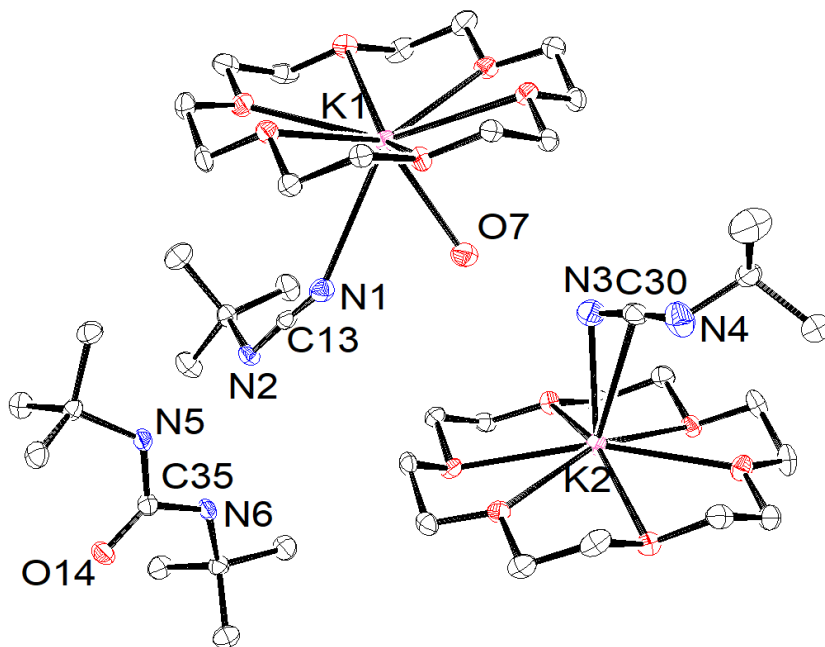
Figure 1.1. Representation of tert-butylcyanamide anions bound side-on and end-on, and 1,3-di-tert-butyl urea, all drawn with ellipsoids at the 50% probability level. Hydrogen atoms are excluded for clarity.

Carbon Disulfide. CS_2 was chosen as a reagent since it had been previously studied with complexes of the traditional $4f^6$, $4f^7$, and $4f^{14}$ ions, Sm(II), Eu(II), and Yb(II). A variety of products were identified from these reactions including $(CS_2)^{2-}$,[16,17] coupled $(SCS–CS_2)^{2-}$,[18,19] and $(SC{\equiv}CS)^{2-}$,[17] as well as the potassium salts, K_2CS_3, $K_2C_2S_4$, and $K_2C_3S_5$.[20] CS_2 reduction has also been studied with actinide reducing reagents, and complexes containing trithiocarbonate, $(CS_3)^{2-}$, have been isolated.[21,22] CS_2 was also of interest since an *in situ* $Y(NR_2)_3/KC_8/18$-c-6/CS_2 reaction

previously had generated crystals of a trithiocarbonate, {[K(18-c-6)$_2$(THF)$_2$]$_2$[(R$_2$N)$_2$Y(μ-CS$_3$-κ^2S,S')]$_2$}(18-c-6).[23]

A Trithiocarbonate From CS$_2$ and 1. The dropwise addition of excess CS$_2$ to a dark blue solution of the 18-c-6 complex, [K(18-c-6)$_2$][Gd(NR$_2$)$_3$], **1,** dissolved in Et$_2$O at −35 °C under Ar immediately formed a dark yellow solution. Within 24 hours, small amounts of light yellow crystals grew on top of a red oil that solidified at −35 °C. The yellow crystals were characterized by X-ray diffraction as the trithiocarbonate complex, {[K(18-c-6)](μ_3-CS$_3$-$\kappa S, \kappa^2 S', S''$)[Gd(NR$_2$)$_2$]}$_2$, **3**, Figure 1.2, eq 1.1.

13
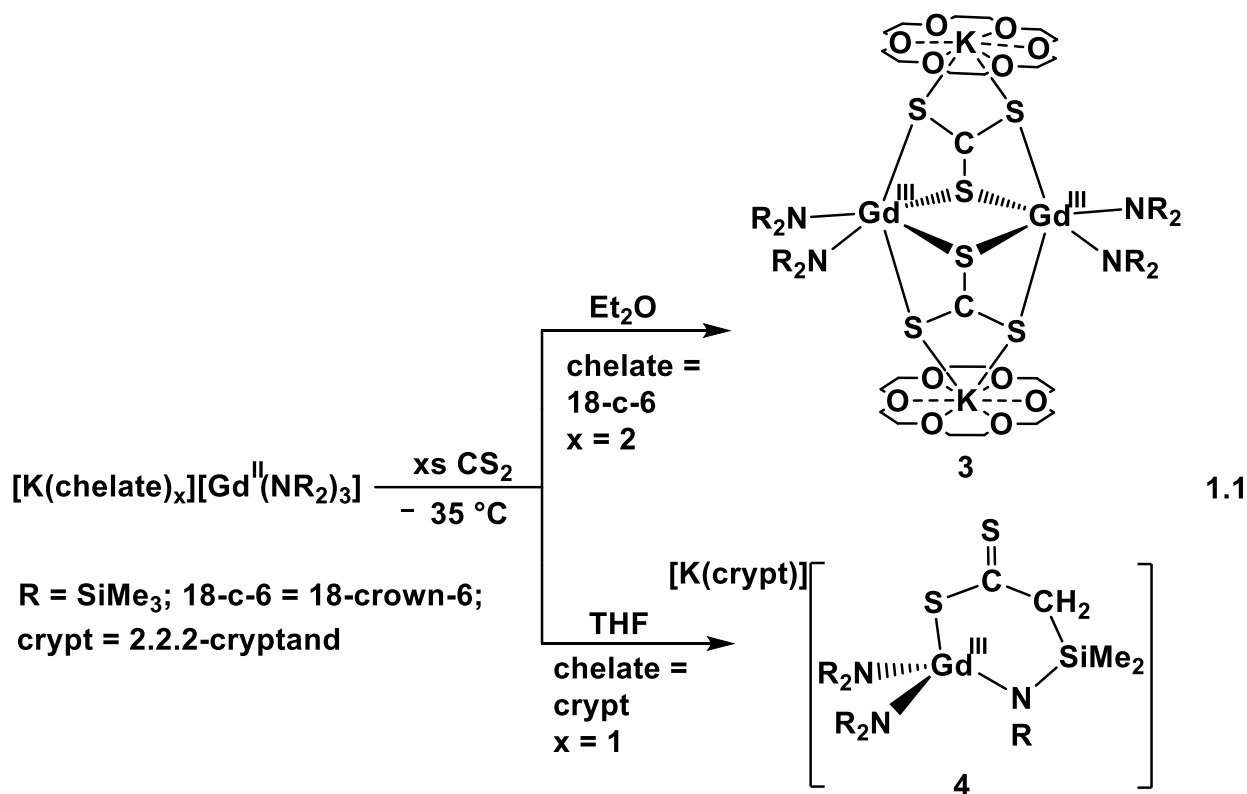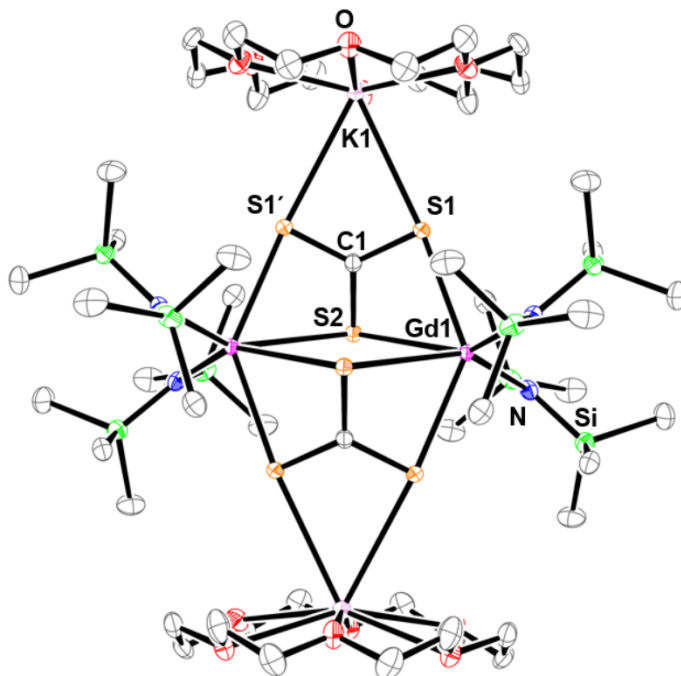
Figure 1.2. Representation of {[K(18-c-6)](μ_3-CS$_3$-kS,k^2S′,S″)[Gd(NR$_2$)$_2$]}$_2$, **3** with atomic displacement parameters drawn at the 50% probability level. Hydrogen atoms are omitted for clarity.

Attempts to crystallize the red oil were unsuccessful although its IR (Figure 1.3) and UV-visible spectra (Figure 1.4) are very similar to that of the yellow crystals. The stoichiometry with respect to CS$_2$ did not affect the outcome of the reaction: similar results are observed from reactions of **1** with 1 equivalent and with excess CS$_2$.
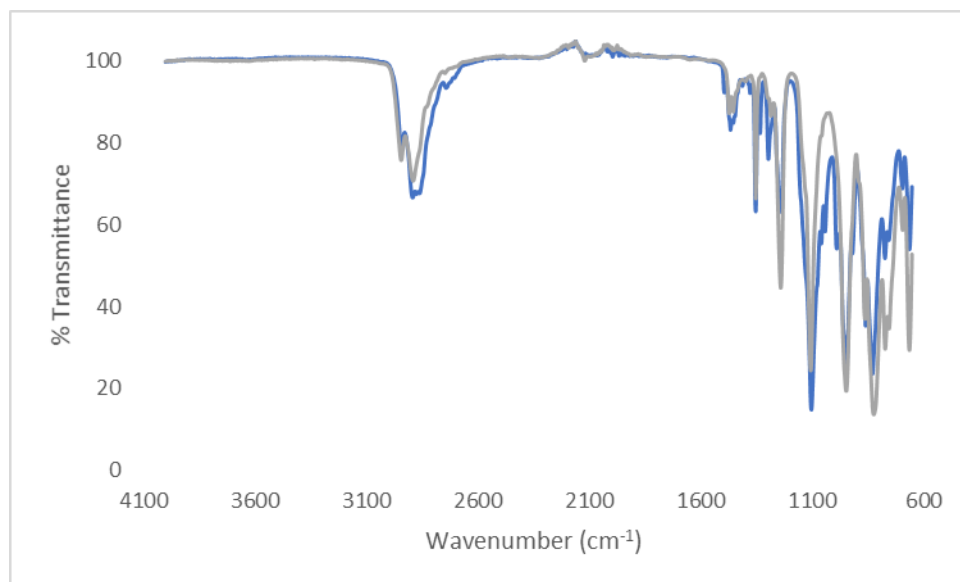
Figure 1.3. IR spectrum of red oil (grey) and {[K(18-c-6)](μ_3-CS$_3$-κS,κ^2S′,S″)[Gd(NR$_2$)$_2$]}$_2$, **3** (blue).
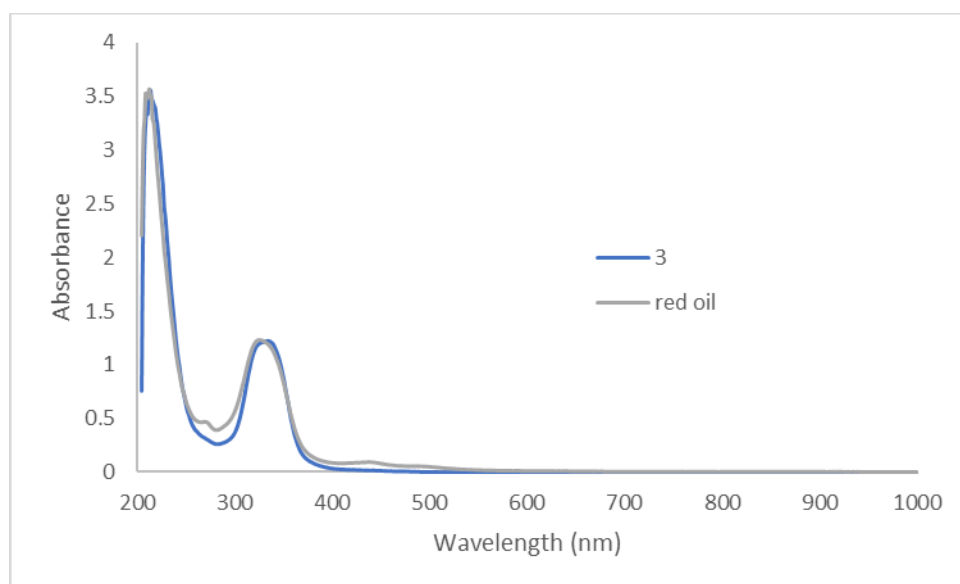
Figure 1.4. UV-vis spectra of red oil (grey) and {[K(18-c-6)](μ_3-CS$_3$-κS,κ^2S′,S″)[Gd(NR$_2$)$_2$]}$_2$, **3** (blue) in THF.

Complex **3** is a tetrametallic compound that contains two trithiocarbonate dianions (CS$_3$)$^{2-}$ with each sulfur involved in a bridge between two metals. It crystallizes in the monoclinic P2$_{1/c}$ space group with one formula unit per unit cell. One sulfur from each (CS$_3$)$^{2-}$ ligand bridges two

Gd(III) ions each ligated by two $(NR_2)^{1-}$ ligands. The other two sulfur atoms bridge a Gd(III) ion and a potassium ion bound to an 18-c-6 ligand. This type of κ^3 $(CS_3)^{2-}$ has been observed previously in the extended 3D-polymeric structure of $(K_2CS_3)_5(DMSO)_{12}$ in which each sulfur bridges three potassium ions and each potassium is coordinated by three thiocarbonate sulfur atoms and three DMSO ligands,[20] Figure 1.5. It has also been found in $(RO)_4U(CS_3)[(K(18\text{-crown-}6)]_2$ $(R = OSi(OCMe_3)_3)^{[22]}$ and in $(RR'N)_2Fe(CS_3)[K(18\text{-crown-}6)]_2$ $(R = SiMe_3; R' = 2,6\text{-}$diisopropylphenyl),[24] Figure 1.5. The U and Fe structures differ from **3** in that there are two [K(18-crown-6)]$^{1+}$ units coordinating to the κ^3 $(CS_3)^{2-}$ and only one other metal (U, Fe) rather than one potassium and two Gd as in **3**. The product of the *in situ* Y(NR$_2$)$_3$/KC$_8$/18-c-6/CS$_2$ reaction is also shown in Figure 1.5.
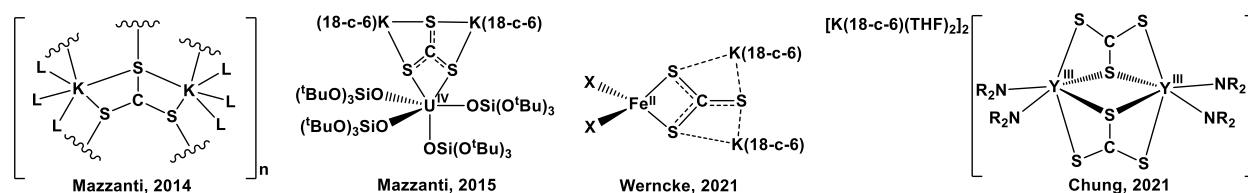
Figure 1.5. $(CS_3)^{2-}$ complexes: $[(K_2C_3S_5)_5(L)_{12}]_n$ (L = DMSO),[20] $\{U[OSi(O^tBu)_3]_4(\mu_3\text{-}\kappa^2{:}\kappa^2{:}\kappa^2CS_3)K_2(18\text{-c-}6)_2\}$,[22] $[K(18\text{-c-}6)]_2[X_2Fe(\eta^2\text{-}CS_3)]$ (X = N(Dipp)SiMe$_3$, Dipp = 2,6-diisopropylphenyl)[24] and $\{[K(18\text{-c-}6)_2(THF)_2]_2[(R_2N)_2Y(\mu\text{-}CS_3\text{-}\kappa^2S,S')]_2\}(18\text{-c-}6)$ ((R = SiMe$_3$).[23]

In Table 1.1, the metrical parameters on **3** are compared with those of the related yttrium complex, $\{[K(18\text{-c-}6)_2(THF)_2]_2[(R_2N)_2Y(\mu\text{-}CS_3\text{-}\kappa^2S,S')]_2\}(18\text{-c-}6)$. Although the structures differ in that potassium is not coordinated to the $(CS_3)^{2-}$ ion in the yttrium complex, the metrical parameters are very similar after taking into account that the ionic radius of Y(III) is approximately 0.03-0.04 Å shorter than that of Gd(III).[25]

Table 1.1. Selected metrical parameters for $\{[K(18\text{-}c\text{-}6)](\mu_3\text{-}CS_3\text{-}\kappa S,\kappa^2 S',S'')[Gd(NR_2)_2]\}_2$ (**3**) and $\{[K(18\text{-}c\text{-}6)_2(THF)_2]_2[(R_2N)_2Y(\mu\text{-}CS_3\text{-}\kappa^2 S,S')]_2\}(18\text{-}c\text{-}6)$ (Å, deg).

$\{[K(18\text{-}c\text{-}6)](\mu_3\text{-}CS_3\text{-}\kappa S,\kappa^2 S',S'')[Gd(NR_2)_2]\}_2$		$\{[K(18\text{-}c\text{-}6)_2(THF)_2]_2[(R_2N)_2Y(\mu\text{-}CS_3\text{-}\kappa^2 S,S')]_2\}(18c6)$	
Gd1–N1	2.285(4)	Y1–N1	2.260(2)
		Y1–N2	2.258(2)
Gd1–S1	2.8350(11)	Y1–S1	2.8055(8)
Gd1–S1′	2.8349(11)	Y1–S3	2.7930(7)
Gd1–S2	3.0180(9)	Y1–S2	2.9442(7)
S1–C1	1.712(3)	S1–C13	1.702(3)
S2–C1	1.718(7)	S2–C13	1.731(3)
S1′–C1	1.712(3)	S3–C13	1.702(3)
S1–C1–S1′	120.8(4)	S1–C13–S3	122.38(16)
S1–C1–S2	119.53(19)	S1–C13–S2	119.25(16)
S1′–C1–S2	119.53(19)	S3–C13–S2	118.23(16)

Despite the two types of sulfur bridges in **3**, i.e. Ln–S–Ln and Ln–S–K, the metrical parameters of the $(CS_3)^{2-}$ ligands are quite uniform. The S−C−S angles span a small range: 119.1(2)°, 120.8(4)°, and 119.1(2)°. The 1.712(3) Å (C1–S1), 1.712(3) Å (C1–S1′), and 1.718(7) Å (C1–S2) C–S distances are between the values typical for a C–S single bond, 1.819 Å, and a C=S double bond, 1.671 Å,[26] which suggests that the charge is delocalized across all three C–S bonds. These bond distances are similar to those in $[\{((^{Ad}ArO)_3N)U\}_2(\mu\text{-}CS_3\text{-}\kappa S,\kappa S')]$, with C–S

bond distances of 1.724(4), 1.707(4), and 1.710(4) Å.[21] The metrical parameters of the $(CS_3)^{2-}$ unit in $\{[K(18\text{-}c\text{-}6)_2(THF)_2]_2[(R_2N)_2Y(\mu\text{-}CS_3\text{-}\kappa^2S,S')]_2\}(18\text{-}c\text{-}6)$ are similar to those in **3** even though potassium is not bound. This indicates that the $[K(18\text{-}c\text{-}6)]^{1+}$ ions are not significantly perturbing the core structure in **3**.

In **3**, the planar Gd, Gd′, S2, S2′ quadrilateral is perpendicular to the plane defined by C1, S2, C1′, and S2′. $\{[K(18\text{-}c\text{-}6)_2(THF)_2]_2[(R_2N)_2Y(\mu\text{-}CS_3\text{-}\kappa^2S,S')]_2\}(18\text{-}c\text{-}6)$ has a similarly symmetrical arrangement, but the 2.9442(7) Å Y1–S2 distance differs slightly from the 2.9814(7) Å Y1–S2′ distance. In **3**, the quadrilateral is rhombic with 3.0189(9) Å Gd1–S2 and Gd1–S2′ distances. All the other Ln–N and Ln–S distances in **3** and the yttrium analog are similar when the difference in ionic radii is taken into account. The 2.8350(11) Å Gd1–S1 and 2.8349(11) Å Gd1–S1′ distances in **3** for the sulfur atoms bridging to potassium are shorter than those in the Gd–S–Gd bridging unit, 3.0180(9) Å. The 113.8(5)° Gd–S–Gd angle is also more acute than the 168.5(5)° Gd–S–K angle. The 2.285(4) Å Gd−N(NR$_2$) distances in **3** are only slightly longer than the 2.230(6) and 2.244(6) Å analogs in the complex with simple $(SR)^{1-}$ bridging ligands in $[(R_2N)_2Gd(\mu\text{-}SBu^t)]_2$.[27]

A CS₂ Insertion Product from 2. Like **1** above, the crypt complex, [K(crypt)][Gd(NR$_2$)$_3$], **2**, reacts immediately with CS$_2$ with **2** with a color change from dark blue to yellow in THF. However, the crystalline product isolated in this case was $[K(crypt)]\{(R_2N)_2Gd[SCS(CH_2)Si(Me_2)N(SiMe_3)\text{-}\kappa N,\kappa S]\}$, **4**, Figure 1.6, eq 1.1.
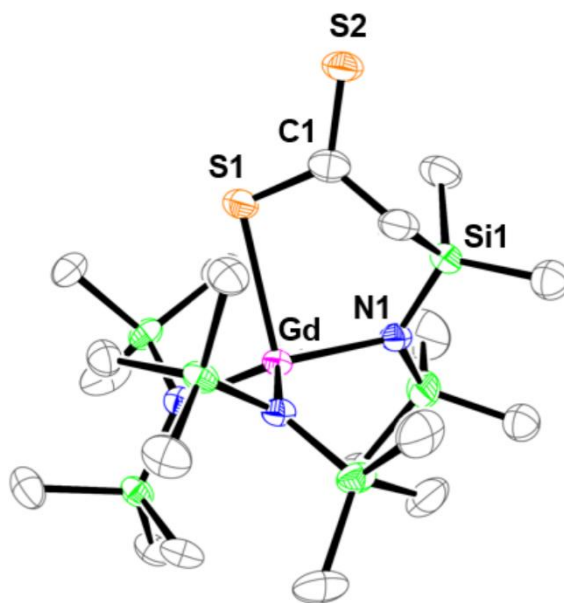
Figure 1.6. Representation of anion of [K(crypt)]{(R_2N)_2Gd[SCS(CH_2)Si(Me_2)N(SiMe_3)-$\kappa N, \kappa S$]}, **4**, with atomic displacement parameters drawn at the 50% probability level. Hydrogen atoms are omitted for clarity.

Complex **4** formally appears to be the product of insertion of CS_2 into the Gd–C bond of a cyclometallated amide unit "{(R_2N)_2Gd[(CH_2SiMe_2)N(SiMe_3)-kC,kN]}$^{1-}$". Cyclometalation of N(SiMe_3)_2 ligands is a common reaction for this ligand[28,29,38–43,30–37] and examples of C–H bond activation have been observed previously in reductive Ln(II) chemistry.[44–46] Hence, it is conceivable that the cyclometallated product is generated in this reaction. The only other known lanthanide-based CS_2 insertion product is an Yb(II) dithiocarbamate, Yb(S_2CNR_2)_2, which was obtained from the reaction of [Yb(NR_2)_2(OEt_2)_2] with CS_2, but was not crystallographically characterized.[47]

No examples of insertion of CS_2 into a Gd–C bond of a cyclometallated amide were found in the literature for comparison with **4**. Complex **4** crystallizes in the monoclinic P2_{1/n} space group

with one formula unit per unit cell. The 1.726(4) Å S1–C bond length is shorter than a typical C–S bond length of 1.819 Å, whereas the 1.659(3) Å C–S2 bond is close to that of a C=S double bond, 1.671 Å.[26] The 2.288(3) Å Gd–N1 cyclometallated nitrogen bond length is indistinguishable from the 2.286(2) Å Gd–N3 and 2.292(2) Å Gd–N2 terminal amide distances. All of these Gd–N distances are similar to those in **3**. The 2.7490(9) Å Gd–S1 bond length in **4** is shorter than the Gd–S bonds of **3**, which involves sulfur bridging two metal atoms. The newly formed C–C bond distance is 1.506(5) Å, in the typical single bond range.

S_8. Since reduction of S_8 has also been examined with the traditional Sm(II) and Yb(II), it was also investigated as part of this sulfur study. In the past, the Ln(II) reductions of S_8 generated complexes of S^{2-},[48] $(S_2)^{2-}$,[49] and $(S_3)^{2-}$.[16] When a dark blue solution of **1** in Et_2O at –35 °C was added to a slurry of S_8 in Et_2O, the color changed to light yellow. After the solution was layered with chilled hexanes in the freezer overnight, yellow crystals were isolated, but these were not of high enough quality for X-ray diffraction.

When the same S_8 reaction was performed with the crypt complex in THF, [K(crypt)][Gd(NR$_2$)$_3$], **2**, yellow crystals were similarly isolated. However, in this case they could be identified by X-ray diffraction as the bis-disulfide bridged complex, [K(crypt)]$_2${[(R$_2$N)$_2$Gd]$_2$(μ-S$_2$)$_2$}, **5**, Figure 1.7, eq 1.2. Unfortunately, the crystal data were not good enough to provide for metrical parameters. In further efforts to get structural data on this system, the reaction of [K(crypt)][Tb(NR$_2$)$_3$], **5-Tb**, with S_8 was examined.[23] Yellow crystals were also isolated from this reaction and had a unit cell that matched **5**, but like the Gd analog, the crystal data were not sufficient for detailed analysis.
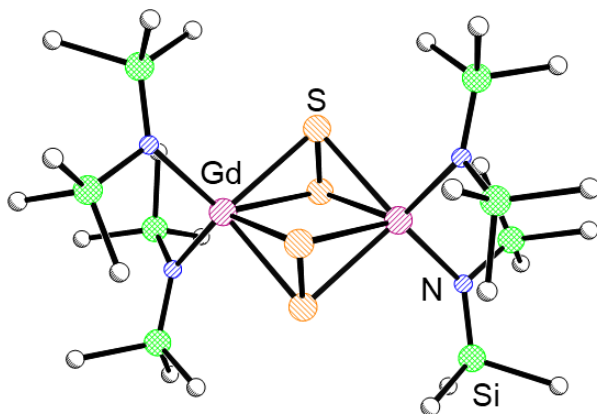
Figure 1.7. Ball and stick representation of **5**. Hydrogen atoms were excluded for clarity.

5
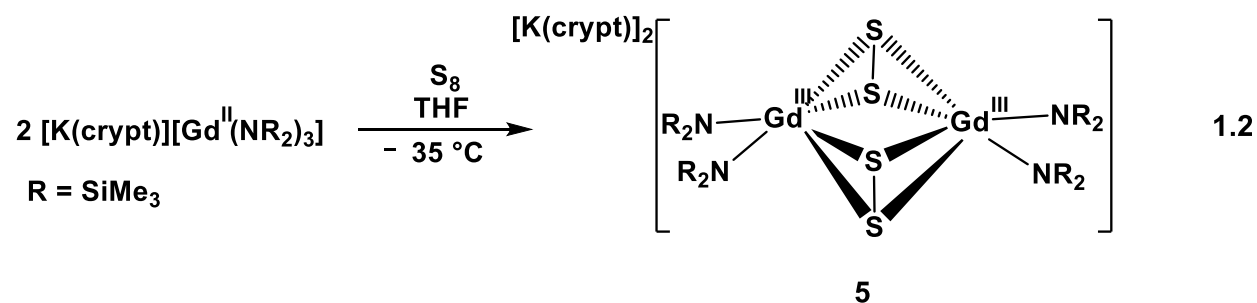
[K(crypt)][S₃NR₂]. In the reaction of **5-Tb** with S_8, a second set of crystals was isolated and identified by X-ray diffraction as [K(crypt)][S_2NR_2].[23] This was an interesting byproduct because each of the lanthanide products reported for the S_8 reaction had two $(NR_2)^{1-}$ ligands per metal and each started with three per metal. The fate of the lost amide ligand was unknown, but the isolation of [K(crypt)][S_2NR_2] could mean that it was trapped by sulfur. Independent synthesis of [K(crypt)][S_2NR_2] was attempted through the reaction of KNR_2, crypt, and S_8. However, instead of [K(crypt)][S_2NR_2] the product, [K(crypt)][S_3NR_2] was isolated, shown in Figure 1.8. This does show that one of the byproduct $(NR_2)^{1-}$ ligands could be trapped with sulfur.
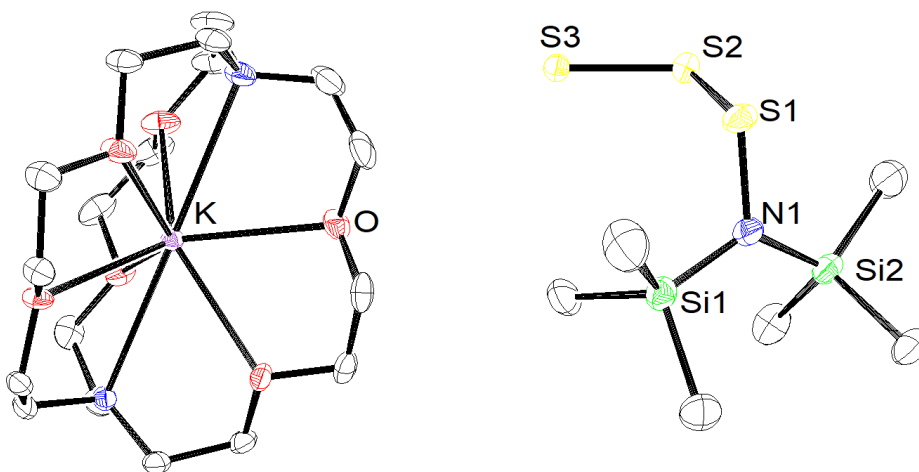
Figure 1.8. Representation of [K(crypt)][S$_3$NR$_2$] drawn at the 50% probability level. Hydrogen atoms and a molecule of [K(crypt)][S$_3$NR$_2$] are excluded for clarity.

Pyridine Reductive Coupling From 1 and 2. Pyridine is another reagent that has been examined with other low oxidation state lanthanide and actinide complexes, so there is precedent for investigating its reactivity with Gd(II). Reductive coupling has been observed with Sm(II)[50] Tm(II),[51,52] U(II),[53] and Th(III).[54] Reductive coupling with transition metals is also known.[55]

Dropwise addition of excess pyridine to a dark blue solution of **1** in Et$_2$O at −35 °C in an argon-filled glovebox immediately formed a light pink solution. This solution was layered into hexanes and the product was crystallized at −35 °C within 24 hours as pink crystals. X-ray diffraction revealed that these crystals were the reductively coupled pyridine complex, {[K(18-c-6)(NC$_5$H$_5$)$_2$]}$_2${[(R$_2$N)$_3$Gd]$_2$[μ-(NC$_5$H$_4$-C$_5$H$_4$N)$_2$]}, **6**, Figure 1.9, eq 1.3, with a pyridine-ligated potassium 18-c-6 countercation.
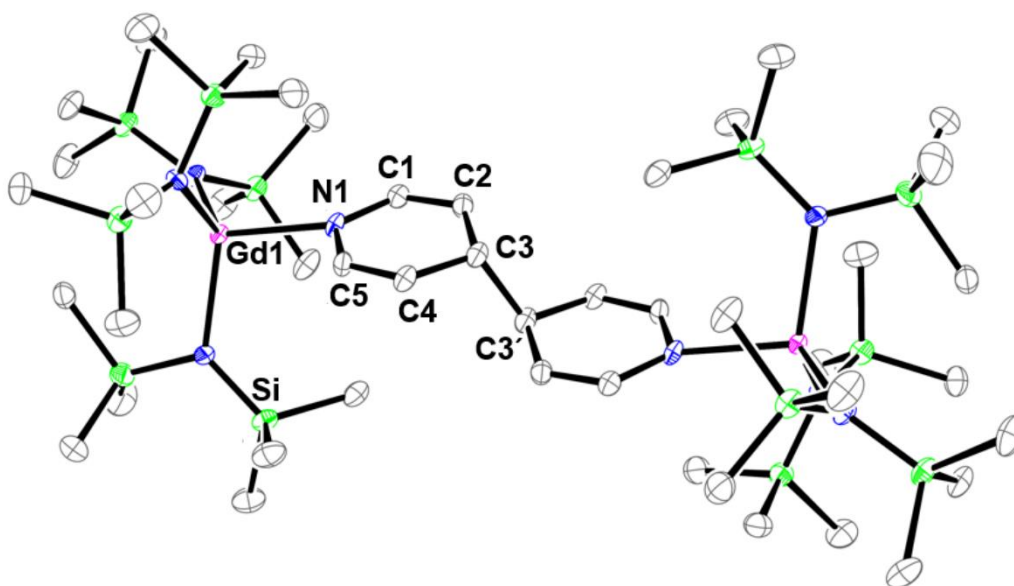
Figure 1.9. Representation of {[K(18-c-6)(NC$_5$H$_5$)$_2$]}$_2${[(R$_2$N)$_3$Gd]$_2$[μ-(NC$_5$H$_4$-C$_5$H$_4$N)$_2$]}, **6**, with atomic displacement parameters drawn at the 50% probability level. Hydrogen atoms and [K(18-c-6)(NC$_5$H$_5$)$_2$]$^{1+}$ were omitted for clarity.
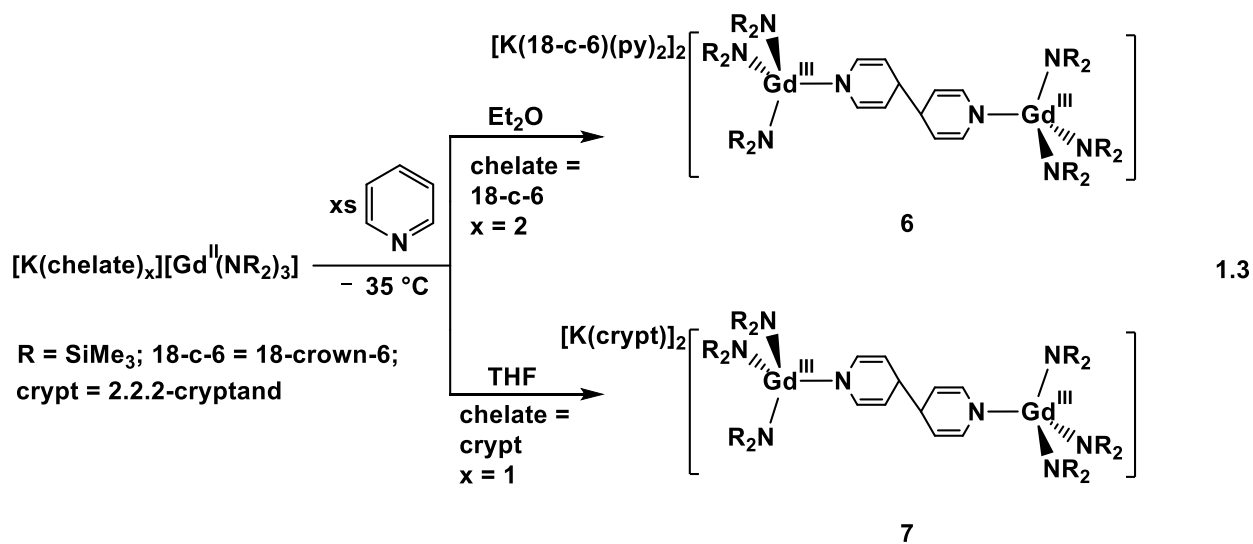
The reaction analogous to the pyridine/**1** reaction was also explored with a dark blue solution of **2** in THF and this afforded the similarly-coupled pyridine complex,

[K(crypt)]$_2${[(NR$_2$)$_3$Gd]$_2$[μ-(NC$_5$H$_4$-C$_5$H$_4$N)]}$_2$, **7**, eq 1.3, Figure 1.25, that differed only in the countercation. Complex **7** crystallizes with two molecules of the bimetallic Gd complex in the unit cell along with four [K(crypt)]$^{1+}$ countercations and six THF molecules in the crystal lattice. For **7**, the data were not of high enough quality for a detailed structural discussion.

Selected bond distances of **6** are listed in Table 1.2. Complex **6** crystallizes in the monoclinic P2$_{1/n}$ space group with one formula unit per unit cell. The C–C bonds between C2–C3 (1.518(8) Å), C4–C3 (1.498(8) Å), and C3–C3′ (1.565(10) Å) are typical C–C single bond lengths.[26] The C1–C2 (1.342(8) Å) and C5–C4 (1.335(8) Å) distances are typical for C=C bonds.[26] The 2.287(4) Å Gd–N[μ-(NC$_5$H$_4$-C$_5$H$_4$N)] distance in **6** is close to the 2.298(4) – 2.337(4) Å range of Gd–N(amide) single bond distances. In comparison, the recently reported uranium complex [K(crypt)]$_2${[(R$_2$N)$_3$U]$_2$[μ-(NC$_5$H$_4$-C$_5$H$_4$N)]}[53] has an average 2.385(5) Å U–N(amide) distance similar to the U–N[μ-(NC$_5$H$_4$-C$_5$H$_4$N)] distance of 2.404(7) Å. The longer uranium distances are consistent with the fact that the Shannon radius of U(III) is 0.087 Å larger than that of Gd(III).[25] The C3–C3′ bond distance of 1.565(10) Å for **6** is within error to the uranium complex distance which was 1.570(17) Å.[53] These distances are also consistent with a single bond and close to the range of 1.559(4) – 1.563(6) Å distances reported for iron,[55] samarium,[50] thulium,[51,52] and thorium[54] complexes featuring reductively coupled pyridines.

Table 1.2. Selected bond distances (Å) for **6.**

Gd–N1(py)	2.287(4)
Gd–N$_{amide}$	2.298(4), 2.334(5), 2.337(4)
N1–C1	1.395(7)
N1–C5	1.392(7)
C1–C2	1.342(8)
C5–C4	1.335(8)
C2–C3	1.518(8)
C4–C3	1.498(8)
C3–C3´	1.565(10)

Reduction of (2,2,6,6-Tetramethylpiperidin-1-yl)oxyl (TEMPO) by 1 and 2. To examine the radical reactivity of the $4f^7 5d^1$ ion, TEMPO reactions were studied. When an orange solution of TEMPO in Et$_2$O at –35 °C was added to a dark blue solution containing **1** in Et$_2$O at –35 °C, the solution turned light pink. Colorless crystals were obtained from this solution layered under hexanes and were characterized by X-ray diffraction to be {[(18-c-6)K][(μ-Me$_3$Si)(Me$_3$Si)N]$_2$[Gd(NR$_2$)(η^1-ONC$_5$H$_6$Me$_4$)]}$_n$, **8**, Figure 1.10, eq 1.4. In the solid state, this complex has an extended structure generated by interactions on either side of the [K(18-c-6)]$^{1+}$ cation with silylmethyl groups of the (NR$_2$)$^{1-}$ ligands, Figure 1.11.
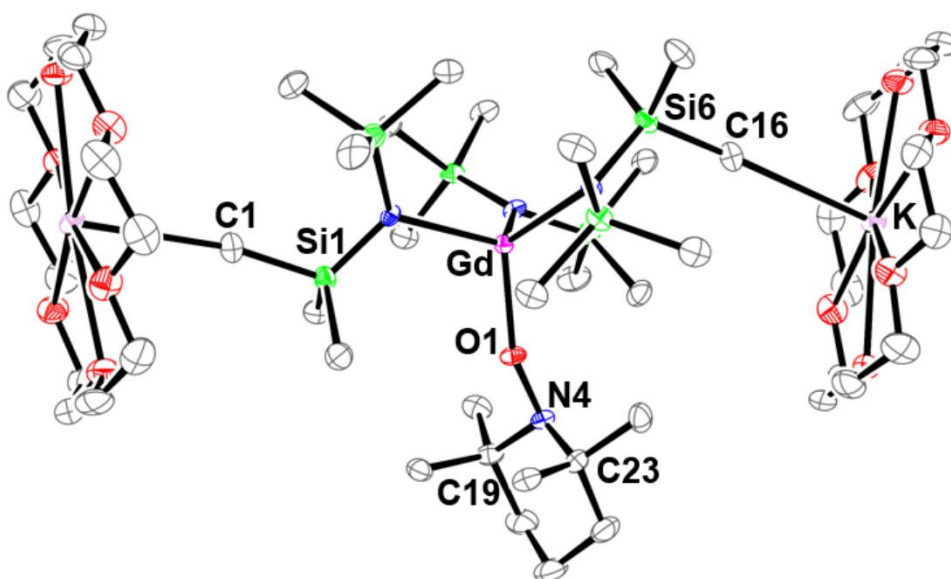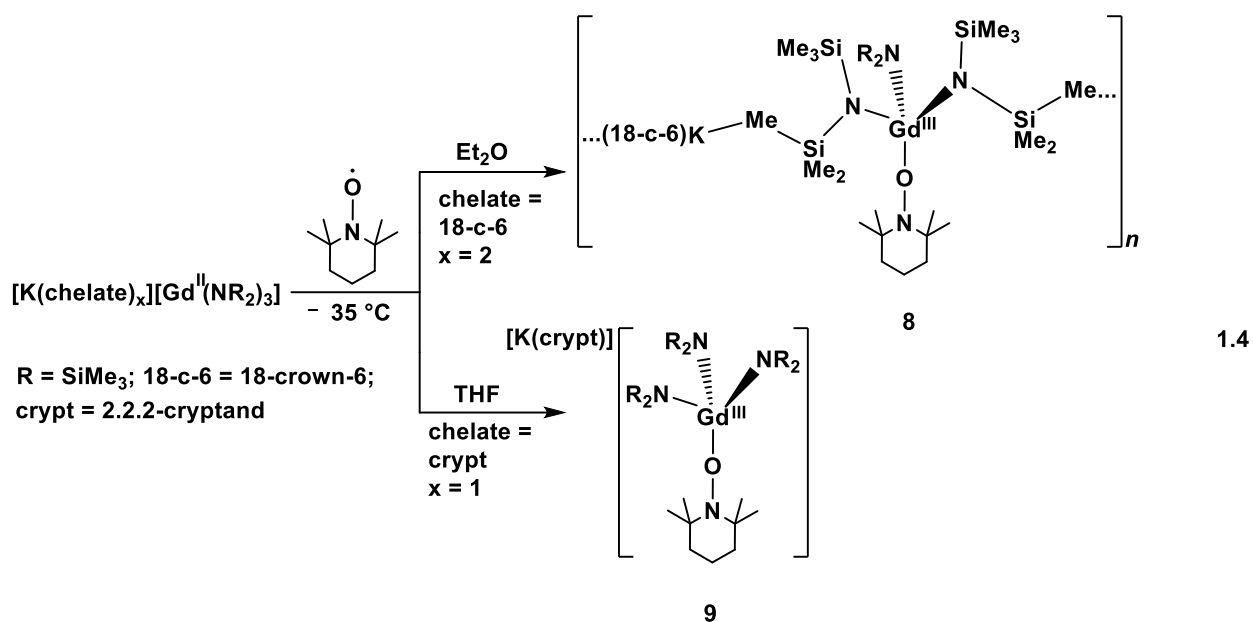
Figure 1.10. Representation of $\{[(18\text{-c-}6)\text{K}][(\mu\text{-Me}_3\text{Si})(\text{Me}_3\text{Si})\text{N}]_2[\text{Gd}(\text{NR}_2)(\eta^1\text{-ONC}_5\text{H}_6\text{Me}_4)]\}_n$, **8**, plus an additional $\text{K}(18\text{-c-}6)]^{1+}$ unit to show the connectivity of the polymer, with atomic displacement parameters drawn at the 50% probability level. Hydrogen atoms were omitted for clarity.
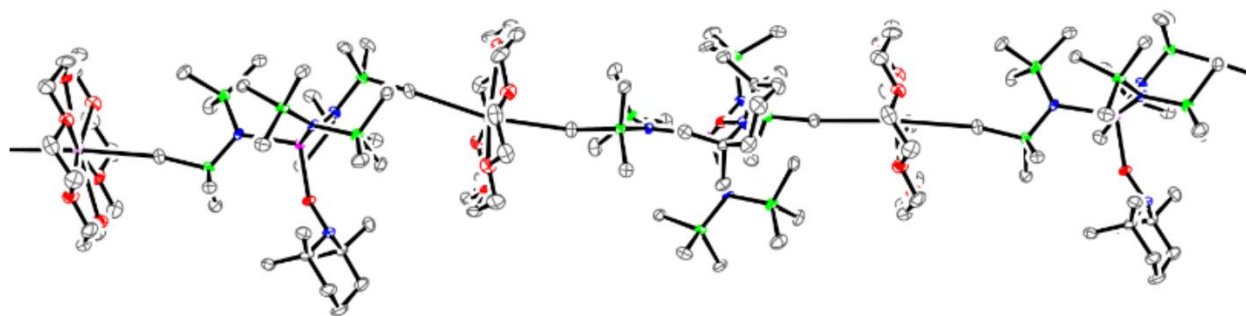
Figure 1.11. Representation of the extended structure of {[(18-c-6)K][(μ-Me$_3$Si)(Me$_3$Si)N]$_2$[Gd(NR$_2$)(η^1-ONC$_5$H$_6$Me$_4$)]}$_n$, **8**, with atomic displacement parameters drawn at the 50% probability level. Hydrogen atoms were omitted for clarity.

Each Gd(III) center is attached to two bridging (NR$_2$)$^{1-}$ groups, one terminal (NR$_2$)$^{1-}$, and the TEMPO anion. The reaction of **2** with TEMPO in THF afforded an analogous complex [K(crypt)(THF)][(R$_2$N)$_3$Gd(η^1-ONC$_5$H$_6$Me$_4$)], **9,** Figure 1.12, eq 1.4, but with the [K(crypt)(THF)]$^{1+}$ countercation,[56,57] an extended structure was not formed.
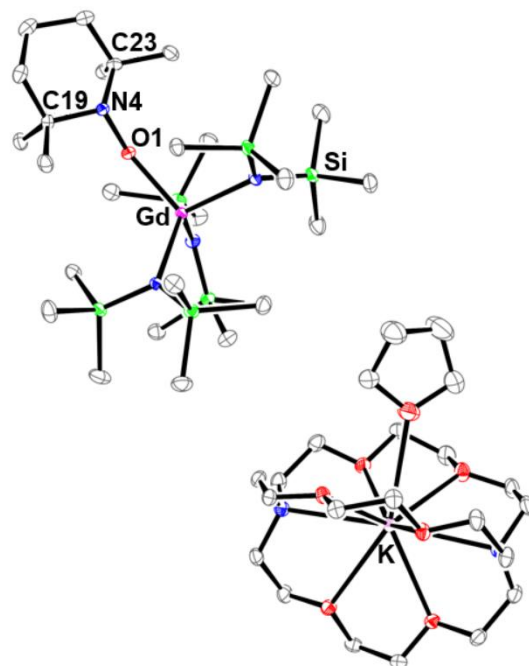
Figure 1.12. Representation of [K(crypt)(THF)][(R$_2$N)$_3$Gd(η^1-ONC$_5$H$_6$Me$_4$)], **9**, with atomic displacement parameters drawn at the 50% probability level. Hydrogen atoms were omitted for clarity.

Both **8** and **9** crystallize in the monoclinic P2$_{1/n}$ space group, but an extended structure is found only in **8**. Complexes **8** and **9** contain η^1-TEMPO^{1-} anions like those in (η^5-C$_5$Me$_5$)$_2$Th(Me)(η^1-ONC$_5$H$_6$Me$_4$).[58] The Gd–O(TEMPO) distances in **8** and **9**, 2.1313(18) Å and 2.1342(10) Å, Table 1.3, are similar to those in the thorium complex which is consistent with the fact that Gd(III) and Th(IV) have similar ionic radii.[25] The O1–N4 distances and the O–N–C angles in both **8** and **9** are typical for a TEMPO^{1-} anion.[58–63] Similarly, the sums of the angles around the nitrogen center, 335.8° for **8** and 336.8° for **9**, are consistent with a pyramidal geometry about the nitrogen in a fully reduced TEMPO^{1-} anion.[58–63]

The extended structure of **8** has precedent in that K···Me(SiMe$_3$) linkages have been observed before with [K(18-c-6)]$^{1+}$ cations,[64–67] but not on both sides of the potassium crown entity

to our knowledge. The six donor oxygen atoms of 18-c-6 are planar to within 0.1721 Å and the potassium is 0.1549 Å out of the plane. The K···C(Me$_3$Si) distances are 3.130(3) and 3.172(3) Å with the C···K vector making an 85.7° angle for C(1) and a 104.8° angle for C(16) with the plane of the six oxygen donor atoms of 18-c-6.

Table 1.3. Selected metrical parameters for **8** and **9**. (Å, deg)

	8	9
Gd–N$_{amide}$	2.333(2), 2.359(2), 2.366(2)	2.3361(12), 2.3638(12), 2.3734(12)
Gd–O1	2.1313(18)	2.1342(10)
O1–N4	1.439(3)	1.4386(15)
O1–N4–C19	108.98(19)	109.46(10)
O1–N4–C23	108.9(2)	109.26(10)

Formation of a Gd–Bi Complex from 2 and BiPh$_3$. The reaction BiPh$_3$ with the Gd(II) complexes was investigated to determine if there was any connection between the previously reported reaction of the Sm(II) complex, (C$_5$Me$_5$)$_2$Sm, with BiPh$_3$ that forms (C$_5$Me$_5$)$_2$Sm]$_2$(μ-η^2:η^2:-Bi$_2$) along with (C$_5$Me$_5$)$_2$SmPh.[68] Addition of solid **1** to a solution of BiPh$_3$ in Et$_2$O at room temperature results in an immediate color change from colorless to orange. Crystallization at −35 °C under hexanes yielded an orange/brown oil and blue crystals. The crystals were identified by X-ray crystallography as the Bi−C(Ph) cleavage product, [K(18-c-6)$_2$][PhGd(NR$_2$)$_3$], , eq 1.5.[23]

The same reaction performed with **2** produced similar color changes, but crystallization at −35 °C yielded bright green crystals as well as an orange oil. X-ray diffraction revealed that the green crystals were [K(crypt)][(Ph$_2$Bi)Gd(NR$_2$)$_3$], **10**, Figure 1.13, eq 1.5, the bismuth product expected after one Bi−C(Ph) cleavage reaction. The only other crystallographically characterized

complex containing bismuth and gadolinium is the Zintl cluster, $[K(crypt)]_4[Gd@Pb_4Bi_9]$,[69] which

has 13 cage atoms around the Gd. Five of the cage atoms are identified by crystallography as Bi,

but the identity of the other eight cage atoms could not be determined due to the similar atomic

number of Pb and Bi. Hence **10** provides the first example of a simple coordination complex with

a single Gd−Bi bond. Complexes containing f-element to Bi bonds are rare in general.[68,70] The

structure of $[K(crypt)][BiPh_2]$ (Figure 1.15) was also identified from this reaction system which is

summarized in eq 1.5. We found no other structures of the $(BiPh_2)^{1-}$ anion in a CCDC search.

1.5

10
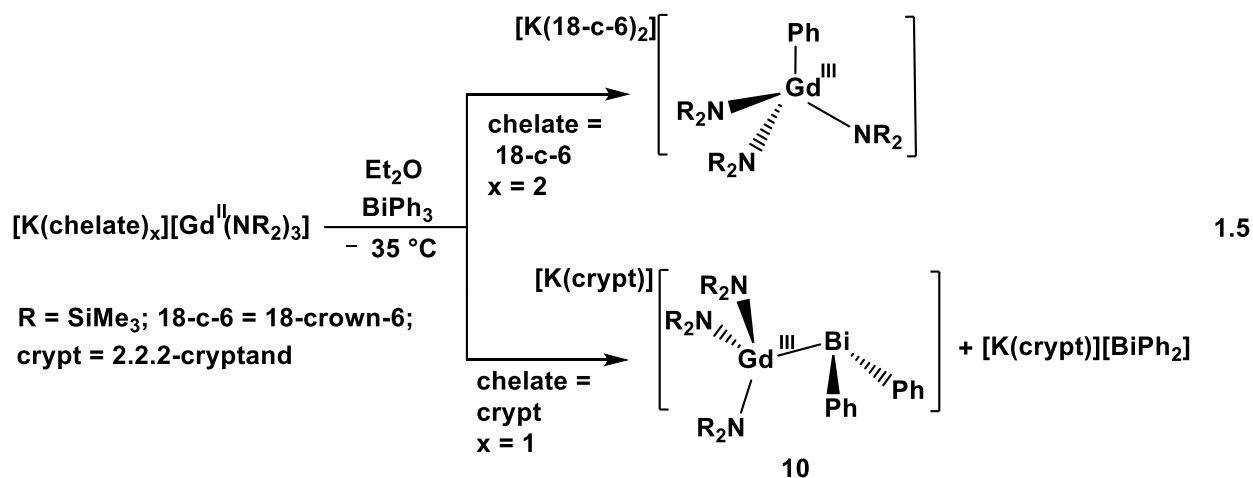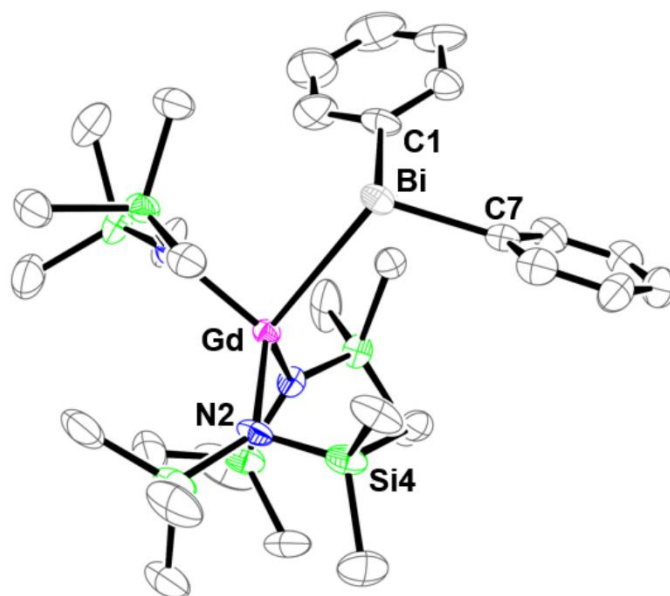
Figure 1.13. Representation of [K(crypt)][(Ph$_2$Bi)Gd(NR$_2$)$_3$], **10**, with atomic displacement parameters drawn at the 50% probability level. Hydrogen atoms, disordered SiMe$_3$ group, and [K(crypt)]$^{1+}$ were omitted for clarity.
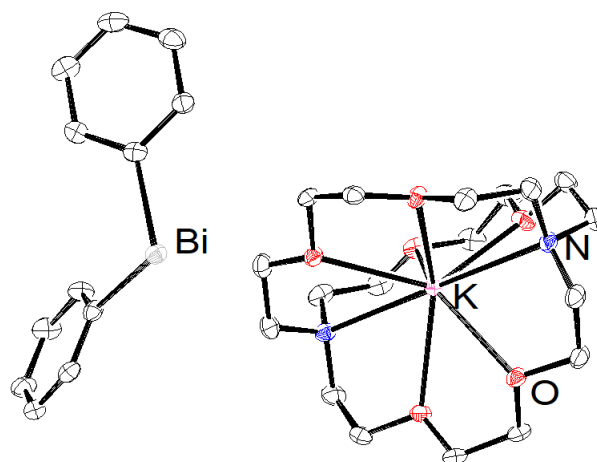
Figure 1.14. Representation of [K(crypt)][BiPh$_2$] with atomic displacement parameters drawn at the 50% probability level. Hydrogen atoms were omitted for clarity.

One sample of **10** was found to crystallize in the triclinic P$\bar{1}$ space group and a subsequent crystallization gave **10** in the monoclinic P2$_{1/c}$ space group. In both cases, there is only one formula unit per unit cell. The molecular parameters are similar in both cases and data from only the monoclinic crystal are discussed here. The structure of **10** has an irregular pseudo-tetrahedral coordination environment around the Gd ion generated by three NR$_2$ ligands and one BiPh$_2$ ligand with 107.07(8)° to 115.46(8)° N−Gd−N and 102.49° N−Gd−Bi angles. There is also one Me$_3$Si group that is oriented toward Gd with a 110.39(11)° Gd−N(2)−Si(4) angle that is more acute than the other Gd−N−Si angles that range from 115.95(11)° to 131.24(11)°. The three coordinate bismuth atom has 95.09(7)° and 112.43(7)° Gd−Bi−C(Ph) angles and a range of 115.5(2) – 127.3(2)° C(Ph)−Bi−C(Ph) angles which leaves a large amount of open space in the coordination sphere as is typical for bismuth.[71,72] The 3.3466(2) Å Gd−Bi bond in **10** is similar to the 3.3208(4) Å U−Bi bond in {(Me$_3$Si)$_2$Bi]U(TrenDMBS)} (TrenDMBS = N(CH$_2$CH$_2$NSiMe$_2$Bu^t)$_3$)[70] when the 0.05 Å larger ionic radius of Gd(III) versus U(IV) is considered. The similarities in metrical parameters extend to the M−N(amide) bonds with distances ranging from, 2.274(2) Å – 2.314(2) Å for **10** vs 2.232(6) – 2.247(6) Å in {(Me$_3$Si)$_2$Bi]U(TrenDMBS)}.

Ph-Sn Cleavage with Ph$_4$Sn. To further explore reductive cleavage of Ph-main group element bonds, the reaction of **2** with SnPh$_4$ was examined. However, only the crystallographically characterizable product was [K(crypt)][SnPh$_3$](THF) (Figure 1.15). The X-ray crystal structures of [K(18-crown-6)]{SnPh$_3$},[73] [Ba(18-crown-6)(HMPA)$_2$][SnPh$_3$]$_2$,[74] and (Me$_2$NCH$_2$CH$_2$)$_2$NMe)LiSnPh$_3$[75] have previously been reported.
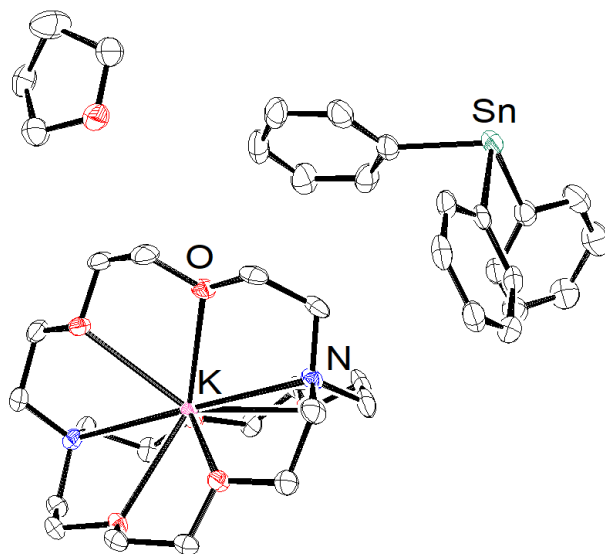
Figure 1.15. Representation of [K(crypt)][SnPh$_3$](THF) with atomic displacement parameters drawn at the 50% probability level. Hydrogen atoms were omitted for clarity.

`**Other Reactions.** The reactions of [K(18-c-6)$_2$][Gd(NR$_2$)$_3$], **1**, with CO$_2$ and NO were also examined. The reaction of a dark blue solution of **1** in Et$_2$O was exposed CO$_2$. The reaction was swirled and after a few seconds, it turned to a white slurry. This slurry was then filtered and layered into hexanes. However, there were no isolable products from this reaction. The same reaction was performed with NO and the resulting solution turned to a dark orange. Again, there were no isolable products from the reaction.

Conclusion

Both [K(18-c-6)$_2$][Gd(NR$_2$)$_3$], **1**, and the crypt analog, [K(crypt)][Gd(NR$_2$)$_3$], **2**, can perform a variety of reductive reactions and provide new synthetic pathways to Gd-containing compounds. The reactions with pyridine show reductive coupling reactivity for the Gd(II) ion while the reactions with BiPh$_3$ show that reductive cleavage is viable in this case with a Bi–Ph bond. With CS$_2$, the reactions show a combination of cleavage and coupling reactions, while the reaction with TEMPO reinforces the radical nature of Gd(II). In some cases, the reductive

reactivity results in loss of a $(NR_2)^{1-}$ ligand to form products of the $[(R_2N)_2Gd]^{1+}$ cation, but in other cases, anionic complexes of $Gd(NR_2)_3$ are formed that retain all the amide ligands in the starting materials. With some reagents, the $[K(18\text{-}c\text{-}6)_2]^{1+}$ and $[K(crypt)]^{1+}$ salts give different products and with others, both species give the same reductive chemistry. For each chelate, a specific solvent combination was used, namely Et_2O with 18-c-6 and THF with crypt (with the exception of the reactivity with $BiPh_3$). Using the alternative solvent and chelate combinations, i.e. Et_2O and crypt and THF and 18-c-6, made product isolation more difficult. Since 18-c-6 with potassium prefers to form extended structures or countercations in the form of $[K(18\text{-}c\text{-}6)_2]^{1+}$, it is hypothesized that THF is an inferior solvent for this chelate since it would interfere with the formation of these countercations. Clearly, extensive reactivity is available through Gd(II), and the selection of solvent and potassium chelate can be very influential in terms of product isolation.

Experimental Details

All manipulations and syntheses described below were conducted with the rigorous exclusion of air and water using standard Schlenk line and glovebox techniques under an argon or dinitrogen atmosphere. Solvents were sparged with UHP argon and dried by passage through columns containing Q-5 and molecular sieves prior to use. Elemental analyses were conducted on a Perkin-Elmer 2400 Series II CHNS elemental analyzer. Infrared spectra were collected on an Agilent Cary 630 equipped with a diamond ATR attachment. UV−visible spectra were collected in THF or Et_2O at room temperature in a 1 mm cell fitted with a Teflon stopcock using an Agilent Cary 60 UV−visible spectrophotometer. 2.2.2-Cryptand (crypt, Merck) was placed under vacuum (10^{-4} torr) for 12 h before use. 18-Crown-6 (18-c-6, Alfa Aesar) was sublimed before use. TEMPO (98%, Sigma-Aldrich) was sublimed before use. CS_2 (Sigma-Aldrich) and pyridine (Sigma-Aldrich) were freeze-pump-thawed and stored over 3Å molecular sieves for one week

before use. BiPh$_3$ (Alfa Aesar) was used as received. [K(18-c-6)$_2$][Gd(NR$_2$)$_3$], **1**, and [K(crypt)][Gd(NR$_2$)$_3$], **2**, were synthesized via literature procedures.[1,11]

[K(18-crown-6)(H$_2$O)][NCNCMe$_3$-κN], [K(18-crown-6)][κ^2-NCNCMe$_3$], CO(NH$_2$)$_2$.

In an argon filled glovebox, N,N′-di-tert-butylcarbodiimide was added dropwise to a dark blue solution of [K(18-c-6)$_2$][Gd(NR$_2$)$_3$] (R = SiMe$_3$) (30 mg, 0.02 mmol) in diethyl ether (5 mL) at −35˚C. The solution changed from dark blue to colorless after a few minutes. Methylcyclohexane was layered into the solution and the solution was kept at −35˚C, but no crystals were obtained. Solvent was removed to produce a white solid which was dissolved in toluene and placed in a vapor diffusion set up with hexanes. After 5 days, small colorless crystals of [K(18-crown-6)(H$_2$O)][NCNCMe$_3$-κN], [K(18-crown-6)][κ^2-NCNCMe$_3$], CO(NH$_2$)$_2$ were collected and identified by X-ray crystallography.

{[K(18-c-6)](μ_3-CS$_3$-$\kappa S, \kappa^2 S′, S″$)Gd(NR$_2$)$_2$]}$_2$, 3. In an argon filled glovebox, [K(18-c-6)$_2$][Gd(NR$_2$)$_3$] (50 mg, 0.04 mmol) was dissolved in Et$_2$O (2 mL) chilled to −35 °C and excess CS$_2$ was added dropwise. The solution changed from dark blue to yellow. The solution was layered into cold hexanes and placed in a −35 °C freezer producing a red oil and yellow crystals suitable for X-ray diffraction (6 mg, 8%). IR (cm^{-1}): 2890m, 1465w, 1352m, 1237m, 1102s, 943s, 827s, 767w, 696w, 661s. IR (cm^{-1}): red oil: 2889m, 1471w, 1351w, 1239m, 1105s, 945s, 823s, 765w, 696w, 662m. UV-Vis in THF: λ_{max} = 333 nm (ε = 3619 M^{-1} cm^{-1}). Anal. Calcd for C$_{50}$H$_{122}$N$_4$O$_{12}$S$_6$Si$_8$K$_2$Gd$_2$: C, 33.71; H, 6.90; N, 3.15. Found: C, 33.68; H, 6.58; N, 2.71.

[K(crypt)]{(R$_2$N)$_2$Gd[SCS(CH$_2$)Si(Me$_2$)N(SiMe$_3$)-$\kappa N, \kappa S$]}, 4.   In an argon filled glovebox, [K(crypt)][Gd(NR$_2$)$_3$] (50 mg, 0.05 mmol), was dissolved in THF (2 mL) chilled to −35 °C and excess CS$_2$ was added dropwise. The solution went from dark blue to yellow and was layered into cold hexanes and placed in a −35 °C freezer. A few yellow crystals suitable for X-

ray diffraction were isolated. IR (cm^{-1}): 2948w, 2880w, 2812w, 2409w, 1475w, 1443w, 1397w, 1353m, 1295w, 1238m, 1150m, 1014w, 947m, 827m, 750w, 664w. Anal. Calcd for $C_{37}H_{90}N_5O_6S_2Si_6KGd$: C, 39.32; H, 8.03; N, 6.02. Found: C, 33.73; H, 7.83; N, 5.95. The low values indicate incomplete combustion as has been previously observed in *f*-element chemistry.[76-83]

[K(crypt)]$_2$[(R$_2$N)$_2$Gd]$_2$(μ-S$_2$)$_2$ 5. In an argon filled glovebox, [K(crypt)][Gd(NR$_2$)$_3$] (50 mg, 0.05 mmol) was dissolved in THF (2 mL) chilled to −35 °C and added to a vial containing S$_8$ also chilled to −35 °C. The solution went from dark blue to light yellow. Filtration followed by layering into hexanes and storage at −35 °C produced yellow crystals of **5** suitable for X-ray diffraction (33 mg, 36%). IR(cm^{-1}): 2944w, 2878w, 2809w, 1470w, 1444w, 1355w, 1298w, 1255w, 1232w, 1095m, 1074m, 988w, 945m, 928m, 817m, 747m, 661w. UV-Vis in THF: λ_{max} = 345 nm (ε = 1357 M^{-1} cm^{-1}) and 400 nm (ε = 530 M^{-1} cm^{-1}). Anal. Calcd for $C_{60}H_{144}N_8K_2O_{12}Si_8S_4Gd_2$: C, 37.62; H, 7.58; N, 5.85. Found: C, 37.27; H, 7.62; N, 5.96. The low values are consistent with incomplete combustion as has been previously observed in *f*-element chemistry.[76-83] The experimental values give a $C_{60}H_{152}N_8$ formula based on C which is close to the calculated value.

[K(crypt)][S$_3$NR$_2$]. In an argon filled glovebox, a solution was of S$_8$ (10 mg, 0.04 mmol) and crypt (7 mg, 0.02 mmol) in THF was chilled to −35 °C and added to a chilled vial KNR$_2$ (4 mg, 0.02 mmol) dissolved in THF. The solution turned yellow to a purple/red color. Filtration followed by layering hexanes onto the solution and storage at −35 °C produced **6** as small purple crystals.

{[K(18-c-6)(NC$_5$H$_5$)$_2$]}$_2${[(R$_2$N)$_3$Gd]$_2$[μ-(NC$_5$H$_4$-C$_5$H$_4$N)$_2$]}, 6.   In an argon filled glovebox, [K(18-c-6)$_2$][Gd(NR$_2$)$_3$] (100 mg, 0.08 mmol) was dissolved in Et$_2$O (2 mL) chilled to

−35 °C and excess pyridine , also chilled to −35 °C, was added dropwise. The solution went from dark blue to light pink. The resulting solution was layered under cold hexanes and placed in a −35 °C freezer. Pink crystals suitable for X-ray diffraction were isolated (39 mg, 43%). IR (cm^{-1}): 2941w, 2889w, 1634w, 1453w, 1351w, 1237m, 1105s, 958s, 868m, 819s, 770m, 747m, 702w, 660m. Anal. Calcd for $C_{71}H_{168}N_8O_{12}Si_{12}K_2Gd_2$: C, 41.48; H, 8.24; N, 5.45. Found: C, 41.36; H, 8.23; N, 5.54.

[K(crypt)]$_2$\{[(NR$_2$)$_3$Gd]$_2$[μ-(NC$_5$H$_4$-C$_5$H$_4$N)$_2$]\}, 7. In an argon filled glovebox, [K(crypt)][Gd(NR$_2$)$_3$] (100 mg, 0.09 mmol), was dissolved in THF (2 mL) chilled to −35 °C and excess pyridine, chilled to −35 °C, was added dropwise. The solution went from dark blue to light pink. The resulting solution was layered under cold hexanes and placed in a −35 °C freezer. Pink crystals suitable for X-ray diffraction were isolated (89 mg, 83%). IR (cm^{-1}): 2944w, 2882w, 2812w, 1637w, 1562w, 1476w, 1354w, 1236m, 1103m, 961m, 868m, 821m, 770m, 747m, 702w, 660m.

[K(18-c-6)][(R$_2$N)$_3$Gd(η^1-ONC$_5$H$_6$Me$_4$)], 8. In an argon filled glovebox, [K(18-c-6)$_2$][Gd(NR$_2$)$_3$] (50 mg, 0.05 mmol) was dissolved in Et$_2$O (2 mL) chilled to −35 °C. A solution of TEMPO (13 mg, 0.080 mmol) dissolved in Et$_2$O (2 mL) chilled to −35 °C was added dropwise to the dark blue solution of [K(18-c-6)$_2$][Gd(NR$_2$)$_3$]. The solution went from dark blue to light pink. The resulting solution was layered under cold hexanes and placed in a −35 °C freezer. Colorless crystals suitable for X-ray diffraction were isolated (54 mg, 59%). IR (cm^{-1}): 2887m, 1470w, 1452w, 1352w, 1296w, 1106s, 956s, 864m, 824s, 770m, 700w, 660m.

[K(crypt)][(R$_2$N)$_3$Gd(η^1-ONC$_5$H$_6$Me$_4$)], 9. In an argon-filled glovebox, [K(crypt)][Gd(NR$_2$)$_3$] (100 mg, 0.09 mmol) was dissolved in THF (2 mL) chilled to −35 °C. A solution of TEMPO (14 mg, 0.090 mmol) dissolved in THF (2 mL) chilled to −35 °C was added

dropwise to the dark blue solution of [K(crypt)][Gd(NR$_2$)$_3$]. The solution went from dark blue to light pink. The resulting solution was layered under cold hexanes and placed in a −35 °C freezer. Colorless crystals suitable for X-ray diffraction were isolated (57 mg, 44%). IR (cm^{-1}): 2938w, 2885w, 2815w, 1477w, 1444w, 1354w, 1296w, 1235m, 1133w, 1104m, 1078w, 951s, 864m, 824s, 770m, 752m, 700w, 660m. Anal. Calcd for C$_{45}$H$_{108}$N$_6$O$_7$Si$_6$KGd: C, 44.66; H, 9.00; N, 6.94. Found: C, 44.99; H, 9.47; N, 6.80.

[K(crypt)][Ph$_2$BiGd(NR$_2$)$_3$], 10. In an argon filled glovebox, solid [K(crypt)][Gd(NR$_2$)$_3$] (60 mg, 0.06 mmol) was added to a solution of BiPh$_3$ in Et$_2$O (9 mg, 0.02 mmol) at room temperature resulting in an immediate color change from colorless to orange. The solution was allowed to react for about 1 minute before being filtered and layered into hexanes. After the sample was in the glovebox freezer at −35 °C overnight, an orange/brown oil collected in the bottom of the vial. After another 24 hours in the freezer, small bright green triclinic crystals of **10** grew from the oil. Repeating this reaction in the same manner with crystallization set up for slow evaporation of a concentrated orange Et$_2$O solution resulted in bright yellow monoclinic crystals of **10**. UV-Vis in Et$_2$O: λ$_{max}$ = 291 nm (ε = 145 M^{-1} cm^{-1}).

[K(crypt)][BiPh$_2$]. In an argon filled glovebox, solid [K(crypt)][Gd(NR$_2$)$_3$] (60 mg, 0.06 mmol) was added to a solution of BiPh$_3$ in Et$_2$O (9 mg, 0.02 mmol) at room temperature resulting in an immediate color change from colorless to orange. The solution was allowed to react for about 1 minute before being filtered and layered into hexanes. After the sample was in the glovebox freezer at −35 °C overnight, an orange/brown oil collected in the bottom of the vial. Subsequently, red crystals identified as [K(crypt)][BiPh$_2$], were obtained.

[K(crypt)][SnPh$_3$](THF). In an argon filled glovebox, solid [K(crypt)][Gd(NR$_2$)$_3$] (60 mg, 0.06 mmol) was added to a solution of SnPh$_4$ in Et$_2$O (24 mg, 0.060 mmol) at room

temperature resulting in an immediate color change from colorless to yellow. The solution was

allowed to react for about 1 minute before being filtered and layered into hexanes. After the sample

was in the glovebox freezer at −35 °C overnight, a yellow oil collected in the bottom of the vial.

Colorless crystals were identified as [K(crypt)][SnPh$_3$](THF).

Additional Characterization of Complexes
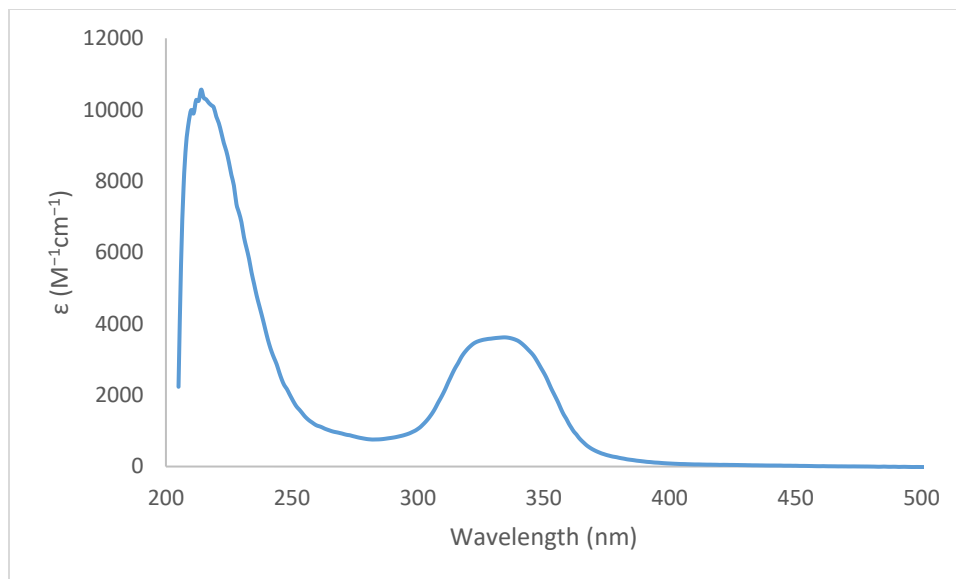
Figure 1.16. UV-vis spectrum of {[K(18-c-6)](μ_3-CS$_3$-κS,κ^2S′,S″)[Gd(NR$_2$)$_2$]}$_2$, **3** (0.3 mmol) in THF.
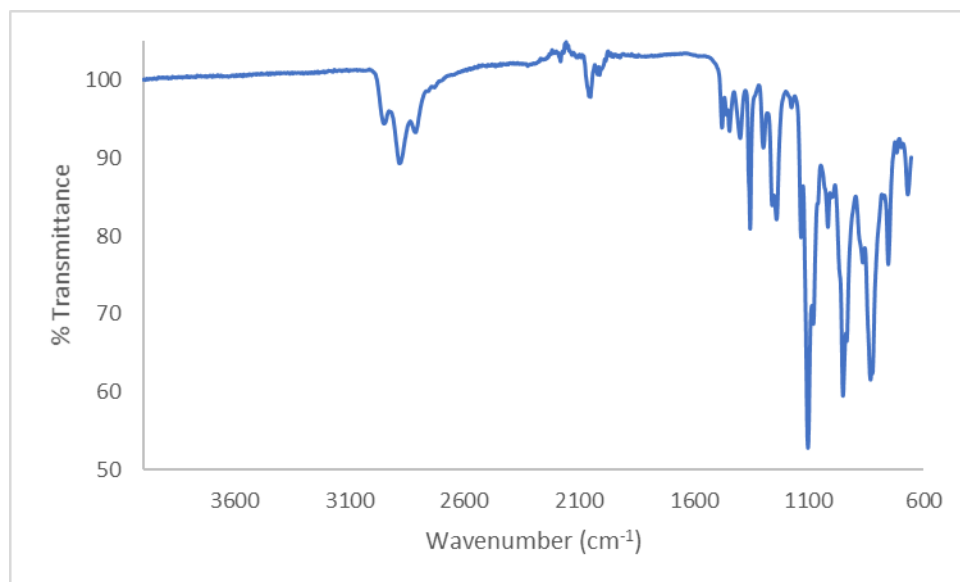
Figure 1.17. IR spectrum of [K(crypt)]{(R$_2$N)$_2$Gd[SCS(CH$_2$)Si(Me$_2$)N(SiMe$_3$)-$\kappa N, \kappa S$]}, **4.**
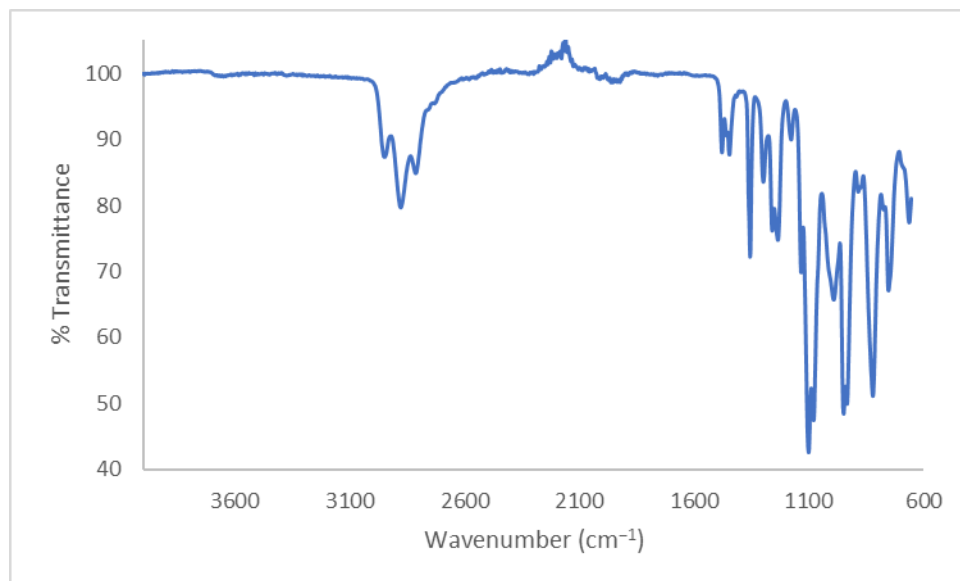
Figure 1.18. IR spectrum of [K(crypt)]$_2$[(R$_2$N)$_2$Gd]$_2$(μ-S$_2$)$_2$, **5.**
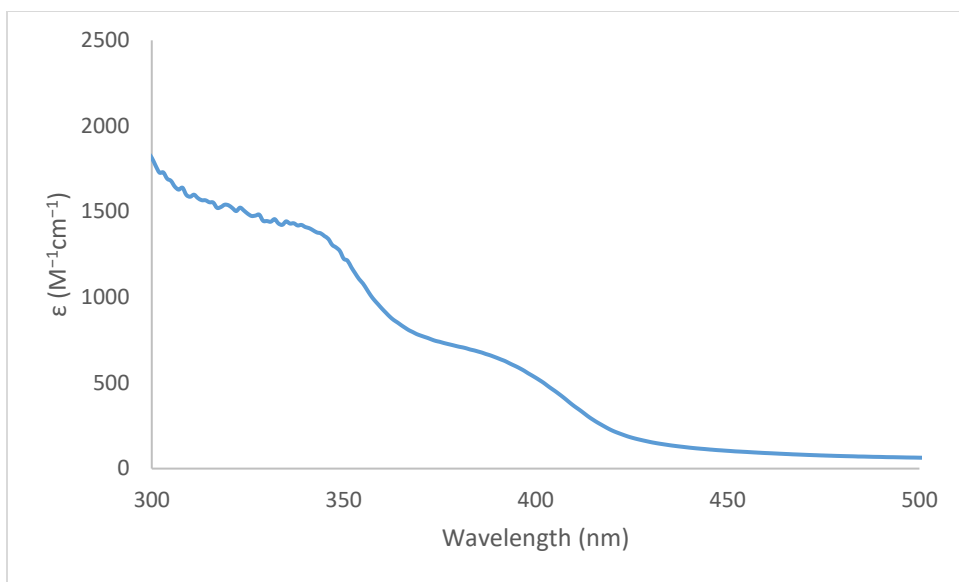
Figure 1.19. UV-Vis spectrum of [K(crypt)]$_2$[(R$_2$N)$_2$Gd]$_2$(μ-S$_2$)$_2$, **5**, in 20 mmol in THF.
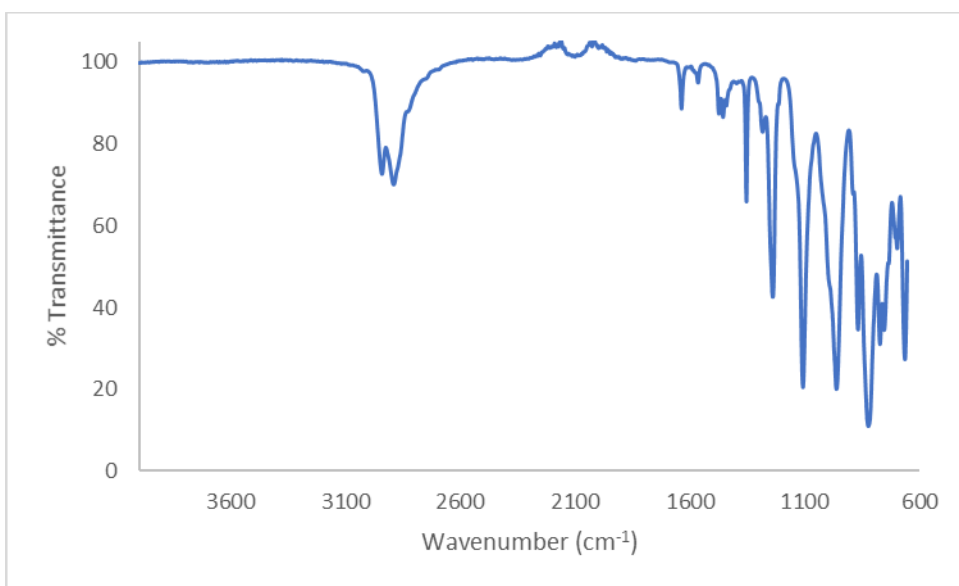
Figure 1.20. IR spectrum of [{K(18-c-6)(NC$_5$H$_5$)$_2$}]$_2$[{(R$_2$N)$_3$Gd}$_2${μ-(NC$_5$H$_4$-C$_5$H$_4$N)$_2$}], **6**.
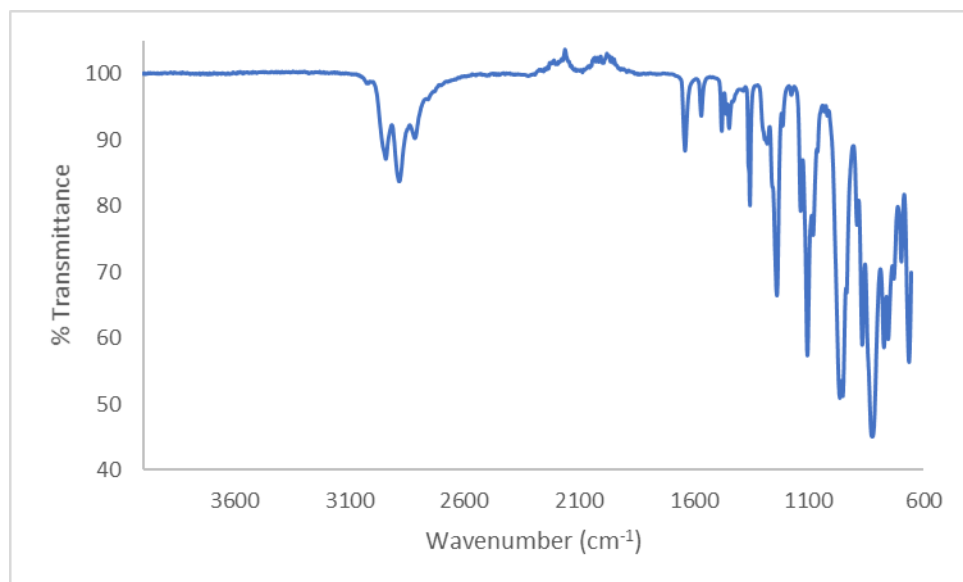
Figure 1.21. IR spectrum of $[K(\text{crypt})]_2[\{(NR_2)_3Gd\}_2\{\mu\text{-}(NC_5H_4\text{-}C_5H_4N)\}]_2$, **7**.
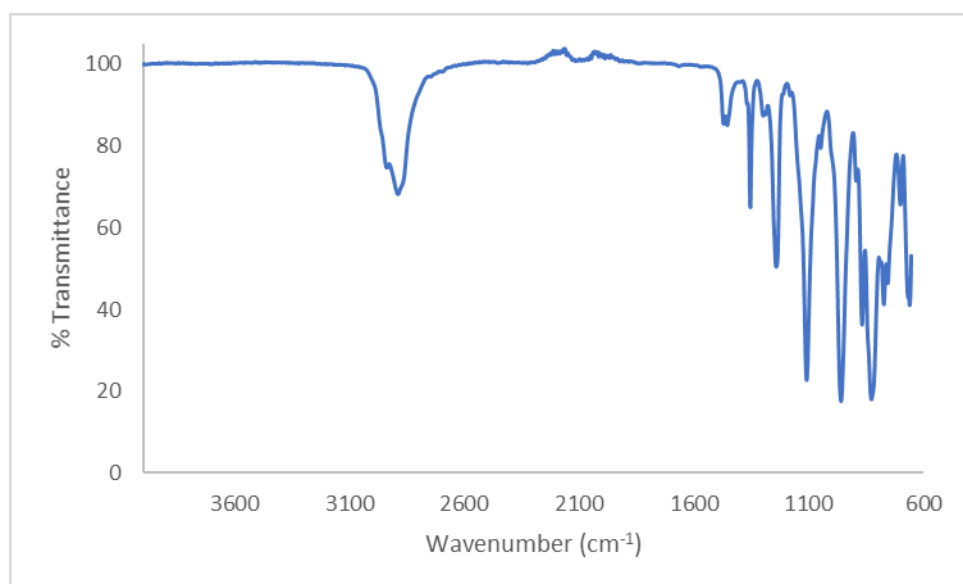
Figure 1.22. IR spectrum of $\{[(18\text{-c-}6)K][(\mu\text{-}Me_3Si)(Me_3Si)N]_2[Gd(NR_2)(\eta^1\text{-}ONC_5H_6Me_4)]\}_n$, **8.**
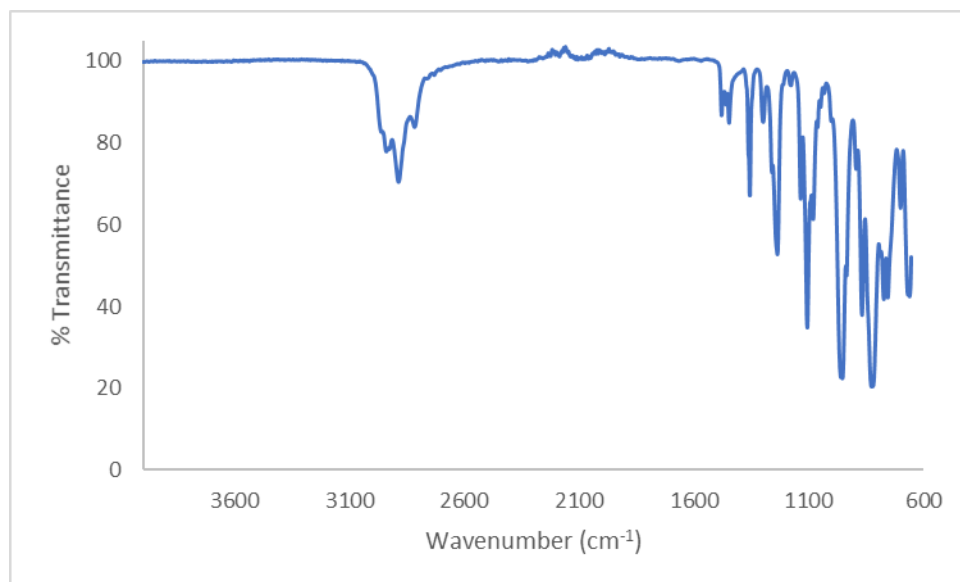
Figure 1.23. IR spectrum of [K(crypt)(THF)][(R$_2$N)$_3$Gd(η^1-ONC$_5$H$_6$Me$_4$)], **9.**
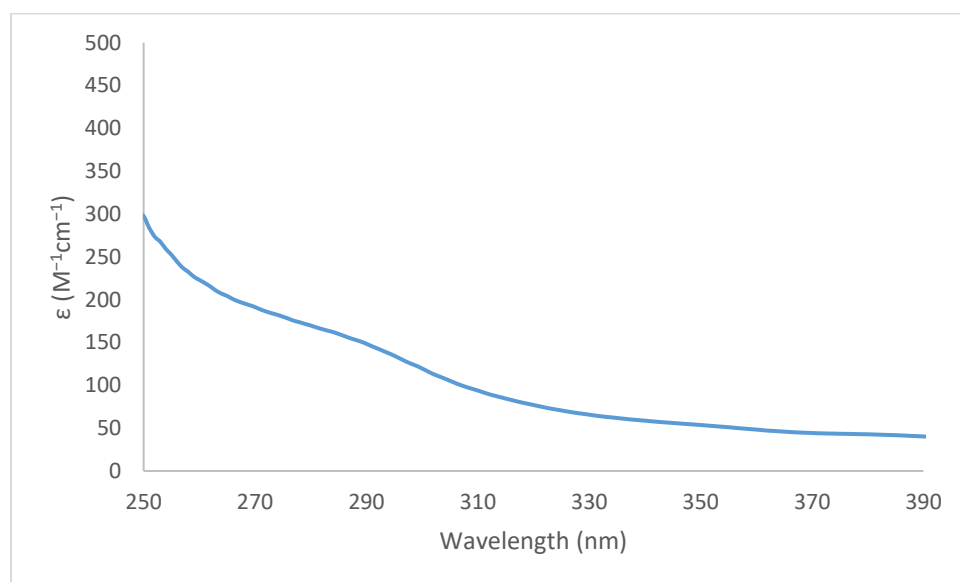
Figure 1.24. UV-vis spectrum of [K(crypt)][(Ph$_2$Bi)Gd(NR$_2$)$_3$], **10**, 11 mmol in Et$_2$O.

X-ray Data Collection, Structure, Solution, Refinement

X-ray data, collection, structure, solution, and refinement can also be found in reference 23.
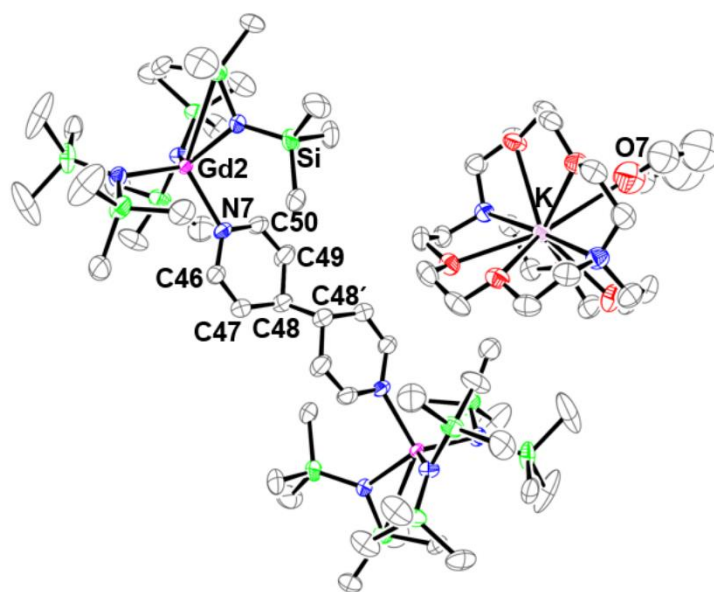
Figure 1.25. Representation of [K(crypt)]₂[{(NR₂)₃Gd}₂{μ-(NC₅H₄-C₅H₄N)}]₂, **7**, with atomic displacement parameters drawn at the 50% probability level. Hydrogen atoms, two THF molecules, and one ion pair were omitted for clarity.

Table 1.4. Crystal data and structure refinement for **[K(18-crown-6)(H₂O)][NCNCMe₃-κN], [K(18-crown-6)][κ^2-NCNCMe₃], CO(NH₂)₂.**

Identification code	abc2 (Amanda Chung)
Empirical formula	$C_{43} H_{88} K_2 N_6 O_{14}$
Formula weight	991.39
Temperature	88(2) K
Wavelength	0.71073 Å
Crystal system	Orthorhombic
Space group	*Pna2₁*
Unit cell dimensions	a = 21.1326(10) Å $\alpha = 90°$.
	b = 8.5470(4) Å $\beta = 90°$.
	c = 29.9188(14) Å $\gamma = 90°$.
Volume	5403.9(4) Å³
Z	4

Density (calculated)	1.219 Mg/m^3
Absorption coefficient	0.238 mm^{-1}
F(000)	2152
Crystal color	colorless
Crystal size	0.474 x 0.150 x 0.143 mm^3
Theta range for data collection	1.361 to 26.392°
Index ranges	$-26 \leq h \leq 26$, $-10 \leq k \leq 10$, $-37 \leq l \leq 36$
Reflections collected	42763
Independent reflections	11018 [R(int) = 0.0405]
Completeness to theta = 25.500°	100.0 %
Absorption correction	Semi-empirical from equivalents
Max. and min. transmission	0.7454 and 0.6996
Refinement method	Full-matrix least-squares on F^2
Data / restraints / parameters	11018 / 1 / 614
Goodness-of-fit on F^2	1.017
Final R indices [I>2sigma(I) = 9556 data]	R1 = 0.0326, wR2 = 0.0606
R indices (all data, 0.80 Å)	R1 = 0.0455, wR2 = 0.0649
Absolute structure parameter	0.015(13)
Largest diff. peak and hole	0.188 and -0.189 e.Å^{-3}

Table 1.5. Selected bond lengths [Å] and angles [°] for **[K(18-crown-6)(H₂O)][NCNCMe₃-*κN*]**, **[K(18-crown-6)][κ²-NCNCMe₃], CO(NH₂)₂.**

K(1)-O(7)	2.707(2)
K(1)-N(1)	3.027(2)
K(1)-H(7A)	2.75(4)
O(7)-H(7A)	0.81(4)
O(7)-H(7B)	0.95(4)
N(1)-C(13)	1.179(3)
N(2)-C(13)	1.294(3)
N(2)-C(14)	1.487(3)
K(2)-N(3)	2.690(2)
K(2)-C(30)	3.197(3)
N(3)-C(30)	1.185(4)
N(4)-C(30)	1.267(4)

N(4)-C(31)	1.457(4)
O(14)-C(35)	1.233(3)
N(5)-C(35)	1.374(3)
N(5)-C(36)	1.477(3)
N(5)-H(5)	0.80(3)
N(6)-C(35)	1.367(3)
N(6)-C(40)	1.479(3)
N(6)-H(6)	0.82(3)
O(7)-K(1)-N(1)	59.57(7)
O(7)-K(1)-H(7A)	17.1(8)
N(1)-K(1)-H(7A)	42.5(8)
C(13)-N(1)-K(1)	132.71(19)
C(13)-N(2)-C(14)	115.3(2)
N(3)-K(2)-C(30)	21.04(8)
C(30)-N(3)-K(2)	104.3(2)
C(30)-N(4)-C(31)	120.3(3)
N(3)-C(30)-N(4)	173.8(3)
N(3)-C(30)-K(2)	54.62(17)
N(4)-C(30)-K(2)	122.8(2)
O(14)-C(35)-N(6)	123.5(2)
O(14)-C(35)-N(5)	123.5(2)
N(6)-C(35)-N(5)	113.0(2)

Table 1.6. Crystal data and structure refinement for **3**.

Identification code	abc11 (Amanda Chung)	
Empirical formula	$C_{50} H_{120} Gd_2 K_2 N_4 O_{12} S_6 Si_8$	
Formula weight	1779.27	
Temperature	93(2) K	
Wavelength	0.71073 Å	
Crystal system	Monoclinic	
Space group	*C2/m*	
Unit cell dimensions	a = 22.150(4) Å	$\alpha = 90°$.
	b = 18.298(3) Å	$\beta = 99.134(3)°$.

	c = 12.156(2) Å γ = 90°.
Volume	4864.5(15) Å^3
Z	2
Density (calculated)	1.215 Mg/m^3
Absorption coefficient	1.706 mm^{-1}
F(000)	1836
Crystal color	yellow
Crystal size	0.237 x 0.213 x 0.201 mm^3
Theta range for data collection	1.451 to 28.489°
Index ranges	-29 ≤ h ≤ 29, -24 ≤ k ≤ 24, -16 ≤ l ≤ 16
Reflections collected	28566
Independent reflections	6295 [R(int) = 0.0528]
Completeness to theta = 25.242°	99.9 %
Absorption correction	Semi-empirical from equivalents
Max. and min. transmission	0.7457 and 0.5790
Refinement method	Full-matrix least-squares on F^2
Data / restraints / parameters	6295 / 0 / 204
Goodness-of-fit on F^2	1.047
Final R indices [I>2sigma(I) = 5567 data]	R1 = 0.0538, wR2 = 0.1343
R indices (all data, 0.75 Å)	R1 = 0.0610, wR2 = 0.1391
Largest diff. peak and hole	6.282 and -1.128 e.Å^{-3}

Table 1.7. Selected bond lengths [Å] and angles [°] for **3**.

Gd(1)-N(1)	2.285(4)
Gd(1)-N(1)#1	2.285(4)
Gd(1)-S(1)#1	2.8349(11)
Gd(1)-S(1)	2.8350(11)
Gd(1)-S(2)#2	3.0180(9)
Gd(1)-S(2)	3.0180(9)
K(1)-S(1)	3.3137(16)
K(1)-S(1)#3	3.3138(16)
S(1)-C(1)	1.712(3)
S(2)-C(1)	1.718(7)
S(2)-Gd(1)#2	3.0180(9)

C(1)-S(1)#3	1.712(3)
N(1)-Gd(1)-S(1)#1	89.75(10)
N(1)#1-Gd(1)-S(1)#1	116.35(10)
N(1)-Gd(1)-S(1)	116.35(10)
N(1)#1-Gd(1)-S(1)	89.75(10)
S(1)#1-Gd(1)-S(1)	136.96(5)
N(1)-Gd(1)-S(2)#2	147.61(9)
N(1)#1-Gd(1)-S(2)#2	99.17(10)
S(1)#1-Gd(1)-S(2)#2	60.76(4)
S(1)-Gd(1)-S(2)#2	82.75(4)
N(1)-Gd(1)-S(2)	99.17(10)
N(1)#1-Gd(1)-S(2)	147.61(9)
S(1)#1-Gd(1)-S(2)	82.76(4)
S(1)-Gd(1)-S(2)	60.76(4)
S(2)#2-Gd(1)-S(2)	66.18(5)
S(1)-K(1)-S(1)#3	53.39(4)
C(1)-S(1)-Gd(1)	88.00(19)
C(1)-S(1)-K(1)	89.87(19)
Gd(1)-S(1)-K(1)	168.47(5)
C(1)-S(2)-Gd(1)	82.07(11)
C(1)-S(2)-Gd(1)#2	82.07(11)
Gd(1)-S(2)-Gd(1)#2	113.82(5)
S(1)#3-C(1)-S(1)	120.8(4)
S(1)#3-C(1)-S(2)	119.53(19)
S(1)-C(1)-S(2)	119.53(19)

Symmetry transformations used to generate equivalent atoms:

#1 -x+1,y,-z+1   #2 -x+1,-y+1,-z+1   #3 x,-y+1,z

Table 1.8. Crystal data and structure refinement for **4**.

Identification code	abc10 (Amanda Chung)
Empirical formula	$C_{37} H_{89} Gd K N_5 O_6 S_2 Si_6$
Formula weight	1129.14
Temperature	133(2) K

Wavelength	0.71073 Å	
Crystal system	Monoclinic	
Space group	$P2_1/c$	
Unit cell dimensions	a = 11.4800(16) Å	$\alpha = 90°$.
	b = 16.473(2) Å	$\beta = 93.8683(19)°$.
	c = 32.251(5) Å	$\gamma = 90°$.
Volume	6085.2(15) Å^3	
Z	4	
Density (calculated)	1.232 Mg/m^3	
Absorption coefficient	1.384 mm^{-1}	
F(000)	2372	
Crystal color	orange	
Crystal size	0.445 x 0.179 x 0.174 mm^3	
Theta range for data collection	1.266 to 27.103°	
Index ranges	-14 ≤ h ≤ 14, -21 ≤ k ≤ 21, -41 ≤ l ≤ 41	
Reflections collected	69551	
Independent reflections	13431 [R(int) = 0.0348]	
Completeness to theta = 25.500°	100.0 %	
Absorption correction	Semi-empirical from equivalents	
Max. and min. transmission	0.7458 and 0.6319	
Refinement method	Full-matrix least-squares on F^2	
Data / restraints / parameters	13431 / 0 / 559	
Goodness-of-fit on F^2	1.075	
Final R indices [I>2sigma(I) = 11668 data]	R1 = 0.0372, wR2 = 0.0852	
R indices (all data, 0.73 Å)	R1 = 0.0451, wR2 = 0.0888	
Largest diff. peak and hole	1.468 and -0.810 e.Å^{-3}	

Table 1.9. Selected bond lengths [Å] and angles [°] for **4**.

Gd(1)-N(3)	2.286(2)
Gd(1)-N(1)	2.287(3)
Gd(1)-N(2)	2.292(2)
Gd(1)-S(1)	2.7489(9)
S(1)-C(1)	1.725(4)
S(2)-C(1)	1.659(3)

Si(1)-N(1)	1.708(3)
Si(1)-C(4)	1.858(10)
Si(1)-C(3)	1.861(4)
Si(1)-C(4B)	1.881(9)
Si(1)-C(2)	1.934(4)
C(1)-C(2)	1.507(5)
N(3)-Gd(1)-S(1)	102.84(6)
N(1)-Gd(1)-S(1)	95.46(7)
N(2)-Gd(1)-S(1)	99.61(6)
C(1)-S(1)-Gd(1)	102.37(12)
C(2)-C(1)-S(2)	119.9(3)
C(2)-C(1)-S(1)	117.5(2)
S(2)-C(1)-S(1)	122.6(2)
C(1)-C(2)-Si(1)	114.2(2)

Table 1.10. Crystal data and structure refinement for **[K(crypt)][S₃NR₂].**

Identification code	abc25 (Amanda Chung)
Empirical formula	C_{24} H_{54} K N_3 O_6 S_3 Si_2
Formula weight	672.16
Temperature	133(2) K
Wavelength	0.71073 Å
Crystal system	Triclinic
Space group	$P\bar{1}$
Unit cell dimensions	a = 11.3807(9) Å α = 84.3794(13)°.
	b = 18.0429(14) Å β = 78.9033(13)°.
	c = 18.5774(15) Å γ = 73.2617(12)°.
Volume	3581.1(5) Å³
Z	4
Density (calculated)	1.247 Mg/m³
Absorption coefficient	0.428 mm⁻¹
F(000)	1448
Crystal color	purple
Crystal size	0.372 x 0.200 x 0.102 mm³

Theta range for data collection	1.118 to 27.168°
Index ranges	$-14 \leq h \leq 14, -23 \leq k \leq 23, -23 \leq l \leq 23$
Reflections collected	42796
Independent reflections	15855 [R(int) = 0.0416]
Completeness to theta = 25.242°	100.0 %
Absorption correction	Semi-empirical from equivalents
Max. and min. transmission	0.8014 and 0.7194
Refinement method	Full-matrix least-squares on F^2
Data / restraints / parameters	15855 / 0 / 715
Goodness-of-fit on F^2	1.032
Final R indices [I>2sigma(I) = 11323 data]	R1 = 0.0505, wR2 = 0.1192
R indices (all data, 0.78 Å)	R1 = 0.0798, wR2 = 0.1334
Largest diff. peak and hole	1.154 and -0.503 e.Å^{-3}

Table 1.11. Selected bond lengths [Å] and angles [°] for **[K(crypt)][S$_3$NR$_2$]**.

S(1)-N(1)	1.731(2)
S(1)-S(2)	2.0420(10)
S(2)-S(3)	2.0323(10)
S(4)-N(2)	1.720(2)
S(4)-S(5)	2.0387(10)
S(5)-S(6)	2.0357(10)
N(1)-S(1)-S(2)	110.62(9)
S(3)-S(2)-S(1)	112.85(5)
S(1)-N(1)-Si(2)	117.29(14)
S(1)-N(1)-Si(1)	114.24(13)
N(2)-S(4)-S(5)	111.00(8)
S(6)-S(5)-S(4)	112.27(4)
S(4)-N(2)-Si(4)	113.01(13)
S(4)-N(2)-Si(3)	116.33(13)

Table 1.12. Crystal data and structure refinement for **6**.

Identification code	abc19 (Amanda Chung)
Empirical formula	$C_{90} H_{186} Gd_2 K_2 N_{12} O_{12} Si_{12}$
Formula weight	2358.28
Temperature	93(2) K
Wavelength	0.71073 Å
Crystal system	Monoclinic
Space group	$P2_1/n$
Unit cell dimensions	a = 20.8448(17) Å $\quad$ α = 90°.
	b = 15.3223(13) Å $\quad$ β = 115.3332(13)°.
	c = 21.4853(18) Å $\quad$ γ = 90°.
Volume	6202.3(9) Å^3
Z	2
Density (calculated)	1.263 Mg/m^3
Absorption coefficient	1.296 mm^{-1}
F(000)	2480
Crystal color	pink
Crystal size	0.379 x 0.158 x 0.141 mm^3
Theta range for data collection	1.693 to 25.349°
Index ranges	$-25 \leq h \leq 22, 0 \leq k \leq 18, 0 \leq l \leq 25$
Reflections collected	11366
Completeness to theta = 25.242°	100.0 %
Absorption correction	Semi-empirical from equivalents
Max. and min. transmission	0.7457 and 0.6251
Refinement method	Full-matrix least-squares on F^2
Data / restraints / parameters	11366 / 0 / 605
Goodness-of-fit on F^2	1.148
Final R indices [I>2sigma(I) = 9681 data]	R1 = 0.0510, wR2 = 0.0958
R indices (all data, 0.83 Å)	R1 = 0.0661, wR2 = 0.1020
Largest diff. peak and hole	1.436 and -0.931 e.Å^{-3}

Table 1.13. Selected bond lengths [Å] and angles [°] for **6**.

Gd(1)-N(1)	2.287(4)
Gd(1)-N(4)	2.298(4)
Gd(1)-N(2)	2.334(5)

Gd(1)-N(3)	2.337(4)
N(1)-C(5)	1.392(7)
N(1)-C(1)	1.395(7)
C(1)-C(2)	1.342(8)
C(2)-C(3)	1.518(8)
C(3)-C(4)	1.498(8)
C(3)-C(3)#1	1.565(10)
C(4)-C(5)	1.335(8)
N(1)-Gd(1)-N(4)	90.99(16)
N(1)-Gd(1)-N(2)	103.04(16)
N(4)-Gd(1)-N(2)	117.81(17)
N(1)-Gd(1)-N(3)	114.92(16)
N(4)-Gd(1)-N(3)	115.48(16)
N(2)-Gd(1)-N(3)	112.13(16)
C(5)-N(1)-C(1)	111.3(4)
C(5)-N(1)-Gd(1)	107.9(3)
C(1)-N(1)-Gd(1)	140.7(4)
C(2)-C(1)-N(1)	126.6(5)
C(1)-C(2)-C(3)	123.0(5)
C(4)-C(3)-C(2)	107.6(4)
C(4)-C(3)-C(3)#1	112.4(6)
C(2)-C(3)-C(3)#1	112.6(5)
C(5)-C(4)-C(3)	123.0(5)
C(4)-C(5)-N(1)	127.6(5)
C(4)-C(5)-Gd(1)	171.9(4)
N(1)-C(5)-Gd(1)	46.1(3)

Symmetry transformations used to generate equivalent atoms:

#1 -x+1,-y+2,-z+1

Table 1.14. Crystal data and structure refinement for **8**.

Identification code	abc38 (Amanda Chung)
Empirical formula	$[C_{39} H_{96} Gd K N_4 O_7 Si_6]_{\infty}$
Formula weight	1098.08
Temperature	93(2) K

Wavelength	0.71073 Å
Crystal system	Monoclinic
Space group	$P2_1/n$
Unit cell dimensions	a = 14.8515(17) Å $\alpha = 90°$.
	b = 17.892(2) Å $\beta = 105.9616(19)°$.
	c = 23.166(3) Å $\gamma = 90°$.
Volume	5918.6(12) Å^3
Z	4
Density (calculated)	1.232 Mg/m^3
Absorption coefficient	1.353 mm^{-1}
F(000)	2324
Crystal color	colorless
Crystal size	0.437 x 0.295 x 0.257 mm^3
Theta range for data collection	1.460 to 31.589°
Index ranges	$-21 \leq h \leq 21, -25 \leq k \leq 26, -33 \leq l \leq 33$
Reflections collected	147735
Independent reflections	18621 [R(int) = 0.0716]
Completeness to theta = 25.242°	100.0 %
Absorption correction	Semi-empirical from equivalents
Max. and min. transmission	0.7463 and 0.6580
Refinement method	Full-matrix least-squares on F^2
Data / restraints / parameters	18621 / 0 / 545
Goodness-of-fit on F^2	1.047
Final R indices [I>2sigma(I) = 14461 data]	R1 = 0.0413, wR2 = 0.0788
R indices (all data, 0.68 Å)	R1 = 0.0653, wR2 = 0.0881
Largest diff. peak and hole	3.472 and -0.807 e.Å^{-3}

Table 1.15. Selected bond lengths [Å] and angles [°] for **8**.

Gd(1)-O(1)	2.1313(18)
Gd(1)-N(2)	2.333(2)
Gd(1)-N(3)	2.359(2)
Gd(1)-N(1)	2.366(2)
O(1)-N(4)	1.439(3)
N(4)-C(19)	1.488(4)
N(4)-C(23)	1.494(4)

C(1)-K(1)	3.130(3)
C(16)-K(1)#1	3.172(3)
C(19)-C(24)	1.530(4)
C(19)-C(25)	1.537(4)
C(19)-C(20)	1.541(4)
C(20)-C(21)	1.523(5)
C(21)-C(22)	1.517(5)
C(22)-C(23)	1.543(4)
C(23)-C(26)	1.531(4)
C(23)-C(27)	1.543(4)
K(1)-C(16)#2	3.172(3)
O(1)-Gd(1)-N(2)	105.14(7)
O(1)-Gd(1)-N(3)	114.12(7)
N(2)-Gd(1)-N(3)	109.92(7)
O(1)-Gd(1)-N(1)	107.89(7)
N(2)-Gd(1)-N(1)	111.73(7)
N(3)-Gd(1)-N(1)	108.07(8)
N(4)-O(1)-Gd(1)	153.09(15)
O(1)-N(4)-C(19)	108.98(19)
O(1)-N(4)-C(23)	108.9(2)
C(19)-N(4)-C(23)	117.9(2)
Si(1)-C(1)-K(1)	168.10(16)
Si(6)-C(16)-K(1)#1	174.94(15)
N(4)-C(19)-C(24)	106.6(2)
N(4)-C(19)-C(25)	115.0(2)
C(24)-C(19)-C(25)	109.1(2)
N(4)-C(19)-C(20)	107.7(2)
C(24)-C(19)-C(20)	107.6(2)
C(25)-C(19)-C(20)	110.5(2)
C(21)-C(20)-C(19)	113.5(3)
C(22)-C(21)-C(20)	107.9(3)
C(21)-C(22)-C(23)	113.3(3)
N(4)-C(23)-C(26)	106.4(2)
N(4)-C(23)-C(22)	107.7(2)
C(26)-C(23)-C(22)	107.4(2)

N(4)-C(23)-C(27)	115.5(2)
C(26)-C(23)-C(27)	109.4(2)
C(22)-C(23)-C(27)	110.1(2)
C(1)-K(1)-C(16)#2	169.35(8)

Symmetry transformations used to generate equivalent atoms:

#1 x+1/2,-y+3/2,z-1/2   #2 x-1/2,-y+3/2,z+1/2

Table 1.16. Crystal data and structure refinement for **9**.

Identification code	abc20 (Amanda Chung)
Empirical formula	$C_{49} H_{116} Gd K N_6 O_8 Si_6$
Formula weight	1282.36
Temperature	93(2) K
Wavelength	0.71073 Å
Crystal system	Triclinic
Space group	$P\bar{1}$
Unit cell dimensions	a = 12.4688(13) Å α = 94.4047(14)°.
	b = 16.6943(17) Å β = 92.8951(15)°.
	c = 16.7111(17) Å γ = 95.3820(15)°.
Volume	3447.1(6) Å^3
Z	2
Density (calculated)	1.235 Mg/m^3
Absorption coefficient	1.173 mm^{-1}
F(000)	1366
Crystal color	colorless
Crystal size	0.400 x 0.300 x 0.222 mm^3
Theta range for data collection	1.224 to 30.508°
Index ranges	$-17 \leq h \leq 17, -23 \leq k \leq 23, -23 \leq l \leq 23$
Reflections collected	52280
Independent reflections	20353 [R(int) = 0.0231]
Completeness to theta = 25.242°	100.0 %
Absorption correction	Semi-empirical from equivalents
Max. and min. transmission	0.7462 and 0.6545
Refinement method	Full-matrix least-squares on F^2
Data / restraints / parameters	20353 / 0 / 662
Goodness-of-fit on F^2	1.075

Final R indices [I>2sigma(I) = 18608 data] R1 = 0.0243, wR2 = 0.0563
R indices (all data, 0.70 Å) R1 = 0.0285, wR2 = 0.0580
Largest diff. peak and hole 1.030 and -0.862 e.Å^{-3}

Table 1.17. Selected bond lengths [Å] and angles [°] for **9**.

Gd(1)-O(1)	2.1342(10)
Gd(1)-N(1)	2.3361(12)
Gd(1)-N(2)	2.3638(12)
Gd(1)-N(3)	2.3734(12)
O(1)-N(4)	1.4386(15)
N(4)-C(23)	1.4914(18)
N(4)-C(19)	1.4917(18)
C(19)-C(25)	1.532(2)
C(19)-C(24)	1.536(2)
C(19)-C(20)	1.542(2)
C(20)-C(21)	1.522(2)
C(21)-C(22)	1.517(2)
C(22)-C(23)	1.536(2)
C(23)-C(27)	1.529(2)
C(23)-C(26)	1.544(2)
O(1)-Gd(1)-N(1)	105.87(4)
O(1)-Gd(1)-N(2)	115.37(4)
N(1)-Gd(1)-N(2)	107.95(4)
O(1)-Gd(1)-N(3)	106.21(4)
N(1)-Gd(1)-N(3)	113.19(4)
N(2)-Gd(1)-N(3)	108.40(4)
O(1)-N(4)-C(23)	109.26(10)
O(1)-N(4)-C(19)	109.46(10)
C(23)-N(4)-C(19)	117.95(11)
N(4)-C(19)-C(25)	106.45(12)
N(4)-C(19)-C(24)	115.39(12)
C(25)-C(19)-C(24)	109.46(13)
N(4)-C(19)-C(20)	107.93(12)
C(25)-C(19)-C(20)	106.76(12)

C(24)-C(19)-C(20)	110.44(12)
C(21)-C(20)-C(19)	113.97(13)
C(22)-C(21)-C(20)	108.45(13)
C(21)-C(22)-C(23)	112.80(13)
N(4)-C(23)-C(27)	106.41(12)
N(4)-C(23)-C(22)	107.64(12)
C(27)-C(23)-C(22)	106.85(12)
N(4)-C(23)-C(26)	115.51(12)
C(27)-C(23)-C(26)	109.34(13)
C(22)-C(23)-C(26)	110.68(12)

Table 1.18. Crystal data and structure refinement for **10**.

Identification code	abc50 (Amanda Chung)
Empirical formula	$C_{48} H_{100} Bi Gd K N_5 O_6 Si_6$
Formula weight	1417.19
Temperature	93(2) K
Wavelength	0.71073 Å
Crystal system	Monoclinic
Space group	$P2_1/c$
Unit cell dimensions	a = 16.1118(10) Å $\alpha = 90°$.
	b = 21.9948(14) Å $\beta = 99.4558(11)°$.
	c = 18.4834(12) Å $\gamma = 90°$.
Volume	6461.1(7) Å^3
Z	4
Density (calculated)	1.457 Mg/m^3
Absorption coefficient	3.957 mm^{-1}
F(000)	2884
Crystal color	yellow
Crystal size	0.453 x 0.285 x 0.148 mm^3
Theta range for data collection	1.451 to 26.372°
Index ranges	$-20 \leq h \leq 20, -27 \leq k \leq 27, -23 \leq l \leq 23$
Reflections collected	129292
Independent reflections	13194 [R(int) = 0.0361]
Completeness to theta = 25.242°	100.0 %
Absorption correction	Semi-empirical from equivalents

Max. and min. transmission	0.3373 and 0.2371
Refinement method	Full-matrix least-squares on F^2
Data / restraints / parameters	13194 / 0 / 634
Goodness-of-fit on F^2	1.047
Final R indices [I>2sigma(I) = 12210 data]	R1 = 0.0211, wR2 = 0.0493
R indices (all data, 0.80 Å)	R1 = 0.0246, wR2 = 0.0506
Largest diff. peak and hole	1.576 and -0.967 e.Å^{-3}

Table 1.19. Selected bond lengths [Å] and angles [°] for **10**.

Bi(1)-C(7)	2.268(3)
Bi(1)-C(1)	2.285(3)
Bi(1)-Gd(1)	3.3466(2)
Gd(1)-N(2)	2.274(2)
Gd(1)-N(1)	2.305(2)
Gd(1)-N(3)	2.314(2)
C(1)-C(2)	1.398(4)
C(1)-C(6)	1.401(4)
C(2)-C(3)	1.400(4)
C(3)-C(4)	1.387(4)
C(4)-C(5)	1.389(4)
C(5)-C(6)	1.391(4)
C(7)-C(8)	1.395(4)
C(7)-C(12)	1.397(4)
C(8)-C(9)	1.385(4)
C(9)-C(10)	1.384(4)
C(10)-C(11)	1.373(5)
C(11)-C(12)	1.389(4)
C(7)-Bi(1)-C(1)	97.60(10)
C(7)-Bi(1)-Gd(1)	95.09(7)
C(1)-Bi(1)-Gd(1)	112.43(7)
N(2)-Gd(1)-N(1)	107.07(8)
N(2)-Gd(1)-N(3)	114.54(7)
N(1)-Gd(1)-N(3)	115.46(8)

C(2)-C(1)-C(6)	117.2(3)
C(2)-C(1)-Bi(1)	127.3(2)
C(6)-C(1)-Bi(1)	115.5(2)
C(1)-C(2)-C(3)	121.2(3)
C(4)-C(3)-C(2)	120.4(3)
C(3)-C(4)-C(5)	119.2(3)
C(4)-C(5)-C(6)	120.2(3)
C(5)-C(6)-C(1)	121.7(3)
C(8)-C(7)-C(12)	117.2(3)
C(8)-C(7)-Bi(1)	122.5(2)
C(12)-C(7)-Bi(1)	120.3(2)
C(9)-C(8)-C(7)	121.7(3)
C(10)-C(9)-C(8)	120.1(3)
C(11)-C(10)-C(9)	119.2(3)
C(10)-C(11)-C(12)	121.0(3)
C(11)-C(12)-C(7)	120.8(3)

Table 1.20. Crystal data and structure refinement for **[K(crypt)][BiPh$_2$]**.

Identification code	abc30 (Amanda Chung)
Empirical formula	C$_{30}$ H$_{46}$ Bi K N$_2$ O$_6$
Formula weight	778.77
Temperature	93(2) K
Wavelength	0.71073 Å
Crystal system	Monoclinic
Space group	$P2_1/c$
Unit cell dimensions	a = 13.0303(7) Å $\alpha = 90°$.
	b = 13.9504(7) Å $\beta = 95.8719(9)°$.
	c = 18.2757(9) Å $\gamma = 90°$.
Volume	3304.7(3) Å^3
Z	4
Density (calculated)	1.565 Mg/m^3
Absorption coefficient	5.502 mm^{-1}
F(000)	1560
Crystal color	purple
Crystal size	0.238 x 0.154 x 0.134 mm^3

Theta range for data collection	1.571 to 29.129°
Index ranges	$-17 \leq h \leq 17$, $-19 \leq k \leq 19$, $-25 \leq l \leq 25$
Reflections collected	78212
Independent reflections	8886 [R(int) = 0.0565]
Completeness to theta = 25.242°	100.0 %
Absorption correction	Semi-empirical from equivalents
Max. and min. transmission	0.2657 and 0.1912
Refinement method	Full-matrix least-squares on F^2
Data / restraints / parameters	8886 / 0 / 361
Goodness-of-fit on F^2	1.029
Final R indices [I>2sigma(I) = 7308 data]	R1 = 0.0264, wR2 = 0.0524
R indices (all data, 0.73 Å)	R1 = 0.0403, wR2 = 0.0570
Largest diff. peak and hole	2.021 and -0.675 e.Å^{-3}

Table 1.21. Selected bond lengths [Å] and angles [°] for **[K(crypt)][BiPh₂]**.

Bi(1)-C(7)	2.273(3)
Bi(1)-C(1)	2.279(3)
C(1)-C(2)	1.403(4)
C(1)-C(6)	1.408(4)
C(2)-C(3)	1.392(4)
C(3)-C(4)	1.388(4)
C(4)-C(5)	1.380(4)
C(5)-C(6)	1.394(4)
C(7)-C(8)	1.396(4)
C(7)-C(12)	1.400(4)
C(8)-C(9)	1.390(4)
C(9)-C(10)	1.380(4)
C(10)-C(11)	1.388(4)
C(11)-C(12)	1.389(4)
C(7)-Bi(1)-C(1)	98.01(9)
C(2)-C(1)-C(6)	116.1(2)
C(2)-C(1)-Bi(1)	125.40(19)
C(6)-C(1)-Bi(1)	118.25(19)

C(3)-C(2)-C(1)	122.1(3)
C(4)-C(3)-C(2)	120.1(3)
C(5)-C(4)-C(3)	119.5(3)
C(4)-C(5)-C(6)	120.1(3)
C(5)-C(6)-C(1)	122.1(3)
C(8)-C(7)-C(12)	116.2(2)
C(8)-C(7)-Bi(1)	125.8(2)
C(12)-C(7)-Bi(1)	117.89(18)
C(9)-C(8)-C(7)	121.9(3)
C(10)-C(9)-C(8)	120.7(3)
C(9)-C(10)-C(11)	118.9(3)
C(10)-C(11)-C(12)	119.9(3)
C(11)-C(12)-C(7)	122.4(2)

_____

Table 1.22. Crystal data and structure refinement for **[K(crypt)][SnPh₃](THF).**

Identification code	abc40 (Amanda Chung)
Empirical formula	$C_{40} H_{59} K N_2 O_7 Sn$
Formula weight	837.68
Temperature	93(2) K
Wavelength	0.71073 Å
Crystal system	Monoclinic
Space group	$P2_1/c$
Unit cell dimensions	a = 13.9183(9) Å $\quad$ $\alpha = 90°$.
	b = 21.6195(14) Å $\quad$ $\beta = 98.2302(12)°$.
	c = 13.7646(9) Å $\quad$ $\gamma = 90°$.
Volume	4099.2(5) Å^3
Z	4
Density (calculated)	1.357 Mg/m^3
Absorption coefficient	0.773 mm^{-1}
F(000)	1752
Crystal color	colorless
Crystal size	0.509 x 0.374 x 0.170 mm^3
Theta range for data collection	1.478 to 27.103°
Index ranges	$-17 \le h \le 17$, $-27 \le k \le 27$, $-17 \le l \le 17$

Reflections collected	75738
Independent reflections	9043 [R(int) = 0.0409]
Completeness to theta = 25.242°	100.0 %
Absorption correction	Semi-empirical from equivalents
Max. and min. transmission	0.8017 and 0.7069
Refinement method	Full-matrix least-squares on F^2
Data / restraints / parameters	9043 / 0 / 478
Goodness-of-fit on F^2	1.085
Final R indices [I>2sigma(I) = 7931 data]	R1 = 0.0539, wR2 = 0.1190
R indices (all data, 0.78 Å)	R1 = 0.0630, wR2 = 0.1239
Largest diff. peak and hole	3.295 and -1.924 e.Å^{-3}

Table 1.23. Selected bond lengths [Å] and angles [°] for **[K(crypt)][SnPh3](THF).**

Sn(1)-C(13)	2.238(4)
Sn(1)-C(1)	2.238(4)
Sn(1)-C(7)	2.245(4)
C(1)-C(6)	1.392(6)
C(1)-C(2)	1.404(5)
C(2)-C(3)	1.399(6)
C(3)-C(4)	1.387(6)
C(4)-C(5)	1.383(6)
C(5)-C(6)	1.391(6)
C(7)-C(8)	1.384(6)
C(7)-C(12)	1.395(6)
C(8)-C(9)	1.398(6)
C(9)-C(10)	1.380(7)
C(10)-C(11)	1.396(7)
C(11)-C(12)	1.393(6)
C(13)-C(14)	1.403(6)
C(13)-C(18)	1.405(5)
C(14)-C(15)	1.397(7)
C(15)-C(16)	1.388(7)

C(16)-C(17)	1.386(6)
C(17)-C(18)	1.382(6)
C(13)-Sn(1)-C(1)	95.17(14)
C(13)-Sn(1)-C(7)	96.11(15)
C(1)-Sn(1)-C(7)	94.04(13)
C(6)-C(1)-C(2)	116.3(4)
C(6)-C(1)-Sn(1)	122.1(3)
C(2)-C(1)-Sn(1)	121.5(3)
C(3)-C(2)-C(1)	122.0(4)
C(4)-C(3)-C(2)	119.9(4)
C(5)-C(4)-C(3)	119.1(4)
C(4)-C(5)-C(6)	120.5(4)
C(5)-C(6)-C(1)	122.2(4)
C(8)-C(7)-C(12)	115.7(4)
C(8)-C(7)-Sn(1)	124.1(3)
C(12)-C(7)-Sn(1)	120.1(3)
C(7)-C(8)-C(9)	122.9(4)
C(10)-C(9)-C(8)	120.0(4)
C(9)-C(10)-C(11)	118.8(4)
C(12)-C(11)-C(10)	119.6(4)
C(11)-C(12)-C(7)	122.9(4)
C(14)-C(13)-C(18)	115.3(4)
C(14)-C(13)-Sn(1)	121.0(3)
C(18)-C(13)-Sn(1)	123.7(3)
C(15)-C(14)-C(13)	122.5(4)
C(16)-C(15)-C(14)	120.1(4)
C(17)-C(16)-C(15)	118.7(4)
C(18)-C(17)-C(16)	120.6(4)
C(17)-C(18)-C(13)	122.8(4)

References

(1)   Ryan, A. J.; Darago, L. E.; Balasubramani, G.; Chen, G. P.; Ziller, J. W.; Furche, F.; Long, J. R.; Evans, W. J. *Chem. Eur. J.* **2018**, No. 2, 7702–7709.

(2)   Woen, D. H.; Chen, G. P.; Ziller, J. W.; Boyle, T. J.; Furche, F.; Evans, W. J. *Angew. Chem. Int. Ed.* **2017**, *129*, 2082–2085.

(3)   MacDonald, M. R.; Ziller, J. W.; Evans, W. J. *J. Am. Chem. Soc.* **2011**, *133* (40), 15914–15917.

(4)   MacDonald, M. R.; Bates, J. E.; Fieser, M. E.; Ziller, J. W.; Furche, F.; Evans, W. J. *J. Am. Chem. Soc.* **2012**, *134* (20), 8420–8423.

(5)   Macdonald, M. R.; Bates, E.; Ziller, J. W.; Furche, F.; Evans, W. J. *J. Am. Chem. Soc.* **2013**, *135*, 9857–9868.

(6)   Evans, W. J. *Organometallics* **2016**, *35*, 3088–3100.

(7)   Woen, D. H.; Evans, W. J. In *Handbook on the Physics and Chemistry of Rare Earths*; Elsevier B.V., 2016; pp 1–57.

(8)   Fieser, M. E.; Macdonald, M. R.; Krull, B. T.; Bates, J. E.; Ziller, J. W.; Furche, F.; Evans, W. J. *J. Am. Chem. Soc.* **2015**, *137* (1), 369–382.

(9)   Woen, D. H.; Chen, G. P.; Ziller, J. W.; Boyle, T. J.; Furche, F.; Evans, W. J. *J. Am. Chem. Soc.* **2017**, *139*, 14861–14864.

(10)   Ryan, A. J.; Balasubramani, S.; Ziller, J. W.; Furche, F.; Evans, W. J. *J. Am. Chem. Soc.* **2020**, *142* (20), 9302–9313.

(11)   Ryan, A. J.; Ziller, J. W.; Evans, W. J. *Chem. Sci.* **2020**, No. 11, 2006–2014.

(12)   Tilley, T. D.; Andersen, R. A.; Zalkin, A. *Inorg. Chem.* **1984**, *23* (15), 2271–2276.

(13)   Evans, W. J.; Johnston, M. A.; Clark, R. D.; Anwander, R.; Ziller, J. W. *Polyhedron* **2001**, *20* (19), 2483–2490.

(14)   Palumbo, C. T.; Fieser, M. E.; Ziller, J. W.; Evans, W. J. *Organometallics* **2017**, *36* (19), 3721–3728.

(15)   Deacon, G. B.; Forsyth, C. M.; Junk, P. C.; Wang, J. *Inorg. Chem.* **2007**, *46* (23), 10022–10030.

(16)   Werner, D.; Deacon, G. B.; Junk, P. C. *Inorg. Chem.* **2019**, *58* (3), 1912–1918.

(17)   Toniolo, D.; Willauer, A. R.; Andrez, J.; Yang, Y.; Scopelliti, R.; Maron, L.; Mazzanti, M. *Chem. Eur. J.* **2019**, *25* (33), 7831–7834.

(18)   Heitmann, D.; Jones, C.; Mills, D. P.; Stasch, A. *Dalt. Trans.* **2010**, *39* (7), 1877–1882.

(19)   Deacon, G. B.; Junk, P. C.; Wang, J.; Werner, D. *Inorg. Chem.* **2014**, *53* (23), 12553–12563.

(20)   Andrez, J.; Pøcaut, J.; Bayle, P.; Mazzanti, M. *Angew. Chem. Int. Ed.* **2014**, *53*, 10448–10452.

(21)   Lam, O. P.; Castro, L.; Kosog, B.; Heinemann, F. W.; Maron, L.; Meyer, K. *Inorg. Chem.* **2012**, *51* (2), 781–783.

(22)   Camp, C.; Cooper, O.; Andrez, J.; Pécaut, J.; Mazzanti, M. *Dalt. Trans.* **2015**, *44* (6), 2650–2656.

(23)   Chung, A. B.; Ryan, A. J.; Fang, M.; Ziller, J. W.; Evans, W. J. *Inorg. Chem.* **2021**, *60* (20), 15635–15645.

(24)   Schneider, C.; Demeshko, S.; Meyer, F.; Werncke, C. G. *Chem. Eur. J.* **2021**, *27* (20), 6348–6353.

(25)   Shannon, R. D. *Acta Crystallogr., Sect. A Cryst. Phys., Diffr., Theor. Gen. Crystallogr.* **1976**, *32*, 751–767.

(26)   Allen, F. H.; Kennard, O.; Watson, D. G.; Brammer, L.; Orpen, A. G.; Taylor, R. *J. Chem. Soc. Perkin Trans. 2* **1987**, 1–19.

(27)   Aspinall, H. C.; Bradley, D. C.; Hursthouse, M. B.; Sales, K. D.; Walker, N. P. C. *J.*

Chem. Soc. - Ser. Chem. Commun. **1985**, *2* (22), 1585–1586.

(28) Simpson, S. J.; Turner, H. W.; Andersen, R. A. *J. Am. Chem. Soc.* **1979**, *101* (26), 7728–7729.

(29) Andersen, R. A. *Inorg. Chem.* **1979**, *18* (6), 1724–1725.

(30) Han, F.; Zhang, J.; Yi, W.; Zhang, Z.; Yu, J.; Weng, L.; Zhou, X. *Inorg. Chem.* **2010**, *49*, 2793–2798.

(31) Fortier, S.; Wu, G.; Hayton, T. W. *J. Am. Chem. Soc.* **2010**, *132* (20), 6888–6889.

(32) Fang, M.; Bates, J. E.; Lorenz, S. E.; Lee, D. S.; Rego, D. B.; Ziller, J. W.; Furche, F.; Evans, W. J. *Inorg. Chem.* **2011**, *50* (4), 1459–1469.

(33) Fortier, S.; Kaltsoyannis, N.; Wu, G.; Hayton, T. W. *J. Am. Chem. Soc.* **2011**, *133* (36), 14224–14227.

(34) Lewis, A. J.; Williams, U. J.; Carroll, P. J.; Schelter, E. J. *Inorg. Chem.* **2013**, *52* (13), 7326–7328.

(35) Smiles, D. E.; Wu, G.; Hayton, T. W. *New J. Chem.* **2015**, *39* (10), 7563–7566.

(36) Simpson, S. J.; Turner, H. W.; Andersen, R. A. *Inorg. Chem.* **1981**, *20* (9), 2991–2995.

(37) Moore, M.; Gambarotta, S.; Bensimon, C. *Organometallics* **1997**, *16* (5), 1086–1088.

(38) Galsworthy, J. R.; Green, M. L. H.; Müller, M. *J. Chem. Soc. Dalt. Trans.* **1998**, *868*, 387–392.

(39) Karl, M.; Harms, K.; Seybert, G.; Massa, W.; Fau, S.; Frenking, G.; Dehnicke, K. *Z. Anorg. Allg. Chem.* **1999**, *625* (12), 2055–2063.

(40) Yu, X.; Bi, S.; Guzei, I. A.; Lin, Z.; Xue, Z. L. *Inorg. Chem.* **2004**, *43* (22), 7111–7119.

(41) Niemeyer, M. *Inorg. Chem.* **2006**, *45* (22), 9085–9095.

(42) Graves, C. R.; Schelter, E. J.; Cantat, T.; Scott, B. L.; Kiplinger, J. L. *Organometallics* **2008**, *27* (20), 5371–5378.

(43) Gardner, B. M.; McMaster, J.; Lewis, W.; Blake, A. J.; Liddle, S. T. *J. Am. Chem. Soc.* **2009**, *131* (30), 10388–10389.

(44) Corbey, J. F.; Woen, D. H.; Palumbo, C. T.; Fieser, M. E.; Ziller, J. W.; Furche, F.; Evans, W. J. *Organometallics* **2015**, *34* (15), 3909–3921.

(45) Jaroschik, F.; Momin, A.; Nief, F.; Goff, X. Le; Deacon, G. B.; Junk, P. C. *Angew. Chem. Int. Ed.* **2009**, *48*, 1117–1121.

(46) Fieser, M. E.; Palumbo, C. T.; La Pierre, H. S.; Halter, D. P.; Voora, V. K.; Ziller, J. W.; Furche, F.; Meyer, K.; Evans, W. J. *Chem. Sci.* **2017**, *8* (11), 7424–7433.

(47) Hende, J. R. Van Den; Hitchcock, P. B.; Lappert, M. F. *J. Chem. Soc. Dalt. Trans.* **1995**, 2251–2258.

(48) Evans, W. J.; Rabe, G. W.; Ziller, J. W.; Doedens, R. J. *Inorg. Chem.* **1994**, *33* (13), 2719–2726.

(49) Corbey, J. F.; Fang, M.; Ziller, J. W.; Evans, W. J. *Inorg. Chem.* **2015**, *54*, 801–807.

(50) Labouille, S.; Nief, F.; Le Goff, X. F.; Maron, L.; Kindra, D. R.; Houghton, H. L.; Ziller, J. W.; Evans, W. J. *Organometallics* **2012**, *31* (14), 5196–5203.

(51) Fedushkin, I. L.; Nevodchikov, V. I.; Bochkarev, M. N.; Dechert, S.; Schumann, H. *Russ. Chem. Bull. Int. Ed. Izv. Akad. Nauk. Seriya Khimicheskaya* **2003**, *52* (1), 154–159.

(52) Jaroschik, F.; Nief, F.; Le Goff, X. F.; Ricard, L. *Organometallics* **2007**, *26* (14), 3552–3558.

(53) Mazzanti, M.; Modder, D. K.; Palumbo, C. T.; Douair, I.; Fadaei-Tirani, F.; Maron, L. *Angew. Chem. Int. Ed.* **2020**.

(54) Formanuik, A.; Ortu, F.; Liu, J.; Nodaraki, L. E.; Tuna, F.; Kerridge, A.; Mills, D. P.

Chem. Eur. J. **2017**, *23* (10), 2290–2293.

(55) Dugan, T. R.; Bill, E.; MacLeod, K. C.; Christian, G. J.; Cowley, R. E.; Brennessel, W. W.; Ye, S.; Neese, F.; Holland, P. L. *J. Am. Chem. Soc.* **2012**, *134* (50), 20352–20364.

(56) Demir, S.; Gonzalez, M. I.; Darago, L. E.; Evans, W. J.; Long, J. R. *Nat. Commun.* **2017**, *8*, 1–9.

(57) Bartholomew, A. K.; Teesdale, J. J.; Sanchez, R. H.; Malbrecht, B. J.; Jude, C. E.; Menard, G.; Bu, W.; Iovan, D. A.; Mikhailine, A. A.; Zheng, S.-L.; et al. *CSD Commun.* **2019**.

(58) Langeslay, R. R.; Walensky, J. R.; Ziller, J. W.; Evans, W. J. *Inorg. Chem.* **2014**, *53* (16), 8455–8463.

(59) Farnaby, J. H.; Fang, M.; Ziller, J. W.; Evans, W. J. *Inorg. Chem.* **2012**, *51* (20), 11168–11176.

(60) Dickman, M. H.; Doedens, R. J. *Inorg. Chem.* **1982**, *21* (2), 682–684.

(61) Mahanthappa, M. K.; Huang, K. W.; Cole, A. P.; Waymouth, R. M. *Chem. Commun.* **2002**, *2* (5), 502–503.

(62) Evans, W. J.; Perotti, J. M.; Doedens, R. J.; Ziller, J. W. *Chem. Commun.* **2001**, *1* (22), 2326–2327.

(63) Jaitner, P.; Huber, W.; Hunter, G.; Scheidsteger, O. *J. Organomet. Chem.* **1983**, *259* (1), 3–7.

(64) Westerhausen, M.; Weinrich, S.; Schmid, B.; Schneiderbauer, S.; Suter, M.; Noth, H.; Piotrowski, H. *Zeitschrift Fur Anorg. Und Allg. Chemie* **2003**, *629* (4), 625–633.

(65) Likhar, P. R.; Zirngast, M.; Baumgartner, J.; Marschner, C. *Chem. Commun.* **2004**, *4* (15), 1764–1765.

(66) Zitz, R.; Hlina, J.; Arp, H.; Kinschel, D.; Marschner, C.; Baumgartner, J. *Inorg. Chem.* **2019**, *58* (10), 7107–7117.

(67) Evans, W. J.; Giarikos, D. G.; Workman, P. S.; Ziller, J. W. *Inorg. Chem.* **2004**, *43* (18), 5754–5760.

(68) Evans, W. J.; Gonzales, S. L.; Ziller, J. W. *J. Am. Chem. Soc.* **1991**, *113* (26), 9880–9882.

(69) Ababei, R.; Massa, W.; Weinert, B.; Pollak, P.; Xie, X.; Clérac, R.; Weigend, F.; Dehnen, S. *Chem. Eur. J.* **2015**, *21* (1), 386–394.

(70) Rookes, T. M.; Wildman, E. P.; Balázs, G.; Gardner, B. M.; Wooles, A. J.; Gregson, M.; Tuna, F.; Scheer, M.; Liddle, S. T. *Angew. Chem. Int. Ed.* **2018**, *57* (5), 1332–1336.

(71) Kindra, D. R.; Casely, I. J.; Fieser, M. E.; Ziller, J. W.; Furche, F.; Evans, W. J. *J. Am. Chem. Soc.* **2013**, *135* (20), 7777–7787.

(72) Silvestru, C.; Breunig, H. J.; Althaus, H. *Chem. Rev.* **1999**, *99* (11), 3277–3327.

(73) Birchall, T.; Vetrone, J. A. *J. Chem. Soc. Chem. Commun.* **1988**, No. 13, 877–879.

(74) Englich, U.; Ruhlandt-Senge, K.; Uhlig, F. *J. Organomet. Chem.* **2000**, *613* (2), 139–147.

(75) Reed, D.; Stalke, D.; Wright, D. S. *Angew. Chem. Int. Ed.* **1991**, *11*, 1459–1460.

(76) Jenkins, T. F.; Woen, D. H.; Mohanam, L. N.; Ziller, J. W.; Furche, F.; Evans, W. J. *Organometallics* **2018**, *37* (21), 3863–3873.

(77) Chilton, N. F.; Goodwin, C. A. P.; Mills, D. P.; Winpenny, R. E. P. *Chem. Commun.* **2015**, *51* (1), 101–103.

(78) Goodwin, C. A. P.; Chilton, N. F.; Vettese, G. F.; Moreno Pineda, E.; Crowe, I. F.; Ziller, J. W.; Winpenny, R. E. P.; Evans, W. J.; Mills, D. P. *Inorg. Chem.* **2016**, *55* (20), 10057–10067.

(79) Ortu, F.; Packer, D.; Liu, J.; Burton, M.; Formanuik, A.; Mills, D. P. *J. Organomet. Chem.*

2018, *857*, 45–51.

(80) Huh, D. N.; Roy, S.; Ziller, J. W.; Furche, F.; Evans, W. J. *J. Am. Chem. Soc.* **2019**, *141* (32), 12458–12463.

(81) Gabbaï, F. P.; Chirik, P. J.; Fogg, D. E.; Meyer, K.; Mindiola, D. J.; Schafer, L. L.; You, S. L. *Organometallics* **2016**, *35* (19), 3255–3256.

(82) Moehring, S. A.; Miehlich, M.; Hoerger, C. J.; Meyer, K.; Ziller, J. W.; Evans, W. J. *Inorg. Chem.* **2020**, *59* (5), 3207–3214.

(83) Goodwin, C. A. P.; Reta, D.; Ortu, F.; Chilton, N. F.; Mills, D. P. *J. Am. Chem. Soc.* **2017**, *139* (51), 18714–18724.

Chapter 2

Reductive C–O Cleavage of Ethereal Solvents and 18-Crown-6

in Ln(NR$_2$)$_3$/KC$_8$ Reactions (R = SiMe$_3$)

Introduction

This Chapter describes the solvent decomposition reactions by Ln(NR$_2$)$_3$/K reactions with

the smaller rare earth metals, Ln = Y, Ho, Er, and Lu. As outlined in the Introduction, attempts

were made to synthesize molecular complexes of rare earth metals in the +2 oxidation state[1–9]

beyond the known examples with the traditional Ln(II) ions, namely, Eu(II), Yb(II), Sm(II),

Tm(II), Dy(II), and Nd(II).[10–14] These initial studies, done by Professor Michael F. Lappert,

concerning reduction of tris(cyclopentadienyl) rare-earth metal complexes with potassium and

lithium in dimethoxyethane (DME), led to cleavage of the solvent and formation of methoxide

complexes, eq 2.1.[1]

$$\text{Ln = La, Ce, Nd}$$
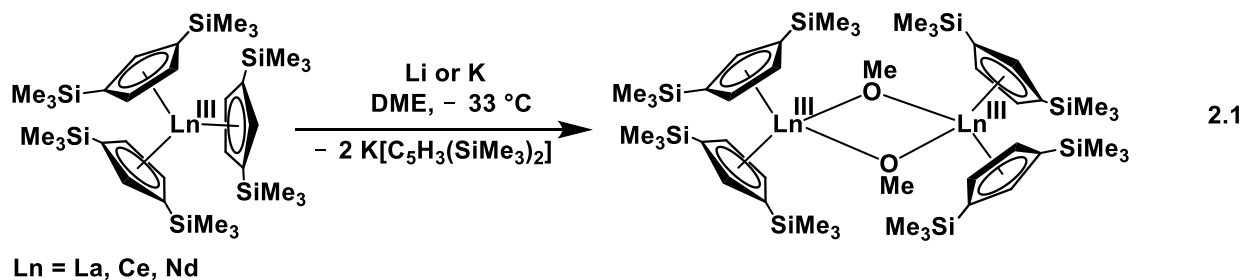
These DME reactions yielded mixtures of methoxide products, such as [Cp″$_2$ Ln(μ-OMe)]$_2$

[Ln = La,[3] Ce,[1] and Nd;[3] Cp″ = C$_5$H$_3$(SiMe$_3$)$_2$], and [Cp″$_2$Nd(μ-OMe)$_2$Li(DME)],[1] along with

KCp″ and unidentified polymetallic methoxide complexes. These results were consistent with

earlier predictions that any Ln(II) ion beyond Eu, Yb, Sm, Tm, Dy, and Nd would be so reducing

that they would decompose any solvent in which they were soluble.[11,13–15] However, when Lappert

switched to THF and Et$_2$O solvents in the presence of 18-crown-6 (18-c-6) and 2.2.2-cryptand

(crypt), La(II) and Ce(II) complexes could be identified.[8] Subsequently, using $(C_5H_4SiMe_3)_3Ln$ precursors, Ln(II) complexes were isolated for the whole lanthanide series in THF, eq 2.2.[16]
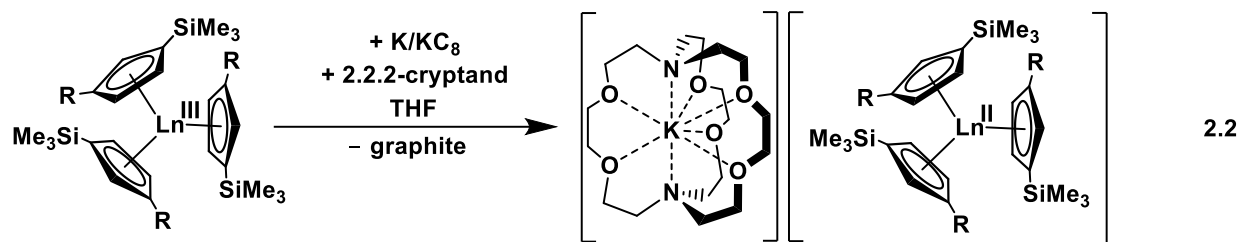
R = SiMe$_3$; Ln = La, Ce, Pr, Nd

R = H; Ln = La, Ce, Pr, Nd, Sm, Gd, Tb, Dy, Ho, Er, Tm, Yb, Lu, Y

The reactivity of isolated $(Cp''_3Ln^{II})^{1-}$ complexes with DME was subsequently investigated and it was found that the isolated Ln(II) complexes slowly react with DME, but do not form the methoxide complexes generated by in situ Cp''_3Ln/K reactions.[17] This was one of several examples of the difference in reactivity of isolated Ln(II) complexes, $[Ln^{II}A_3]^{1-}$ (A = anion) versus in situ $Ln^{III}A_3/M$ reactions.[18–20] Later studies of the reduction of Cp^{Me}_3Ln ($Cp^{Me} = C_5H_4Me$) in THF revealed another way in which in situ LnA_3/M reactions can decompose solvents. For Ln = La and Pr, this led to ring opening of THF to form the $(OCH_2CH_2CH_2CH_2)^{2-}$ dianion, eq 2.3.[21]
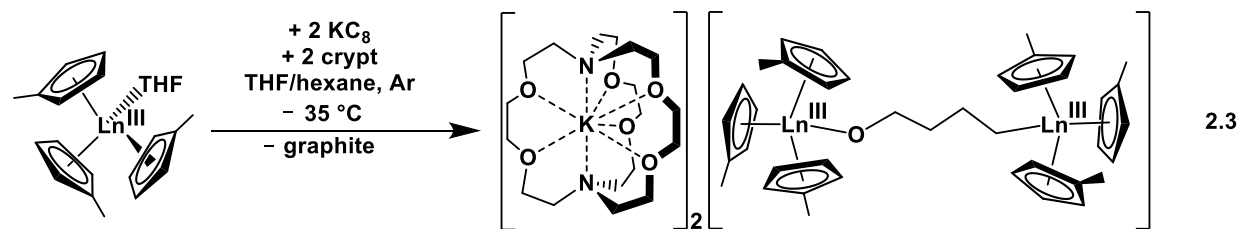
Ln = La, Pr

Although solvent decomposition by Cp^x_3Ln/K (x = Cp'', Cp^{Me}) reactions has been described in several cyclopentadienyl systems, little information is available on the amide reaction manifold, $Ln(NR_2)_3/K$. This Chapter provides more information on solvent reactivity in these

70

reductive systems by describing a series of C–O cleavage products isolated from Ln(NR$_2$)$_3$/K reactions with ethers.

Results and Discussion

Dimethoxyethane (DME). The reduction of Y(NR$_2$)$_3$ in a DME solution at −35 °C using excess cold KC$_8$ in the presence of 2.2.2-cryptand (crypt) produces a dark blue solution that immediately turns to a light-yellow. After removal of spent KC$_8$ by filtration and crystallization under hexanes, colorless crystals form which were identified by X-ray crystallography as [K(crypt)][(R$_2$N)$_3$Y(OCH$_2$CH$_2$OCH$_3$)], **1-Y,** eq 2.4, Figure 2.1.
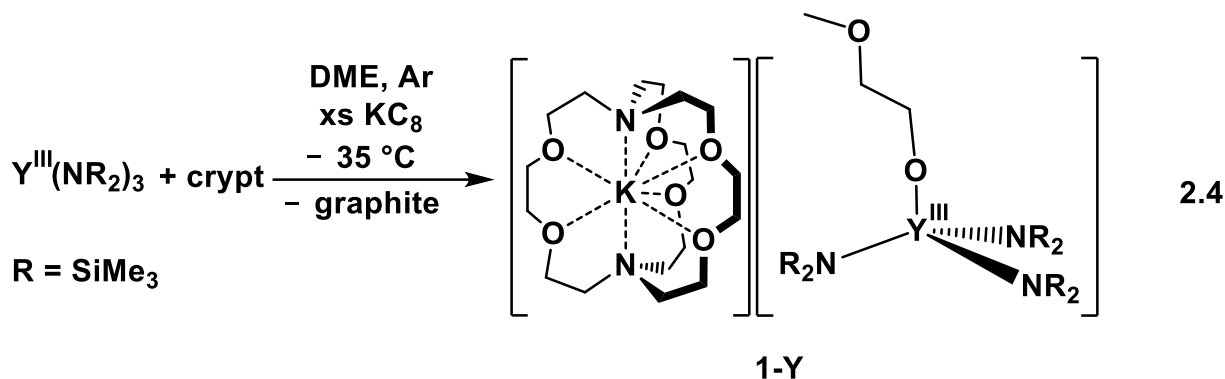
Complex **1-Y** is evidently formed by cleavage of a Me–O bond of DME and differs from the DME cleavage products in Lappert's studies that involved cleavage of an O–CH$_2$ linkage. Analogous reactions in DME in the presence of 18-crown-6 (18-c-6) instead of crypt also display dark blue to yellow color transitions, but the crystal structures of these products could not be solved.
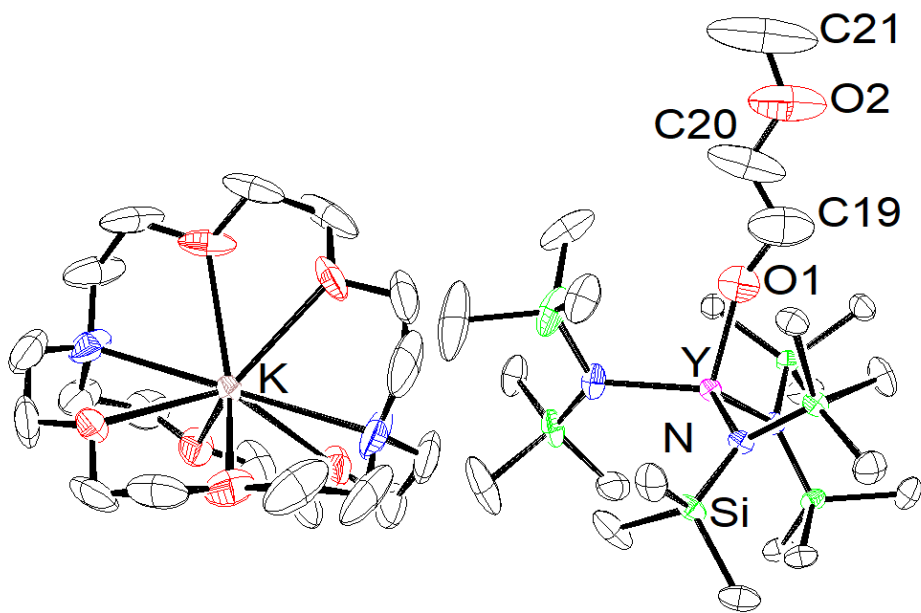
Figure 2.1. Representation of [K(crypt)][(R$_2$N)$_3$Y(OCH$_2$CH$_2$OCH$_3$)], **1-Y**, with atomic displacement parameters drawn at the 50% probability level. Hydrogen atoms were excluded for clarity.

Complex **1-Y** can also be generated by adding DME to a pre-formed solution of [Y(NR$_2$)$_3$]$^{1-}$ in Et$_2$O. Specifically, addition of a −35 °C chilled Et$_2$O solution of Y(NR$_2$)$_3$ and crypt to excess chilled KC$_8$ generates a dark blue solution characteristic of Y(II).[18] After filtration to remove graphite and unreacted KC$_8$, addition of a stoichiometric or excess amount of DME, chilled to −35 °C, immediately turns the solution light yellow. Recrystallization under hexanes at −35 °C produces colorless crystals of **1-Y** which were definitively characterized via crystallography.

Ln(NR$_2$)$_3$/KC$_8$ reactions in DME in the presence of crypt and 18-c-6 were also examined with three lanthanide metals of similar size to yttrium, namely Ln = Ho, Er, and Lu.[22] In all cases, reduction of the Ln(NR$_2$)$_3$ complexes in DME solutions at −35 °C using excess cold KC$_8$, in the presence of either crypt or 18-c-6, produces dark blue solutions that immediately turn to light-

yellow. Only the $Lu(NR_2)_3$ reaction in the presence of 18-c-6 gave a crystallographically characterizable product. After removal of spent KC_8 by filtration and crystallization under hexanes, colorless crystals form which were identified by X-ray crystallography as $[K_2(18\text{-c-}6)_3]\{[(R_2N)_3Lu]_2[(\mu\text{-OCH}_2CH_2O)]\}$, **2-Lu,** eq 2.5, Figure 2.2.
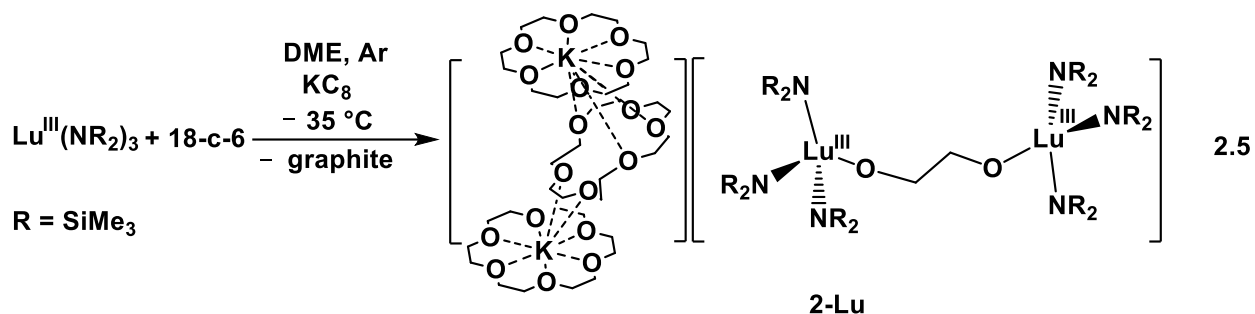
Like **1-Y**, this product is formed by cleavage of Me–O bonds, but in this case both of the C–O bonds of a DME molecule were cleaved and the resulting $(OCH_2CH_2O)^{2-}$ dianion was trapped between two lutetium centers. The isolation of **2-Lu** containing a dianionic DME cleavage fragment may be facilitated by the presence of 18-crown-6 instead of crypt since it can form the dicationic $[K_2(18\text{-c-}6)_3]^{2+}$ countercation. It is possible that both products, **1-Y** and **2-Lu**, form in both reactions, however only one of the products were isolable from each reaction.
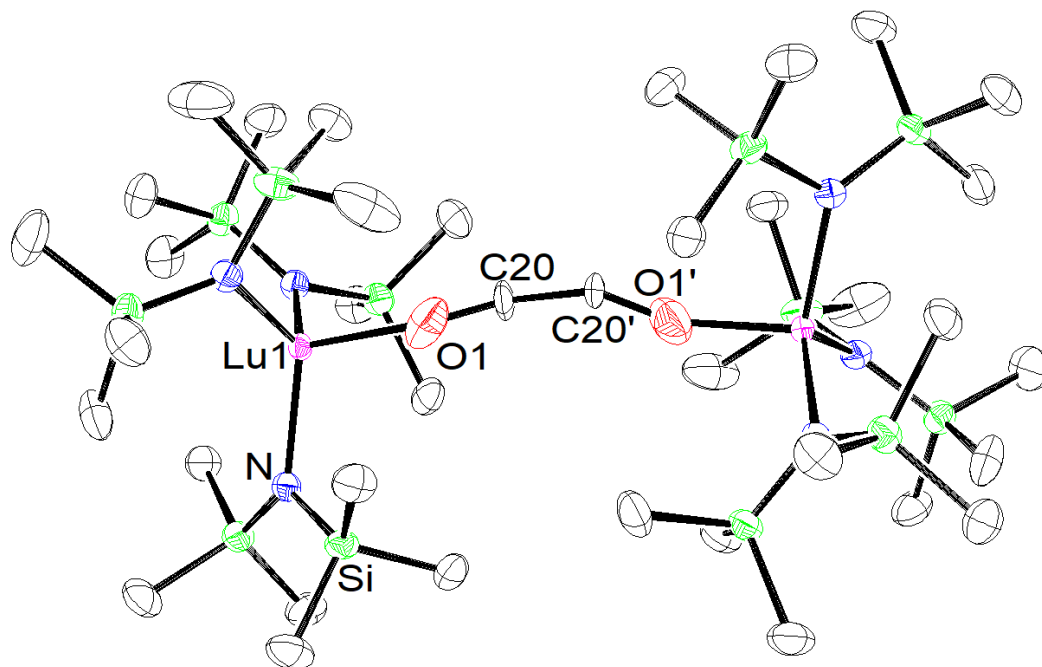
Figure 2.2. Representation of the $[K_2(18\text{-}c\text{-}6)_3]\{[(R_2N)_3Lu]_2[(\mu\text{-}OCH_2CH_2O)]\}$, **2-Lu,** with atomic displacement parameters drawn at the 50% probability level. Hydrogen atoms, $[K_2(18\text{-}c\text{-}6)_3]^{2+}$, a molecule of Et_2O, and a molecule of hexanes are excluded for clarity.

Tetrahydrofuran (THF). Reduction of a $-35\ °C$ solution of $Y(NR_2)_3$ in THF, using excess KC_8 in the presence of crypt, also produces a dark blue solution as it does in DME. After the spent KC_8 is removed by filtration, the dark blue solution remains colored at $-35\ °C$ for about an hour before it turns yellow. Crystallization at $-35\ °C$ under hexanes yielded colorless crystals which were identified by X-ray crystallography as $[K(crypt)][(R_2N)_3Y(OCH_2CH_2CH_2CH_3)]$, **3-Y,** eq 2.6, Figure 2.3. The formation of **3-Y** results from ring opening cleavage of THF, which is well known,[23–39] plus the capture of hydrogen to make an n-butoxide ligand.
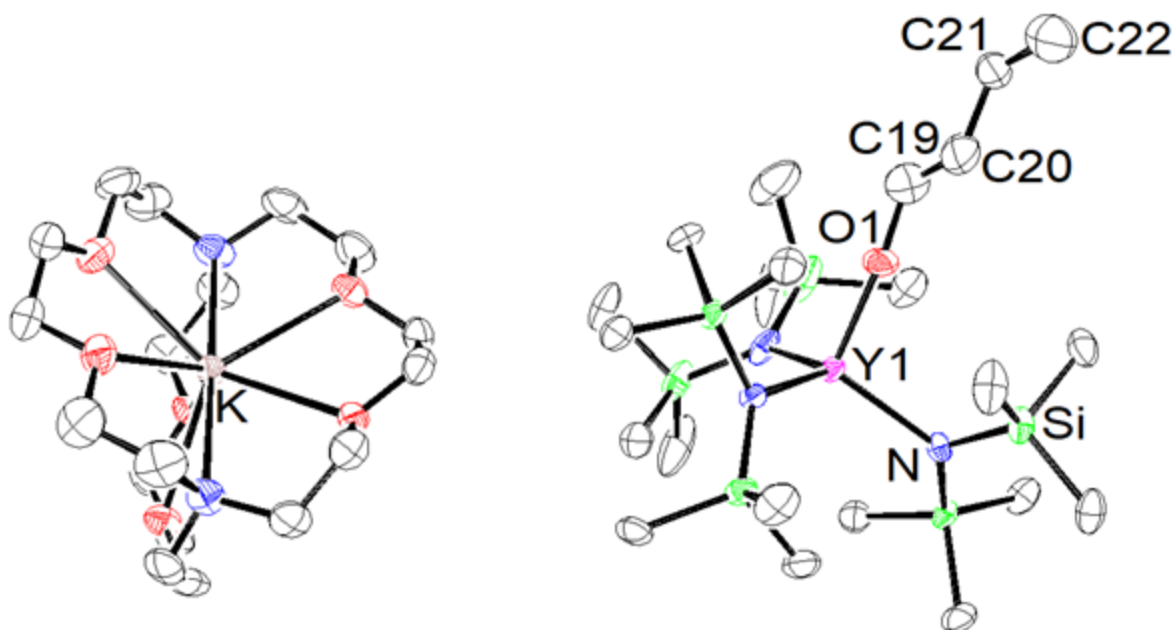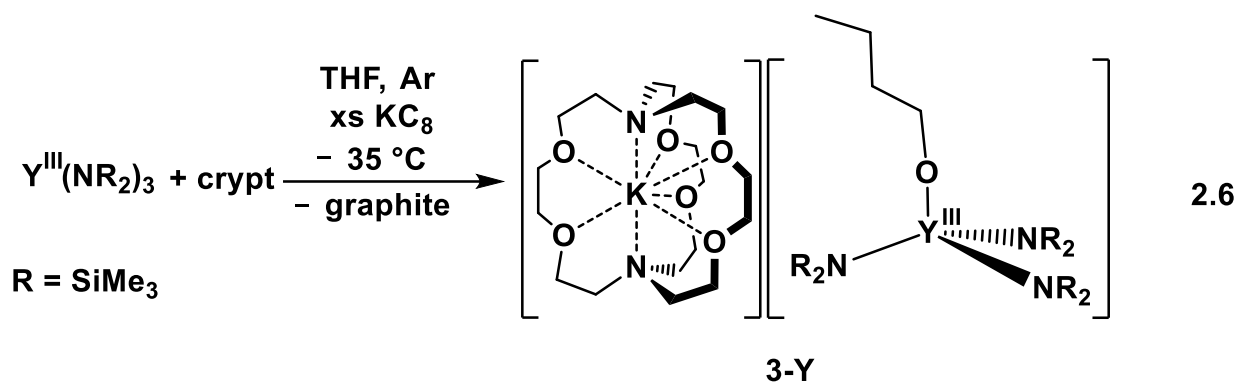
Figure 2.3.   Representation of **3-Y**, [K(crypt)][(R$_2$N)$_3$Y(OCH$_2$CH$_2$CH$_2$CH$_3$)], with atomic displacement parameters drawn at the 50% probability level. Hydrogen atoms are excluded for clarity.

There are many reports in the literature of the ring opening of THF,[23–25,32,34,36–39] but most involve formation of complexes of the (OCH=CH$_2$)$^{1-}$ monoanion. [23,26–28,32] THF decomposition products containing (OCH$_2$CH$_2$CH=CH$_2$)$^{1-}$ [29] and O^{2-} [30,31,34] have also been reported as well as

complexes of the $(OCH_2CH_2CH_2CH_2)^{2-}$ dianion.[21] There are a few examples of the complexes of

the $(OCH_2CH_2CH_2CH_3)^{1-}$ ligand derived from THF.[40–47]

Oxetane (C_3H_6O). Ring opening of the cyclic ether, oxetane, was also examined. When

dark blue solutions of $[Ln^{II}(NR_2)_3]^{1-}$, generated by reduction of chilled Et_2O solutions of $Ln(NR_2)_3$

and 18-c-6 with chilled excess KC_8, were treated with oxetane and swirled, they turned yellow.

No crystallographically characterizable products were isolated for Ln = Y, but for Ln = Ho and Er,

the ring opened oxetane complex $[K(18-c-6)(OC_3H_6)][(R_2N)_3Ln(OCH_2CH_2CH_3)]$, **4-Ln** (Ln = Ho,

Er), eq 2.7, Figure 2.4, could be isolated (Ln = Er, Figure 2.8). This reaction is similar to that in

equation 2.6 in which the ether is ring opened and captures a hydrogen to make an alkoxide, in

this case, n-propoxide.

76
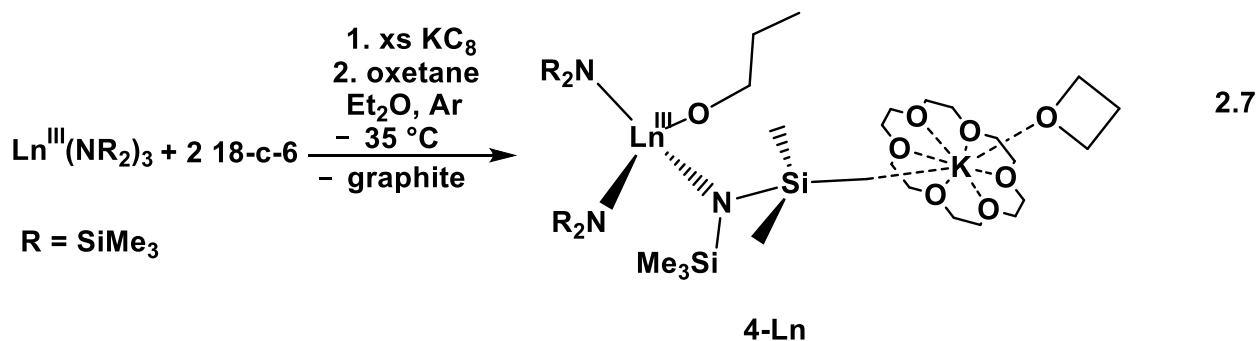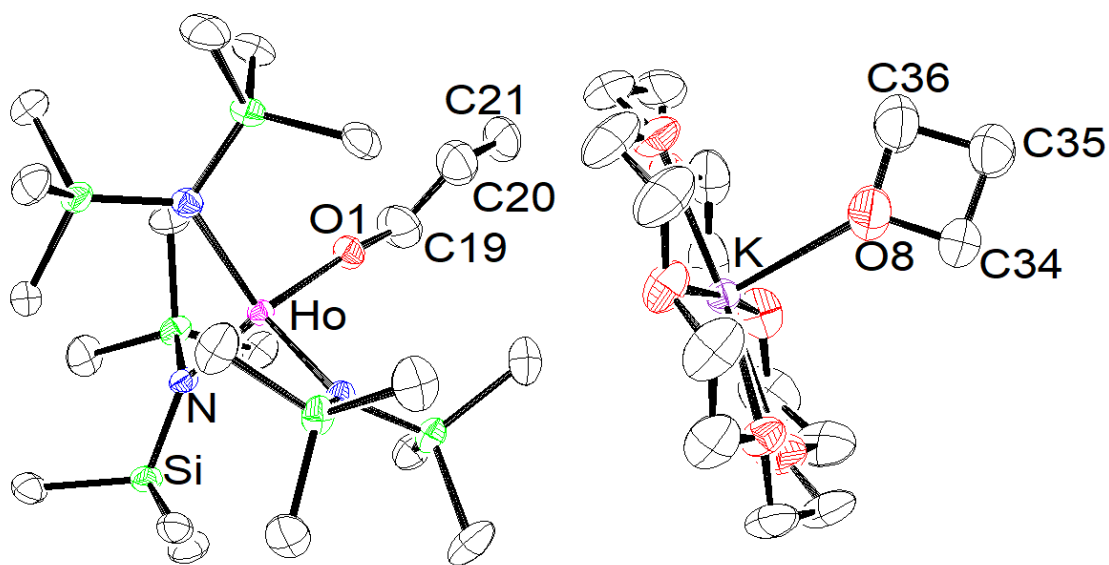
Figure 2.4. Representation of [K(18-c-6)OCH$_2$CH$_2$CH$_2$][(R$_2$N)$_3$Ho(OCH$_2$CH$_2$CH$_3$)], **4-Ho,** with atomic displacement parameters drawn at the 50% probability level. Hydrogen atoms are excluded for clarity.

An intact oxetane is also found in the crystal structure coordinating to the potassium 18-c-6 moiety. The X-ray crystal structure shows a methyl group of an (NR$_2$)$^{1-}$ ligand oriented toward the potassium in the crown on the side opposite the coordinated oxetane. This type of structure has been observed before with the [K(18-c-6)]$^{1+}$ cation.[48–52]

Formation of Cyclometalated Decomposition Products. In addition to the C–O cleavage products isolated from the reductions of amide-ligated rare-earth metal complexes in this study, products of C–H bond activation were also identified. In the Y(NR$_2$)$_3$/KC$_8$ reaction system in Et$_2$O in the presence of crypt, the [K(crypt)]{(R$_2$N)$_2$Y[N(SiMe$_3$)(SiMe$_2$CH$_2$)-κC,κN]}, **5-Y,**

complex, was isolated and crystallographically characterized, eq 2.8, Figure 2.5.

$$Y^{III}(NR_2)_3 + crypt \xrightarrow[\substack{- \text{ graphite}}]{\substack{\text{THF, Ar} \\ \text{xs } KC_8 \\ - \text{ 35 °C}}}$$

R = SiMe$_3$

5-Y

2.8
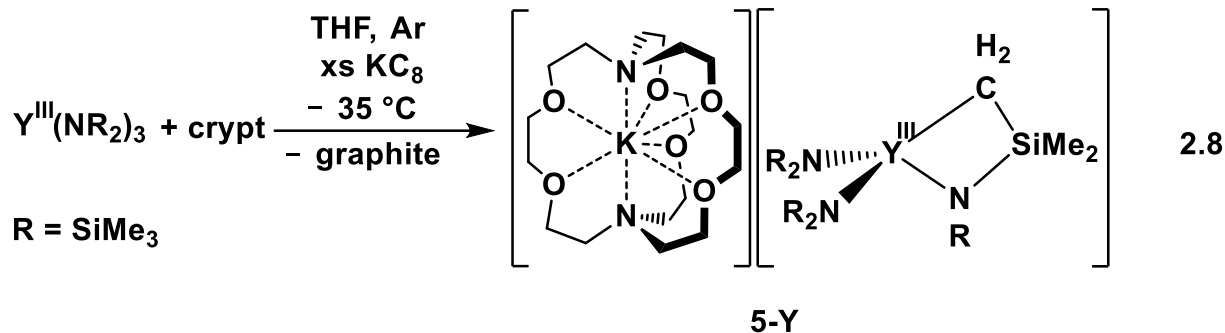
The anion in **5-Y** was previously reported as the $[K(C_6H_6)_2]^{1+}$ salt from the reaction of Y[N(SiMe$_3$)$_2$]$_3$ with KSi(SiMe$_3$)$_3$[53], and as the $[K(18\text{-c-}6)(THF)(toluene)]^{1+}$ salt from the a Y(NR$_2$)$_3$/KC$_8$ reaction in THF at room temperature in the absence of a potassium chelate.[54]
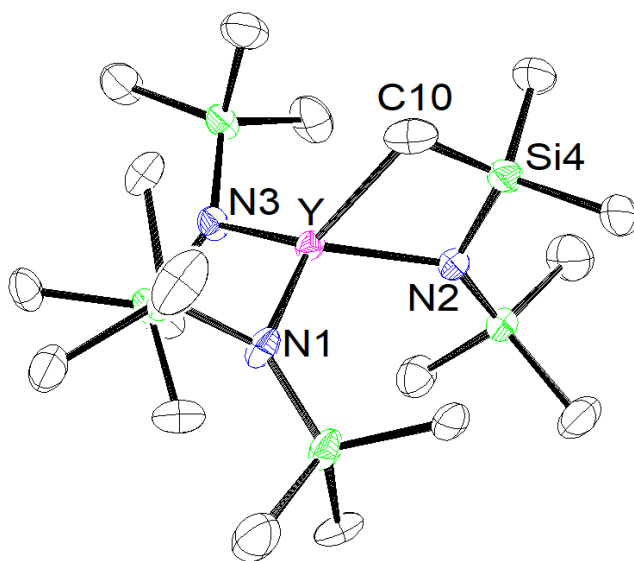
Figure 2.5. Representation of $[K(crypt)]\{(R_2N)_2Y[N(SiMe_3)(SiMe_2CH_2)\text{-}\kappa C,\kappa N]\}$, **5-Y,** with atomic displacement parameters drawn at the 50% probability level. Hydrogen atoms, the $[K(crypt)]^{1+}$ countercation, and 99:1 disorder of the Y position are excluded for clarity.

The [N(SiMe$_3$)$_2$]$^{1-}$ ligand is well known to form cyclometalated products containing the [N(SiMe$_3$)(SiMe$_2$CH$_2$)-κC,κN]$^{2-}$ dianion.[53–61] Furthermore, formation of this dianion by C–H bond activation has also been specifically found in numerous reduction reactions involving rare-earth and actinide metals.[9,55,60–74] Complex **5-Y** was also isolated from the −35 °C reduction of Y(NR$_2$)$_3$ with excess KC$_8$ in the presence of crypt in a 1:1 solution of DME:THF that was carried out to explore whether Y(II) would ring open THF first or cleave DME. As in the other reactions, the dark blue Y(II) solution quickly turns to a light yellow. However, in this case, the decomposition product that crystallizes best is **5-Y**.

Coincidentally, the structure of complex **5** is isomorphous with the structures of the Ln(II) complexes, [K(crypt)][(R$_2$N)$_3$Ln], **8-Ln**, for Ln = Gd, Tb, Dy, Sc. This has previously been observed for other pairs of complexes involving [N(SiMe$_3$)$_2$]$^{1-}$ and [N(SiMe$_3$)(SiMe$_2$CH$_2$)-κC,κN]$^{2-}$, e.g. [K(crypt)][(C$_5$Me$_5$)$_2$Y{N(SiMe$_3$)(SiMe$_2$CH$_2$)-κC,κN}], [K(crypt)][(C$_5$Me$_5$)$_2$Y(NR$_2$)], [K(crypt)][(C$_5$Me$_4$H)$_2$Y{N(SiMe$_3$)(SiMe$_2$CH$_2$)-κC,κN}] and [K(crypt)][(C$_5$Me$_4$H)$_2$Y(NR$_2$)].[60] Comparison of **5-Y** with **8-Y** for yttrium is not possible since **8-Y** has not been crystallographically characterized. However, the holmium and erbium cyclometalates, [K(crypt)]{(R$_2$N)$_2$Ln[N(SiMe$_3$)(SiMe$_2$CH$_2$)-κC,κN]}, **5-Ln** (Ln = Ho, Er), could be isolated from the reduction of Ln(NR$_2$)$_3$ with excess KC$_8$ in the presence of crypt in Et$_2$O, and they too are isomorphous with **8-Ln** and the other structures (See Figure 2.9 and Figure 2.10).

When 18-c-6 is used instead of crypt in the analogous reaction of Y(NR$_2$)$_3$ with excess KC$_8$ in Et$_2$O, the same anion was isolated with a different countercation, {[K(18-c-6)]{(R$_2$N)$_2$Y[N(SiMe$_3$)(SiMe$_2$CH$_2$)-κC,κN]}}$_n$, **6-Y**, eq 2.9, Figure 2.6.

$Y^{III}(NR_2)_3 + 2$ 18-c-6 $\xrightarrow[\text{-graphite}]{\substack{\text{Et}_2\text{O, Ar} \\ \text{xs KC}_8 \\ -35\,°\text{C}}}$

R = SiMe₃

6-Y + **7-Y**   2.9
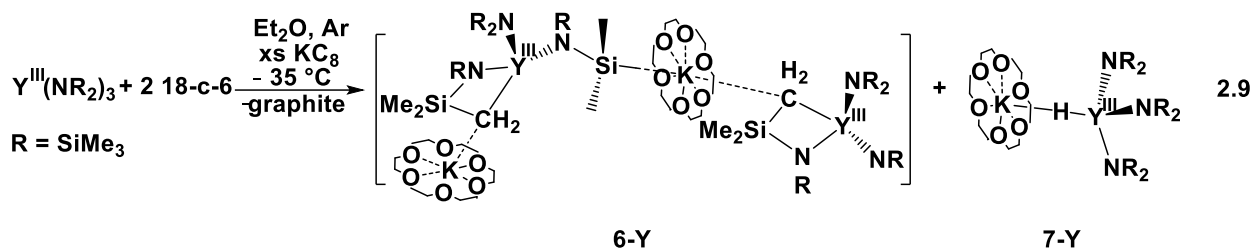
In this case, the complex crystallizes as an extended structure in which the $[\text{K}(18\text{-c-}6)]^{1+}$ cation has a methyl group of a Me₃Si unit on one side, and a methylene of a (SiMe₂CH₂) moiety on the other side. There is precedent in the structural chemistry of the $[\text{K}(18\text{-c-}6)]^{1+}$ cation to form extended structures with silylmethyl groups oriented toward the potassium.[48–51] In the (2,2,6,6-tetramethylpiperidin-1-yl)oxyl complex, $\{[(18\text{-c-}6)\text{K}][(\mu\text{-Me}_3\text{Si})(\text{Me}_3\text{Si})\text{N}]_2[\text{Gd}(\text{NR}_2)(\eta^1\text{-}$ $\text{ONC}_5\text{H}_6\text{Me}_4)]\}_n$, trimethylsilyl groups are oriented to both sides of the $\{[(18\text{-c-}6)\text{K}]^{1+}$ cation.[52]
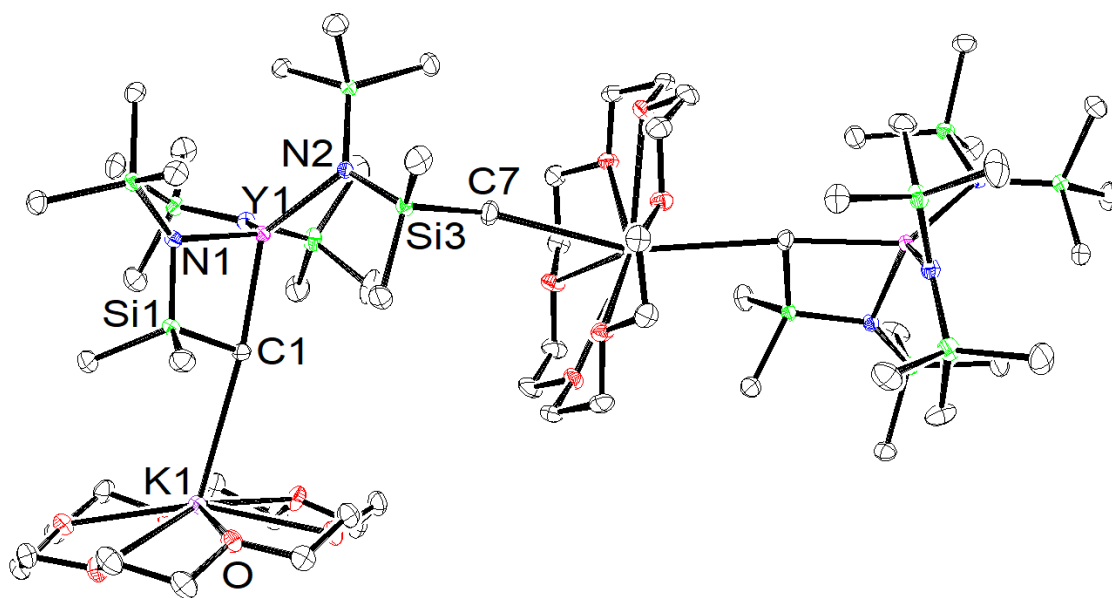
Figure 2.6. Representation of the extended structure of $\{[\text{K}(18\text{-c-}6)]\{(\text{R}_2\text{N})_2\text{Y}[\text{N}(\text{R})(\text{SiMe}_2\text{CH}_2)\text{-}$ $\kappa\text{C},\kappa\text{N}]\}\}_n$, **6-Y**, with atomic displacement parameters drawn at the 50% probability level. Hydrogen atoms are excluded for clarity.

The Y(NR$_2$)$_3$/KC$_8$ reaction system has also yielded a hydride product, [K(18-c-6)][(R$_2$N)$_3$YH], **7-Y**, eq 2.9, Figure 2.7, which was also isolated from the reduction of Y(NR$_2$)$_3$ with excess KC$_8$ in Et$_2$O in the presence of 18-c-6. The hydride ligand in **7-Y** is formally the other product of a reductive C–H cleavage that forms the [N(SiMe$_3$)(SiMe$_2$CH$_2$)-κC,κN]$^{2-}$ dianion. Formation of hydride byproducts in rare-earth reduction reactions has been observed before in the reduction of [((^{Ad,Me}ArO)$_3$mes)Ln],[69–71] and of [((^{Ad,Me}ArO)$_3$mes)U].[75,76] This yttrium hydride is unusual in that the hydride ligand is oriented toward the [K(18-c-6)]$^{1+}$ cation.
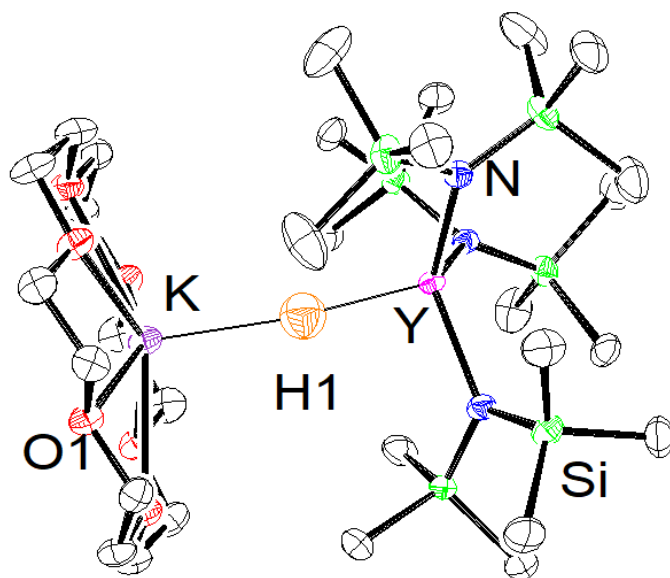
Figure 2.7. Representation of [K(18-c-6)][(R$_2$N)$_3$YH], **7-Y,** with atomic displacement parameters drawn at the 50% probability level. Hydrogen atoms are excluded for clarity.

Crystallographic Details. Ln–O Structures. The four structures containing Ln–O bonds derived from C–O bond cleavage reactions have metals coordinated by three amide ligands and an anionic oxygen donor atom ligand, and thus require countercations for charge balance: [K(crypt)][(R$_2$N)$_3$Y(OCH$_2$CH$_2$OCH$_3$)], **1-Y**, [K$_2$(18-c-6)$_3$]{[(R$_2$N)$_3$Lu]$_2$[(μ-OCH$_2$CH$_2$O$_2$)]}, **2-**

Lu, [K(crypt)][(R$_2$N)$_3$Y(OCH$_2$CH$_2$CH$_2$CH$_3$)], **3-Y,** and [K(18-c-6)(OC$_3$H$_6$)][(R$_2$N)$_3$Ln(OCH$_2$CH$_2$CH$_3$)], **4-Ln,** Table 2.1.

Complexes **1-Y**, **2-Lu**, **3-Y**, and **4-Ln** all have a distorted tetrahedral coordination environment around the metal formed by the three amide ligands and one O-bound ligand. As shown in Table 2.1, the Ln–N distances fall in the narrow range of 2.25-2.30 Å since the structures are similar and the metals are close in radial size. The Ln–O distances and Ln–O–C angles are also similar, as are the N–Ln–N and N–Ln–O angles. In **4-Ln¸** both show interaction between a SiMe$_3$–C bond and the potassium, with a C–K distance of 3.280(3) Å and 3.285(3) Å, for Ho and Er respectively.

Table 2.1. Selected bond distances (Å) and angles (°) for [K(crypt)][(R$_2$N)$_3$Y(OCH$_2$CH$_2$OCH$_3$)], **1-Y**, [K$_2$(18-c-6)$_3$]{[(R$_2$N)$_3$Lu]$_2$[(μ-OCH$_2$CH$_2$O$_2$)]}, **2-Lu,** [K(crypt)][(R$_2$N)$_3$Y(OCH$_2$CH$_2$CH$_2$-CH$_3$)], **3-Y¸** and [K(18-c-6)(OC$_3$H$_6$)][(R$_2$N)$_3$Ln(OCH$_2$CH$_2$CH$_3$)], **4-Ln**.

	Ln–O	Ln–N	C–O–Ln	N–Ln–N	N–Ln–O
1-Y	2.115(4)	2.25(1) – 2.30(1)	159.0(5)	114.7(1) – 117.0(5)	102.0(1) – 104.6(1)
2-Lu	2.113(3)	2.234(2) – 2.247(2)	159.2(4)	113.02(8) – 117.08(8)	101.21(10) – 106.10(10)
3-Y	2.038(4)	2.288(4) – 2.298(4)	161.4(5)	113.39(14) – 116.04(13)	101.85(17) – 103.00(14)
4-Ho	2.045(2)	2.280(2) – 2.293(2)	165.2(2)	112.89(8) – 116.33(8)	103.27(9) – 103.91(9)
4-Er	2.036(2)	2.270(2) – 2.288(2)	164.9(2)	112.77(7) – 116.09(7)	103.69(7) – 104.27(7)

The [K(crypt)]{(R$_2$N)$_2$Y[N(SiMe$_3$)(SiMe$_2$CH$_2$)-κC,κN]}), **5-Y**, complexes have two conventional (R$_2$N)$^{1-}$ amides ligands per metal along with another amide that has been metalated to form a dianion. All the Ln–N distances are in the range of 2.24-2.30 Å similar to those above. The Ln–C distances are longer at 2.44-2.70 Å.

The (18-c-6)K(μ-H)Y(R$_2$N)$_3$Y complex, **6-Y**, is a tris-amide complex with an unusual hydride ligand oriented toward the potassium in the 18-c-6 ligand. The Y–N distances fall within the range of the other complexes which demonstrates that these bond lengths are rather uniform across a range of complexes. The metal hydride distances could not be determined with great accuracy, but it appears the hydride is much closer to yttrium (2.18(4) Å) than potassium (2.61(4) Å). Hence, **6-Y** constitutes yet another example of how the [K(18-c-6)]$^{1+}$ cation orients in crystals to add electron density around potassium.

Conclusion

The high reactivity of Ln(NR$_2$)$_3$/KC$_8$ reduction system is demonstrated by X-ray crystal structures of four different types of C–O bond cleavage products that result from decomposition of DME, THF, and oxetane. When other substrates are absent, and if the low temperatures needed to isolate the Ln(II) complexes, [Ln(NR$_2$)$_3$]$^{1-}$, are not maintained, the systems will clearly decompose solvents. As shown here, a variety of alkoxide products result from these reactions including (OCH$_2$CH$_2$OCH$_3$)$^{1-}$, (OCH$_2$CH$_2$CH$_2$CH$_3$)$^{1-}$, and (OCH$_2$CH$_2$CH$_3$)$^{1-}$. Although Et$_2$O is not attacked by this system, decomposition can occur in this solvent via C–H bond activation that generates complexes of [N(SiMe$_3$)(SiMe$_2$CH$_2$)]$^{2-}$ and H^{1-} ligands.

Experimental Details

All manipulations and syntheses described below were conducted with the rigorous exclusion of air and water using standard Schlenk line and glovebox techniques under an argon or dinitrogen atmosphere. Solvents were sparged with UHP argon and dried by passage through columns containing Q-5 and molecular sieves prior to use. Dimethoxyethane (DME) and oxetane were dried over Na/benzophenone then freeze-pump-thawed and stored over 3Å molecular sieves. All solvents were stored over 3Å molecular sieves. 2.2.2-Cryptand (crypt, Merck) was placed under vacuum (10^{-4} torr) for 12 h before use. 18-Crown-6 (18-c-6, Alfa Aesar) was sublimed before use. $Ln(NR_2)_3$ was synthesized according to literature procedures.[77]

[K(crypt)][(R₂N)₃Y(OCH₂CH₂OCH₃)], 1-Y. In an argon filled glovebox, a DME solution of $Y(NR_2)_3$ (50 mg, 0.09 mmol) and crypt (33 mg, 0.090 mmol) was cooled to −35 °C and was added to a −35 °C chilled vial of excess KC_8. The colorless solution went to dark blue and was swirled for a few seconds before turning light yellow. This light yellow solution was filtered layered into a −35 °C chilled vial of hexanes and placed in a −35 °C freezer to crystallize. Colorless crystals were isolated and crystallographically characterized as **1-Y**.

[K₂(18-c-6)₃]{[(R₂N)₃Lu]₂[(μ-OCH₂CH₂O₂)]}, 2-Lu. In an argon filled glovebox, a DME solution of $Lu(NR_2)_3$ (50 mg, 0.08 mmol) and 18-c-6 (40. mg, 0.15 mmol) was cooled to −35 °C and was added to a −35 °C chilled vial of excess KC_8. The colorless solution went to dark blue and was swirled for a few seconds before turning light yellow. This light yellow solution was filtered layered into a −35 °C chilled vial of hexanes and placed in a −35 °C freezer to crystallize. Colorless crystals were isolated and crystallographically characterized as **2-Lu**.

[K(crypt)][(R₂N)₃Y(OCH₂CH₂CH₂CH₃)], 3-Y. In an argon filled glovebox, a THF solution of $Y(NR_2)_3$ (50 mg, 0.09 mmol) and crypt (33 mg, 0.090 mmol) was cooled to −35 °C and was added to a −35 °C chilled vial of excess KC_8. The colorless solution went to dark blue

and was swirled for a few seconds before turning light yellow. This light yellow solution was filtered layered into a −35 °C chilled vial of hexanes and placed in a −35 °C freezer to crystallize. Colorless crystals were isolated and crystallographically characterized as **3-Y**.

[K(18-c-6)OCH₂CH₂CH₂][(R₂N)₃Ho(OCH₂CH₂CH₃)], 4-Ho. In an argon filled glovebox, an Et₂O solution of Ho(NR₂)₃ (50 mg, 0.08 mmol) and 18-c-6 (41 mg, 0.15 mmol) was cooled to −35 °C and was added to a −35 °C chilled vial of excess KC₈. The colorless solution went to dark blue and was filtered. Oxetane (5 µL, 0.08 mmol), chilled to −35 °C, was then added dropwise and the solution was swirled for a few seconds before turning from dark blue to light pink. This light pink solution was filtered layered into a −35 °C chilled vial of hexanes and placed in a −35 °C freezer to crystallize. Yellow crystals were isolated and crystallographically characterized as **4-Ho**.

[K(18-c-6)OCH₂CH₂CH₂][(R₂N)₃Er(OCH₂CH₂CH₃)], 4-Er. In an argon filled glovebox, an Et₂O solution of Er(NR₂)₃ (50 mg, 0.08 mmol) and 18-c-6 (41 mg, 0.15 mmol) was cooled to −35 °C and was added to a −35 °C chilled vial of excess KC₈. The colorless solution went to dark blue and was filtered. Oxetane (5 µL, 0.08 mmol), chilled to −35 °C, was then added dropwise and the solution was swirled for a few seconds before turning from dark blue to light pink. This light pink solution was filtered layered into a −35 °C chilled vial of hexanes and placed in a −35 °C freezer to crystallize. Yellow crystals were isolated and crystallographically characterized as **4-Er**.

[K(crypt)]{(R₂N)₂Y[N(SiMe₃)(SiMe₂CH₂)-*κ*C,*κ*N]}), 5-Y. In an argon filled glovebox, a THF:DME (1:1) solution of Y(NR₂)₃ (50 mg, 0.09 mmol) and crypt (33 mg, 0.090 mmol) was cooled to −35 °C and was added to a −35 °C chilled vial of excess KC₈. The colorless solution went to dark blue and was swirled for a few seconds before turning light yellow. This light yellow

solution was filtered layered into a −35 °C chilled vial of hexanes and placed in a −35 °C freezer to crystallize. Colorless crystals were isolated and crystallographically characterized as **5-Y**.

[K(crypt)]{(R₂N)₂Er[N(SiMe₃)(SiMe₂CH₂)-*κ*C,*κ*N]}), 5-Er. In an argon filled glovebox, a THF solution of Er(NR₂)₃ (50 mg, 0.08 mmol) and crypt (29 mg, 0.080 mmol) was cooled to −35 °C and was added to a −35 °C chilled vial of excess KC₈. The light pink solution went to dark blue. This dark blue solution was filtered layered into a −35 °C chilled vial of hexanes and placed in a −35 °C freezer to crystallize. Overnight, the dark blue solution turned light pink. Colorless crystals were isolated and crystallographically characterized as **5-Er**.

[K(crypt)]{(R₂N)₂Ho[N(SiMe₃)(SiMe₂CH₂)-*κ*C,*κ*N]}), 5-Ho. In an argon filled glovebox, a THF solution of Ho(NR₂)₃ (50 mg, 0.08 mmol) and crypt (29 mg, 0.080 mmol) was cooled to −35 °C and was added to a −35 °C chilled vial of excess KC₈. The light pink solution went to dark blue. This dark blue solution was filtered layered into a −35 °C chilled vial of hexanes and placed in a −35 °C freezer to crystallize. Overnight, the dark blue solution turned light pink. Colorless crystals were isolated and crystallographically characterized as **5-Ho**.

[K(18-c-6)]{(R₂N)₂Y[N(SiMe₃)(SiMe₂CH₂)-*κ*C,*κ*N]}, 6-Y. In an argon filled glovebox, an Et₂O solution of Y(NR₂)₃ (50 mg, 0.09 mmol) and 18-c-6 (46 mg, 0.18 mmol) was cooled to −35 °C and was added to a −35 °C chilled vial of excess KC₈. The colorless solution went to dark blue and was swirled for a minute before turning light yellow. This light yellow solution was filtered layered into a −35 °C chilled vial of hexanes and placed in a −35 °C freezer to crystallize. Colorless crystals were isolated and crystallographically characterized as **6-Y**.

[K(18-c-6)][(R₂N)₃YH], 7-Y. In an argon filled glovebox, an Et₂O solution of Y(NR₂)₃ (50 mg, 0.09 mmol) and 18-c-6 (46 mg, 0.18 mmol) was cooled to −35 °C and was added to a −35

°C chilled vial of excess KC$_8$. The colorless solution went to dark blue and was swirled for a minute before turning light yellow. This light yellow solution was filtered layered into a −35 °C chilled vial of hexanes and placed in a −35 °C freezer to crystallize. Colorless crystals were isolated and crystallographically characterized as **7-Y**.

X-ray Data Collection, Structure, Solution, Refinement
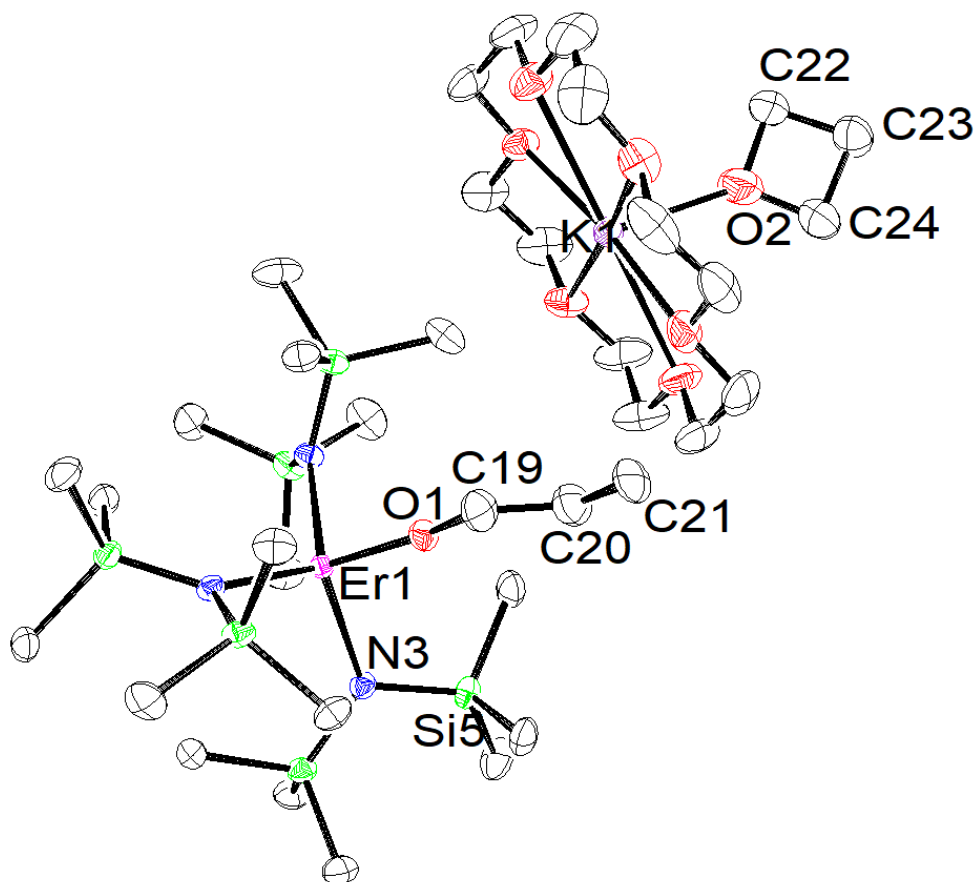
Figure 2.8. Representation of [K(18-c-6)OCH$_2$CH$_2$CH$_2$][(R$_2$N)$_3$Er(OCH$_2$CH$_2$CH$_3$)], **4-Er,** with atomic displacement parameters drawn at the 50% probability level. Hydrogen atoms are excluded for clarity.
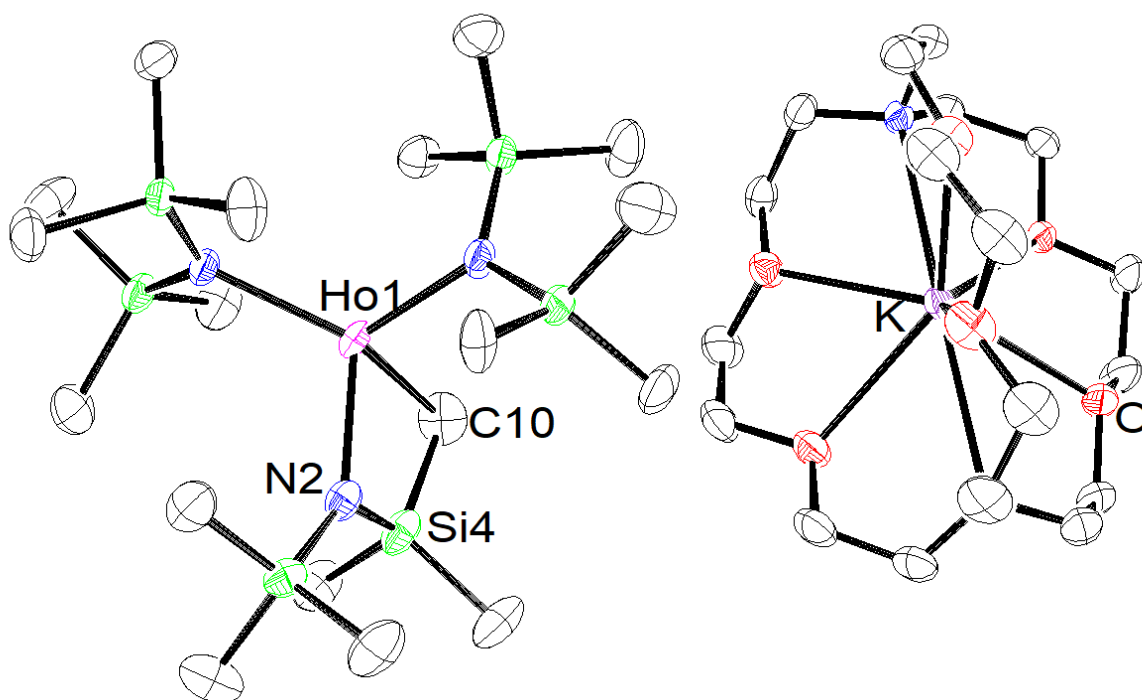
Figure 2.9. Representation of [K(crypt)]{(R$_2$N)$_2$Ho[N(SiMe$_3$)(SiMe$_2$CH$_2$)-κC,κN]}, **5-Ho,** with atomic displacement parameters drawn at the 50% probability level. Hydrogen atoms and disorder are excluded for clarity. There is disorder for the Er atom that sits slightly above the plane made by the N atoms and below the plane.
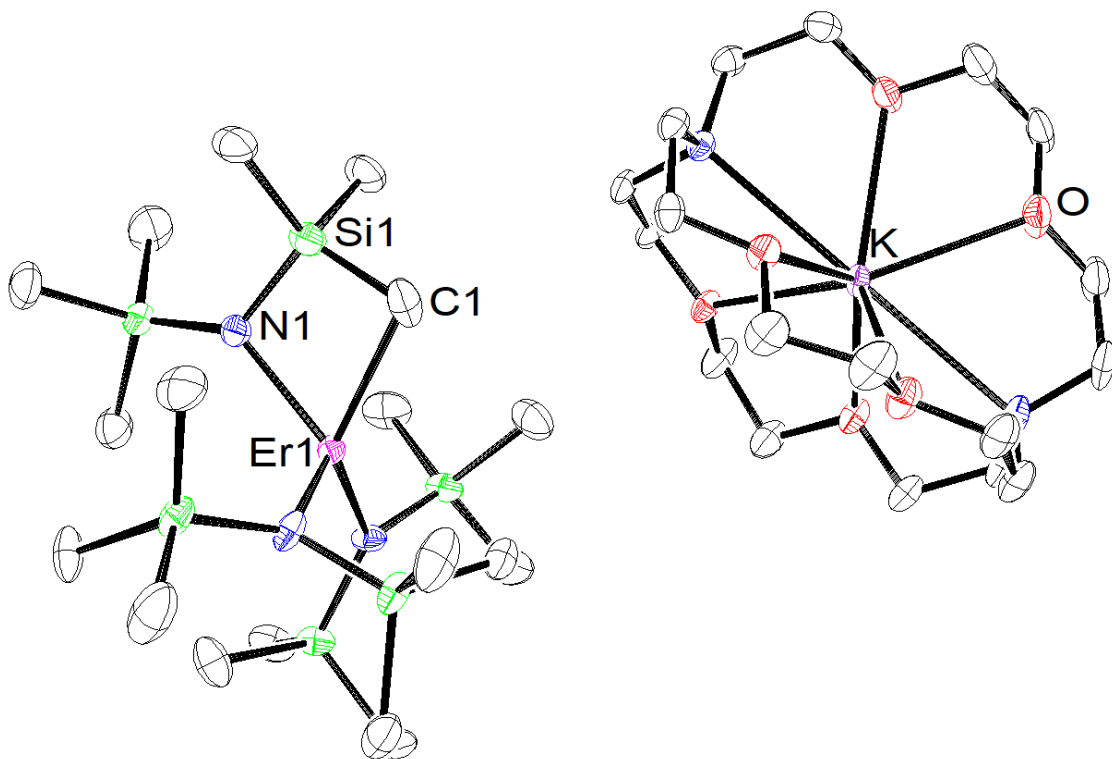
Figure 2.10. Representation of [K(crypt)]{(R$_2$N)$_2$Er[N(SiMe$_3$)(SiMe$_2$CH$_2$)-κC,κN]}, **5-Er,** with atomic displacement parameters drawn at the 50% probability level. Hydrogen atoms and disorder are excluded for clarity. There is disorder for the Er atom that sits slightly above the plane made by the N atoms and below the plane.

Table 2.2. Crystal data and structure refinement for **1-Y**.

Identification code	abc52 (Amanda Chung)
Empirical formula	C$_{39}$ H$_{97}$ K N$_5$ O$_8$ Si$_6$ Y
Formula weight	1060.76
Temperature	93(2) K
Wavelength	0.71073 Å
Crystal system	Monoclinic
Space group	*P2$_1$/c*
Unit cell dimensions	a = 17.9727(7) Å α = 90°.
	b = 13.5766(6) Å β = 93.9471(7)°.
	c = 24.0001(10) Å γ = 90°.

Volume	5842.3(4) Å^3
Z	4
Density (calculated)	1.206 Mg/m^3
Absorption coefficient	1.238 mm^{-1}
F(000)	2288
Crystal color	colorless
Crystal size	0.388 x 0.252 x 0.220 mm^3
Theta range for data collection	1.701 to 27.074°
Index ranges	-22 ≤ h ≤ 23, -17 ≤ k ≤ 17, -30 ≤ l ≤ 30
Reflections collected	93382
Independent reflections	12815 [R(int) = 0.0553]
Completeness to theta = 25.242°	100.0 %
Absorption correction	Semi-empirical from equivalents
Max. and min. transmission	0.7455 and 0.6803
Refinement method	Full-matrix least-squares on F^2
Data / restraints / parameters	12815 / 0 / 569
Goodness-of-fit on F^2	1.128
Final R indices [I>2sigma(I) = 10875 data]	R1 = 0.0704, wR2 = 0.1478
R indices (all data, 0.78 Å)	R1 = 0.0841, wR2 = 0.1539
Largest diff. peak and hole	2.103 and -1.636 e.Å^{-3}

Table 2.3. Selected bond lengths [Å] and angles [°] for **1-Y**.

Y(1)-O(1)	2.115(4)
Y(1)-N(2)	2.293(3)
Y(1)-N(1)	2.294(3)
Y(1)-N(3)	2.296(4)
Y(2)-N(3)	2.247(13)
Y(2)-N(1)	2.296(11)
Y(2)-N(2)	2.303(10)
O(1)-C(19)	1.368(9)
O(2)-C(21)	1.357(13)
O(2)-C(20)	1.380(10)
C(19)-C(20)	1.385(13)

O(1)-Y(1)-N(2)	102.03(13)
O(1)-Y(1)-N(1)	104.61(13)
N(2)-Y(1)-N(1)	115.15(11)
O(1)-Y(1)-N(3)	102.40(16)
N(2)-Y(1)-N(3)	115.45(12)
N(1)-Y(1)-N(3)	114.66(12)
N(3)-Y(2)-N(1)	116.5(5)
N(3)-Y(2)-N(2)	117.0(5)
N(1)-Y(2)-N(2)	114.7(5)
C(19)-O(1)-Y(1)	159.0(5)
C(21)-O(2)-C(20)	125.7(12)
O(1)-C(19)-C(20)	115.5(9)
O(2)-C(20)-C(19)	117.3(11)

_____

Table 2.4. Crystal data and structure refinement for **2-Lu**.

Identification code	abc71 (Amanda Chung)
Empirical formula	$C_{84} H_{208} K_2 Lu_2 N_6 O_{21} Si_{12}$
Formula weight	2403.77
Temperature	133(2) K
Wavelength	0.71073 Å
Crystal system	Monoclinic
Space group	*C2/c*
Unit cell dimensions	a = 28.370(6) Å $\quad$ α = 90°.
	b = 17.809(4) Å $\quad$ β = 106.343(3)°.
	c = 25.850(6) Å $\quad$ γ = 90°.
Volume	12533(5) Å^3
Z	4
Density (calculated)	1.274 Mg/m^3
Absorption coefficient	1.804 mm^{-1}
F(000)	5080
Crystal color	purple
Crystal size	0.567 x 0.497 x 0.144 mm^3
Theta range for data collection	1.366 to 29.206°
Index ranges	$-38 \le h \le 38$, $-24 \le k \le 24$, $-35 \le l \le 35$
Reflections collected	147532

Independent reflections   16944 [R(int) = 0.0347]

Completeness to theta = 25.242°   100.0 %

Absorption correction   Semi-empirical from equivalents

Max. and min. transmission   0.7458 and 0.5535

Refinement method   Full-matrix least-squares on F^2

Data / restraints / parameters   16944 / 0 / 602

Goodness-of-fit on F^2 1.058

Final R indices [I>2sigma(I) = 14757 data]   R1 = 0.0328, wR2 = 0.0728

R indices (all data, 0.73 Å)   R1 = 0.0417, wR2 = 0.0800

Largest diff. peak and hole   1.874 and -1.106 e.Å^{-3}

Table 2.5. Selected bond lengths [Å] and angles [°] for **2-Lu**.

_____

Lu(1)-O(1)	2.113(3)
Lu(1)-N(2)	2.234(2)
Lu(1)-N(1)	2.245(2)
Lu(1)-N(3)	2.247(2)
O(1)-C(20)	1.286(6)
O(1)-C(19)	1.640(6)
C(19)-C(19)#1	0.870(11)
C(20)-C(20)#1	1.529(10)
O(1)-Lu(1)-N(2)	101.21(10)
O(1)-Lu(1)-N(1)	106.10(10)
N(2)-Lu(1)-N(1)	115.32(8)
O(1)-Lu(1)-N(3)	101.34(10)
N(2)-Lu(1)-N(3)	113.02(8)
N(1)-Lu(1)-N(3)	117.08(8)
C(20)-O(1)-Lu(1)	159.2(4)
C(19)-O(1)-Lu(1)	151.2(3)
C(19)#1-C(19)-O(1)	139.1(9)
O(1)-C(20)-C(20)#1	149.7(6)

_____

Symmetry transformations used to generate equivalent atoms:

#1 -x+1,y,-z+1/2   #2 -x+1,-y+1,-z+1   #3 -x+1,y,-z+3/2

#4 -x+3/2,-y+1/2,-z+1

Table 2.6. Crystal data and structure refinement for **3-Y**.

Identification code	abc58 (Amanda Chung)
Empirical formula	$C_{40} H_{99} K N_5 O_7 Si_6 Y$
Formula weight	1058.79
Temperature	93(2) K
Wavelength	0.71073 Å
Crystal system	Monoclinic
Space group	$P2_1/c$
Unit cell dimensions	a = 17.813(5) Å $\quad$ $\alpha = 90°$.
	b = 13.782(4) Å $\quad$ $\beta = 92.364(6)°$.
	c = 24.253(7) Å $\quad$ $\gamma = 90°$.
Volume	5949(3) $Å^3$
Z	4
Density (calculated)	1.182 Mg/m^3
Absorption coefficient	1.214 mm^{-1}
F(000)	2288
Crystal color	colorless
Crystal size	0.301 x 0.290 x 0.273 mm^3
Theta range for data collection	1.681 to 25.349°
Index ranges	$-20 \leq h \leq 21, -16 \leq k \leq 16, -29 \leq l \leq 19$
Reflections collected	24020
Independent reflections	10167 [R(int) = 0.0542]
Completeness to theta = 25.242°	93.3 %
Absorption correction	Semi-empirical from equivalents
Max. and min. transmission	0.7454 and 0.5229
Refinement method	Full-matrix least-squares on F^2
Data / restraints / parameters	10167 / 0 / 560
Goodness-of-fit on F^2	1.053
Final R indices [I>2sigma(I) = 7267 data]	R1 = 0.0635, wR2 = 0.1566
R indices (all data, 0.83 Å)	R1 = 0.0959, wR2 = 0.1734
Largest diff. peak and hole	1.475 and -0.951 e.$Å^{-3}$

Table 2.7. Selected bond lengths [Å] and angles [°] for **3-Y**.

Y(1)-O(1)	2.038(4)
Y(1)-N(2)	2.288(4)
Y(1)-N(3)	2.295(4)
Y(1)-N(1)	2.298(4)
O(1)-C(19)	1.433(8)
C(19)-C(20)	1.430(10)
C(20)-C(21)	1.517(9)
C(21)-C(22)	1.469(10)
O(1)-Y(1)-N(2)	103.00(14)
O(1)-Y(1)-N(3)	105.37(15)
N(2)-Y(1)-N(3)	116.04(13)
O(1)-Y(1)-N(1)	101.85(17)
N(2)-Y(1)-N(1)	114.93(14)
N(3)-Y(1)-N(1)	113.39(14)
C(19)-O(1)-Y(1)	161.4(5)
C(20)-C(19)-O(1)	113.0(7)
C(19)-C(20)-C(21)	116.8(7)
C(22)-C(21)-C(20)	116.1(7)

Table 2.8. Crystal data and structure refinement for **4-Ho**.

Identification code	abc63 (Amanda Chung)	
Empirical formula	$C_{36} H_{91} Ho K N_3 O_8 Si_6$	
Formula weight	1066.68	
Temperature	133(2) K	
Wavelength	0.71073 Å	
Crystal system	Monoclinic	
Space group	$P2_1/n$	
Unit cell dimensions	a = 21.1536(12) Å	$\alpha = 90°$.
	b = 13.4533(7) Å	$\beta = 111.9887(9)°$.
	c = 21.5030(12) Å	$\gamma = 90°$.

Volume	5674.3(5) Å^3
Z	4
Density (calculated)	1.249 Mg/m^3
Absorption coefficient	1.635 mm^{-1}
F(000)	2248
Crystal color	yellow
Crystal size	0.448 x 0.346 x 0.221 mm^3
Theta range for data collection	1.152 to 26.942°
Index ranges	$-26 \leq h \leq 17, -17 \leq k \leq 15, -27 \leq l \leq 27$
Reflections collected	40882
Independent reflections	12278 [R(int) = 0.0353]
Completeness to theta = 25.242°	99.9 %
Absorption correction	Semi-empirical from equivalents
Max. and min. transmission	0.7455 and 0.6290
Refinement method	Full-matrix least-squares on F^2
Data / restraints / parameters	12278 / 0 / 515
Goodness-of-fit on F^2	1.031
Final R indices [I>2sigma(I) = 10514 data]	R1 = 0.0304, wR2 = 0.0717
R indices (all data, 0.79 Å)	R1 = 0.0392, wR2 = 0.0758
Largest diff. peak and hole	1.203 and -0.520 e.Å^{-3}

Table 2.9. Selected bond lengths [Å] and angles [°] for **4-Ho**.

Ho(1)-O(1)	2.045(2)
Ho(1)-N(1)	2.280(2)
Ho(1)-N(2)	2.281(2)
Ho(1)-N(3)	2.293(2)
O(1)-C(19)	1.407(4)
C(15)-K(1)	3.280(3)
C(19)-C(20)	1.439(6)
C(20)-C(21)	1.540(6)
K(1)-O(8)	2.681(3)
O(8)-C(36)	1.404(6)
O(8)-C(34)	1.418(5)
C(34)-C(35)	1.466(7)
C(34)-C(36)	2.034(7)

C(35)-C(36)	1.496(6)

O(1)-Ho(1)-N(1)	103.27(9)
O(1)-Ho(1)-N(2)	103.96(9)
N(1)-Ho(1)-N(2)	112.89(8)
O(1)-Ho(1)-N(3)	103.91(9)
N(1)-Ho(1)-N(3)	114.45(8)
N(2)-Ho(1)-N(3)	116.33(8)
Si(5)-C(15)-K(1)	158.26(19)
O(1)-C(19)-C(20)	116.2(4)
C(19)-C(20)-C(21)	111.1(4)
C(36)-O(8)-C(34)	92.2(3)
C(36)-O(8)-K(1)	133.6(3)
C(34)-O(8)-K(1)	129.0(3)
O(8)-C(34)-C(35)	90.8(4)
O(8)-C(34)-C(36)	43.6(2)
C(35)-C(34)-C(36)	47.2(3)
C(34)-C(35)-C(36)	86.7(4)
O(8)-C(36)-C(35)	90.1(4)
O(8)-C(36)-C(34)	44.2(2)
C(35)-C(36)-C(34)	46.0(3)

Table 2.10. Crystal data and structure refinement for **4-Er**.

Identification code	abc69 (Amanda Chung)	
Empirical formula	$C_{36} H_{91} Er K N_3 O_8 Si_6$	
Formula weight	1069.01	
Temperature	93(2) K	
Wavelength	0.71073 Å	
Crystal system	Monoclinic	
Space group	$P2_1/n$	
Unit cell dimensions	a = 21.1062(11) Å	$\alpha = 90°$.
	b = 13.4465(7) Å	$\beta = 111.8833(9)°$.
	c = 21.4812(12) Å	$\gamma = 90°$.
Volume	5657.2(5) Å^3	
Z	4	

Density (calculated)	1.255 Mg/m^3
Absorption coefficient	1.725 mm^{-1}
F(000)	2252
Crystal color	pink
Crystal size	0.589 x 0.385 x 0.344 mm^3
Theta range for data collection	1.708 to 29.575°
Index ranges	$-29 \leq h \leq 29, -18 \leq k \leq 18, -29 \leq l \leq 29$
Reflections collected	84026
Independent reflections	15862 [R(int) = 0.0257]
Completeness to theta = 25.242°	99.9 %
Absorption correction	Semi-empirical from equivalents
Max. and min. transmission	0.7462 and 0.5309
Refinement method	Full-matrix least-squares on F^2
Data / restraints / parameters	15862 / 0 / 515
Goodness-of-fit on F^2	1.049
Final R indices [I>2sigma(I) = 13724 data]	R1 = 0.0284, wR2 = 0.0689
R indices (all data, 0.72 Å)	R1 = 0.0358, wR2 = 0.0717
Largest diff. peak and hole	1.640 and -0.717 e.Å^{-3}

Table 2.11. Selected bond lengths [Å] and angles [°] for **4-Er**.

Er(1)-O(1)	2.0362(17)
Er(1)-N(3)	2.2703(19)
Er(1)-N(2)	2.2712(19)
Er(1)-N(1)	2.2881(19)
K(1)-O(2)	2.681(3)
O(1)-C(19)	1.401(3)
O(2)-C(24)	1.423(5)
O(2)-C(22)	1.431(4)
C(19)-C(20)	1.475(4)
C(20)-C(21)	1.545(4)
C(22)-C(23)	1.482(5)
C(23)-C(24)	1.513(5)
O(1)-Er(1)-N(3)	103.69(7)

O(1)-Er(1)-N(2)	104.27(7)
N(3)-Er(1)-N(2)	112.77(7)
O(1)-Er(1)-N(1)	104.12(7)
N(3)-Er(1)-N(1)	114.09(7)
N(2)-Er(1)-N(1)	116.09(7)
C(19)-O(1)-Er(1)	164.87(18)
C(24)-O(2)-C(22)	91.7(3)
C(24)-O(2)-K(1)	132.0(2)
C(22)-O(2)-K(1)	129.8(2)
O(1)-C(19)-C(20)	115.3(3)
C(19)-C(20)-C(21)	110.7(3)
O(2)-C(22)-C(23)	91.4(3)
C(22)-C(23)-C(24)	86.3(3)
O(2)-C(24)-C(23)	90.4(3)

Table 2.12. Crystal data and structure refinement for **5-Y**.

Identification code	abc60 (Amanda Chung)
Empirical formula	$C_{36} H_{89} K N_5 O_6 Si_6 Y$
Formula weight	984.67
Temperature	133(2) K
Wavelength	0.71073 Å
Crystal system	Triclinic
Space group	$P\bar{1}$
Unit cell dimensions	a = 11.451(4) Å $\quad$ α = 83.975(5)°.
	b = 15.605(5) Å $\quad$ β = 77.001(5)°.
	c = 16.709(5) Å $\quad$ γ = 89.589(5)°.
Volume	2892.8(16) Å^3
Z	2
Density (calculated)	1.130 Mg/m^3
Absorption coefficient	1.243 mm^{-1}
F(000)	1060
Crystal color	colorless
Crystal size	0.467 x 0.375 x 0.260 mm^3
Theta range for data collection	1.258 to 28.700°
Index ranges	$-15 \leq h \leq 15$, $-21 \leq k \leq 21$, $-22 \leq l \leq 22$

Reflections collected	67096
Independent reflections	14932 [R(int) = 0.0423]
Completeness to theta = 25.242°	99.9 %
Absorption correction	Semi-empirical from equivalents
Max. and min. transmission	0.7462 and 0.6442
Refinement method	Full-matrix least-squares on F^2
Data / restraints / parameters	14932 / 0 / 542
Goodness-of-fit on F^2	1.024
Final R indices [I>2sigma(I) = 12463 data]	R1 = 0.0429, wR2 = 0.1075
R indices (all data, 0.74 Å)	R1 = 0.0548, wR2 = 0.1138
Largest diff. peak and hole	1.485 and -0.528 e.Å^{-3}

Table 2.13. Selected bond lengths [Å] and angles [°] for **5-Y**.

Y(1)-N(1)	2.2437(18)
Y(1)-N(2)	2.2459(17)
Y(1)-N(3)	2.2965(15)
Y(1)-C(10)	2.454(3)
Y(2)-N(3)	2.2412(17)
Y(2)-N(1)	2.2596(19)
Y(2)-N(2)	2.2795(18)
Y(2)-C(14)	2.698(3)
Si(4)-N(2)	1.7258(18)
Si(4)-C(10)	1.856(3)
Si(4)-C(11)	1.880(2)
Si(4)-C(12)	1.885(2)
Si(5)-N(3)	1.7047(17)
Si(5)-C(14)	1.859(2)
Si(5)-C(15)	1.875(2)
Si(5)-C(13)	1.877(2)
N(1)-Y(1)-N(2)	115.85(6)
N(1)-Y(1)-N(3)	116.79(6)
N(2)-Y(1)-N(3)	110.73(6)
N(1)-Y(1)-C(10)	99.97(8)

N(2)-Y(1)-C(10)	73.65(7)
N(3)-Y(1)-C(10)	133.22(7)
N(3)-Y(2)-N(1)	118.45(6)
N(3)-Y(2)-N(2)	111.53(6)
N(1)-Y(2)-N(2)	113.89(7)
N(3)-Y(2)-C(14)	71.86(7)
N(1)-Y(2)-C(14)	93.49(7)
N(2)-Y(2)-C(14)	143.12(8)
N(2)-Si(4)-C(10)	103.91(10)
N(2)-Si(4)-C(11)	111.79(10)
C(10)-Si(4)-C(11)	114.05(14)
N(2)-Si(4)-C(12)	112.22(11)
C(10)-Si(4)-C(12)	107.95(12)
C(11)-Si(4)-C(12)	106.97(12)
N(3)-Si(5)-C(14)	110.09(10)

Table 2.14. Crystal data and structure refinement for **5-Ho**.

Identification code	abc64 (Amanda Chung)
Empirical formula	$C_{36} H_{89} Ho K N_5 O_6 Si_6$
Formula weight	1060.69
Temperature	133(2) K
Wavelength	0.71073 Å
Crystal system	Triclinic
Space group	$P\bar{1}$
Unit cell dimensions	a = 11.4433(11) Å α = 83.8242(15)°.
	b = 15.6667(15) Å β = 77.0120(14)°.
	c = 16.7298(16) Å γ = 89.5598(15)°.
Volume	2905.2(5) Å^3
Z	2
Density (calculated)	1.213 Mg/m^3
Absorption coefficient	1.595 mm^{-1}
F(000)	1116
Crystal color	pink

Crystal size	0.614 x 0.284 x 0.153 mm^3
Theta range for data collection	1.257 to 27.103°
Index ranges	$-14 \leq h \leq 14$, $-20 \leq k \leq 20$, $-21 \leq l \leq 21$
Reflections collected	58529
Independent reflections	12828 [R(int) = 0.0277]
Completeness to theta = 25.242°	100.0 %
Absorption correction	Semi-empirical from equivalents
Max. and min. transmission	0.7461 and 0.5932
Refinement method	Full-matrix least-squares on F^2
Data / restraints / parameters	12828 / 0 / 542
Goodness-of-fit on F^2	1.152
Final R indices [I>2sigma(I) = 12082 data]	R1 = 0.0427, wR2 = 0.0984
R indices (all data, 0.78 Å)	R1 = 0.0460, wR2 = 0.1003
Largest diff. peak and hole	3.152 and -1.500 e.Å^{-3}

Table 2.15. Selected bond lengths [Å] and angles [°] for **5-Ho**.

Ho(1)-N(1)	2.244(3)
Ho(1)-N(2)	2.244(3)
Ho(1)-N(3)	2.294(2)
Ho(1)-C(10)	2.447(4)
Ho(2)-N(3)	2.241(3)
Ho(2)-N(1)	2.259(3)
Ho(2)-N(2)	2.277(3)
Ho(2)-C(14)	2.693(4)
Si(4)-N(2)	1.727(3)
Si(4)-C(10)	1.858(4)
Si(4)-C(11)	1.880(4)
Si(4)-C(12)	1.893(4)
Si(5)-N(3)	1.710(3)
Si(5)-C(14)	1.860(4)
Si(5)-C(15)	1.876(4)
Si(5)-C(13)	1.876(4)
N(1)-Ho(1)-N(2)	116.22(10)

N(1)-Ho(1)-N(3)	117.42(10)
N(2)-Ho(1)-N(3)	110.79(10)
N(1)-Ho(1)-C(10)	99.56(13)
N(2)-Ho(1)-C(10)	73.99(12)
N(3)-Ho(1)-C(10)	132.18(12)
N(3)-Ho(2)-N(1)	119.02(10)
N(3)-Ho(2)-N(2)	111.54(10)
N(1)-Ho(2)-N(2)	114.27(10)
N(3)-Ho(2)-C(14)	72.07(10)
N(1)-Ho(2)-C(14)	93.38(12)
N(2)-Ho(2)-C(14)	142.10(12)
C(10)-Si(4)-C(11)	114.2(2)
N(2)-Si(4)-C(12)	112.43(17)
C(10)-Si(4)-C(12)	107.9(2)
C(11)-Si(4)-C(12)	106.73(19)
N(3)-Si(5)-C(14)	110.02(16)
N(3)-Si(5)-C(15)	112.57(16)
C(14)-Si(5)-C(15)	107.11(19)
N(3)-Si(5)-C(13)	112.84(17)
C(14)-Si(5)-C(13)	106.30(19)
C(15)-Si(5)-C(13)	107.65(18)

Table 2.16. Crystal data and structure refinement for **5-Er**.

Identification code	abc70 (Amanda Chung)
Empirical formula	$C_{36} H_{89} Er K N_5 O_6 Si_6$
Formula weight	1063.02
Temperature	93(2) K
Wavelength	0.71073 Å
Crystal system	Triclinic
Space group	$P\bar{1}$
Unit cell dimensions	a = 11.4128(8) Å α = 83.8334(12)°.
	b = 15.6667(11) Å β = 77.0660(11)°.
	c = 16.7278(11) Å γ = 89.6465(12)°.
Volume	2897.7(3) Å^3
Z	2

Density (calculated)	1.218 Mg/m^3
Absorption coefficient	1.682 mm^{-1}
F(000)	1118
Crystal color	yellow
Crystal size	0.428 x 0.241 x 0.212 mm^3
Theta range for data collection	1.712 to 29.129°
Index ranges	$-15 \le h \le 15$, $-20 \le k \le 21$, $-22 \le l \le 22$
Reflections collected	40999
Independent reflections	15216 [R(int) = 0.0229]
Completeness to theta = 25.242°	99.7 %
Absorption correction	Semi-empirical from equivalents
Max. and min. transmission	0.7461 and 0.6186
Refinement method	Full-matrix least-squares on F^2
Data / restraints / parameters	15216 / 0 / 542
Goodness-of-fit on F^2	1.059
Final R indices [I>2sigma(I) = 13162 data]	R1 = 0.0430, wR2 = 0.0926
R indices (all data, 0.73 Å)	R1 = 0.0538, wR2 = 0.0971
Largest diff. peak and hole	3.130 and -1.655 e.Å^{-3}

Table 2.17. Selected bond lengths [Å] and angles [°] for **5-Er**.

Er(1)-N(1)	2.234(3)
Er(1)-N(2)	2.238(3)
Er(1)-N(3)	2.287(2)
Er(1)-C(1)	2.431(4)
Er(2)-N(3)	2.232(2)
Er(2)-N(2)	2.260(2)
Er(2)-N(1)	2.260(3)
Er(2)-C(13)	2.695(4)
Si(1)-N(1)	1.734(3)
Si(1)-C(1)	1.860(4)
Si(1)-C(2)	1.885(3)
Si(1)-C(3)	1.893(3)
Si(5)-N(3)	1.710(2)
Si(5)-C(13)	1.861(3)
Si(5)-C(15)	1.876(3)

Si(5)-C(14)	1.879(3)

N(1)-Er(1)-N(2)	116.10(9)
N(1)-Er(1)-N(3)	110.30(9)
N(2)-Er(1)-N(3)	117.33(9)
N(1)-Er(1)-C(1)	74.48(11)
N(2)-Er(1)-C(1)	100.00(11)
N(3)-Er(1)-C(1)	132.09(11)
N(3)-Er(2)-N(2)	118.75(9)
N(3)-Er(2)-N(1)	111.38(9)
N(2)-Er(2)-N(1)	114.22(9)
N(3)-Er(2)-C(13)	72.37(9)
N(2)-Er(2)-C(13)	93.04(10)
N(1)-Er(2)-C(13)	142.71(11)
N(1)-Si(1)-C(1)	103.71(15)
N(1)-Si(1)-C(2)	111.70(14)
C(1)-Si(1)-C(2)	114.29(19)
N(1)-Si(1)-C(3)	112.39(15)
C(1)-Si(1)-C(3)	108.14(17)
C(2)-Si(1)-C(3)	106.70(17)
N(3)-Si(5)-C(13)	110.31(15)
N(3)-Si(5)-C(15)	112.54(14)
C(13)-Si(5)-C(15)	107.09(17)
N(3)-Si(5)-C(14)	112.89(15)
C(13)-Si(5)-C(14)	106.12(17)
C(15)-Si(5)-C(14)	107.53(16)

Table 2.18. Crystal data and structure refinement for **6-Y**.

Identification code	abc78 (Amanda Chung)
Empirical formula	$C_{60} H_{154} K_2 N_6 O_{12} Si_{12} Y_2$
Formula weight	1744.98
Temperature	93(2) K
Wavelength	0.71073 Å
Crystal system	Monoclinic
Space group	$P2_1/c$

Unit cell dimensions	a = 23.160(3) Å	α = 90°.
	b = 20.223(3) Å	β = 114.045(3)°.
	c = 22.877(3) Å	γ = 90°.
Volume	9785(2) Å^3	
Z	4	
Density (calculated)	1.184 Mg/m^3	
Absorption coefficient	1.460 mm^{-1}	
F(000)	3744	
Crystal color	colorless	
Crystal size	0.502 x 0.348 x 0.338 mm^3	
Theta range for data collection	0.963 to 29.602°	
Index ranges	-32 ≤ h ≤ 32, -27 ≤ k ≤ 28, -31 ≤ l ≤ 31	
Reflections collected	151938	
Independent reflections	27337 [R(int) = 0.0442]	
Completeness to theta = 25.242°	100.0 %	
Absorption correction	Semi-empirical from equivalents	
Max. and min. transmission	0.7459 and 0.6456	
Refinement method	Full-matrix least-squares on F^2	
Data / restraints / parameters	27337 / 0 / 881	
Goodness-of-fit on F^2	1.041	
Final R indices [I>2sigma(I) = 20313 data]	R1 = 0.0318, wR2 = 0.0659	
R indices (all data, 0.72 Å)	R1 = 0.0567, wR2 = 0.0723	
Largest diff. peak and hole	0.391 and -0.388 e.Å^{-3}	

Table 2.19. Selected bond lengths [Å] and angles [°] for **6-Y**.

Y(1)-N(1)	2.2302(12)
Y(1)-N(3)	2.2728(12)
Y(1)-N(2)	2.2797(12)
Y(1)-C(1)	2.4336(14)
Si(1)-N(1)	1.7362(12)
Si(1)-C(1)	1.8449(15)
Si(1)-C(3)	1.8787(15)
Si(1)-C(2)	1.8815(16)
C(1)-K(1)	3.1808(15)
C(7)-K(2)	3.1346(15)

Y(2)-N(4)	2.2216(12)
Y(2)-N(5)	2.2729(12)
Y(2)-N(6)	2.2874(12)
Y(2)-C(19)	2.4417(14)
Si(7)-N(4)	1.7283(12)
Si(7)-C(19)	1.8448(16)
Si(7)-C(21)	1.8790(15)
Si(7)-C(20)	1.8807(16)
C(19)-K(2)	3.1535(15)
C(33)-K(1)#1	3.1755(15)
N(1)-Y(1)-N(3)	120.25(4)
N(1)-Y(1)-N(2)	109.86(4)
N(3)-Y(1)-N(2)	116.08(4)
N(1)-Y(1)-C(1)	73.91(5)
N(3)-Y(1)-C(1)	103.88(5)
N(2)-Y(1)-C(1)	127.14(5)
N(1)-Si(1)-C(1)	103.27(6)
N(1)-Si(1)-C(3)	111.37(7)
C(1)-Si(1)-C(3)	111.59(7)
N(1)-Si(1)-C(2)	111.71(7)
C(1)-Si(1)-C(2)	112.49(7)
C(3)-Si(1)-C(2)	106.52(8)
Si(1)-C(1)-Y(1)	86.70(6)
Si(1)-C(1)-K(1)	94.74(5)
Y(1)-C(1)-K(1)	168.41(6)
Si(3)-C(7)-K(2)	167.70(7)
N(4)-Y(2)-N(5)	117.85(4)
N(4)-Y(2)-N(6)	108.37(4)
N(5)-Y(2)-N(6)	119.49(4)
N(4)-Y(2)-C(19)	73.58(5)
N(5)-Y(2)-C(19)	100.34(5)
N(6)-Y(2)-C(19)	129.71(5)
N(4)-Si(7)-C(19)	103.05(6)
N(4)-Si(7)-C(21)	110.88(7)
C(19)-Si(7)-C(21)	112.33(8)

N(4)-Si(7)-C(20)	112.93(7)
C(19)-Si(7)-C(20)	112.15(7)
C(21)-Si(7)-C(20)	105.69(8)
Si(7)-C(19)-Y(2)	86.53(6)
Si(7)-C(19)-K(2)	95.32(5)
Y(2)-C(19)-K(2)	168.69(6)
Si(9)-C(26)-Y(2)	77.96(5)
Si(11)-C(33)-K(1)#1	170.20(8)

Symmetry transformations used to generate equivalent atoms:

#1 x,y+1,z

Table 2.20. Crystal data and structure refinement for **7-Y**.

Identification code	abc67 (Amanda Chung)
Empirical formula	$C_{30} H_{79} K N_3 O_6 Si_6 Y \cdot \frac{1}{2}(C_6H_{14})$
Formula weight	917.59
Temperature	133(2) K
Wavelength	0.71073 Å
Crystal system	Orthorhombic
Space group	*Pbca*
Unit cell dimensions	a = 20.9439(16) Å $\alpha = 90°$.
	b = 20.4048(16) Å $\beta = 90°$.
	c = 24.3008(19) Å $\gamma = 90°$.
Volume	10385.1(14) Å^3
Z	8
Density (calculated)	1.174 Mg/m^3
Absorption coefficient	1.379 mm^{-1}
F(000)	3960
Crystal color	colorless
Crystal size	0.460 x 0.309 x 0.220 mm^3
Theta range for data collection	1.626 to 29.201°
Index ranges	$-28 \leq h \leq 28, -27 \leq k \leq 27, -33 \leq l \leq 33$
Reflections collected	192865
Independent reflections	14024 [R(int) = 0.0614]
Completeness to theta = 25.242°	100.0 %
Absorption correction	Semi-empirical from equivalents

Max. and min. transmission	0.7458 and 0.6576
Refinement method	Full-matrix least-squares on F^2
Data / restraints / parameters	14024 / 0 / 473
Goodness-of-fit on F^2	1.020
Final R indices [I>2sigma(I) = 11110 data]	R1 = 0.0459, wR2 = 0.1154
R indices (all data, 0.73 Å)	R1 = 0.0639, wR2 = 0.1262
Largest diff. peak and hole	1.701 and -0.880 e.Å^{-3}

Table 2.21. Selected bond lengths [Å] and angles [°] for **7-Y**.

Y(1)-N(2)	2.259(2)
Y(1)-N(1)	2.270(2)
Y(1)-N(3)	2.280(2)
Y(1)-Si(1)	3.3205(7)
Y(1)-H(1)	2.18(4)
K(1)-H(1)	2.61(4)
N(2)-Y(1)-N(1)	115.98(7)
N(2)-Y(1)-N(3)	115.20(7)
N(1)-Y(1)-N(3)	107.92(7)
N(2)-Y(1)-H(1)	97.8(11)
N(1)-Y(1)-H(1)	105.4(11)
N(3)-Y(1)-H(1)	114.0(11)
Y(1)-H(1)-K(1)	170.3(12)

Symmetry transformations used to generate equivalent atoms:

#1 -x+2,-y+1,-z+1

References

(1)   Gun'ko, Y. K.; Hitchcock, P. B.; Lappert, M. F. *J. Organomet. Chem.* **1995**, *499*, 213–219.
(2)   Cassani, M. C.; Gun, Y. K.; Hitchcock, P. B.; Lappert, M. F. *Chem. Commun.* **1996**, *3*, 1987–1988.
(3)   Cassani, M. C.; Lappert, M. F.; Laschi, F. *Chem. Commun.* **1997**, *2* (16), 1563–1564.
(4)   Cassani, M. C.; Duncalf, D. J.; Lappert, M. F. *J. Am. Chem. Soc.* **1998**, *120* (49), 12958–

12959.

(5) Cassani, M. C.; Gun, Y. K.; Hitchcock, P. B.; Lappert, M. F.; Laschi, F. *Organometallics* **1999**, *18*, 5539–5547.

(6) Gun, Y. K.; Hitchcock, P. B.; Lappert, M. F. *Organometallics* **2000**, *19*, 2832–2834.

(7) Cristina Cassani, M.; Gun'ko, Y. K.; Hitchcock, P. B.; Hulkes, A. G.; Khvostov, A. V.; Lappert, M. F.; Protchenko, A. V. *J. Organometalic Chem.* **2002**, *647*, 71–83.

(8) Hitchcock, P. B.; Lappert, M. F.; Maron, L.; Protchenko, A. V. *Angew. Chem. Int. Ed.* **2008**, No. 47, 1488–1491.

(9) Coles, M. P.; Hitchcock, P. B.; Lappert, M. F.; Protchenko, A. V. *Organometallics* **2012**, *31*, 2682–2690.

(10) Tilley, T. D.; Boncella, J. M.; Berg, D. J.; Burns, C. J.; Andersen, R. A.; Lawless, G. A.; Edelman, M. A.; Lappert, M. F. *Inorg. Synth.* **1990**, *27*, 146.

(11) Woen, D. H.; Evans, W. J. In *Handbook on the Physics and Chemistry of Rare Earths*; Elsevier B.V., 2016; pp 1–57.

(12) Corbett, J. D. *Rev. Chim. Min.* **1973**, *10*, 239–257.

(13) Nief, F. In *Handbook on the Physics and Chemistry of Rare Earths*; 2010; pp 241–300.

(14) Bochkarev, M. N. *Coord. Chem. Rev.* **2004**, *248* (9–10), 835–851.

(15) Morss, L. R. *Chem. Rev.* **1975**, *76* (6), 827–841.

(16) Macdonald, M. R.; Bates, E.; Ziller, J. W.; Furche, F.; Evans, W. J. *J. Am. Chem. Soc.* **2013**, *135*, 9857–9868.

(17) Palumbo, C. T.; Darago, L. E.; Windorff, C. J.; Ziller, J. W.; Evans, W. J. *Organometallics* **2018**, *37* (6), 900–905.

(18) Ryan, A. J.; Ziller, J. W.; Evans, W. J. *Chem. Sci.* **2020**, No. 11, 2006–2014.

(19) Ryan, A. J.; Balasubramani, S. ganesh; Ziller, J. W.; Furche, F.; Evans, W. J. *J. Am. Chem. Soc.* **2020**, *142* (20), 9302–9313.

(20) Woen, D. H.; Chen, G. P.; Ziller, J. W.; Boyle, T. J.; Furche, F.; Evans, W. J. *J. Am. Chem. Soc.* **2017**, *139*, 14861–14864.

(21) Woen, D. H.; Huh, D. N.; Ziller, J. W.; Evans, W. J. *Organometallics* **2018**, *37* (18), 3055–3063.

(22) Shannon, R. D. *Acta Crystallogr., Sect. A Cryst. Phys., Diffr., Theor. Gen. Crystallogr.* **1976**, *32*, 751–767.

(23) Kroposki, L. M.; Potter, D. E.; Bates, R. B.; Kroposki, L. M.; Potter, D. E. *J. Organomet. Chem.* **1972**, *37* (4), 560–562.

(24) Geier, S. J.; Stephan, D. W. *J. Am. Chem. Soc.* **2009**, *131* (10), 3476–3477.

(25) Wu, Z. Z.; Huang, Z. E.; Cai, R. F.; Xu, Z.; You, X. Z.; Huang, X. Y. *Polyhedron* **1996**, *15* (1), 13–22.

(26) Zhu, H.; Chen, E. Y. X. *Inorg. Chem.* **2007**, *46* (4), 1481–1487.

(27) Stanetty, P.; Roller, H.; Mihovilovic, M. *J. Org. Chem.* **1992**, *57* (25), 6833–6837.

(28) Schwamm, R. J.; Coles, M. P.; Hill, M. S.; Mahon, M. F.; McMullin, C. L.; Rajabi, N. A.; Wilson, A. S. S. *Angew. Chem. Int. Ed.* **2020**, *59* (10), 3928–3932.

(29) Clayden, J.; Yasin, S. A. *New J. Chem.* **2002**, *26* (2), 191–192.

(30) Guan, J.; Dubé, T.; Gambarotta, S.; Yap, G. P. A. *Organometallics* **2000**, *19* (23), 4820–4827.

(31) Korobkov, I.; Gambarotta, S.; Yap, G. P. A. *Organometallics* **2001**, *20* (12), 2552–2559.

(32) Maercker, A. *Angew. Chem. Int. Ed. English* **1987**, *26* (10), 972–989.

(33) Kennedy, A. R.; Klett, J.; Mulvey, R. E.; Wright, D. S. *Science (80).* **2010**, *706* (2009),

706–709.

(34) Mulvey, R. E.; Blair, V. L.; Clegg, W.; Kennedy, A. R.; Klett, J.; Russo, L. *Nat. Chem.* **2010**, *2* (7), 588–591.

(35) Covert, K. J.; Mayol, A. R.; Wolczanski, P. T. *Inorganica Chim. Acta* **1997**, *263*, 263–278.

(36) Lugmair, C. G.; Tilley, T. D. *Z. Naturforsch* **2004**, *3*, 1540–1547.

(37) Jones, C.; Schulten, C.; Nembenna, S.; Stasch, A. *J. Chem. Crystallogr.* **2012**, *42* (8), 866–870.

(38) Solovyev, A.; Lacôte, E.; Curran, D. P. *Dalt. Trans.* **2013**, *42* (3), 695–700.

(39) Birkmann, B.; Voss, T.; Geier, S. J.; Ullrich, M.; Kehr, G.; Erker, G.; Stephan, D. W. *Organometallics* **2010**, *29* (21), 5310–5319.

(40) Luo, Y.; Feng, X. *J. Rare Earths* **2011**, *29* (1), 24–27.

(41) Spinney, H. A.; Clough, C. R.; Cummins, C. C. *Dalt. Trans.* **2015**, *44* (15), 6784–6796.

(42) Liu, D.; Wang, Y.; Chan, H. S.; Tang, Y.; Xie, Z. *Organometallics* **2008**, *27* (20), 5295–5302.

(43) Mukherjee, D.; Osseili, H.; Truong, K. N.; Spaniol, T. P.; Okuda, J. *Chem. Commun.* **2017**, *53* (24), 3493–3496.

(44) Fryzuk, M. D.; Clentsmith, G. K. B.; Rettig, S. J. *Inorganica Chim. Acta* **1997**, *259*, 51–59.

(45) Boncella, J. M.; Cajigal, M. L.; Gamble, A. S.; Abboud, K. A. *Polyhedron* **1996**, *15* (12), 2071–2078.

(46) Cheng, J.; Wang, H.; Nishiura, M.; Hou, Z. *Chem. Sci.* **2012**, *3* (7), 2230–2233.

(47) Bonnet, F.; Da Costa Violante, C.; Roussel, P.; Mortreux, A.; Visseaux, M. *Chem. Commun.* **2009**, 3380–3382.

(48) Westerhausen, M.; Weinrich, S.; Schmid, B.; Schneiderbauer, S.; Suter, M.; Noth, H.; Piotrowski, H. *Zeitschrift Fur Anorg. Und Allg. Chemie* **2003**, *629* (4), 625–633.

(49) Likhar, P. R.; Zirngast, M.; Baumgartner, J.; Marschner, C. *Chem. Commun.* **2004**, *4* (15), 1764–1765.

(50) Zitz, R.; Hlina, J.; Arp, H.; Kinschel, D.; Marschner, C.; Baumgartner, J. *Inorg. Chem.* **2019**, *58* (10), 7107–7117.

(51) Evans, W. J.; Giarikos, D. G.; Workman, P. S.; Ziller, J. W. *Inorg. Chem.* **2004**, *43* (18), 5754–5760.

(52) Chung, A. B.; Ryan, A. J.; Fang, M.; Ziller, J. W.; Evans, W. J. *Inorg. Chem.* **2021**, *60* (20), 15635–15645.

(53) Niemeyer, M. *Inorg. Chem.* **2006**, *45* (22), 9085–9095.

(54) Fang, M.; Bates, J. E.; Lorenz, S. E.; Lee, D. S.; Rego, D. B.; Ziller, J. W.; Furche, F.; Evans, W. J. *Inorg. Chem.* **2011**, *50* (4), 1459–1469.

(55) Simpson, S. J.; Turner, H. W.; Andersen, R. A. *Inorg. Chem.* **1981**, *20* (9), 2991–2995.

(56) Karl, M.; Harms, K.; Seybert, G.; Massa, W.; Fau, S.; Frenking, G.; Dehnicke, K. *Z. Anorg. Allg. Chem.* **1999**, *625* (12), 2055–2063.

(57) Deacon, G. B.; Forsyth, C. M. *Chem. Commun.* **2002**, *314* (21), 2522–2523.

(58) Wang, J.; Gardiner, M. G. *Chem. Commun.* **2005**, 1589–1591.

(59) Deacon, G. B.; Forsyth, C. M.; Junk, P. C.; Wang, J. *Inorg. Chem.* **2007**, *46* (23), 10022–10030.

(60) Jenkins, T. F.; Bekoe, S.; Ziller, J. W.; Furche, F.; Evans, W. J. *Organometallics* **2021**, *40* (23), 3917–3925.

(61)   Wedal, J. C.; Ziller, J. W.; Furche, F.; Evans, W. J. *Inorg. Chem.* **2022**, *61*, 7365–7376.
(62)   Trnka, T. M.; Bonanno, J. B.; Bridgewater, B. M.; Parkin, G. *Organometallics* **2001**, *20* (15), 3255–3264.
(63)   Fortier, S.; Wu, G.; Hayton, T. W. *J. Am. Chem. Soc.* **2010**, *132* (20), 6888–6889.
(64)   Fortier, S.; Kaltsoyannis, N.; Wu, G.; Hayton, T. W. *J. Am. Chem. Soc.* **2011**, *133* (36), 14224–14227.
(65)   Hervé, A.; Bouzidi, Y.; Berthet, J. C.; Belkhiri, L.; Thuéry, P.; Boucekkine, A.; Ephritikhine, M. *Inorg. Chem.* **2015**, *54* (5), 2474–2490.
(66)   Rookes, T. M.; Wildman, E. P.; Balázs, G.; Gardner, B. M.; Wooles, A. J.; Gregson, M.; Tuna, F.; Scheer, M.; Liddle, S. T. *Angew. Chem. Int. Ed.* **2018**, *57* (5), 1332–1336.
(67)   Staun, S. L.; Sergentu, D. C.; Wu, G.; Autschbach, J.; Hayton, T. W. *Chem. Sci.* **2019**, *10* (26), 6431–6436.
(68)   Wedal, J. C.; Bekoe, S.; Ziller, J. W.; Furche, F.; Evans, W. J. *Organometallics* **2020**, *39* (18), 3425–3432.
(69)   Fieser, M. E.; Palumbo, C. T.; La Pierre, H. S.; Halter, D. P.; Voora, V. K.; Ziller, J. W.; Furche, F.; Meyer, K.; Evans, W. J.; Pierre, H. S. La; et al. *Chem. Sci.* **2017**, *8* (11), 7424–7433.
(70)   Palumbo, C. T.; Halter, D. P.; Voora, V. K.; Chen, G. P.; Chan, A. K.; Fieser, M. E.; Ziller, J. W.; Hieringer, W.; Furche, F.; Meyer, K.; et al. *Inorg. Chem.* **2018**, *57* (5), 2823–2833.
(71)   Palumbo, C. T.; Halter, D. P.; Voora, V. K.; Chen, G. P.; Ziller, J. W.; Gembicky, M.; Rheingold, A. L.; Furche, F.; Meyer, K.; Evans, W. J. *Inorg. Chem.* **2018**, *57* (20), 12876–12884.
(72)   Jaroschik, F.; Nief, F.; Le Goff, X. F.; Ricard, L. *Organometallics* **2007**, *26* (5), 1123–1125.
(73)   Corbey, J. F.; Woen, D. H.; Palumbo, C. T.; Fieser, M. E.; Ziller, J. W.; Furche, F.; Evans, W. J. *Organometallics* **2015**, *34* (15), 3909–3921.
(74)   Dormond, A.; Bouadili, A. A. El; Moise, C. *J. Chem. Soc. - Ser. Chem. Commun.* **1985**, *26* (13), 914–916.
(75)   Lapierre, H. S.; Kameo, H.; Halter, D. P.; Heinemann, F. W.; Meyer, K. *Angew. Chem. Int. Ed.* **2014**, *53* (28), 7154–7157.
(76)   Fieser, M. E.; Palumbo, C. T.; La Pierre, H. S.; Halter, D. P.; Voora, V. K.; Ziller, J. W.; Furche, F.; Meyer, K.; Evans, W. J. *Chem. Sci.* **2017**, *8* (11), 7424–7433.
(77)   Aspinall, H. C.; Bradley, D. C.; Hursthouse, M. B.; Sales, K. D.; Walker, N. P. C.; Hussain, B. *J. Chem. Soc. Dalton. Trans.* **1989**, No. 1, 623–626.

Chapter 3

2.2.2-Cryptand as a Bidentate Ligand in Rare-Earth Metal Chemistry

Introduction*

This Chapter describes the investigation of the reductive chemistry with the *in-situ* Ce(NR$_2$)$_3$/M/N$_2$ reaction. As outlined in the Introduction, crystallographically-characterizable molecular complexes of La(II), Ce(II), Pr(II), Gd(II), Tb(II), Ho(II), Er(II), Lu(II), and Y(II) were discovered with the ligands C$_5$H$_3$(SiMe$_3$)$_2$ (Cp″) and C$_5$H$_4$SiMe$_3$, (Cp′).[1–9] The reduction reactions that generated the new Ln(II) ions utilized the 2.2.2-cryptand ligand (crypt) extensively to encapsulate the alkali metal ion formed in the reaction. The crypt-chelated alkali metal units constituted good counter-cations for the (Cp′$_3$Ln^{II})$^{1-}$ and (Cp″$_3$Ln^{II})$^{1-}$ anions (Cp′ = C$_5$H$_4$SiMe$_3$; Cp″ = C$_5$H$_3$(SiMe$_3$)$_2$), which facilitated crystallographic characterization of the reaction products. Ln(II) metal complexes are now known with [M(crypt)]$^{1+}$ counter-cations for M = Li, Na, K, Rb, and Cs in structures such as [Li(crypt)][Cp′$_3$Ln],[10] [Na(crypt)][Cp′$_3$Ln],[11] [K(crypt)][Cp″$_3$Ln],[1,9] [K(crypt)][Cp^{tet}$_3$Ln] (Ln = La, Ce, Pr, Nd, Sm, Gd, Tb, Dy); Cp^{tet} = C$_5$Me$_4$H),[12] [K(crypt)][Cp^t$_3$Dy]$_2$ (Cp^t = C$_5$H$_4$CMe$_3$),[13] [K(crypt)][Cp^{Me}$_3$Dy] (Cp^{Me} = C$_5$H$_4$Me),[14] [K(crypt)][Sc(OAr′)$_3$ (OAr′ = OC$_6$H$_2$tBu$_2$-2,6-Me-4),[15] [K(crypt)][((^{Ad,Me}ArO)$_3$mes)Ln] (Ln = Nd, Gd, Dy, Er; (^{Ad,Me}ArO)$_3$mes = (2-Ad-4-Me-C$_6$H$_2$O)$_3$(2,4,6-Me$_3$C$_6$H$_2$); Ad = 1-adamantyl),[8] [K(crypt)][Y(OAr$^{Ad,Ad,t-Bu}$)$_3$] (OAr$^{Ad,Ad,t-Bu}$ = 2,6-Ad$_2$-4-*t*-Bu-C$_6$H$_2$O),[16] [Rb(crypt)][Ln(NR$_2$)$_3$] (Ln = Nd, Ho, Er),[17] and [Cs(crypt)][Sc(NR$_2$)$_3$] (R = SiMe$_3$).[18]

Additionally, the crypt ligand in $[Li(crypt)]^{1+}$ counter-cations has also been found as crypt-κ^6 in three different binding modes: N_2O_4,[10,19] NO_5,[10,19–25] and O_6.[10]

However, the crypt ligand can also encapsulate rare-earth metals ions as well as alkali metal ions. A variety of such metal complexes have been crystallographically characterized, involving both divalent and trivalent ions, usually with one or two additional coordinated ligands that could be anions or neutral species. Examples include $[Ln^{II}(crypt)(THF)_x][Cp'_3Ln]$ (x = 1, Ln = Sm, Eu; x = 0, Ln = Yb),[26] $[Sm^{II}(crypt)(DippForm)][DippForm]$ (DippForm = N,N′-bis(2,6-diisopropylphenyl)-formamidinate),[27] $[Sm^{II}(crypt)(PCO)_2]$,[27] $[Eu^{II}(crypt)Cl][Cl]$,[28] $[Yb^{II}(crypt)I][I]$,[29] $[Ln^{III}(crypt)(THF)][BPh_4]_2$ (Ln = Sm, Eu),[30] $[Ln^{III}(crypt)(THF)_x][Cp'_3Ln^{II}]_2$ (x = 1, Ln = Sm, Eu; x = 0, Ln = Yb),[26] $[La^{III}(crypt)Cl_2][Cl]$,[31] $[Ln^{II}(crypt)(DMF)_x][X]_2$ (x = 2, Ln = Sm, Eu; x = 1, Ln = Yb; X = I, BPh_4),[32] $[Ln^{III}(crypt)(OTf)_2][OTf]$ and $[Ln^{II}(crypt)(OTf)_2]$ (Ln = Nd, Sm)[33] among others.[34–38]

A new coordination mode for crypt with rare-earth metal ions was discovered that is an intermediate between the 8-coordinate mode with the rare-earth metal ion inside crypt and the situation in which crypt is not coordinating the rare-earth metal ion at all. In this Chapter it is shown that crypt can function as a bidentate ligand to rare-earth ions.

Results and Discussion

The first example of a bidentate crypt metal complex of a rare-earth metal ion was discovered while examining the reduction of dinitrogen with $Ce(NR_2)_3$ (R = $SiMe_3$) and potassium graphite. Numerous LnA_3/M reactions (A = anion; M = alkali metal) of this type have been performed in the past and generated both $(N=N)^{2-}$ and $(N_2)^{3-}$ metal complexes.[39–44] For example, crystallographically-characterized examples of $[(R_2N)_2(THF)Ln]_2(\mu-\eta^2:\eta^2-N_2)$ have been isolated

in this way from reactions in THF for the smaller rare-earths, Ln = Nd, Gd, Tb, Dy, Ho, Y, Er, Tm, and Lu, eq 3.1.[40]

$$2\ Ln^{III}(NR_2)_3 + 2\ K \quad \xrightarrow[-\ 2\ KNR_2]{\substack{N_2 \\ THF}} \quad$$

3.1
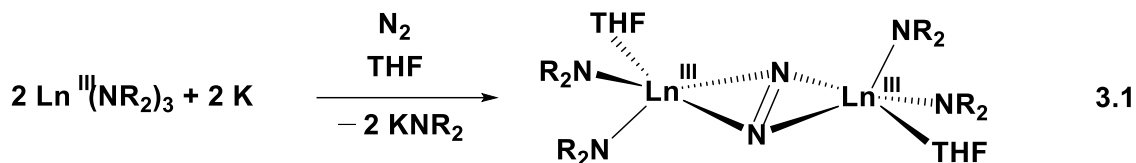
Ln = Nd, Gd, Tb, Dy, Ho, Y, Er, Tm, Lu
R = SiMe$_3$

Analogous reactions with the larger lanthanides, La, Ce, and Pr, appeared to proceed similarly, but crystallographic confirmation of the products was not obtained. ^{1}H and ^{15}N NMR data on the La product were similar to those on the Y and Lu products.[40,42] Hence, it was likely that $(N=N)^{2-}$ products of La, Ce, and Pr formed, but the metal complexes were too sterically unsaturated with these larger metals to crystallize well. Further evidence of reaction in eq 3.1 with the large lanthanides was obtained by isolation and crystallographic characterization of the tetrakis(amide) products, [K(THF)$_6$][Ln(NR$_2$)$_4$] for La and Pr, and [Na(THF$_4$)(Et$_2$O)][Ce(NR$_2$)$_4$] for Ce. These tetrakis(amides) can form by complexation to the Ln(NR$_2$)$_3$ starting material of the $(NR_2)^{1-}$ ligands lost by each metal in a successful dinitrogen reduction.[40]

When the LnA$_3$/M reaction was conducted in Et$_2$O using Ce(NR$_2$)$_3$ and KC$_8$ in the presence of crypt, the $(N=N)^{2-}$ metal complex, [{(R$_2$N)$_2$Ce(crypt-κ^2-O,O′)}$_2$(μ-η^2:η^2-N$_2$)], **1**, was isolated and identified by X-ray diffraction, eq 3.2, Figure 3.1. This was the first cerium amide $(N=N)^{2-}$ metal complex that could be crystallized.

Ce^{II}(NR$_2$)$_3$ + 2.2.2-cryptand + xs KC$_8$ $\xrightarrow[\substack{-35\,°C \\ -\,\text{graphite}}]{\substack{N_2 \\ Et_2O}}$

1

3.2
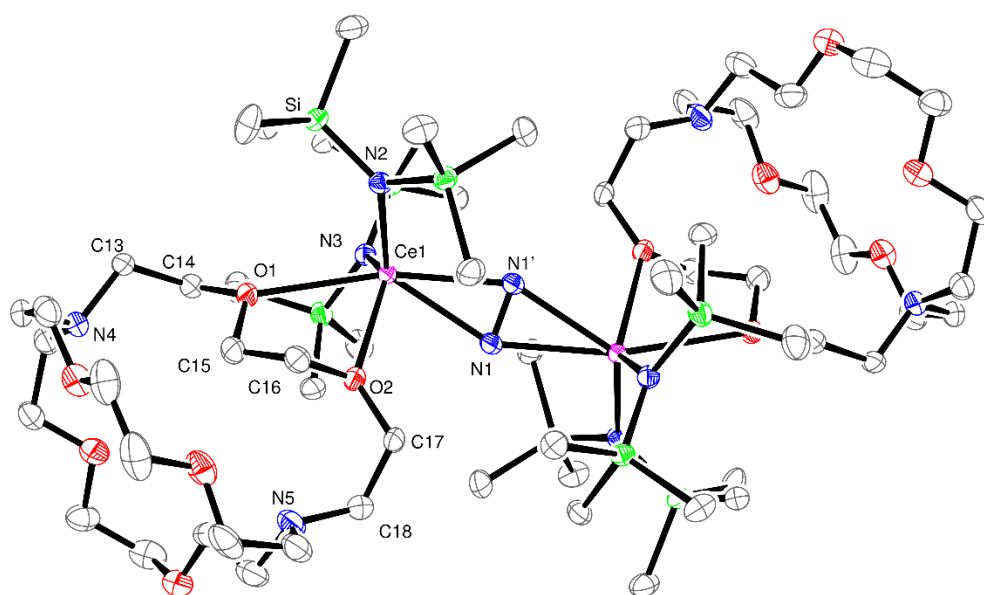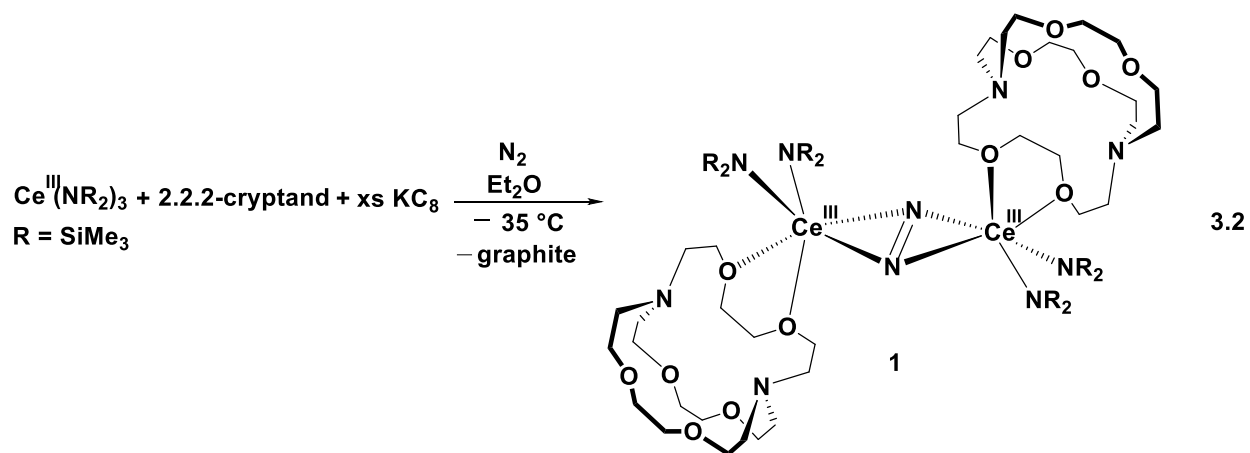
Figure 3.1. Representation of [{(R$_2$N)$_2$Ce(crypt-κ^2-O,O′)}$_2$(μ-η^2:η^2-N$_2$)], **1**, with atomic displacement parameters drawn at the 50% probability level. Hydrogen atoms and an Et$_2$O in the lattice are excluded for clarity.

The crystal structure of **1**, shows that it is a neutral metal complex with a side-on bound $(N=N)^{2-}$, and two amide ligands bound to each cerium. This is similar to the known series of THF adducts in eq 3.1, $[\{(THF)(R_2N)_2Ln\}_2(\mu\text{-}\eta^2\text{:}\eta^2\text{-}N_2)]$,[40] except instead of one THF molecule per metal, a crypt ligand coordinates to each metal through two oxygen atoms. In this case, crypt is acting as a $\kappa^2\text{-}O,O'$ "exo-crypt" with binding similar to that of a dimethoxyethane (DME) ligand. Presumably, with the extra steric bulk of crypt versus THF, the $Ce(N=N)^{2-}$ product is sterically saturated enough to allow isolation and crystallization.

Compound **1** is sparingly soluble in both toluene and benzene. A ^1H NMR spectrum was taken in both toluene-d_8 and C_6D_6, Figure 3.2 and Figure 3.3. The crypt resonances align with free cryptand in solution and only one resonance is seen for the methyl group of the silyl amides, which is shifted upfield.
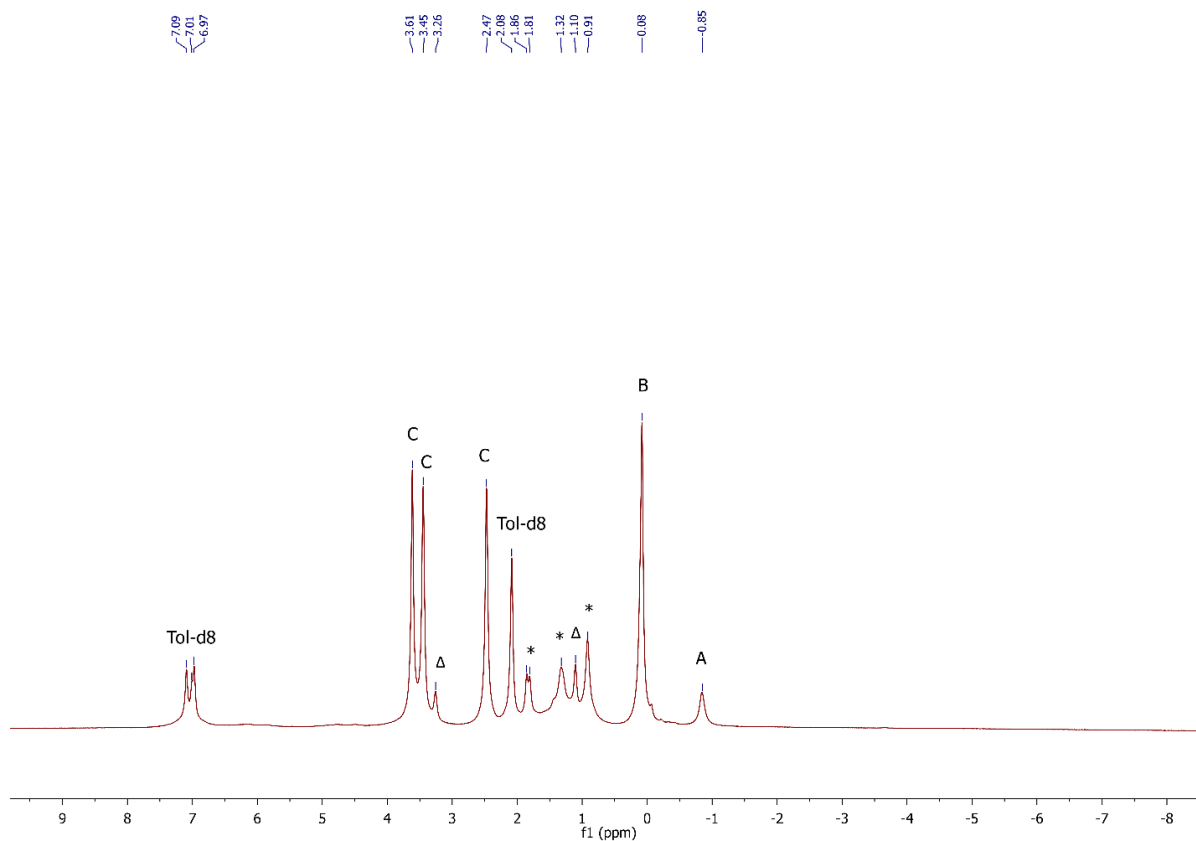
Figure 3.2. ^{1}H NMR spectrum of **1** in toluene-d$_8$. A: Si*Me$_3$* of **1**; B: HN*; C: crypt; Δ: diethyl ether; *unidentified.

117
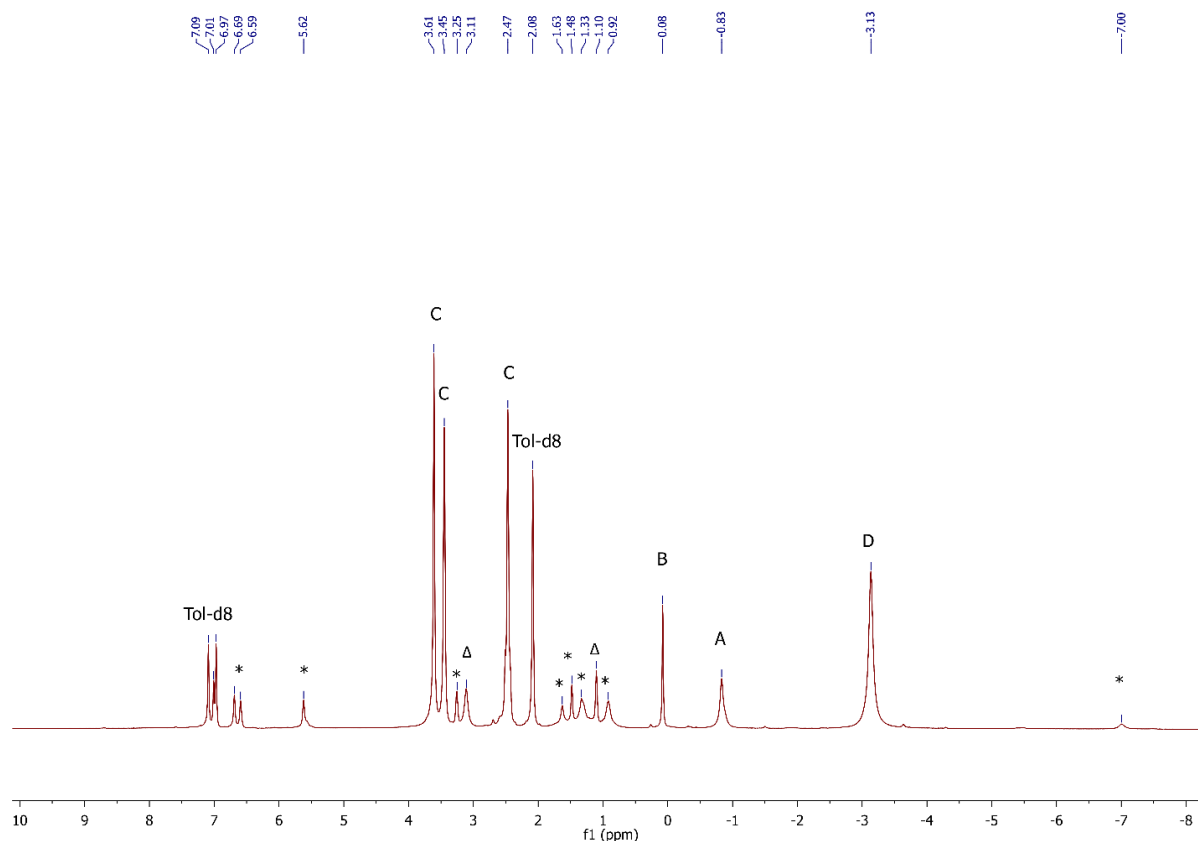
Figure 3.3. ^{1}H NMR spectrum of **1** reaction mixture in toluene-d$_8$. A: Si*Me$_3$* of **1**; B: HN*; C: crypt; D: Si*Me$_3$* of Ce(NR$_2$)$_3$; Δ: diethyl ether; *unidentified.

The 1.233(4) Å N–N distance in **1** is similar to those in the metal complexes in eq 3.1, 1.258(3)-1.305(6) Å, and is consistent with a double bond, i.e. (N=N)$^{2-}$.[45,46] The exo-crypt in **1** does not bind symmetrically and has Ce–O distances in **1** of 2.545(2) Å for Ce–O1, and 2.796(2) Å for Ce–O2. In comparison, the Ce–O(THF) distances in the cyclopentadienyl cerium dinitrogen complexes, [(C$_5$Me$_5$)$_2$(THF)Ce]$_2$[μ-η^2:η^2-N$_2$] and [(C$_5$Me$_4$H)$_2$(THF)Ce]$_2$[μ-η^2:η^2-N$_2$], are 2.607(4) Å and 2.589(3) Å, respectively.[42] Hence, the crypt coordination could also be described as a monodentate ligand with a long secondary interaction. The 2.545(2) Å Ce–O(crypt) distance is similar to the 2.518(1) Å Nd–O(THF) distance in [(R$_2$N)$_2$(THF)Nd]$_2$(μ-η^2:η^2-N$_2$) when the 0.027 Å ionic radius increase from Nd to Ce is considered.[47]

Within the coordinated crypt, the 1.437(3)-1.443(3) Å C–O distances involving the coordinating O1 and O2 are within the error limits of the other 1.399(4)-1.424(4) Å C–O distances, as shown in Table 3.1. The C–C distances and the angles involving the bound oxygen atoms are similar to those in the rest of the crypt molecule.

Table 3.1. Selected distances (Å) and angles (°) for **1**.

Ce1–N3$_{amide}$	2.409(2)	Ce1–N1	2.451(2)
Ce1–N2$_{amide}$	2.411(2)	Ce1–N1′	2.468(2)
Ce1–O1	2.7957(18)	Ce1–O2	2.5453(18)
N1–N1′	1.233(4)		
Crypt O–C Distance			
O1–C14	1.439(3)	O1–C15	1.437(3)
O2–C16	1.438(3)	O2–C17	1.443(3)
O3–C20	1.422(4)	O3–C21	1.418(4)
O4–C22	1.413(4)	O4–C23	1.418(4)
O5–C26	1.424(4)	O5–C27	1.417(4)
O6–C28	1.413(4)	O6–C29	1.399(4)
Crypt C–C Distance			
C13–C14	1.525(4)	C15–C16	1.485(4)
C17–C18	1.512(4)	C19–C20	1.504(4)
C21–C22	1.489(5)	C23–C24	1.507(5)
C25–26	1.510(4)	C27–C28	1.495(5)
C29–C30	1.525(5)		

Conclusion

Although 2.2.2-cryptand can stabilize alkali metal ions to generate favorable lattices for crystallization of rare-earth metal complexes and encapsulate rare-earth ions as an octadentate ligand, it can also function as a stabilizing bidentate κ^2-chelating ligand for rare-earth metal ions as shown in $[\{(R_2N)_2Ce(crypt-\kappa^2-O,O')\}_2(\mu-\eta^2:\eta^2-N_2)]$, **1**. The diverse nature of this metal complex suggests that crypt could coordinate to rare-earth metal ions in a variety of different coordination environments.

To the extent that it binds like dimethoxyethane, it constitutes a sterically bulky variation of this commonly-used ether. The size and 3-dimensional nature of crypt means that it can substantially fill the coordination environment of a sterically unsaturated compound. In the case of the $[\{(R_2N)_2Ln\}_2(\mu-\eta^2:\eta^2-N_2)]$, which crystallizes for smaller metals, Nd-Lu, sans Ce, it is possible that a single THF ligand was not enough to sterically saturate the coordination environment to yield single crystals for X-ray diffraction. Crypt coordination in **1** led to successful crystallization of this cerium $(N=N)^{2-}$ compound. Attempts to crystallize "$[\{(R_2N)_2Ce\}_2(\mu-\eta^2:\eta^2-N_2)]$" with DME have been unsuccessful.

Experimental Details

All manipulations and syntheses described below were conducted with the rigorous exclusion of air and water using standard Schlenk line and glovebox techniques under an argon or dinitrogen atmosphere. Solvents were sparged with UHP argon and dried by passage through columns containing Q-5 and molecular sieves prior to use. Deuterated NMR solvents were dried over NaK alloy or Na/benzophenone, degassed by three freeze−pump−thaw cycles, and vacuum-transferred before use. ^{1}H NMR spectra were recorded on a Bruker AVANCE 600 spectrometer (^{1}H operating at 600 MHz) at 298 K, unless otherwise stated, and referenced internally to residual

protio-solvent resonances. 2.2.2-cryptand (Sigma-Aldrich) was placed under vacuum (10^{-3} Torr) before use. Ce(NR$_2$)$_3$[61] was synthesized according to literature procedures.

[{(R$_2$N)$_2$Ce(crypt-κ^2-O,O′)}$_2$(μ-η^2:η^2-N$_2$)], 1. A dinitrogen-saturated Et$_2$O (3 mL) solution of Ce(NR$_2$)$_3$ (R = SiMe$_3$) (60 mg, 0.1 mmol) and 2.2.2.-cryptand (36 mg, 0.10 mmol), chilled to −35 °C, was added to a vial containing excess KC$_8$ (20 mg 0.1 mmol), that had been chilled in a cold well with a liquid nitrogen bath. This generated a yellow solution. Bright yellow crystals were isolated by filtering and placing the Et$_2$O solution in a −35 °C freezer for several days (20 mg, 24%). These were identified as **1** by X-ray diffraction.

X-ray Data Collection, Structure, Solution, Refinement

X-ray data, collection, structure, solution, and refinement can also be found in Chung, A. B.; Huh, D. N.; Ziller, J. W.; Evans, W. J. *Inorg. Chem. Front.* **2020**, *7* (22), 4445–4451.

Table 3.2. Crystal data and structure refinement for **1**.

Identification code	abc16 (Amanda Chung)
Empirical formula	C$_{60}$ H$_{144}$ Ce$_2$ N$_{10}$ O$_{12}$ Si$_8$ • 2(C$_4$H$_{10}$O)
Formula weight	1851.04
Temperature	133(2) K
Wavelength	0.71073 Å
Crystal system	Triclinic
Space group	$P\bar{1}$
Unit cell dimensions	a = 12.8760(12) Å α = 113.0740(14)°.
	b = 14.4999(14) Å β = 92.3513(15)°.
	c = 15.4460(15) Å γ = 110.9522(14)°.
Volume	2421.9(4) Å^3
Z	1
Density (calculated)	1.269 Mg/m^3
Absorption coefficient	1.082 mm^{-1}
F(000)	982
Crystal color	yellow
Crystal size	0.335 x 0.187 x 0.164 mm^3

Theta range for data collection	1.466 to 29.575°
Index ranges	$-17 \leq h \leq 17, -20 \leq k \leq 18, -21 \leq l \leq 21$
Reflections collected	32715
Independent reflections	13437 [R(int) = 0.0347]
Completeness to theta = 25.500°	100.0 %
Absorption correction	Semi-empirical from equivalents
Max. and min. transmission	0.7462 and 0.6682
Refinement method	Full-matrix least-squares on F^2
Data / restraints / parameters	13437 / 0 / 474
Goodness-of-fit on F^2	1.041
Final R indices [I>2sigma(I) = 11059 data]	R1 = 0.0387, wR2 = 0.0898
R indices (all data, 0.72 Å)	R1 = 0.0546, wR2 = 0.0984
Largest diff. peak and hole	1.927 and -0.450 e.Å^{-3}

Table 3.3. Bond lengths [Å] and angles [°] for **1**.

Ce(1)-N(3)	2.409(2)
Ce(1)-N(2)	2.411(2)
Ce(1)-N(1)	2.451(2)
Ce(1)-N(1)#1	2.468(2)
Ce(1)-O(2)	2.5453(18)
Ce(1)-O(1)	2.7957(18)
N(1)-N(1)#1	1.233(4)
N(1)-Ce(1)#1	2.468(2)
N(3)-Ce(1)-N(2)	123.09(7)
N(3)-Ce(1)-N(1)	104.41(7)
N(2)-Ce(1)-N(1)	116.01(7)
N(3)-Ce(1)-N(1)#1	102.44(7)
N(2)-Ce(1)-N(1)#1	95.60(7)
N(1)-Ce(1)-N(1)#1	29.04(9)
N(3)-Ce(1)-O(2)	129.31(7)
N(2)-Ce(1)-O(2)	99.09(7)
N(1)-Ce(1)-O(2)	76.30(6)
N(1)#1-Ce(1)-O(2)	99.65(7)
N(3)-Ce(1)-O(1)	92.74(6)

N(2)-Ce(1)-O(1)	84.78(6)
N(1)-Ce(1)-O(1)	136.28(6)
N(1)#1-Ce(1)-O(1)	161.42(6)
O(2)-Ce(1)-O(1)	62.08(6)

Symmetry transformations used to generate equivalent atoms:

#1 -x+1,-y+2,-z+1

References

(1)   Hitchcock, P. B.; Lappert, M. F.; Maron, L.; Protchenko, A. V. *Angew. Chem. Int. Ed.* **2008**, No. 47, 1488–1491.

(2)   MacDonald, M. R.; Ziller, J. W.; Evans, W. J. *J. Am. Chem. Soc.* **2011**, *133* (40), 15914–15917.

(3)   MacDonald, M. R.; Bates, J. E.; Fieser, M. E.; Ziller, J. W.; Furche, F.; Evans, W. J. *J. Am. Chem. Soc.* **2012**, *134* (20), 8420–8423.

(4)   Macdonald, M. R.; Bates, E.; Ziller, J. W.; Furche, F.; Evans, W. J. *J. Am. Chem. Soc.* **2013**, *135*, 9857–9868.

(5)   Fieser, M. E.; Macdonald, M. R.; Krull, B. T.; Bates, J. E.; Ziller, J. W.; Furche, F.; Evans, W. J. *J. Am. Chem. Soc.* **2015**, *137* (1), 369–382.

(6)   Evans, W. J. *Organometallics* **2016**, *35*, 3088–3100.

(7)   Woen, D. H.; Evans, W. J. In *Handbook on the Physics and Chemistry of Rare Earths*; Elsevier B.V., 2016; pp 1–57.

(8)   Fieser, M. E.; Palumbo, C. T.; La Pierre, H. S.; Halter, D. P.; Voora, V. K.; Ziller, J. W.; Furche, F.; Meyer, K.; Evans, W. J. *Chem. Sci.* **2017**, *8* (11), 7424–7433.

(9)   Palumbo, C. T.; Darago, L. E.; Windorff, C. J.; Ziller, J. W.; Evans, W. J. *Organometallics* **2018**, *37* (6), 900–905.

(10)   Huh, D. N.; Darago, L. E.; Ziller, J. W.; Evans, W. J. *Inorg. Chem.* **2018**, *57* (4), 2096–2102.

(11)   Fieser, M. E. University of California, Irvine, 2015.

(12)   Jenkins, T. F.; Woen, D. H.; Mohanam, L. N.; Ziller, J. W.; Furche, F.; Evans, W. J. *Organometallics* **2018**, *37* (21), 3863–3873.

(13)   Angadol, M. A.; Woen, D. H.; Windorff, C. J.; Ziller, J. W.; Evans, W. J. *Organometallics* **2019**, *38* (5), 1151–1158.

(14)   Huh, D. N.; Ziller, J. W.; Evans, W. J. *Dalt. Trans.* **2018**, *47* (48), 17285–17290.

(15)   Moehring, S. A.; Beltrán-Leiva, M. J.; Páez-Hernández, D.; Arratia-Pérez, R.; Ziller, J. W.; Evans, W. J. *Chem. Eur. J.* **2018**, *24* (68), 18059–18067.

(16)   Moehring, S. A.; Miehlich, M.; Hoerger, C. J.; Meyer, K.; Ziller, J. W.; Evans, W. J. *Inorg. Chem.* **2020**, *59* (5), 3207–3214.

(17)   Ryan, A. J.; Darago, L. E.; Balasubramani, G.; Chen, G. P.; Ziller, J. W.; Furche, F.; Long, J. R.; Evans, W. J. *Chem. Eur. J.* **2018**, No. 2, 7702–7709.

(18)   Woen, D. H.; Chen, G. P.; Ziller, J. W.; Boyle, T. J.; Furche, F.; Evans, W. J. *Angew. Chem. Int. Ed.* **2017**, *129*, 2082–2085.

(19) Han, S. D.; Allen, J. L.; Jónsson, E.; Johansson, P.; McOwen, D. W.; Boyle, P. D.; Henderson, W. A. *J. Phys. Chem. C* **2013**, *117* (11), 5521–5531.

(20) Tirla, C.; Mézailles, N.; Ricard, L.; Mathey, F.; Le Floch, P. *Inorg. Chem.* **2002**, *41* (23), 6032–6037.

(21) Moores, A.; Ricard, L.; Le Floch, P.; Mézailles, N. *Organometallics* **2003**, *22* (9), 1960–1966.

(22) Guzei, I. A.; Spencer, L. C.; Su, J. W.; Burnette, R. R. *Acta Crystallogr. Sect. B Struct. Sci.* **2007**, *63* (1), 93–100.

(23) Rudd Alex, P.; Planas, N.; Bill, E.; Gagliardi, L.; Lu, C. C. *Eur. J. Inorg. Chem.* **2013**, *2* (22–23), 3898–3906.

(24) Assefa, M. K.; Wu, G.; Hayton, T. W. *Chem. Sci.* **2017**, *8* (11), 7873–7878.

(25) Lu, E.; Boronski, J. T.; Gregson, M.; Wooles, A. J.; Liddle, S. T. *Angew. Chemie - Int. Ed.* **2018**, *57* (19), 5506–5511.

(26) Huh, D. N.; Kotyk, C. M.; Gembicky, M.; Rheingold, A. L.; Ziller, J. W.; Evans, W. J. *Chem. Commun.* **2017**, *53* (62), 8664–8666.

(27) Bestgen, S.; Chen, Q.; Rees, N. H.; Goicoechea, J. M. *Dalt. Trans.* **2018**, *47* (37), 13016–13024.

(28) Lenora, C. U.; Carniato, F.; Shen, Y.; Latif, Z.; Haacke, E. M.; Martin, P. D.; Botta, M.; Allen, M. J. *Chem. Eur. J.* **2017**, *23* (61), 15404–15414.

(29) Jenks, T. C.; Kuda-Wedagedara, A. N. W.; Bailey, M. D.; Ward, C. L.; Allen, M. J. *Inorg. Chem.* **2020**.

(30) Marsh, M. L.; White, F. D.; Meeker, D. S.; McKinley, C. D.; Dan, D.; Van Alstine, C.; Poe, T. N.; Gray, D. L.; Hobart, D. E.; Albrecht-Schmitt, T. E. *Inorg. Chem.* **2019**, *58* (15), 9602–9612.

(31) Huh, D. N.; Windorff, C. J.; Ziller, J. W.; Evans, W. J. *Chem. Commun.* **2018**, *54* (73), 10272–10275.

(32) Huh, D. N.; Ziller, J. W.; Evans, W. J. *Inorg. Chem.* **2019**, *58* (15), 9613–9617.

(33) Huh, D. N.; Ciccone, S. R.; Roy, S.; Ziller, J. W.; Furche, F.; Evans, W. J. *Angew. Chem. Int. Ed.* **2020**.

(34) Burns, J. H. *Inorg. Chem.* **1979**, *18* (11), 3044–3047.

(35) Ciampolini, B. M.; Dapporto, P.; Nardi, N. *J. Chem. Soc. Dalt.* **1979**, 974–977.

(36) Benetollo, F.; Bombieri, G.; Cassol, A.; De Paoli, G.; Legendziewicz, J. *Inorganica Chim. Acta* **1985**, *110* (1), 7–13.

(37) Yang, G.; Liu, S.; Jin, Z. *Inorganica Chim. Acta* **1987**, *131* (1), 125–128.

(38) Heinze, U.; Heinze, T.; Klemm, D. *Macromol. Chem. Phys.* **1999**, *200* (2), 896–902.

(39) Evans, W. J.; Lee, D. S.; Lie, C.; Ziller, J. W. *Angew. Chem. Int. Ed.* **2004**, *43* (41), 5517–5519.

(40) Evans, W. J.; Lee, D. S.; Rego, D. B.; Perotti, J. M.; Kozimor, S. A.; Moore, E. K.; Ziller, J. W. *J. Am. Chem. Soc.* **2004**, *126* (44), 14574–14582.

(41) Evans, W. J.; Lee, D. S.; Ziller, J. W. *J. Am. Chem. Soc.* **2004**, *126*, 454–455.

(42) Evans, W. J.; Rego, D. B.; Ziller, J. W. *Inorg. Chem.* **2006**, *45*, 10790–10798.

(43) Rinehart, D.; Fang, M.; Evans, W. J.; Long, R. *J. Am. Chem. Soc.* **2011**, *133*, 14236–14239.

(44) Fang, M.; Lee, D. S.; Ziller, J. W.; Doedens, R. J.; Bates, J. E.; Furche, F.; Evans, W. J. *J. Am. Chem. Soc.* **2011**, *133* (11), 3784–3787.

(45) Allen, F. H.; Kennard, O.; Watson, D. G.; Brammer, L.; Orpen, A. G.; Taylor, R. *J. Chem.*

Soc. Perkin Trans. 2 **1987**, 1–19.

(46)   Fieser, M. E.; Woen, D. H.; Corbey, J. F.; Mueller, T. J.; Ziller, J. W.; Evans, W. J. *Dalt. Trans.* **2016**, *45* (37), 14634–14644.

(47)   Shannon, R. D. *Acta Crystallogr., Sect. A Cryst. Phys., Diffr., Theor. Gen. Crystallogr.* **1976**, *32*, 751–767.

Chapter 4

The Solid State End-on to Side-on Isomerization of $(N=N)^{2-}$ in $\{[(R_2N)_3Nd]_2N_2\}^{2-}$ (R = SiMe$_3$) Connects In Situ $Ln^{III}(NR_2)_3$/K and Isolated $[Ln^{II}(NR_2)_3]^{1-}$ Dinitrogen Reduction

Introduction

This Chapter describes the reductive chemistry of neodymium with *in-situ* Nd(NR$_2$)$_3$/M/N$_2$ reactions and a possible connection between the LnA$_3$/M reductions of N$_2$ and the Ln(II) reductions. As outlined in the Introduction, exposure of dinitrogen to the [Ln(NR$_2$)$_3$]$^{1-}$ complexes (Ln = Sc, Gd, Tb) at low temperatures in Et$_2$O with either 18-c-6 or crypt produced the first end-on bound reduced dinitrogen complexes of the Ln metals, $[\{(R_2N)_3Ln\}_2(\mu\text{-}\eta^1{:}\eta^1\text{-}N_2)]^{2-}$.[1,2] In contrast to the previously isolated neutral complexes, $[(THF)(R_2N)_2Ln]_2[\mu\text{-}\eta^2{:}\eta^2\text{-}N_2]$,[3] with two amide ligands per metal, these complexes were dianionic with three (NR$_2$)$^{1-}$ ligands per metal, $[\{(R_2N)_3Ln\}_2(\mu\text{-}\eta^1{:}\eta^1\text{-}N_2)]^{2-}$. The reactions that formed the end-on complexes, $[\{(R_2N)_3Ln\}_2(\mu\text{-}\eta^1{:}\eta^1\text{-}N_2)]^{2-}$, were performed at −35 °C in Et$_2$O and in the presence of a chelating agent. In comparison, the reactions that formed the side-on complexes, $[(THF)(R_2N)_2Ln]_2[\mu\text{-}\eta^2{:}\eta^2\text{-}N_2]$, were performed at room temperature in THF without the presence of a chelating agent.

Although the Sc and Tb complexes had the end-on structure, $[\{(R_2N)_3Ln\}_2(\mu\text{-}\eta^1{:}\eta^1\text{-}N_2)]^{2-}$, the X-ray crystallographic evidence of the Gd complex showed that it was comprised of a mixture of side-on and end-on bound $(N=N)^{2-}$ units, $[\{(R_2N)_3Gd\}_2(\mu\text{-}\eta^x{:}\eta^x\text{-}N_2)]^{2-}$ (x = 1, 2).[1] The end-on $(N=N)^{2-}$ ions in these complexes, $[\{(R_2N)_3Ln\}_2(\mu\text{-}\eta^1{:}\eta^1\text{-}N_2)]^{2-}$ (Ln = Sc, Tb) and $[\{(R_2N)_3Gd\}_2(\mu\text{-}\eta^x{:}\eta^x\text{-}N_2)]^{2-}$, are potent reductants and can revert back to the highly reactive Ln(II) complexes, [Ln(NR$_2$)$_3$]$^{1-}$.[1,2] This has not been observed for the side-on species.

Since the smaller metals such as Sc and Tb formed end-on $\{[(R_2N)_3Ln]_2[\mu-\eta^1:\eta^1-N_2]\}^{2-}$ complexes and the larger Gd formed a mixture of end-on and side-on species, it was of interest to look at an even larger metal to see if side-on would be favored in this series of dianions.

Results

Synthesis of $[K_2(18\text{-}c\text{-}6)_3][\{(R_2N)_3Nd\}_2(N_2)]$, 1-Nd. Under an atmosphere of N_2, a solution of light blue $Nd(NR_2)_3$ and 18-c-6 in Et_2O, chilled to $-35\ °C$, was added to a vial containing excess KC_8, chilled to $-116\ °C$. The solution became dark yellow and was filtered and placed in a $-35\ °C$ freezer. As the solution warmed to $-35\ °C$, the solution became light green and light green crystals were isolated after several days. As a light green crystal was cooled on the diffractometer from room temperature to $-180\ °C$, it became yellow-brown. Data were collected on the yellow-brown crystal at $-180\ °C$ which revealed it to be the end-on structure $[K_2(18\text{-}c\text{-}6)_3][\{(R_2N)_3Nd\}_2(\mu-\eta^1:\eta^1-N_2)]$, **1-Nd(end-on)**, Figure 4.1.
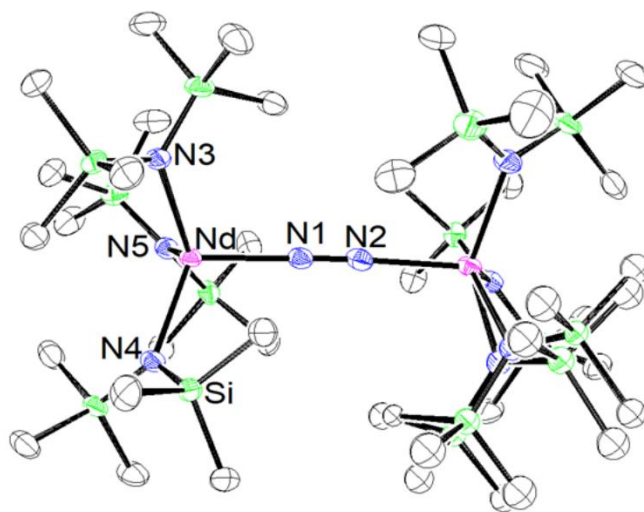
Figure 4.1. Representation of **1-Nd(end-on)** with atomic displacement parameters drawn at the 50% probability level. Hydrogen atoms, the $[K_2(18\text{-}c\text{-}6)_3]^{2+}$ countercation, and an Et_2O molecule in the lattice are not shown.

The color change of this crystal from light green to yellow-brown was observed to be reversible. When the data collection temperature was changed to −25 °C, the crystal became green again and the X-ray data showed that it had a side-on structure, $[K_2(18\text{-}c\text{-}6)_3][\{(R_2N)_3Nd\}_2(\mu\text{-}\eta^2:\eta^2\text{-}N_2)]$, **1-Nd(side-on)**, Figure 4.2, eq 4.1. The data shows that the dinitrogen unit is disordered (see below in Figure 4.3). Green crystals of **1-Nd(side-on)** also become yellow-brown when cooled to −116 °C in the cold well of the glovebox, but in Et_2O solution, the green to dark yellow transformation is not observed.
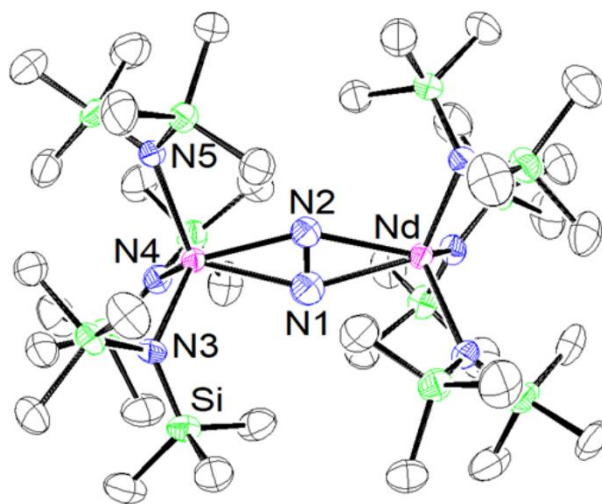
Figure 4.2. Representation of **1-Nd(side-on)** with atomic displacement parameters drawn at the 50% probability level. The N_2 unit is disordered above and below the plane made by the two Nd atoms and the average position of the nitrogen atoms, but only one form is shown here for clarity. Hydrogen atoms, the $[K_2(18\text{-}c\text{-}6)_3]^{2+}$ countercation, and an Et_2O molecule in the lattice are not shown.

Figure 4.3. Representation of **1-Nd(side-on)** with atomic displacement parameters drawn at the 50% probability level with disorder of the N_2 unit shown. Hydrogen atoms, the $[K_2(18\text{-}c\text{-}6)_3]^{2+}$ countercation, and an Et_2O molecule in the lattice are not shown.
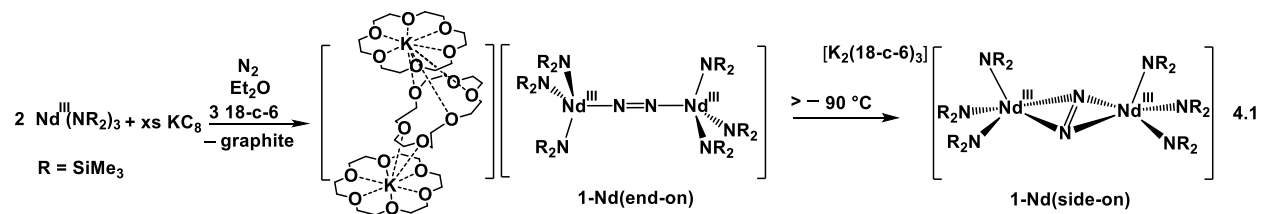
Once the solid-state isomerization of **1-Nd(side-on)** to **1-Nd(end-on)** was observed, X-ray crystallographic data were collected on a single crystal at 10 °C intervals from −50 °C to −130 °C. It was necessary to start at the higher temperature and slowly lower the temperature, because attempts to start at low temperature and raise the temperature cracked the crystals so that useful data could not be obtained at higher temperatures. The error limits on the data did not allow detailed analysis of bond distance changes as a function of temperature, in part due to the quality of the crystal, disorder, thermal motion at higher temperatures, and degradation of the crystal during the 13 day period over which the data were collected. A concern was the choice of space

129

groups. It was possible to solve and refine the structures in both P1 and P$\bar{1}$. Since P1 is less common for organometallic complexes, the structures for **1-Nd** were refined in P$\bar{1}$ for all representations shown and metrical parameters. The data sets collected at −50 °C, −60 °C, −70 °C, and −80 °C showed exclusively side-on $Nd_2(\mu\text{-}\eta^2\text{:}\eta^2\text{-}N_2)$ coordination at the limits of detection. At temperatures below −100 °C, the end-on contribution was seen exclusively at the limits of detection. Between −90 °C and −100 °C, there was a transition from side-on to end-on coordination and the structures are likely to be mixtures of end-on and side-on like those found for gadolinium in $\{[(R_2N)_3Gd]_2[\mu\text{-}\eta^x\text{:}\eta^x\text{-}N_2]\}^{2-}$.[1] When the structures are refined in P1 instead of P$\bar{1}$, the ratios of the equilibrium mixture can be identified, Figure 4.4. Similar to the refinement in P$\bar{1}$, at −50 °C, −60 °C, −70 °C, and −80 °C the structures show exclusively side-on $Nd_2(\mu\text{-}\eta^2\text{:}\eta^2\text{-}N_2)$ coordination. At −90 °C, the data indicated the presence of a small amount of the end-on $Nd_2(\mu\text{-}\eta^1\text{:}\eta^1\text{-}N_2)$ isomer at the 5% detection limit along with the 95% side-on form. At −100°C, the end-on contribution increased to 74% and was 95% at −180°C.
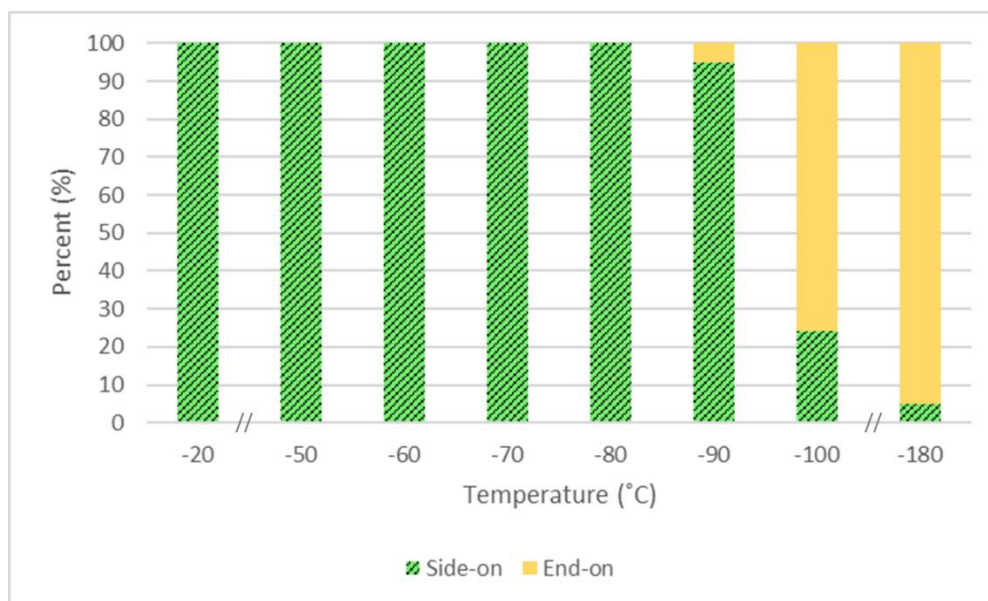
Figure 4.4. Bar graph of % end-on (yellow) and % side-on (green cross-hatch) by variable temperature X-ray crystallography studies of **1-Nd** refined in P1.

Temperature changes led to changes in the unit cell volume consistent with the isomerization analysis given above. The unit cell volume decreases with decreasing temperature from −50 °C (5942.4 Å^3), to −80 °C (5917.1 Å^3). However, in the side-on to end-on transition range, the volume increases from −90 °C (5883.2 Å^3) to −100 °C (5998.4 Å^3).

Variations in Et$_2$O solvent coordination were also observed as the temperature changed. At the higher temperatures, from −25 °C to −80 °C, the Et$_2$O is bound to the potassium atom (K2). At −90 °C and lower temperatures the Et$_2$O is not bound to the potassium. However, the Et$_2$O has distances consistent with hydrogen-bonding between its CH$_2$ component and an oxygen of the crown ether. For example, the C(73B)–O(15) distance is 3.446 Å which is in the range of such interactions.[4–7]

Complex **1-Nd** is isomorphous with the previously-observed [K$_2$(18-c-6)$_3$][{(R$_2$N)$_3$Gd}$_2$(μ-η^x:η^x-N$_2$)],[1] as well as with the newly-characterized [K$_2$(18-c-6)$_3$][{(R$_2$N)$_3$Dy}$_2$(μ-η^x:η^x-N$_2$)] (x = 1, 2) and [K$_2$(18-c-6)$_3$][{(R$_2$N)$_3$Y}$_2$(μ-η^1:η^1-N$_2$)] complexes

131

described below. This system is further complicated by the fact that the oxide complex, [K$_2$(18-c-6)$_3$][{(R$_2$N)$_3$Nd}$_2$(O)], is also isomorphous, Figure 4.5. An analogous oxide was also observed for Gd.[1]
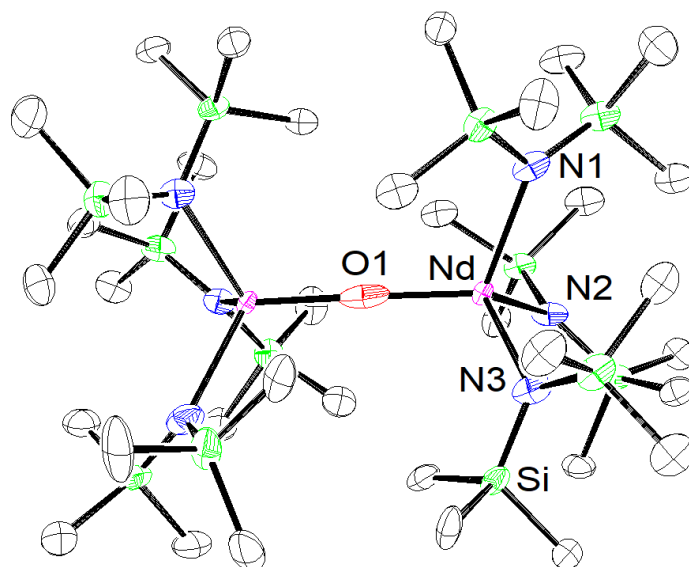
Figure 4.5. Representation of [K$_2$(18-c-6)$_3$]{[(NR$_2$)$_3$Nd]$_2$[μ-O]} with atomic displacement parameters drawn at the 50% probability level. [K$_2$(18-c-6)$_3$]{[(NR$_2$)$_3$Nd]$_2$[μ-O]} is shown without the 25% end-on N$_2$ disorder for clarity. Hydrogen atoms, the [K$_2$(18-c-6)$_3$]$^{2+}$ countercation, and an Et$_2$O molecule in the lattice are not shown.

Synthesis of [K(crypt)][{(THF)(R$_2$N)$_2$Nd}(N$_2$){Nd(NR$_2$)$_3$}], 2-Nd. Reactions using 2.2.2-cryptand (crypt) instead of 18-c-6 as the potassium chelator were also examined. Following the same procedure that generated **1-Nd**, a solution of Nd(NR$_2$)$_3$ and crypt in Et$_2$O, chilled to −35 °C, was added to a vial containing excess KC$_8$, chilled to −116 °C under N$_2$. These reactions generated yellow solutions that become green upon warming. However, crystalline products were not isolable except in one case in which the sample was exposed to THF in the glovebox. Light green crystals were characterized by X-ray crystallography to be a side-on (N=N)$^{2-}$ complex where

one Nd center is ligated by three amides and the other is ligated by two amides and a THF

molecule, [K(crypt)][{(THF)(R$_2$N)$_2$Nd}(μ-η^2:η^2-N$_2$){Nd(NR$_2$)$_3$}], **2-Nd**, Figure 4.6, eq 4.2.

$$\text{Nd}^{\text{III}}(\text{NR}_2)_3 + \text{xs KC}_8 \xrightarrow[\substack{-(\text{NR}_2)^{1-} \\ -\text{graphite}}]{\substack{\text{N}_2 \\ \text{Et}_2\text{O} \\ \text{trace THF} \\ \text{crypt}}} \quad [\text{K(crypt)}] \left[\begin{array}{c} \text{2-Nd} \end{array} \right] \qquad 4.2$$

R = SiMe$_3$

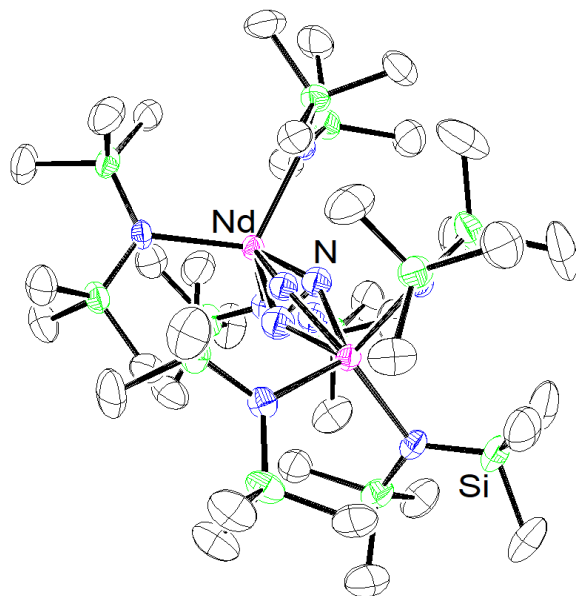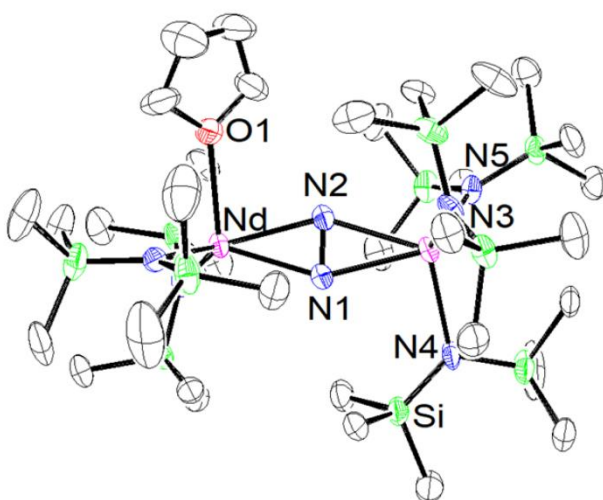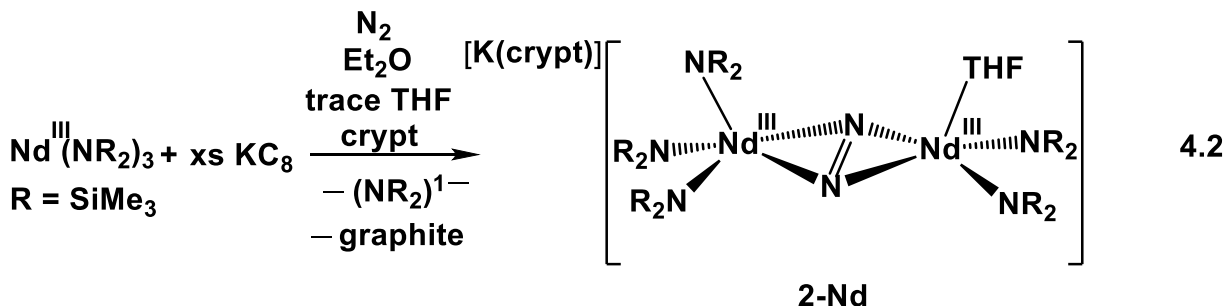**Figure 4.6.** Representation of **2-Nd** with atomic displacement parameters drawn at the 50%

probability level. Hydrogen atoms and the [K(crypt)]$^{1+}$ countercation are not shown.

In attempts to synthesize **2-Nd**, the complex, [K(crypt)][{(THF)(R$_2$N)$_2$Nd}$_2$(μ-η^2:η^2-N$_2$)],

Figure 4.7, was isolated and crystallographically characterized. The N$_2$ unit has been reduced to

N$_2$$^{3-}$ with each Nd center is ligated by a THF molecule and two amides. This complex is similar

to the other isolated N$_2$$^{3-}$ complexes.[8–10]
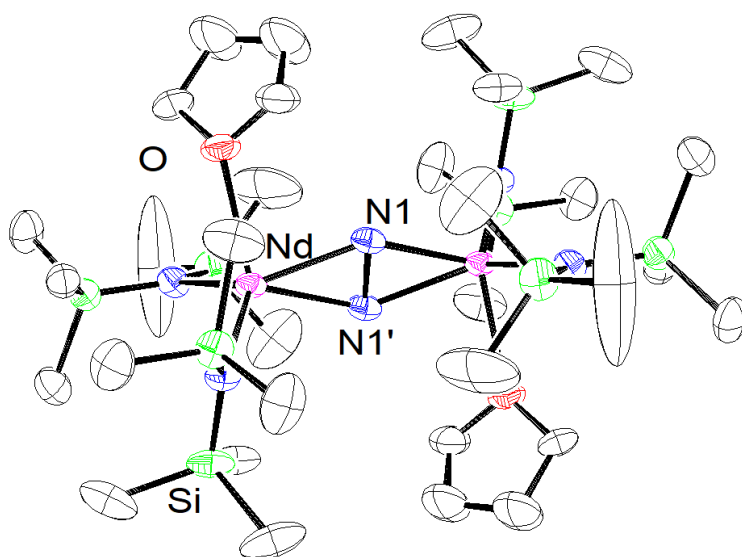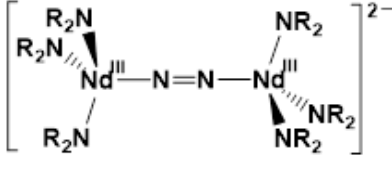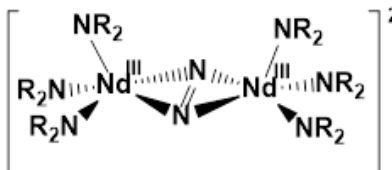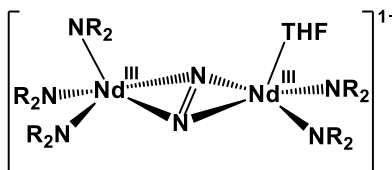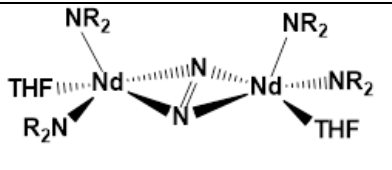
Figure 4.7. Representation of $[K(crypt)][\{(THF)(R_2N)_2Nd\}_2(\mu\text{-}\eta^2{:}\eta^2\text{-}N_2)]$ with atomic displacement parameters drawn at the 50% probability level. Hydrogen atoms, $[K(crypt)]^{1+}$, and Et_2O molecules are omitted for clarity.

Crystallographic Data. Crystallographic data on **1-Nd(end-on)** at −180 °C, **1-Nd(side-on)** at −25 °C, and **2-Nd** at −180 °C were compared with that of the neutral complex, $[(THF)(R_2N)_2Nd]_2(\mu\text{-}\eta^2{:}\eta^2\text{-}N_2)$, **3-Nd**,[3] in Table 4.1, but it should be noted that the data were collected at different temperatures. The 1.205(5) Å N–N distance in **1-Nd(end-on)** is consistent with a double bond, i.e. $(N{=}N)^{2-}$.[11,12] The **1-Nd(side-on)** structure has high thermal motion in some atoms possibly due to the high collection temperature (−25 °C) and the N_2 unit is disordered over two positions which average to a co-planar Nd_2N_2 unit. The N–N distances of 1.185(19) and 1.179(18) Å are equivalent within experimental error of the N–N distances for **1-Nd(end-on)** and shorter than the 1.258(3) Å N–N distance of the neutral side-on bound complex, $[(THF)(R_2N)_2Nd]_2(\mu\text{-}\eta^2{:}\eta^2\text{-}N_2)$, **3-Nd**. However, the high error limits for these high temperature data limit the usefulness of these comparisons. The 1.312(6) Å N–N distance in **2-Nd** is the longest

of these distances. Comparisons with $[\{(R_2N)_3Gd\}_2(\mu\text{-}\eta^x{:}\eta^x\text{-}N_2)]^{2-}$ complexes show the variability of these distances that can occur when different chelating agents are used. For example, $[K_2(18\text{-}c\text{-}6)_3][\{(R_2N)_3Gd\}_2(\mu\text{-}\eta^x{:}\eta^x\text{-}N_2)]$, **1-Gd**, and $[K(crypt)]_2\{[(R_2N)_3Gd]_2(\mu\text{-}\eta^x{:}\eta^x\text{-}N_2)\}$, **1-Gd(crypt)**, have end-on distances of 1.234(9) and 1.271(12) Å, respectively, compared to side-on distances of 1.190(5) and 1.193(9) Å, respectively.[1] The $Nd\text{-}N(N_2)$ distances in **1-Nd(end-on)** are significantly shorter than the analogs in **2-Nd** and **3-Nd**. This was also observed in the Gd system. The $Nd\text{-}N(amide)$ distances in **1-Nd**, **2-Nd**, and **3-Nd** have overlapping ranges that extend from 2.328(1) to 2.467(1) Å.

Table 4.1. Selected metrical parameters for $[K_2(18\text{-}c\text{-}6)_3][\{(R_2N)_3Nd\}_2(\mu\text{-}\eta^x{:}\eta^x\text{-}N_2)]$, **1-Nd** and $[K(crypt)][\{(THF)(R_2N)_2Nd\}(\mu\text{-}\eta^2{:}\eta^2\text{-}N_2)\{Nd(NR_2)_3\}]$, **2-Nd,** and $[(THF)(R_2N)_2Nd]_2(\mu\text{-}\eta^2{:}\eta^2\text{-}N_2)$, **3-Nd**[3] (Å).

	Data Collection Temp (°C)	N–N	Ln–N(N_2)	Ln–N(amide)
	−180	1.205(5)	2.239(4), 2.241(4)	2.389(4) –, 2.466(15)
	−25 to −40	1.185(19), 1.179(18)	2.390(11) –, 2.441(13)	2.421(5) –, 2.466(5)
	−180	1.312(6)	2.357(4) –, 2.425(4)	2.340(4) –, 2.431(4), [Ln–O: 2.528(4)]
	−98	1.258(3)	2.376(2)	2.328(1), 2.347(1), [Ln–O: 2.518(1)]

Synthesis of $[\{(R_2N)_3Dy\}_2(\mu\text{-}\eta^x{:}\eta^x\text{-}N_2)]^{2-}$, $[\{(R_2N)_3Y\}_2(\mu\text{-}\eta^1{:}\eta^1\text{-}N_2)]^{2-}$, **and** $[\{(R_2N)_3Gd\}_2(\mu\text{-}\eta^1{:}\eta^1\text{-}N_2)]^{2-}$**.** Following the procedure in eq 4.1, but with Dy instead of Nd, a colorless solution of $Dy(NR_2)_3$ and 18-c-6 in Et_2O, chilled to −35 °C under an atmosphere of N_2, was added to a vial containing excess KC_8, chilled to −116 °C. The colorless solution changed to

an orange solution and was filtered and placed in a −35 °C freezer. Yellow crystals were isolated after a few days and were identified by X-ray crystallography to be $[K_2(18\text{-}c\text{-}6)_3][\{(R_2N)_3Dy\}_2(\mu\text{-}\eta^x:\eta^x\text{-}N_2)]$, **1-Dy**,[13] i.e. a two-component system as found for the dianion, $\{[(R_2N)_3Gd]_2[\mu\text{-}\eta^x:\eta^x\text{-}N_2]\}^{2-}$, in both the 18-c-6 chelated complex, **1-Gd**, and the crypt analog, **1-Gd(crypt).** The data for **1-Dy** were modelled as a 50% end-on / 50% side-on mixture.

Changing the chelate from 18-c-6 to crypt with Dy again following the same reaction in eq 4.1, allowed the isolation of red crystals that were identified by X-ray crystallography to be $[K(crypt)]_2[\{(R_2N)_3Dy\}_2(\mu\text{-}\eta^x:\eta^x\text{-}N_2)]$, **1-Dy(crypt)**, Figure 4.8. The data were modeled as 30% side-on and 70% end-on.
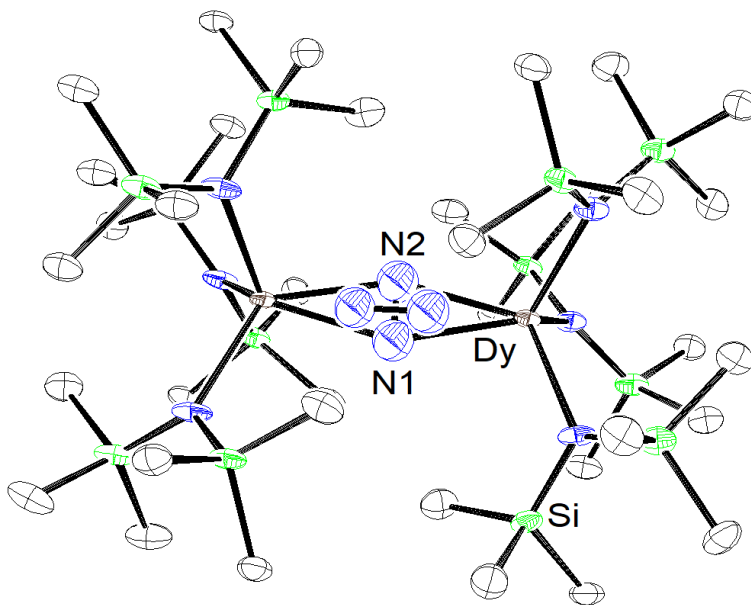
Figure 4.8. Representation of **1-Dy(crypt)** with atomic displacement parameters drawn at the 50% probability level. Hydrogen atoms, two $[K(crypt)]^{1+}$ countercations, and an Et_2O molecule are not shown.

Reactions analogous to eq 4.1 with $Y(NR_2)_3$ generated orange crystals which were identified as $[K_2(18\text{-}c\text{-}6)_3][\{(R_2N)_3Y\}_2(\mu\text{-}\eta^1{:}\eta^1\text{-}N_2)]$, **1-Y**, Figure 4.9, with 18-c-6 as the chelate and $[K(crypt)]_2[\{(R_2N)_3Y\}_2(\mu\text{-}\eta^1{:}\eta^1\text{-}N_2)]$, **1-Y(crypt)**, Figure 4.10, with crypt as the chelate. As indicated in the formulas, both yttrium complexes were exclusively end-on structures.
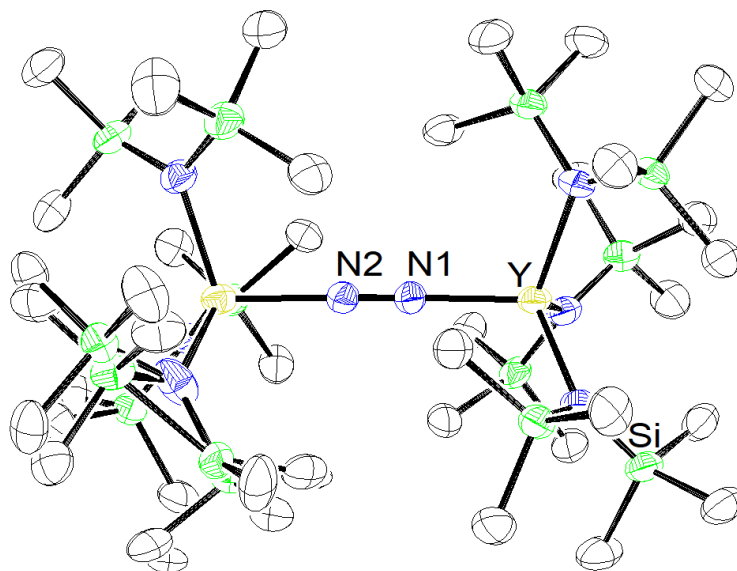
Figure 4.9. Representation of **1-Y** with atomic displacement parameters drawn at the 50% level. Hydrogen atoms, $[K_2(18\text{-}c\text{-}6)_3]^{2+}$ countercation, and two Et_2O molecules are not shown.
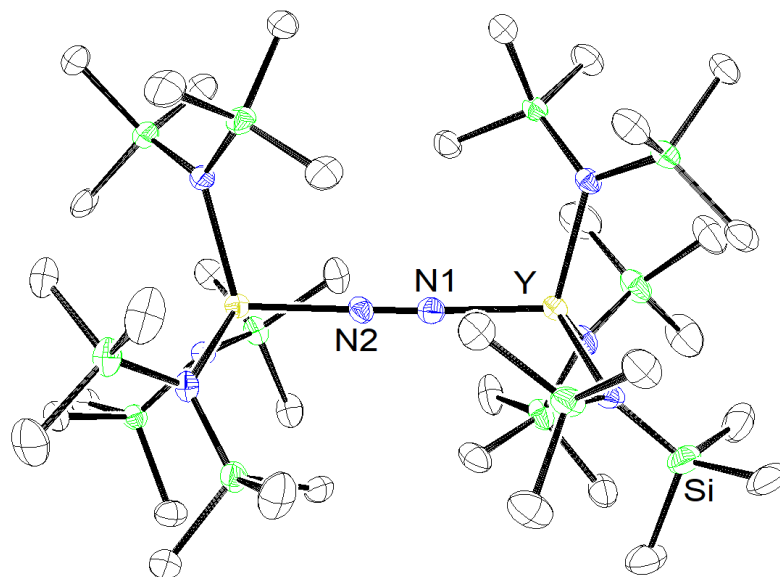
Figure 4.10. Representation of **1-Y(crypt)** with atomic displacement parameters drawn at the 50% level. Hydrogen atoms, two [K(crypt)]$^{1+}$ units, six Et$_2$O molecules, and one unit of [K(crypt)]$_2$\{[(R$_2$N)$_3$Y]$_2$[μ-η^1:η^1-N$_2$]\} are not shown.

The analogous reaction for **1-Ln** was completed with Gd as well since the Gd and Tb complexes were formed from isolated Ln(II). Through using the LnA$_3$/M route, the crystal that was mounted from the reaction was identified by X-ray crystallography to be [K$_2$(18-c-6)$_3$][\{(R$_2$N)$_3$Gd\}$_2$(μ-η^1:η^1-N$_2$)], **1-Gd(end-on),** Figure 4.11, in which the N$_2$ unit was fully end-on. The complexes first discovered with Gd were shown to be a mixture of side-on and end-on.[1]
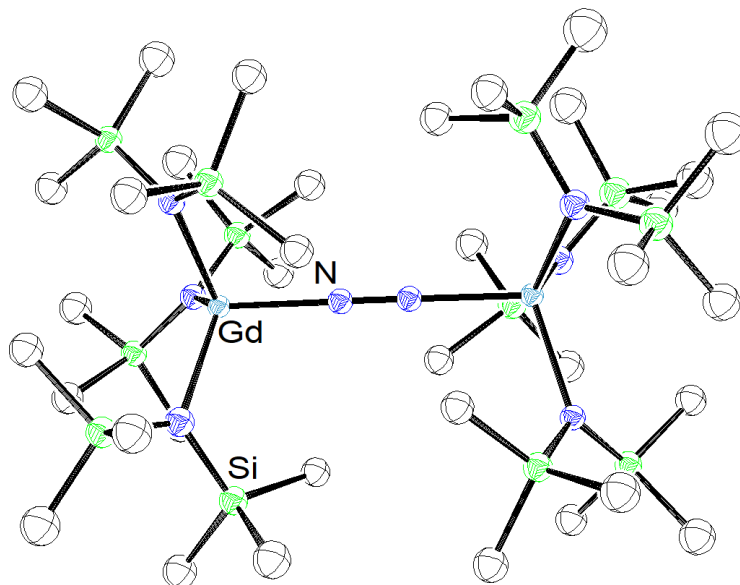
Figure 4.11. Representation of **1-Gd** with atomic displacement parameters drawn at the 50% level. Hydrogen atoms, $[K_2(18\text{-}c\text{-}6)_3]^{2+}$ countercation, and two Et_2O molecules are not shown.

Raman Spectroscopy. Raman data were collected on crystalline samples at room temperature of $[K_2(18\text{-}c\text{-}6)_3][\{(R_2N)_3Nd\}_2(\mu\text{-}\eta^2{:}\eta^2\text{-}N_2)]$, **1-Nd(side-on),** $[K_2(18\text{-}c\text{-}6)_3][\{(R_2N)_3Dy\}_2(\mu\text{-}\eta^x{:}\eta^x\text{-}N_2)]$, **1-Dy**, $K(crypt)]_2[\{(R_2N)_3Dy\}_2(\mu\text{-}\eta^x{:}\eta^x\text{-}N_2)]$, **1-Dy(crypt),** $[K_2(18\text{-}c\text{-}6)_3][\{(R_2N)_3Y\}_2(\mu\text{-}\eta^1{:}\eta^1\text{-}N_2)]$, **1-Y,** and $[K(crypt)]_2[\{(R_2N)_3Y\}_2(\mu\text{-}\eta^x{:}\eta^x\text{-}N_2)]$, **1-Y(crypt)**, Figure 4.12.
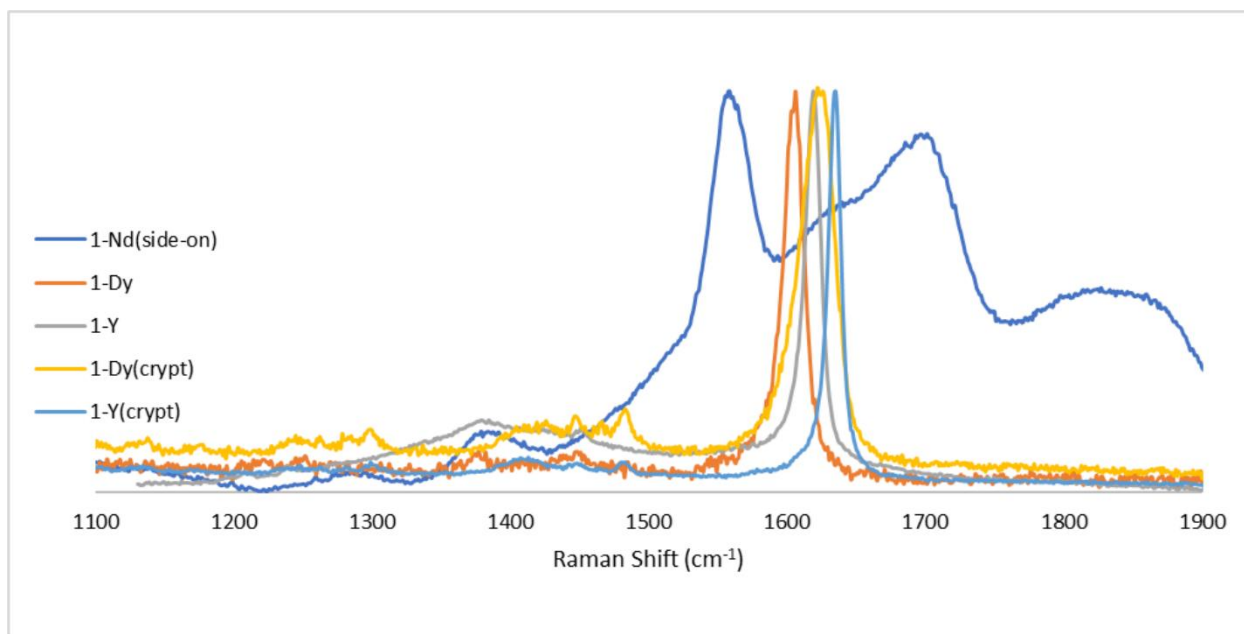
Figure 4.12. Normalized and baseline-corrected Raman spectra of **1-Nd(side-on)** (1557 cm^{-1}), **1-Dy** (1606 cm^{-1}), **1-Dy(crypt)** (1626 cm^{-1}), **1-Y** (1619 cm^{-1}), and **1-Y(crypt)** (1635 cm^{-1}).

Strong resonances in the Raman spectra of **1-Dy** at 1606 cm^{-1}, **1-Dy(crypt)** at 1626 cm^{-1}, **1-Y** at 1619 cm^{-1}, and **1-Y(crypt)** at 1635 cm^{-1}, were very similar to spectra obtained for **1-Sc** at 1644 cm^{-1}, **1-Tb** at 1623 cm^{-1}, and **1-Gd** at 1627 cm^{-1}, Figure 4.13.[1,2]
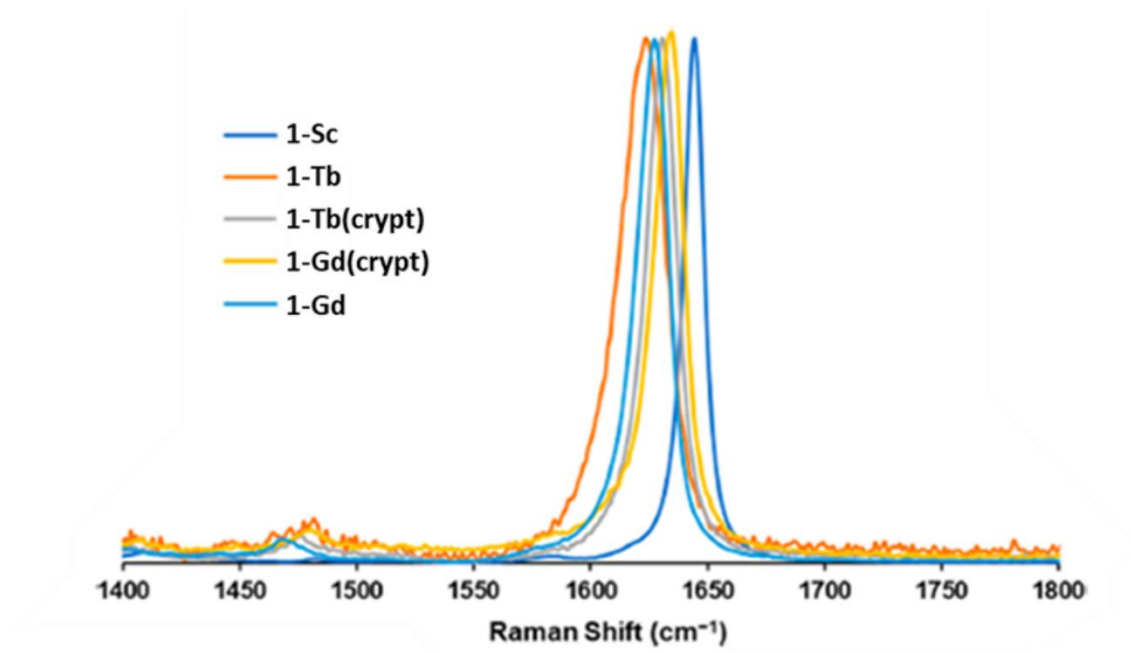
Figure 4.13. Normalized and baseline-corrected Raman spectra of **1-Sc** (1644 cm^{-1}), **1-Tb** (1623cm^{-1}), **1-Tb(crypt)** (1630 cm^{-1}), **1-Gd** (1627 cm^{-1}), and **1-Gd(crypt)** (1634 cm^{-1}).[1,2]

Density functional theory (DFT) studies on the mixed crystal **1-Gd** indicated that the resonance for end-on (N=N)$^{2-}$ was two orders of magnitude more intense than the side-on (N=N)$^{2-}$ stretch, which explains why only the end-on peaks are prominent in Figures 4.12 and 4.13.[1] The neutral side-on complexes, [(R$_2$N)$_2$(THF)Ln]$_2$[μ-η^2:η^2-N$_2$], **3-Ln**, have Raman stretches at 1413–1447 cm^{-1} for Ln = Nd, Gd, Tb, Dy, Ho, Er, and Tm.[14]

The Raman spectrum of **1-Nd** at room temperature showed a different spectrum, however, Figure 4.12. Since this sample should be predominantly the side-on isomer, no end-on resonance is expected. A broad absorption at 1557 cm^{-1} is observed with other bands at higher energy that could not be assigned by DFT analysis (see below).

Optical Spectroscopy. UV-visible spectra of **1-Nd** were taken at −78 °C and at room temperature, Figure 4.14. In the room temperature spectrum of **1-Nd(side-on)**, there is one

absorbance around 600 nm ($\varepsilon = 180$ M^{-1}cm^{-1}). This band is broader and stronger than the hypersensitive $^4I_{9/2}$ → $^4G_{5/2}$, $^2G_{7/2}$ transition which is typical of Nd(III) complexes.[15] In the spectrum of **1-Nd(end-on)** at −78 °C there is an additional absorbance at 556 nm ($\varepsilon = 284$ M^{-1}cm^{-1}) and a broad absorbance at 488 nm ($\varepsilon = 409$ M^{-1}cm^{-1}). The absorptions are analyzed by DFT as described in the next section.
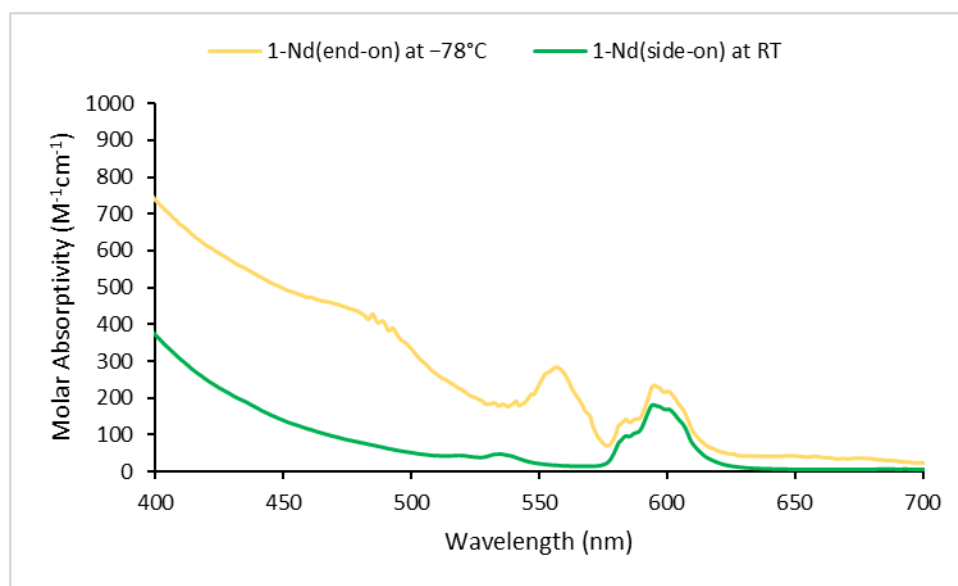
Figure 4.14. UV-visible absorbance spectra in Et$_2$O of **1-Nd(side-on)** at room temperature (green) and **1-Nd(end-on)** at −78 °C (yellow).

Density Functional Theory. Structure optimizations were performed by Dr. Dmitrij Rappaport and Professor Filipp Furche on the end-on and side-on $\{[(R_2N)_3Ln]_2[\mu\text{-}\eta^x{:}\eta^x\text{-}N_2]\}^{2-}$, for Ln = Nd, Gd, Tb, Dy, and Y by DFT using TPSSh hybrid exchange–correlation functional[16] with the Becke–Johnson dispersion correction (D3-BJ),[17,18] def2-SVP basis sets,[19,20] and the resolution-of -the identity (RI-*J*) approximation.[21,22] In contrast to previous calculations on the Gd complexes in which large-core effective core potentials (ECPs) were used,[1] lanthanide atoms were modeled with explicit 4f orbitals and small-core ECPs.[23] The optimized structures were verified

143

by vibrational frequency calculations. The computed harmonic frequencies were scaled by a factor of 0.97.[24]

The $\{[(R_2N)_3Nd]_2[\mu\text{-}\eta^1:\eta^1\text{-}N_2]\}^{2-}$ dianion in **1-Nd(end-on)** has an essentially linear central motif with a 1.19 Å N–N distance (exp: 1.20(1) Å at −180°C) and a 177° Nd–N–N angle. The Nd–N bonds are slightly elongated relative to the X-ray data, d(Nd–N) = 2.28 Å (exp: 2.24(1) Å at −180 °C). The Nd atoms have an approximate f^3 configuration (n/Nd = 3.24) according to the natural population analysis (NPA).[25] The analysis of the spin density on the bridging dinitrogen shows that the unpaired electrons are located in the N p-orbitals (n^{spin}_p(N) = 0.54) and Nd d-orbitals (n^{spin}_d(Nd) = 0.20) and constitute a triplet. The total spin expectation value, $<S^2>$ = 20.01 corresponds to a high-spin configuration with 8 unpaired electrons.

The $\{[(R_2N)_3Nd]_2[\mu\text{-}\eta^2:\eta^2\text{-}N_2]\}^{2-}$ dianion in **1-Nd(side-on)** contains a planar Nd_2N_2 unit with d(N–N) = 1.24 Å (2) (exp: 1.18(2)-1.19(2) Å at −25 °C) and d(Nd–N) =2.41-2.42 Å (exp: 2.39(1)-2.43(1) Å at −25 °C). The Nd atoms have an f^3 configuration (n_f(Nd) = 3.05), while the bridging dinitrogen unit is a singlet. The spin expectation value $<S^2>$ = 12.06 is in line with a spin septet (six unpaired electrons).

Time-dependent density functional theory (TDDFT) calculations were also performed by Dr. Dmitrij Rappaport and Professor Filipp Furche to model the UV-visible spectra. Due to reference-state instabilities in **1-Nd(end-on)** with the PBE0[26] functional, Tamm-Dancoff Approximation (TDA) was applied,[27,28] which is more robust to instabilities. The comparison between TDA and full TDDFT results for the **1-Nd(side-on)** helps to estimate the error of TDA.

The **1-Nd(side-on)** complex is predicted by PBE0/TDA to have a prominent absorption at 543–566 nm stemming from $\pi^*(N_2) \rightarrow$ Nd f excitations, in line with the observed absorption at 600

nm, Figure 4.15. A weaker Nd $f{\rightarrow}f$ band is found at 697 nm which is consistent with Nd(III) complexes.[15] The TDA and full TDDFT spectra are qualitatively similar for the side-on complex. However, TDA causes the strong electronic excitations to be blue-shifted by ca. 40 nm (Figure 4.17).

The predicted electronic absorption spectrum of the dianion in **1-Nd(end-on)**, Figure 4.15, also features a single strong absorption band, in this case at 525 nm, i.e. at higher energy than the **1-Nd(side-on)** prediction. The 525 nm absorption is associated with the excitation from the nearly degenerate HOMO in the complex, which has predominantly $\pi^*(N_2)$ character, into Nd f orbitals. As in **1-Nd(side-on)**, long-wavelength absorptions around 700 nm are also predicted due to the characteristic $f{\rightarrow}f$ transitions of Nd(III).[15]
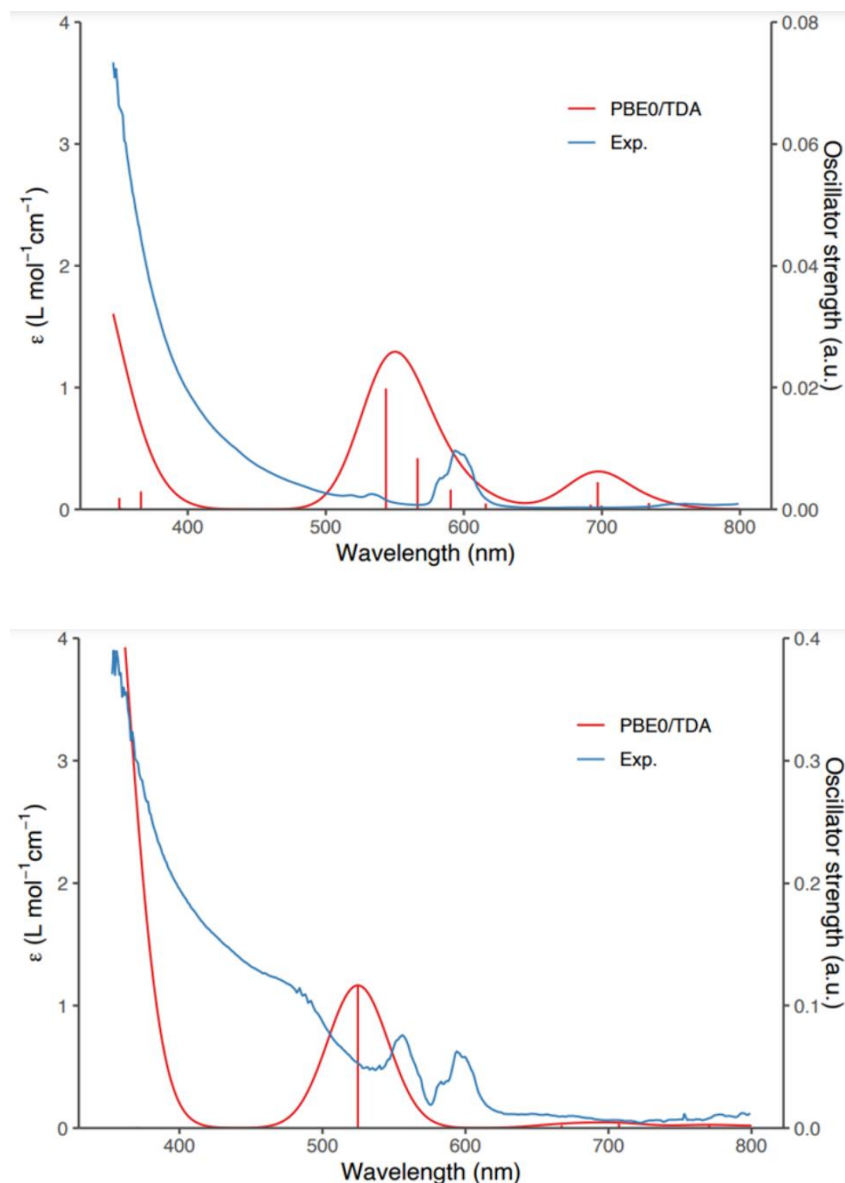
Figure 4.15. Predicted (red) UV-vis spectra of **1-Nd(end-on)** (top) and **1-Nd(side-on)** (bottom) overlayed on experimental (blue).

Experimentally, two absorptions are found in the spectrum of **1-Nd** at −78 °C. One matches that of **1-Nd(side-on)** and the other is at higher energy as predicted by DFT for the end-on isomer. The higher energy absorption disappears within 30 s as the sample warms up (See Computational Details) as expected for an end-on to side-on isomerization. Hence, the −78 °C

146

UV-vis spectrum is likely showing a mixture of the two isomers and the spectra are in good agreement with the calculations.

Calculations by Rappaport and Furche on the Raman spectra also matched the experimental results. The end-on complex is predicted to have an intense stretching Raman mode at 1738 cm^{-1}. The frequency of this mode is strongly downshifted to 1562 cm^{-1} in the side-on complex due to the back-donation from the d(Nd) orbitals to the π^*(N$_2$) orbitals, which leads to weakening of the N–N bond. Vibrational frequencies are somewhat overestimated due to small basis set size. Increasing the basis set size to def2-TZVP[19,20] for the Nd and bridging N atoms gives a vibrational frequency of 1695 cm^{-1} in the end-on complex and 1528 cm^{-1} in the side-on complex.[24] Experimental Raman data were only obtained at room temperature so data on only the side-on isomer can be compared. The 1557 cm^{-1} resonance found for **1-Nd(side-on)** is consistent with the calculations, but the additional resonances in the spectrum, Figure 4.12, were not modeled by the calculations and remain puzzling since they do not seem to be due to fluorescence.

The trend in predicted Raman stretches for the side-on isomers compares well with experimental values; they are 1666, 1541, 1533, 1530, and 1528 cm^{-1} for Gd, Tb, Y, Dy, and Nd, respectively, compared to the experimental values in the same order, 1630, 1623, 1619, 1606, and 1557 cm^{-1}.

Examination of the $\{[(R_2N)_3Gd]_2[\mu\text{-}\eta^x:\eta^x\text{-}N_2]\}^{2-}$ system with explicit treatment of the 4f orbitals revealed low energy distorted end-on structures with the (N=N)$^{2-}$ group rotated relative to the Gd...Gd vector by 27°. The similarities of the energies of the end-on, side-on, and distorted end-on structures suggest that rotation of the (N=N)$^{2-}$ unit between the two metal centers can occur with a low energy barrier. This is consistent with the experimental data that shows mixtures of structures in single crystals.

Discussion

Connecting $Ln^{III}(NR_2)_3/K$ and $[Ln^{II}(NR_2)_3]^{1-}$ Reductions. Examination of the reduction of $Nd(NR_2)_3$ at low temperatures in Et_2O in the presence of 18-crown-6 provides a crystal system, **1-Nd**, that demonstrates a solid-state isomerization of an end-on bound $(N=N)^{2-}$ moiety to the side-on structure found in most of the previously reported rare-earth metal complexes of reduced dinitrogen ligands. The results of this study provide a basis to suggest a connection between the LnA_3/M reductions of N_2 and the Ln(II) reductions, Scheme 4.1, which depends on temperature, solvent, and the presence of a potassium chelating agent.
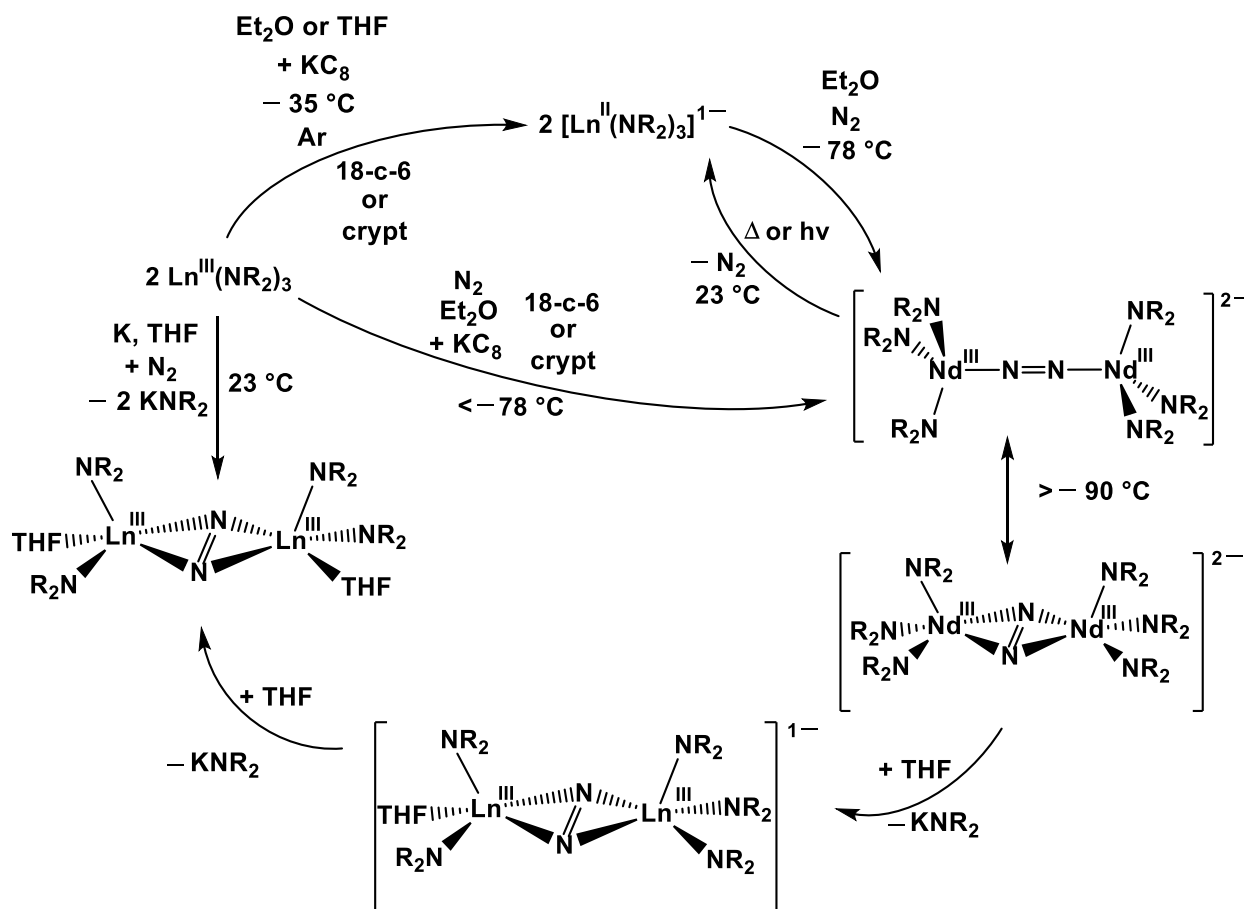
Scheme 4.1. A general scheme showing how reduction of N_2 by LnA_3/M reactions at room temperature could connect to reductions with isolated Ln(II) complexes at low temperature.

Examples of all the complexes in the scheme are known, although not every example is stable enough to be isolated with every rare earth metal.

The $Ln^{III}(NR_2)_3$/K reactions in the absence of N_2 and in the presence of potassium chelating agents can form isolable $[Ln^{II}(NR_2)_3]^{1-}$ compounds, which have been crystallographically characterized for Ln = Nd, Gd, Tb, Dy, Ho, Er, Y, and Sc.[29,30] These will react with N_2 at −78 °C in the dark to form end-on dianions, $\{[(R_2N)_3Ln]_2(\mu\text{-}\eta^1\text{:}\eta^1\text{-}N_2)\}^{2-}$, which have been confirmed by X-ray diffraction for Ln = Nd, Gd, Tb, Dy, Y, Sc.[1,2] For Ln = Nd, the end-on species, observable at low temperature, can isomerize as the temperature increases to the side-on dianion, $\{[(R_2N)_3Ln]_2(\mu\text{-}\eta^2\text{:}\eta^2\text{-}N_2)\}^{2-}$, at temperatures below −90 °C as observed on the diffractometer. This is consistent with the mixed-isomer structures found for Ln = Gd and Dy.

If THF is present, it can displace an NR_2 ligand to form a side-on monoanion, $[(R_2N)_3Ln^{III}(\mu\text{-}\eta^2\text{:}\eta^2\text{-}N_2)Ln^{III}(NR_2)_2(THF)]^{1-}$, as has been crystallographically defined for Ln = Nd and Gd.[1] If this monoanion undergoes one more substitution of amide for THF, the neutral $[(R_2N)_2(THF)Ln]_2[\mu\text{-}\eta^2\text{:}\eta^2\text{-}N_2]$ would result.[3] The latter complexes have been generated by $Ln(NR_2)_3$/K reactions at room temperature in THF in the absence of a potassium chelate for Ln = Nd, Gd, Tb, Dy, and Y.[3]

Hence, in the weaker donor solvent, Et_2O, at low temperature, in the dark, and with a chelate to stabilize the potassium cation, it is possible to access isolable Ln(II) complexes which reduce N_2 to end-on Ln–N=N–Ln species. The end-on dianions, $\{[(R_2N)_3Ln]_2(\mu\text{-}\eta^1\text{:}\eta^1\text{-}N_2)\}^{2-}$, are likely first products of the reaction of $[Ln^{II}(NR_2)_3]^{1-}$ anions with N_2. Subsequent $[\mu\text{-}\eta^1\text{:}\eta^1\text{-}N_2]$ to $[\mu\text{-}\eta^2\text{:}\eta^2\text{-}N_2]$ rearrangement is evidently possible, and substitution of amide ligands by THF with reduction of overall charge of the complex logically leads to the $[(R_2N)_2(THF)Ln]_2[\mu\text{-}\eta^2\text{:}\eta^2\text{-}N_2]$ products isolated from the room temperature reactions in THF without a chelate, Scheme 4.1.

End-on versus Side-on as a Function of Metal. This study was initiated because it seemed that end-on coordination was favored by smaller rare earth metals, e.g. Sc and Tb, and side-on by larger metals since Gd formed mixed isomer species. The Nd result shows that the two forms are close in energy and isomerization can occur in the solid state. The isolation of the pure end-on structures of $[K_2(18\text{-c-6})_3][\{(R_2N)_3Y\}_2(\mu\text{-}\eta^1\text{:}\eta^1\text{-}N_2)]$ and $[K(crypt)]_2[\{(R_2N)_3Y\}_2(\mu\text{-}\eta^1\text{:}\eta^1\text{-}N_2)]$ fits the pattern that end-on is favored by smaller metals. However, isolation of the mixed side-on and end-on Dy complexes, $[K_2(18\text{-c-6})_3][\{(R_2N)_3Dy\}_2(\mu\text{-}\eta^x\text{:}\eta^x\text{-}N_2)]$ and $[K(crypt)_2][\{(R_2N)_3Dy\}_2(\mu\text{-}\eta^1\text{:}\eta^1\text{-}N_2)]$ and a purely end-on Gd complex, $[K_2(18\text{-c-6})_3][\{(R_2N)_3Gd\}_2(\mu\text{-}\eta^1\text{:}\eta^1\text{-}N_2)]$, indicates that there is not a clear-cut correlation between structure and the size of the metal since Dy is smaller than Tb, Figure 4.16.
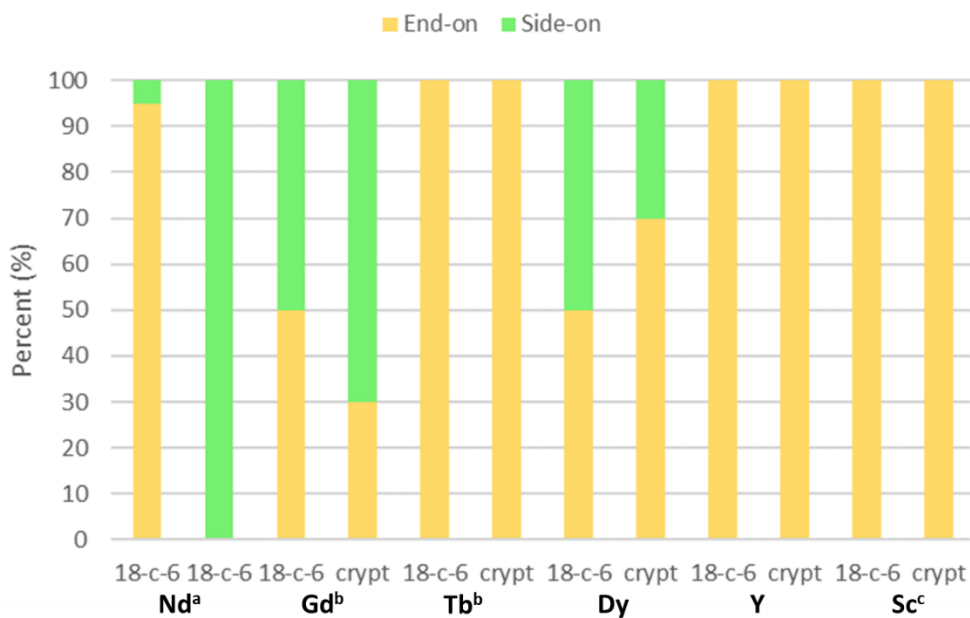
Figure 4.16. Bar graph of % end-on and % side-on of **1-Ln** (Ln = Nd, Gd, Tb, Dy, Y, Sc) and **1-Ln(crypt)** (Ln = Gd, Tb, Dy, Y, Sc). [a] −180 °C, [b] −20 °C, [c] Gd and Tb results shown are taken from literature,[1] and [d] Sc results shown are taken from literature.[2]

Conclusion

The Nd(NR$_2$)$_3$/KC$_8$ dinitrogen reduction system conducted in Et$_2$O at low temperature in the presence of 18-crown-6 provided an ideal metal/ligand combination to elucidate the connection between end-on $\{[(R_2N)_3Ln]_2(\mu\text{-}\eta^1\text{:}\eta^1\text{-}N_2)\}^{2-}$ and side-on $\{[(R_2N)_3Ln]_2(\mu\text{-}\eta^2\text{:}\eta^2\text{-}N_2)\}^{2-}$ (N=N)$^{2-}$ products obtained with rare-earth metal amide complexes. Specifically, the Nd system provided single crystals that isomerize in the solid state from $\{[(R_2N)_3Nd]_2(\mu\text{-}\eta^1\text{:}\eta^1\text{-}N_2)\}^{2-}$ to $\{[(R_2N)_3Nd]_2(\mu\text{-}\eta^2\text{:}\eta^2\text{-}N_2)\}^{2-}$ at temperatures around -90 °C on the diffractometer. This provides the link which connects the Ln(NR$_2$)$_3$/KC$_8$/N$_2$ reactions which give the side-on $[(R_2N)_2(THF)Ln]_2[\mu\text{-}\eta^2\text{:}\eta^2\text{-}N_2]$ products at room temperature in THF to the end-on products observed from reactions at low temperature in Et$_2$O in the presence of potassium chelators. The results emphasize the importance of subtle factors in controlling the reactivity of the rare-earth metal complexes. These are metals are not just simple ionic systems that behave monotonically.

Experimental Details

All manipulations and syntheses described below were conducted with the rigorous exclusion of air and water using standard Schlenk line and glovebox techniques under an argon or dinitrogen atmosphere. Solvents were sparged with UHP argon and dried by passage through columns containing Q-5 and molecular sieves prior to use. Elemental analyses were conducted on a Perkin-Elmer 2400 Series II CHNS elemental analyzer. Infrared spectra were collected on an Agilent Cary 630 equipped with a diamond ATR attachment. UV-visible spectra were collected in Et$_2$O in a 1 mm cell fitted with a Teflon stopcock using an Agilent Cary 60 UV-visible spectrophotometer. Raman spectra were collected on solid samples in a 1 mm quartz cuvette appended with a Teflon stopcock using a Renishaw inVia confocal Raman Microscope, equipped with a 122 mW laser of wavelength 785 nm (laser power 10% and a X5L objective laser).

Measurements were taken on at least three different crystals to confirm reproducibility. 2.2.2-Cryptand (crypt, Merck) was placed under vacuum (10^{-4} torr) for 12 h before use. 18-Crown-6 (18-c-6, Alfa Aesar) was sublimed before use. $Nd(NR_2)_3$, $Gd(NR_2)_3$, $Dy(NR_2)_3$, and $Y(NR_2)_3$ was synthesized according to literature procedures.[31] For all reactions, KC_8 was cooled in a cold well with liquid nitrogen.

[K₂(18-c-6)₃]{[(NR₂)₃Nd]₂[μ-η¹:η¹-N₂]}, 1-Nd(end-on), and [K₂(18-c-6)₃]{[(NR₂)₃Nd]₂[μ-η²:η²-N₂]}, 1-Nd(side-on). In a dinitrogen filled glovebox, $Nd(NR_2)_3$ (50 mg, 0.080 mmol) and 18-crown-6 (32 mg, 0.12 mmol) were dissolved in chilled (−35 °C), nitrogen saturated Et_2O (2 mL) and placed in a −35 °C freezer for one hour. This light blue solution was then added to a vial containing excess KC_8 (24 mg, 0.18 mmol) at −116 °C. The solution was immediately filtered and placed in a −35 °C freezer. As the resulting dark yellow solution warmed to this temperature, it became light green color from which bright green crystals of **1-Nd(side-on)** (34 mg, 38%) suitable for X-ray diffraction were grown. Under the cold stream of the diffractometer (−180 °C), the light green crystals turned to a yellow-brown color of **1-Nd(end-on)**. **1-Nd(side-on)** IR (cm^{-1}): 2994m, 2888m, 1470w, 1453w, 1352s, 1240s, 1107s, 985m, 945s, 862m, 823s, 765m, 699w, 659m. **1-Nd(side-on)** UV-Vis in Et_2O: λ_{max} = 600 nm (ε = 180 M^{-1} cm^{-1}). **1-Nd(end-on)** UV-vis in Et_2O: λ_{max} = 556 nm (ε = 284 M^{-1} cm^{-1}) and 488 nm(ε = 409 M^{-1} cm^{-1}). **1-Nd(side-on)** Anal. Calcd for $C_{70}H_{190}N_8O_{19}Si_{12}K_2Nd_2$: C, 41.81; H, 8.77; N, 4.88. Found: C, 41.67; H, 8.71; N, 3.87. Multiple samples gave low nitrogen values and it is possible that N_2 is lost before combustion is complete.

[K₂(18-c-6)₃]{[(NR₂)₃Nd]₂[μ--O]}. In a dinitrogen filled glovebox, $Nd(NR_2)_3$ (50 mg, 0.08 mmol) and 18-crown-6 (32 mg, 0.12 mmol) were dissolved in −35 °C, nitrogen saturated, Et_2O (2 mL) and placed in a −35 °C freezer for one hour. This light blue solution was then added

to a vial containing excess KC_8 (24 mg, 0.18 mmol) at –116 °C. The solution was immediately filtered and placed in a –35 °C freezer. At some point, the solution was exposed to O_2, from either the box atmosphere being compromised or during the process of preparing the crystal to collect data for x-ray diffraction. The resulting light green solution produced light green crystals of $[K_2(18\text{-}c\text{-}6)_3]\{[(NR_2)_3Nd]_2[\mu\text{-}O]\}$ suitable for x-ray diffraction.

[K(crypt)]{[(THF)(R$_2$N)$_2$Nd][μ-η^2:η^2-N$_2$][Nd(NR$_2$)$_3$]} 2-Nd. In a dinitrogen filled glovebox, $Nd(NR_2)_3$ (50 mg, 0.08 mmol) and 2.2.2-cryptand (30 mg, 0.08 mmol) were dissolved in chilled (−35 °C), nitrogen-saturated Et_2O (2 mL) and placed in a −35 °C freezer for one hour. This light blue solution was then added to a vial containing excess KC_8 (24 mg, 0.18 mmol) at −116 °C. The solution was immediately filtered and placed in a −35 °C freezer overnight. The solution was exposed to trace THF that was present in the box. Bright green crystals of **2-Nd** suitable for X-ray diffraction studies were grown from the resulting green solution.

[K(crypt)][{(THF)(R$_2$N)$_2$Nd}$_2$(μ-η^2:η^2-N$_2$)]. In a dinitrogen filled glovebox, $Nd(NR_2)_3$ (50 mg, 0.08 mmol) and 2.2.2-cryptand (30 mg, 0.08 mmol) were dissolved in chilled (−35 °C), nitrogen-saturated Et_2O (2 mL) and placed in a −35 °C freezer for one hour. This light blue solution was then added to a vial containing excess KC_8 (24 mg, 0.18 mmol) at −116 °C. The solution was immediately filtered and THF (6 μL, 0.08 mmol), chilled to −35 °C, was added and the resulting green solution placed in a −35 °C freezer overnight. Bright green crystals of **[K(crypt)][{(THF)(R$_2$N)$_2$Nd}$_2$(μ-η^2:η^2-N$_2$)]** suitable for X-ray diffraction studies were grown from the resulting green solution.

[K$_2$(18-c-6)$_3$]{[(NR$_2$)$_3$Dy]$_2$[μ-η^x:η^x-N$_2$]}, 1-Dy. In a dinitrogen filled glovebox, $Dy(NR_2)_3$ (50 mg, 0.078 mmol) and 18-crown-6 (31 mg, 0.12 mmol) were dissolved in −35 °C, nitrogen-saturated, Et_2O (2 mL) and placed in a −35 °C freezer for one hour. This colorless solution was

then added to a vial containing excess KC_8 (24 mg, 0.18 mmol) at −116 °C. The solution was immediately filtered and placed in a −35 °C freezer. The resulting dark yellow/orange solution produced yellow crystals of **1-Dy** (23 mg, 26%) suitable for X-ray diffraction. IR (cm^{-1}): 2944w, 2887w, 1473w, 1452w, 1352w, 1237m, 1104m, 943m, 868m, 814m, 770w, 756w, 704w, 652m. UV-Vis in Et_2O: λ_{max} = 360 nm.

[K(crypt)]₂{[(NR₂)₃Dy]₂[μ-ηˣ:ηˣ-N₂]}, 1-Dy(crypt). In a dinitrogen filled glovebox, $Dy(NR_2)_3$ (50 mg, 0.078 mmol) and crypt (29 mg, 0.078 mmol) were dissolved in chilled (−35 °C), nitrogen-saturated, Et_2O (2 mL) and placed in a −35 °C freezer for one hour. This colorless solution was then added to a vial containing excess KC_8 (24 mg, 0.18 mmol) at −116 °C. The solution was immediately filtered and placed in a −35 °C freezer. Red crystals of **1-Dy(crypt)** (27 mg, 32%) that were suitable for X-ray diffraction studies were grown from the resulting yellow/orange solution. IR (cm^{-1}): 2944w, 2884w, 2818w, 1479w, 1445w, 1354w, 1223m, 1132w, 1101m, 943m, 868m, 814m, 770w, 753w, 702w, 652m.

[K₂(18-c-6)₃]{[(NR₂)₃Y]₂[μ-η¹:η¹-N₂]}, 1-Y. In a dinitrogen filled glovebox, $Y(NR_2)_3$ (50 mg, 0.088 mmol) and 18-crown-6 (35 mg, 0.13 mmol) were dissolved in chilled (−35 °C), nitrogen-saturated, Et_2O (2 mL) and placed in a −35 °C freezer for one hour. This colorless solution was then added to a vial containing excess KC_8 (27 mg, 0.20 mmol) at −116 °C. The orange solution was immediately filtered and placed in a −35 °C freezer. Orange crystals of **1-Y** (16 mg, 17%) suitable for X-ray diffraction studies were grown from the resulting yellow/orange solution. IR (cm^{-1}): 2944w, 2888w, 1470w, 1452w, 1352w, 1237m, 1104m, 945m, 865m, 815m, 773w, 750w, 702w, 654m. UV-Vis in Et_2O: λ_{max} = 357 nm (ε = 383 $M^{-1}\,cm^{-1}$)

[K(crypt)]₂{[(NR₂)₃Y]₂[μ-η¹:η¹-N₂]}, 1-Y(crypt). In a dinitrogen filled glovebox, $Y(NR_2)_3$ (50 mg, 0.088 mmol) and crypt (33 mg, 0.088 mmol) were dissolved in chilled (−35 °C),

nitrogen-saturated, Et$_2$O (2 mL) and placed in a −35 °C freezer for one hour. This colorless solution was then added to a vial containing excess KC$_8$ (27 mg, 0.20 mmol) at −116 °C. The solution was immediately filtered and placed in a −35 °C freezer. Orange crystals of **1-Y(crypt)** (17 mg, 19%) suitable for X-ray diffraction studies were grown from the resulting yellow/orange solution. IR (cm^{-1}): 2948w, 2889w, 1476w, 1442w, 1353w, 1298w, 1240m, 1137w, 1103w, 1107m, 962w, 948w, 925w, 865w, 823m, 770w, 753w, 702w, 665w. UV-Vis in Et$_2$O: λ_{max} = 362 nm.

[K$_2$(18-c-6)$_3$]{[(NR$_2$)$_3$Gd]$_2$[μ-η^1:η^1-N$_2$]}, 1-Gd. In a dinitrogen filled glovebox, Gd(NR$_2$)$_3$ (50 mg, 0.070 mmol) and 18-crown-6 (35 mg, 0.14 mmol) were dissolved in chilled (−35 °C), nitrogen saturated Et$_2$O (2 mL) and placed in a −35 °C freezer for one hour. This colorless solution was then added to a vial containing excess KC$_8$ (24 mg, 0.18 mmol) at −116 °C. The resulting dark yellow solution was immediately filtered and placed in a −35 °C freezer. Yellow crystals of **1-Gd** suitable for X-ray diffraction studies were grown from the resulting yellow solution.

Computational Details

Structure optimizations of the end-on and side-on dianions, {[(R$_2$N)$_3$Ln]$_2$[μ-η^x:η^x-N$_2$]}$^{2-}$, were performed for Ln = Nd, Gd, Tb, Dy, and Y. The initial structures of the **1-Nd** and **2-Nd** complexes were extracted from X-ray data of the [K(18-crown-6)$_2$]$^+$ complexes. For the **1-Gd** and **2-Gd** complexes, the X-ray structure of the [K(18-crown-6)$_2$]$^+$ complex[1] was used as a starting point for the structure optimizations. The structure optimizations of **1-Tb** and **1-Dy** compounds were based on the X-ray structure of the [K(crypt)]$^+$ **1-Tb** complex.[1] Additionally, **2-Tb** and **2-Dy** structures were derived from the Gd analog. The structural parameters of the **1-Sc** complex were used as the initial guess for the structure optimizations of the **1-Y** complex.[2] The end-on

complexes were initially treated in D_3 point group symmetry, which was lowered if necessary (see details below). The side-on complexes were assumed to have C_2 symmetry.

Structure optimizations were performed by density functional theory (DFT) with TPSSh hybrid exchange–correlation functional[16] with the Becke–Johnson dispersion correction (D3-BJ)[17,18] and the resolution-of the identity (RI-*J*) approximation.[21,22] def2-SVP basis sets were used for non-hydrogen atoms and def2-SV(P) for hydrogens[19,20] together with small-core relativistic effective core potentials (ECPs) of Dolg and co-workers for the lanthanide atoms.[23] Additional calculations were performed with the larger def2-TZVP basis sets for the lanthanide and bridging N atoms.[19,20] The solvation effects were treated by the conductor-like solvation model (COSMO)[32] using the experimental dielectric constant $\varepsilon_r = 7.52$ and the optical index of refraction $n = 1.4050$ of THF. The optimized structures were confirmed as stable by numerical force constant calculations. Thermodynamic functions were computed in quasi-rigid-rotor–harmonic-oscillator (qRRHO) approximation, in which the contributions from low-frequency vibrations are treated as free rotors.[33] Harmonic vibrational frequencies were scaled down using a global factor of 0.97.[24]

Raman spectra of the **1-Nd** and **2-Nd** complexes were computed using vibrational frequencies from TPSSh calculations and static polarizability derivatives[34] using the PBE0 functional,[26] def2-SVP basis sets, and the COSMO solvation model for THF. Harmonic vibrational frequencies were scaled by an empirical factor 0.97[24] to account for anharmonicity and broadened using Gaussian profiles with empirical line width 20 cm^{-1}.

UV-visible absorption spectra of the optimized **1-Nd** and **2-Nd** complexes were simulated by time-dependent density functional theory (TDDFT) using the PBE0 hybrid functional, def2-SVP basis sets, the RI-*J* approximation, and the COSMO solvation model as in the ground-state calculations. Due to ground-state instabilities, TDDFT calculations using the Tamm–Dancoff

approximation (TDA)[27,28] were additionally performed for both complexes **1-Nd** and **2-Nd**. The computed spectra were broadened using Gaussian profiles with an empirical full width at half-maximum (FWHM) parameter of 50 nm.

DFT Structure Optimizations

The structures of the anions $[(R_2N)_3Ln]_2[\mu\text{-}\eta^1\text{:}\eta^1\text{-}N_2]^{2-}$ (**1-Ln(end-on)**) and $[(R_2N)_3Ln]_2[\mu\text{-}\eta^2\text{:}\eta^2\text{-}N_2]^{2-}$ (**1-Ln(side-on)**) with Ln = Nd, Gd, Dy, Tb, Y were optimized with the TPSSh hybrid exchange–correlation functional[16] with the Becke–Johnson dispersion correction (D3-BJ)[17,18] and the resolution-of -the identity (RI-*J*) approximation.[21] def2-SVP basis sets were used throughout (def2-SV(P) for hydrogens)[19,20] together with small-core relativistic effective core potentials (ECPs) for Ln = Nd, Gd, Dy, Tb.[23] Additional calculations were performed with def2-TZVP basis sets used for the metal and bridging nitrogen atoms. The solvation effects were treated by the conductor-like solvation model (COSMO)[32] using the experimental dielectric constant ε_r = 7.52 and the optical index of refraction n = 1.4050 of THF. All optimized structures were verified as energy minima by numerical force constant calculations. Thermodynamic functions were computed in quasi-rigid-rotor–harmonic-oscillator (qRRHO) approximation, in which the contributions from low-frequency vibrations are treated as free rotors.[33] The computed vibrational frequencies were scaled down using a global factor of 0.97.[24] The **1-Ln(end-on)** complex structures were treated in the D_3 point group symmetry, which was relaxed to C_2 if the D_3-symmetric structures were found to be unstable with respect to symmetry breaking. The electronic configurations were assigned with the help of Natural Population Analysis (NPA) method.[25]

Raman Spectra Simulations

Vibrational Raman spectra of the **1-Nd(end-on)** and **1-Nd(side-on)** complexes were simulated using vibrational frequencies from TPSSh calculations and static polarizability derivatives[34] using the hybrid PBE0 functional[26] and the RI-*J* approximation.[22] The basis sets, ECPs, and COSMO solvation model were the same as in the structure optimizations. The computed vibrational frequencies were scaled by factor 0.97[24] and broadened using Gaussian profiles with empirical line width 20 cm^{-1}.

UV/Vis Spectra Simulations

Simulations of the electronic UV/Vis absorption spectra were performed using time-dependent density functional theory (TDDFT) with the hybrid PBE0 functional[26] and the RI-*J* approximation.[22] The basis sets, ECPs, and COSMO solvation model were the same as in the structure optimizations. The TDDFT calculations exhibited ground-state instabilities in some complexes and were replaced by calculations using the hybrid PBE0 functional and the Tamm–Dancoff approximation (TDA).[27,28] For comparison, excitation calculations using the hybrid TPSSh functional were additionally performed. Current-density corrections were include in the TPSSh excitation calculations.[35] The computed spectra were broadened using Gaussian kernels with an empirical full width at half-maximum (FWHM) parameter of 50 nm.

DFT Results

Structural and Electronic Parameters

Table 4.2. Computed structural and electronic parameters of **1-Nd(end-on)** and **1-Nd(side-on)** complexes. n_u is the number of unpaired electrons, ΔG is reported for T = 213 K. φ is the angle of rotation of the N$_2$ group relative to the Nd–Nd axis

Structure	n_u	**ΔG, kJ/mol^{-1}**	**d(Nd–N$_2$), Å**	**d(N–N), Å**	**φ, deg**	**ν(N–N), cm^{-1}**
side-on	6	0	2.41–2.42	1.24	90	1738
end-on	8	39	2.28	1.19	2	1562

UV/Vis Spectra

Table 4.3. Computed excitation wavelengths λ and oscillator strengths f (in length representation) of the **1-Nd(end-on)** complex with TDDFT using TDA.

Excitation	λ, nm	f	Interpretation
9 B	866	0.002	$\pi^*(N_2) \rightarrow f(Nd)$
13 B	770	0.002	$\pi^*(N_2) \rightarrow f(Nd)$
15 B	707	0.003	$f(Nd) \rightarrow f(Nd)$
18 B	667	0.002	$f(Nd) \rightarrow f(Nd)$
20 B	525	0.117	$\pi^*(N_2) \rightarrow f(Nd)$

Table 4.4. Computed excitation wavelengths λ and oscillator strengths f (in length representation) of the **1-Nd(side-on)** complex with TDDFT.

Excitation	λ, nm	f	Interpretation
15 B	689	0.115	$\pi^*(N_2) \rightarrow f(Nd)$
20 B	539	0.006	$f(Nd) \rightarrow f(Nd)$
24 B	363	0.309	$\pi^*(N_2) \rightarrow d(Nd)$
25 B	351	0.031	$\pi^*(N_2) \rightarrow p(Nd)$
26 B	350	0.005	$\pi^*(N_2) \rightarrow p(Nd)$

Table 4.5. Computed excitation wavelengths λ and oscillator strengths f (in length representation) of the **1-Nd(side-on)** complex with TDDFT using TDA.

Excitation	λ, nm	f	Interpretation
19 A	366	0.003	$\pi^*(N_2) \rightarrow f(Nd)$
8 B	734	0.001	$\pi^*(N_2)/f(Nd) \rightarrow f(Nd)$
10 B	697	0.004	$f(Nd) \rightarrow f(Nd)$
14 B	590	0.003	$\pi^*(N_2) \rightarrow f(Nd)$
15 B	566	0.008	$\pi^*(N_2) \rightarrow f(Nd)$
16 B	543	0.020	$\pi^*(N_2) \rightarrow f(Nd)$
19 B	350	0.002	$\pi^*(N_2) \rightarrow f(Nd)$
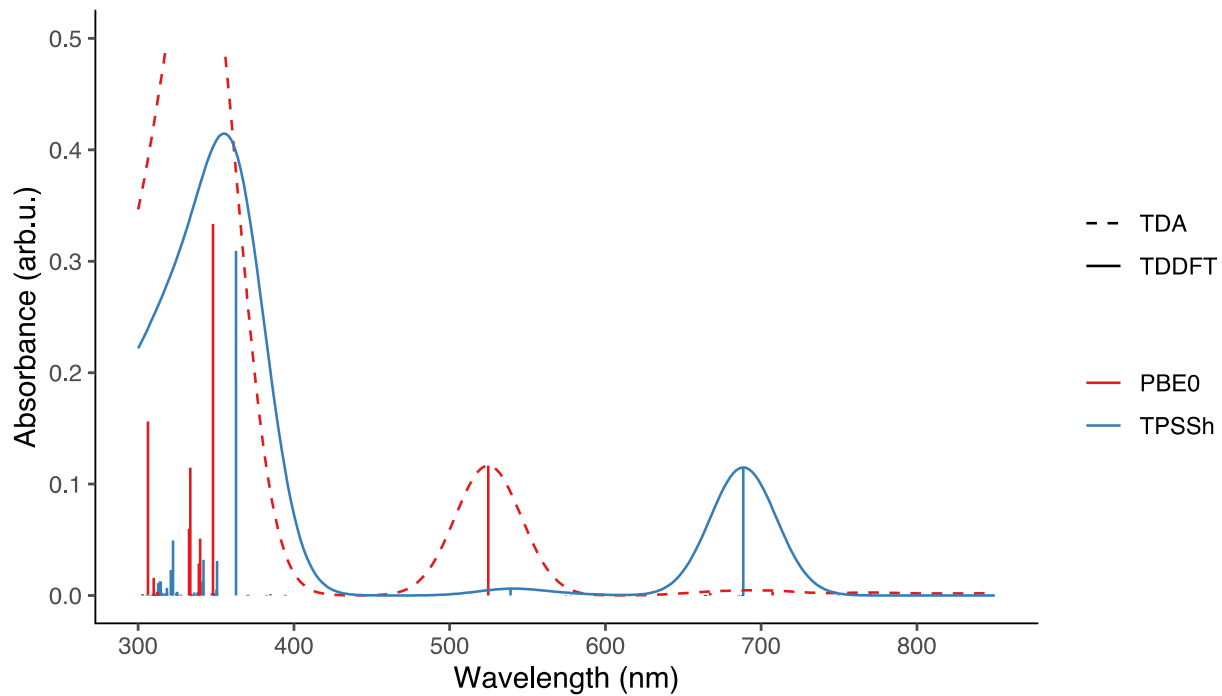
Figure 4.17. Computed electronic UV/Vis spectra of the **1-Nd(end-on)** complex with PBE0 and
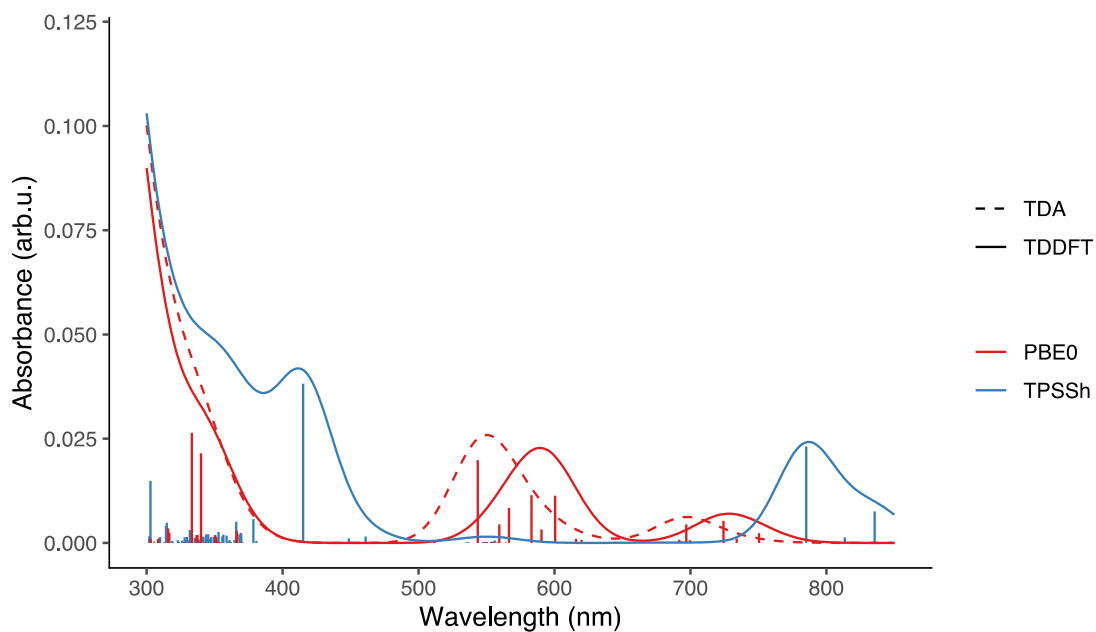
TPSSh functionals.

Figure 4.18. Computed electronic UV/Vis spectra of the **1-Nd(side-on)** complex with PBE0 and

TPSSh functionals.

160
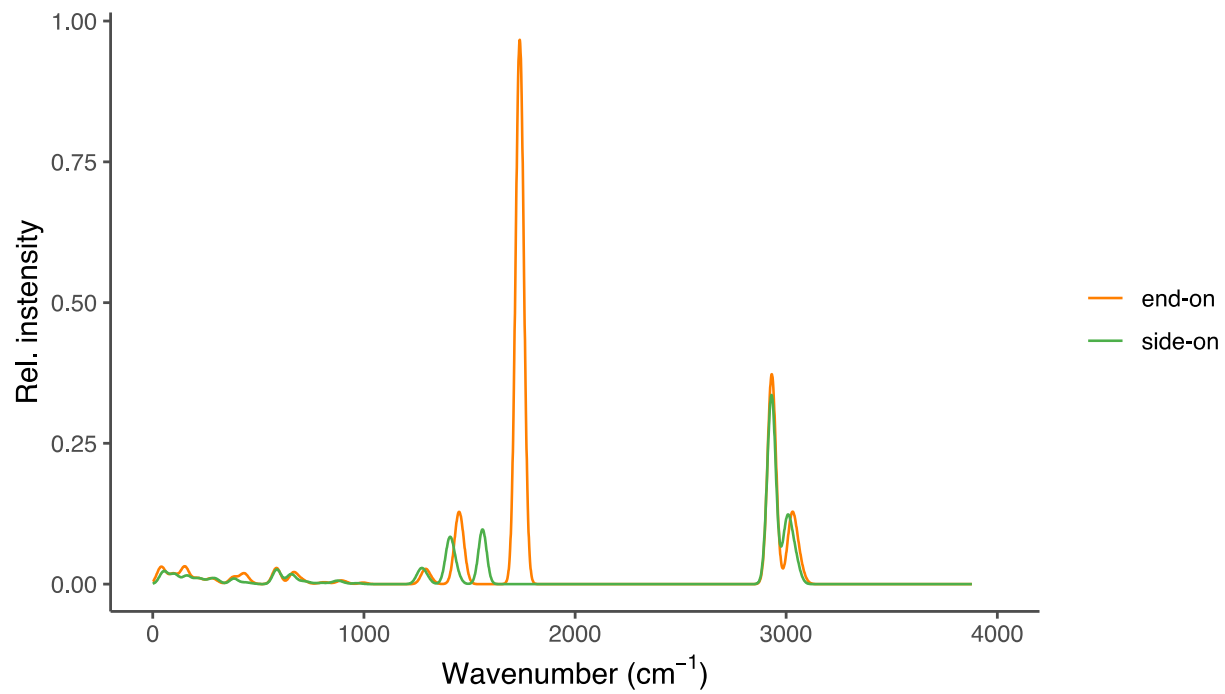
Figure 4.19. Computed vibrational Raman spectra of the **1-Nd(end-on)** and **1-Nd(side-on)** complexes.

Additional Characterization of Complexes
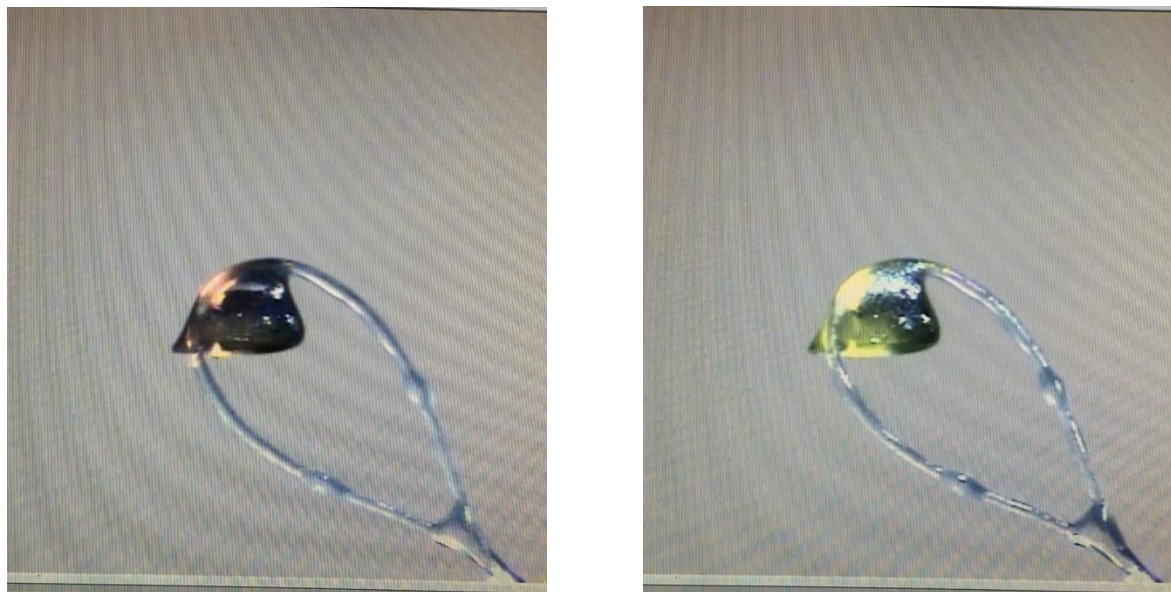
Figure 4.20. Images of **1-Nd** under cold stream of x-ray diffractometer at −180 °C (left) and 23 °C (right).
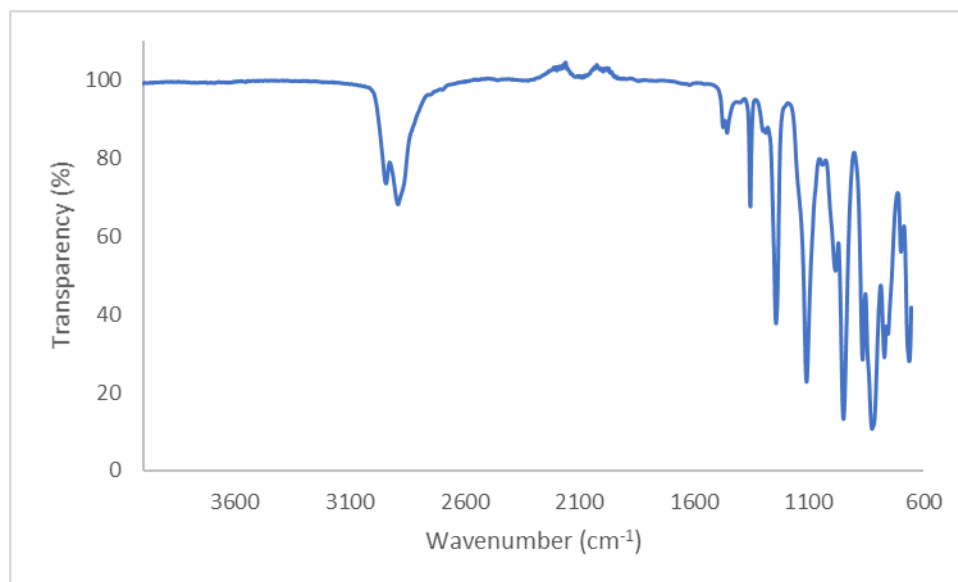
Figure 4.21. IR spectrum of **1-Nd**.
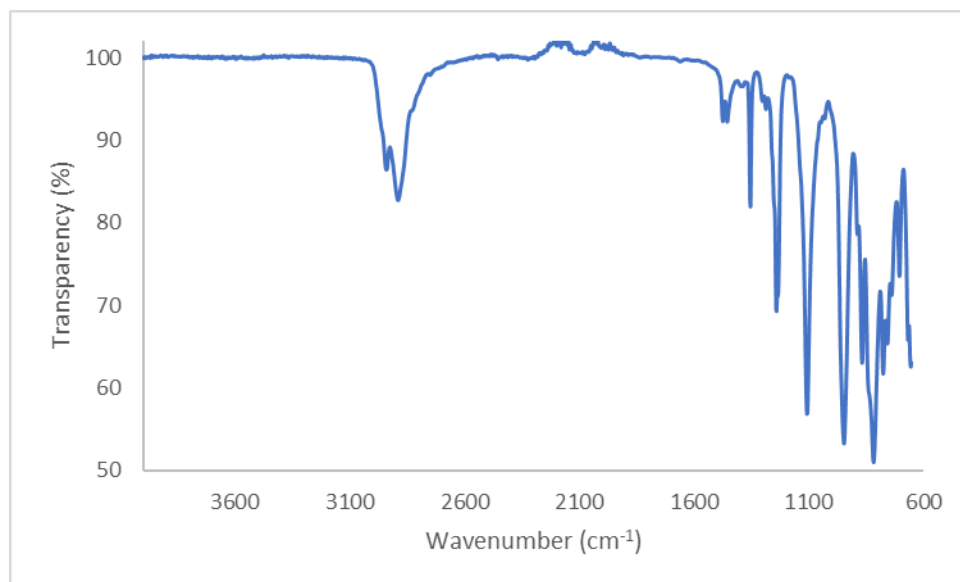
Figure 4.22. IR spectrum of **1-Dy.**
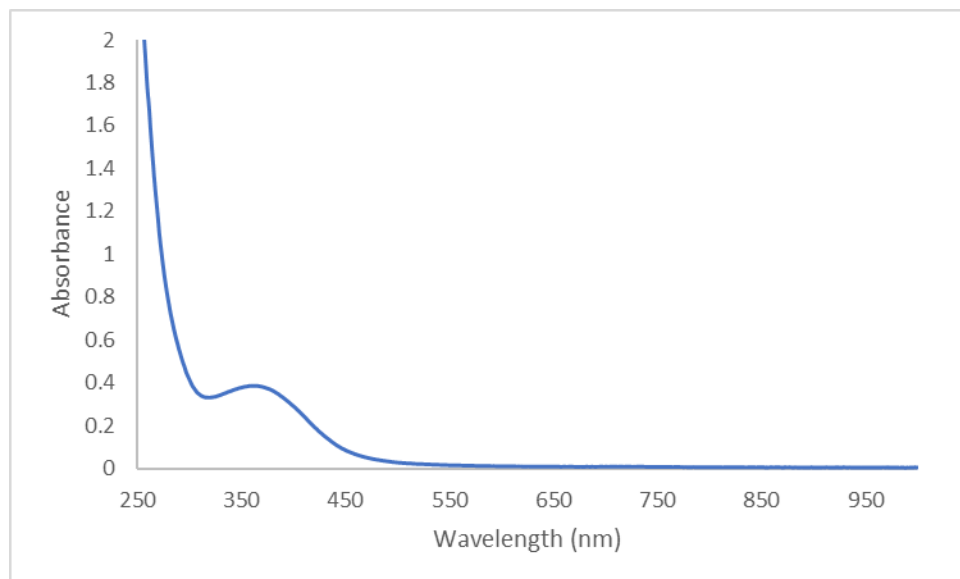
Figure 4.23. UV-vis spectrum of **1-Dy** in Et$_2$O**.**
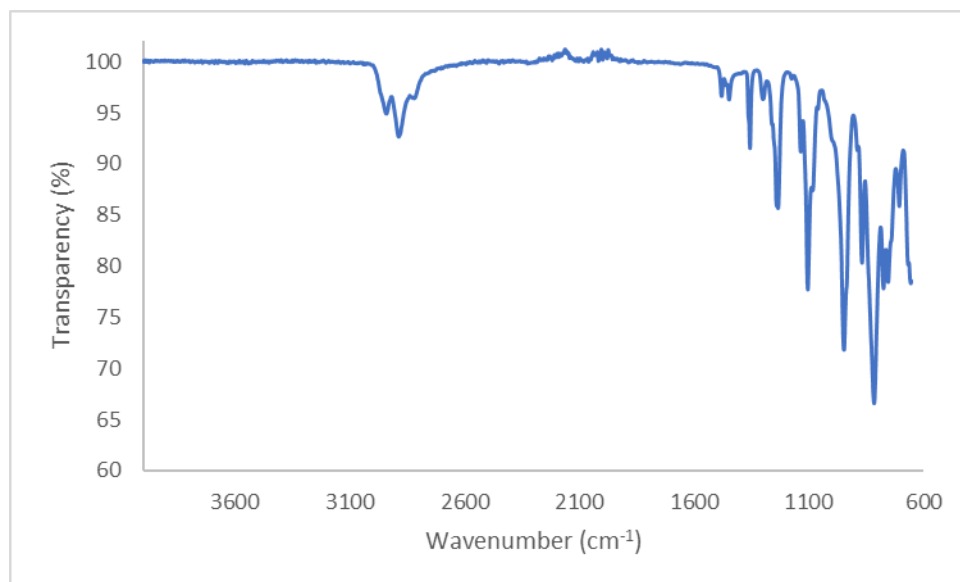
Figure 4.24. IR spectrum of **1-Dy(crypt).**
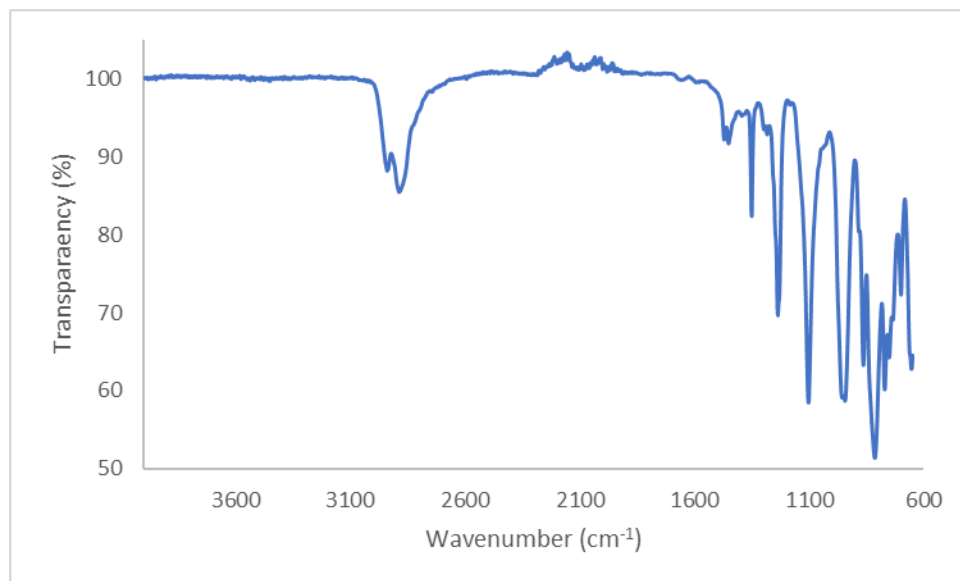
Figure 4.25. IR spectrum of **1-Y**.
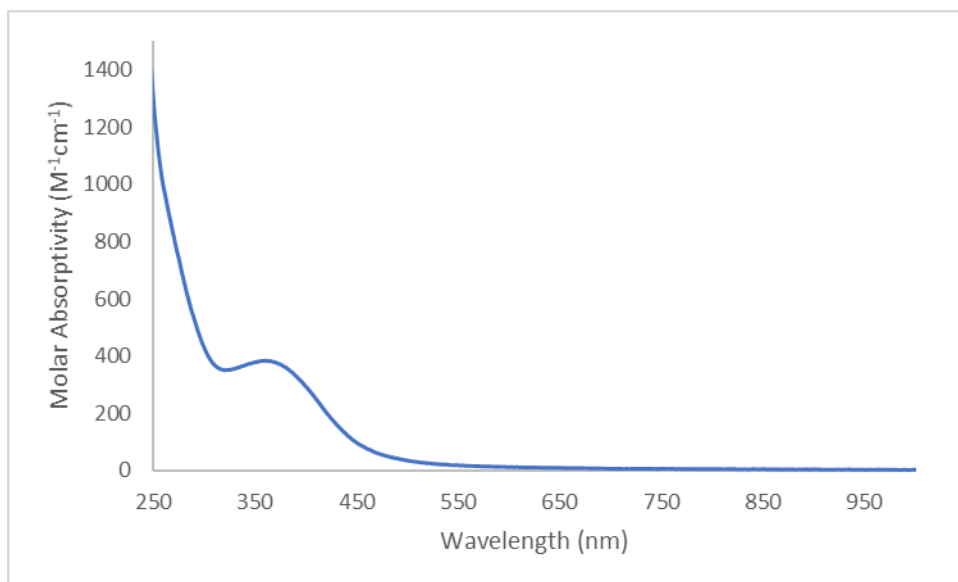
Figure 4.26. UV-vis of **1-Y** in 0.012mM Et$_2$O.
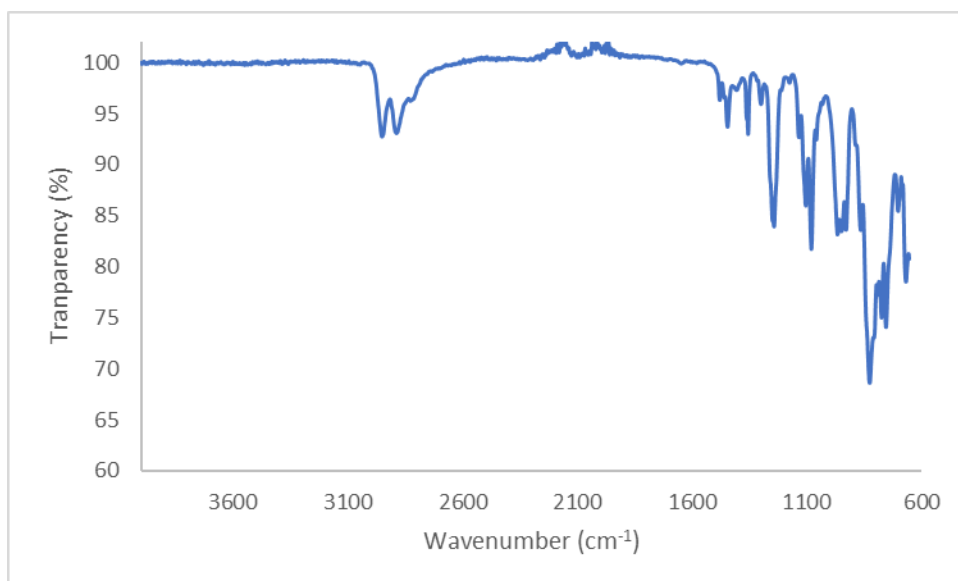
Figure 4.27. IR spectrum of **1-Y(crypt).**

165
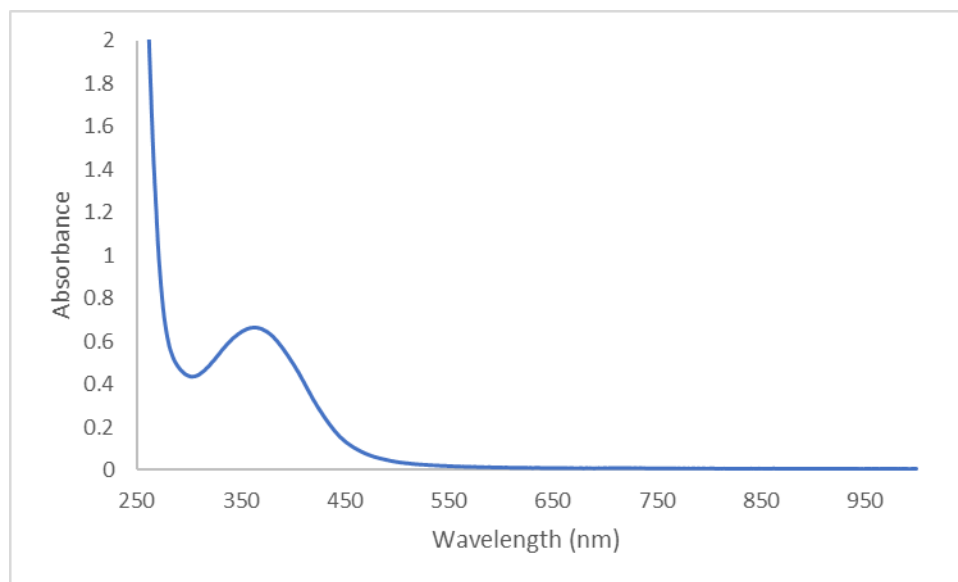
Figure 4.28. UV-vis spectrum of **1-Y(crypt)** in Et$_2$O.

X-ray Data Collection, Structure, Solution, Refinement

Table 4.6. Crystal data and structure refinement for **1-Nd(end-on).**

Identification code	abc14 (Amanda Chung)
Empirical formula	C$_{76}$ H$_{190}$ K$_2$ N$_8$ Nd$_2$ O$_{19}$ Si$_{12}$
Formula weight	2224.11
Temperature	88(2) K
Wavelength	0.71073 Å
Crystal system	Triclinic
Space group	$P\bar{1}$
Unit cell dimensions	a = 15.7791(7) Å α= 79.8704(7)°.
	b = 16.1634(7) Å β= 77.2173(7)°.
	c = 24.1563(11) Å γ= 82.0679(7)°.
Volume	5883.0(5) Å^3
Z	2
Density (calculated)	1.256 Mg/m^3
Absorption coefficient	1.121 mm^{-1}
F(000)	2360
Crystal color	brown
Crystal size	0.292 x 0.231 x 0.162 mm^3
Theta range for data collection	1.287 to 28.349°

Index ranges	$-21 \leq h \leq 21, -21 \leq k \leq 21, -32 \leq l \leq 32$
Reflections collected	82840
Independent reflections	29244 [R(int) = 0.0372]
Completeness to theta = 25.500°	100.0 %
Absorption correction	Semi-empirical from equivalents
Max. and min. transmission	0.7457 and 0.6714
Refinement method	Full-matrix least-squares on F^2
Data / restraints / parameters	29244 / 0 / 1028
Goodness-of-fit on F^2	1.034
Final R indices [I>2sigma(I) = 23041 data]	R1 = 0.0559, wR2 = 0.1204
R indices (all data, 0.75 Å)	R1 = 0.0751, wR2 = 0.1308
Largest diff. peak and hole	3.939 and -1.004 e.Å^{-3}

Table 4.7.   Bond lengths [Å] and angles [°] for **1-Nd(end-on)**.

Nd(1)-N(1)	2.239(4)
Nd(1)-N(5)	2.404(4)
Nd(1)-N(3)	2.404(3)
Nd(1)-N(4)	2.412(3)
Nd(2)-N(2)	2.241(4)
Nd(2)-N(6)	2.389(4)
Nd(2)-N(7A)	2.398(5)
Nd(2)-N(8)	2.402(3)
Nd(2)-N(7B)	2.466(15)
N(1)-N(2)	1.205(5)
N(1)-Nd(1)-N(5)	105.70(12)
N(1)-Nd(1)-N(3)	103.84(12)
N(5)-Nd(1)-N(3)	112.11(12)
N(1)-Nd(1)-N(4)	106.26(12)
N(5)-Nd(1)-N(4)	113.91(12)
N(3)-Nd(1)-N(4)	113.95(11)
N(2)-Nd(2)-N(6)	104.60(13)
N(2)-Nd(2)-N(7A)	105.61(15)
N(6)-Nd(2)-N(7A)	115.24(17)

N(2)-Nd(2)-N(8)	103.51(12)
N(6)-Nd(2)-N(8)	113.50(13)
N(7A)-Nd(2)-N(8)	112.91(15)
N(2)-Nd(2)-N(7B)	110.5(4)
N(6)-Nd(2)-N(7B)	103.1(4)
N(8)-Nd(2)-N(7B)	120.7(4)

Table 4.8. Crystal data and structure refinement for **1-Nd(side-on)**.

Identification code	abc14b (Amanda Chung)
Empirical formula	$C_{76} H_{190} K_2 N_8 Nd_2 O_{19} Si_{12}$
Formula weight	2224.11
Temperature	248(2) K
Wavelength	0.71073 Å
Crystal system	Triclinic
Space group	$P\bar{1}$
Unit cell dimensions	a = 15.768(8) Å α = 78.680(6)°.
	b = 16.120(8) Å β = 77.053(6)°.
	c = 24.570(12) Å γ = 84.299(6)°.
Volume	5958(5) Å^3
Z	2
Density (calculated)	1.240 Mg/m^3
Absorption coefficient	1.107 mm^{-1}
F(000)	2360
Crystal color	green
Crystal size	0.338 x 0.229 x 0.180 mm^3
Theta range for data collection	1.290 to 25.107°
Index ranges	$-18 \le h \le 18$, $-18 \le k \le 18$, $-28 \le l \le 29$
Reflections collected	58209
Independent reflections	20668 [R(int) = 0.0725]
Completeness to theta = 25.107°	97.2 %
Absorption correction	Semi-empirical from equivalents
Max. and min. transmission	0.8011 and 0.6486
Refinement method	Full-matrix least-squares on F^2
Data / restraints / parameters	20668 / 0 / 907

Goodness-of-fit on F^2 1.057

Final R indices [I>2sigma(I) = 14713 data]   R1 = 0.0593, wR2 = 0.1510

R indices (all data, 0.85 Å)   R1 = 0.0861, wR2 = 0.1703

Largest diff. peak and hole   1.914 and -0.934 e.Å^{-3}

Table 4.9. Bond lengths [Å] and angles [°] for **1-Nd(side-on)**.

Nd(1)-N(2)	2.390(11)
Nd(1)-N(1)	2.423(12)
Nd(1)-N(1B)	2.426(11)
Nd(1)-N(2B)	2.433(11)
Nd(1)-N(4)	2.436(5)
Nd(1)-N(3)	2.444(5)
Nd(1)-N(5)	2.466(5)
Nd(2)-N(2B)	2.406(11)
Nd(2)-N(1B)	2.411(11)
Nd(2)-N(7)	2.421(5)
Nd(2)-N(2)	2.426(11)
Nd(2)-N(8)	2.432(5)
Nd(2)-N(1)	2.441(13)
Nd(2)-N(6)	2.455(5)
N(1)-N(2)	1.185(19)
N(1B)-N(2B)	1.179(18)
N(2)-Nd(1)-N(1)	28.5(5)
N(1B)-Nd(1)-N(2B)	28.1(4)
N(2)-Nd(1)-N(4)	115.3(3)
N(1)-Nd(1)-N(4)	103.9(4)
N(1B)-Nd(1)-N(4)	123.7(3)
N(2B)-Nd(1)-N(4)	97.1(3)
N(2)-Nd(1)-N(3)	117.5(3)
N(1)-Nd(1)-N(3)	99.8(4)
N(1B)-Nd(1)-N(3)	98.7(3)
N(2B)-Nd(1)-N(3)	119.0(3)
N(4)-Nd(1)-N(3)	107.35(17)

N(2)-Nd(1)-N(5)	95.2(3)
N(1)-Nd(1)-N(5)	123.5(3)
N(1B)-Nd(1)-N(5)	105.4(3)
N(2B)-Nd(1)-N(5)	111.4(3)
N(4)-Nd(1)-N(5)	110.26(18)
N(3)-Nd(1)-N(5)	110.64(17)
N(2B)-Nd(2)-N(1B)	28.3(4)
N(2B)-Nd(2)-N(7)	116.9(3)
N(1B)-Nd(2)-N(7)	100.1(3)
N(7)-Nd(2)-N(2)	118.9(3)
N(2B)-Nd(2)-N(8)	115.8(3)
N(1B)-Nd(2)-N(8)	103.8(3)
N(7)-Nd(2)-N(8)	107.45(18)
N(2)-Nd(2)-N(8)	97.5(3)
N(7)-Nd(2)-N(1)	97.9(4)
N(2)-Nd(2)-N(1)	28.2(4)
N(8)-Nd(2)-N(1)	123.8(3)
N(2B)-Nd(2)-N(6)	94.3(3)
N(1B)-Nd(2)-N(6)	122.4(3)
N(7)-Nd(2)-N(6)	111.05(17)
N(2)-Nd(2)-N(6)	110.2(3)
N(8)-Nd(2)-N(6)	110.80(18)
N(1)-Nd(2)-N(6)	104.9(4)
N(2)-N(1)-Nd(1)	74.2(8)
N(2)-N(1)-Nd(2)	75.2(8)
Nd(1)-N(1)-Nd(2)	149.4(6)
N(1)-N(2)-Nd(1)	77.3(8)
N(1)-N(2)-Nd(2)	76.6(8)
Nd(1)-N(2)-Nd(2)	153.9(6)
N(2B)-N(1B)-Nd(2)	75.6(8)
N(2B)-N(1B)-Nd(1)	76.3(8)
Nd(2)-N(1B)-Nd(1)	151.9(5)
N(1B)-N(2B)-Nd(2)	76.1(8)
N(1B)-N(2B)-Nd(1)	75.6(8)
Nd(2)-N(2B)-Nd(1)	151.6(6)

Table 4.10. Crystal data and structure refinement for **2-Nd**.

Identification code	abc4 (Amanda Chung)
Empirical formula	$C_{52} H_{134} K N_9 Nd_2 O_7 Si_{10} \cdot \frac{1}{2}(C_6H_{14})$
Formula weight	1649.24
Temperature	88(2) K
Wavelength	0.71073 Å
Crystal system	Triclinic
Space group	$P\bar{1}$
Unit cell dimensions	a = 12.2028(11) Å α = 95.4011(12)°.
	b = 16.4730(14) Å β = 91.3472(12)°.
	c = 21.8501(19) Å γ = 90.9686(12)°.
Volume	4370.7(7) $Å^3$
Z	2
Density (calculated)	1.253 Mg/m^3
Absorption coefficient	1.404 mm^{-1}
F(000)	1738
Crystal color	blue
Crystal size	0.282 x 0.187 x 0.046 mm^3
Theta range for data collection	1.483 to 25.681°
Index ranges	$-14 \leq h \leq 14$, $-20 \leq k \leq 20$, $-26 \leq l \leq 26$
Reflections collected	46019
Independent reflections	16555 [R(int) = 0.0476]
Completeness to theta = 25.500°	99.8 %
Absorption correction	Semi-empirical from equivalents
Max. and min. transmission	0.7454 and 0.6741
Refinement method	Full-matrix least-squares on F^2
Data / restraints / parameters	16555 / 0 / 773
Goodness-of-fit on F^2	1.034
Final R indices [I>2sigma(I) = 12257 data]	R1 = 0.0504, wR2 = 0.1050
R indices (all data, 0.82 Å)	R1 = 0.0772, wR2 = 0.1179
Largest diff. peak and hole	1.817 and -0.853 e.$Å^{-3}$

Table 4.11. Bond lengths [Å] and angles [°] for **2-Nd**.

Nd(1)-N(3)	2.379(4)
Nd(1)-N(4)	2.413(5)
Nd(1)-N(1)	2.422(4)
Nd(1)-N(2)	2.425(4)
Nd(1)-N(5)	2.431(4)
Nd(2)-N(6)	2.340(4)
Nd(2)-N(1)	2.357(4)
Nd(2)-N(2)	2.371(4)
Nd(2)-N(7)	2.382(4)
Nd(2)-O(1)	2.528(4)
O(1)-C(31)	1.437(7)
O(1)-C(34)	1.437(7)
N(1)-N(2)	1.312(6)
C(31)-C(32)	1.459(10)
C(32)-C(33)	1.518(10)
C(33)-C(34)	1.425(9)
N(3)-Nd(1)-N(4)	118.51(16)
N(3)-Nd(1)-N(1)	101.45(15)
N(4)-Nd(1)-N(1)	89.04(14)
N(3)-Nd(1)-N(2)	95.89(15)
N(4)-Nd(1)-N(2)	118.09(14)
N(1)-Nd(1)-N(2)	31.41(14)
N(3)-Nd(1)-N(5)	112.10(14)
N(4)-Nd(1)-N(5)	108.99(15)
N(1)-Nd(1)-N(5)	125.72(15)
N(2)-Nd(1)-N(5)	101.70(15)
N(6)-Nd(2)-N(1)	107.81(15)
N(6)-Nd(2)-N(2)	114.42(15)
N(1)-Nd(2)-N(2)	32.21(15)
N(6)-Nd(2)-N(7)	115.47(14)
N(1)-Nd(2)-N(7)	117.09(15)
N(2)-Nd(2)-N(7)	128.53(15)
N(6)-Nd(2)-O(1)	119.30(14)

N(1)-Nd(2)-O(1)	110.69(14)
N(2)-Nd(2)-O(1)	81.07(14)
N(7)-Nd(2)-O(1)	85.50(13)
C(31)-O(1)-C(34)	108.4(5)
C(31)-O(1)-Nd(2)	125.8(4)
C(34)-O(1)-Nd(2)	125.7(3)
N(2)-N(1)-Nd(2)	74.5(3)
N(2)-N(1)-Nd(1)	74.4(3)
Nd(2)-N(1)-Nd(1)	148.9(2)
N(1)-N(2)-Nd(2)	73.3(3)
N(1)-N(2)-Nd(1)	74.2(3)
Nd(2)-N(2)-Nd(1)	147.4(2)
O(1)-C(31)-C(32)	106.0(6)
C(31)-C(32)-C(33)	104.9(6)
C(34)-C(33)-C(32)	105.4(6)
C(33)-C(34)-O(1)	109.0(6)

Symmetry transformations used to generate equivalent atoms:

#1 -x+2,-y+1,-z+1

Table 4.12. Crystal data and structure refinement for **1-Dy(crypt)**.

Identification code	abc57 (Amanda Chung)
Empirical formula	$C_{72} H_{180} Dy_2 K_2 N_{12} O_{14} Si_{12} \cdot 2(C_4H_{10}O)$
Formula weight	2294.79
Temperature	93(2) K
Wavelength	0.71073 Å
Crystal system	Triclinic
Space group	$P\bar{1}$
Unit cell dimensions	a = 15.329(3) Å α = 101.281(3)°.
	b = 16.100(3) Å β = 96.351(3)°.
	c = 26.050(5) Å γ = 104.153(3)°.
Volume	6028.0(18) Å^3
Z	2
Density (calculated)	1.264 Mg/m^3
Absorption coefficient	1.472 mm^{-1}
F(000)	2428

Crystal color	red
Crystal size	0.950 x 0.696 x 0.653 mm^3
Theta range for data collection	1.486 to 27.103°
Index ranges	$-19 \leq h \leq 17, -20 \leq k \leq 20, -33 \leq l \leq 33$
Reflections collected	72583
Independent reflections	26023 [R(int) = 0.0396]
Completeness to theta = 25.242°	98.7 %
Absorption correction	Semi-empirical from equivalents
Max. and min. transmission	0.7461 and 0.4576
Refinement method	Full-matrix least-squares on F^2
Data / restraints / parameters	26023 / 0 / 1155
Goodness-of-fit on F^2	1.157
Final R indices [I>2sigma(I) = 19190 data]	R1 = 0.0600, wR2 = 0.1055
R indices (all data, 0.78 Å)	R1 = 0.0910, wR2 = 0.1203
Largest diff. peak and hole	2.354 and -1.831 e.Å^{-3}

Table 4.13. Bond lengths [Å] and angles [°] for **1-Dy(crypt)**.

Dy(1)-N(2)	2.329(12)
Dy(1)-N(1)	2.349(12)
Dy(1)-N(6)	2.356(4)
Dy(1)-N(5)	2.370(4)
Dy(1)-N(7)	2.386(4)
Dy(2)-N(1)	2.346(12)
Dy(2)-N(2)	2.349(12)
Dy(2)-N(10)	2.374(4)
Dy(2)-N(9)	2.380(4)
Dy(2)-N(8)	2.399(4)
Dy(3)-N(3)	2.21(2)
Dy(3)-N(7)	2.218(5)
Dy(3)-N(6)	2.228(5)
Dy(3)-N(5)	2.255(5)
Dy(4)-N(4)	2.172(19)
Dy(4)-N(9)	2.216(4)
Dy(4)-N(8)	2.242(4)

Dy(4)-N(10)	2.244(4)
N(1)-N(2)	1.043(14)
N(3)-N(4)	1.26(3)
N(2)-Dy(1)-N(1)	25.8(3)
N(2)-Dy(1)-N(6)	107.9(3)
N(1)-Dy(1)-N(6)	113.8(3)
N(2)-Dy(1)-N(5)	125.0(3)
N(1)-Dy(1)-N(5)	100.2(3)
N(6)-Dy(1)-N(5)	105.97(14)
N(2)-Dy(1)-N(7)	103.1(3)
N(1)-Dy(1)-N(7)	121.7(3)
N(6)-Dy(1)-N(7)	106.69(14)
N(5)-Dy(1)-N(7)	107.02(15)
N(1)-Dy(2)-N(2)	25.7(3)
N(1)-Dy(2)-N(10)	117.9(3)
N(2)-Dy(2)-N(10)	101.6(3)
N(1)-Dy(2)-N(9)	114.8(3)
N(2)-Dy(2)-N(9)	105.7(3)
N(10)-Dy(2)-N(9)	107.78(14)
N(1)-Dy(2)-N(8)	102.1(3)
N(2)-Dy(2)-N(8)	127.3(3)
N(10)-Dy(2)-N(8)	106.14(14)
N(9)-Dy(2)-N(8)	107.03(14)
N(3)-Dy(3)-N(7)	99.0(6)
N(3)-Dy(3)-N(6)	104.8(5)
N(7)-Dy(3)-N(6)	117.6(2)
N(3)-Dy(3)-N(5)	98.5(6)
N(7)-Dy(3)-N(5)	117.5(2)
N(6)-Dy(3)-N(5)	114.6(2)
N(4)-Dy(4)-N(9)	100.1(5)
N(4)-Dy(4)-N(8)	99.2(5)
N(9)-Dy(4)-N(8)	119.06(17)
N(4)-Dy(4)-N(10)	94.3(5)
N(9)-Dy(4)-N(10)	118.87(16)

N(8)-Dy(4)-N(10)	116.52(17)
N(2)-N(1)-Dy(2)	77.4(10)
N(2)-N(1)-Dy(1)	76.1(10)
Dy(2)-N(1)-Dy(1)	153.3(5)
N(1)-N(2)-Dy(1)	78.2(10)
N(1)-N(2)-Dy(2)	77.0(10)
Dy(1)-N(2)-Dy(2)	155.1(5)
N(4)-N(3)-Dy(3)	171.7(15)
N(3)-N(4)-Dy(4)	177.2(16)

_____

Table 4.14. Crystal data and structure refinement for **1-Y**.

Identification code	abc82 (Amanda Chung)
Empirical formula	$C_{76} H_{190} K_2 N_8 O_{19} Si_{12} Y_2$
Formula weight	2113.45
Temperature	93(2) K
Wavelength	1.54178 Å
Crystal system	Triclinic
Space group	$P\bar{1}$
Unit cell dimensions	a = 15.7399(11) Å $\quad$ α = 80.529(4)°.
	b = 16.2051(12) Å $\quad$ β = 76.881(4)°.
	c = 24.0578(17) Å $\quad$ γ = 82.393(4)°.
Volume	5865.8(7) Å^3
Z	2
Density (calculated)	1.197 Mg/m^3
Absorption coefficient	3.585 mm^{-1}
F(000)	2276
Crystal color	orange
Crystal size	0.220 x 0.205 x 0.106 mm^3
Theta range for data collection	2.778 to 69.237°
Index ranges	$-18 \leq h \leq 18$, $-18 \leq k \leq 19$, $-28 \leq l \leq 29$
Reflections collected	69902
Independent reflections	21397 [R(int) = 0.0584]
Completeness to theta = 67.679°	99.2 %
Absorption correction	Semi-empirical from equivalents
Max. and min. transmission	0.3833 and 0.2714

Refinement method	Full-matrix least-squares on F^2
Data / restraints / parameters	21397 / 0 / 1329
Goodness-of-fit on F^2	1.034
Final R indices [I>2sigma(I) = 16535 data]	R1 = 0.0741, wR2 = 0.1918
R indices (all data, 0.82 Å)	R1 = 0.0950, wR2 = 0.2160
Largest diff. peak and hole	2.263 and -0.653 e.Å^{-3}

Table 4.15. Bond lengths [Å] and angles [°] for **1-Y**.

Y(1)-N(1)	2.196(4)
Y(1)-N(5)	2.294(4)
Y(1)-N(4)	2.308(4)
Y(1)-N(3)	2.313(4)
Y(2)-N(2)	2.190(4)
Y(2)-N(7)	2.293(4)
Y(2)-N(8)	2.303(5)
Y(2)-N(6)	2.313(4)
N(1)-N(2)	1.194(6)
N(1)-Y(1)-N(5)	106.16(15)
N(1)-Y(1)-N(4)	107.93(15)
N(5)-Y(1)-N(4)	110.07(15)
N(1)-Y(1)-N(3)	107.63(16)
N(5)-Y(1)-N(3)	112.77(15)
N(4)-Y(1)-N(3)	111.96(15)
N(2)-Y(2)-N(7)	106.87(16)
N(2)-Y(2)-N(8)	107.69(17)
N(7)-Y(2)-N(8)	110.3(2)
N(2)-Y(2)-N(6)	105.90(15)
N(7)-Y(2)-N(6)	112.28(15)
N(8)-Y(2)-N(6)	113.37(17)
N(2)-N(1)-Y(1)	178.7(4)
N(1)-N(2)-Y(2)	179.2(4)

Table 4.16. Crystal data and structure refinement for **1-Y(crypt)**.

Identification code	abc79 (Amanda Chung)
Empirical formula	$C_{36}H_{108}N_8Si_{12}Y_2$ $(KC_{18}H_{36}N_2O_6)_2$ $(C_4H_{10}O)_2$
Formula weight	2147.61
Temperature	133(2) K
Wavelength	0.71073 Å
Crystal system	Triclinic
Space group	$P\bar{1}$

Unit cell dimensions
a = 15.5335(19) Å   α = 92.016(2)°.
b = 16.0142(19) Å   β = 95.107(2)°.
c = 50.658(6) Å   γ = 104.110(2)°.

Volume	12152(3) $Å^3$
Z	4
Density (calculated)	1.174 Mg/m^3
Absorption coefficient	1.190 mm^{-1}
F(000)	4640
Crystal color	orange
Crystal size	0.370 x 0.352 x 0.146 mm^3
Theta range for data collection	1.213 to 26.538°
Index ranges	$-19 \leq h \leq 19, -20 \leq k \leq 20, -63 \leq l \leq 63$
Reflections collected	241472
Independent reflections	50055 [R(int) = 0.1398]
Completeness to theta = 25.242°	100.0 %
Absorption correction	Semi-empirical from equivalents
Max. and min. transmission	0.7454 and 0.6113
Refinement method	Full-matrix least-squares on F^2
Data / restraints / parameters	50055 / 16 / 2258
Goodness-of-fit on F^2	1.024
Final R indices [I>2sigma(I) = 29563 data]	R1 = 0.0715, wR2 = 0.1296
R indices (all data, 0.80 Å)	R1 = 0.1428, wR2 = 0.1528
Largest diff. peak and hole	1.498 and -0.855 e.$Å^{-3}$

Table 4.17. Bond lengths [Å] and angles [°] for **1-Y(crypt)**.

_____

Y(1)-N(1)   2.159(4)

Y(1)-N(3)	2.284(4)
Y(1)-N(5)	2.305(4)
Y(1)-N(4)	2.317(4)
Y(2)-N(2)	2.156(4)
Y(2)-N(6)	2.297(4)
Y(2)-N(7)	2.301(4)
Y(2)-N(8)	2.304(4)
N(1)-N(2)	1.216(5)
Y(3)-N(9)	2.166(4)
Y(3)-N(12)	2.300(4)
Y(3)-N(13)	2.307(4)
Y(3)-N(11)	2.308(4)
Y(4)-N(10)	2.169(4)
Y(4)-N(16)	2.289(4)
Y(4)-N(15)	2.306(4)
Y(4)-N(14)	2.311(4)
N(9)-N(10)	1.231(5)
N(1)-Y(1)-N(3)	107.77(15)
N(1)-Y(1)-N(5)	104.41(14)
N(3)-Y(1)-N(5)	111.46(14)
N(1)-Y(1)-N(4)	108.94(15)
N(3)-Y(1)-N(4)	111.68(15)
N(5)-Y(1)-N(4)	112.20(13)
N(2)-Y(2)-N(6)	109.34(14)
N(2)-Y(2)-N(7)	106.29(14)
N(6)-Y(2)-N(7)	109.16(13)
N(2)-Y(2)-N(8)	106.32(14)
N(6)-Y(2)-N(8)	112.30(13)
N(7)-Y(2)-N(8)	113.17(14)
N(2)-N(1)-Y(1)	178.3(4)
N(1)-N(2)-Y(2)	177.3(3)
N(9)-Y(3)-N(12)	107.68(14)
N(9)-Y(3)-N(13)	110.88(14)
N(12)-Y(3)-N(13)	109.02(14)
N(9)-Y(3)-N(11)	105.48(14)

N(12)-Y(3)-N(11)	112.20(14)
N(13)-Y(3)-N(11)	111.48(14)
N(10)-Y(4)-N(16)	106.97(14)
N(10)-Y(4)-N(15)	105.64(14)
N(16)-Y(4)-N(15)	113.79(13)
N(10)-Y(4)-N(14)	110.53(14)
N(16)-Y(4)-N(14)	108.87(14)
N(15)-Y(4)-N(14)	110.92(14)
N(10)-N(9)-Y(3)	179.6(4)
N(9)-N(10)-Y(4)	178.4(3)

Table 4.18. Crystal data and structure refinement for [K_2(18-c-6)$_3$]{[(R_2N)$_3Nd$]$_2$[μ-O]}

Identification code	abc12 (Amanda Chung)
Empirical formula	$C_{76} H_{190} K_2 N_6 Nd_2 O_{20} Si_{12}$
Temperature	88(2) K
Wavelength	0.71073 Å
Crystal system	Triclinic
Space group	$P\bar{1}$
Unit cell dimensions	a = 15.5895(12) Å α = 78.8674(14)°.
	b = 16.0063(13) Å β = 76.8412(14)°.
	c = 24.3636(19) Å γ = 84.0665(14)°.
Volume	5797.2(8) Å^3
Z	2
Density (calculated)	1.267 Mg/m^3
Absorption coefficient	1.138 mm^{-1}
F(000)	2348
Crystal color	brown
Crystal size	0.246 x 0.225 x 0.078 mm^3
Theta range for data collection	0.872 to 26.372°
Index ranges	$-19 \leq h \leq 19, -20 \leq k \leq 19, -30 \leq l \leq 30$
Reflections collected	69144
Independent reflections	23558 [R(int) = 0.0543]
Completeness to theta = 25.242°	99.5 %
Absorption correction	Semi-empirical from equivalents

Max. and min. transmission   0.7461 and 0.6599

Refinement method   Full-matrix least-squares on F^2

Data / restraints / parameters   23558 / 0 / 915

Goodness-of-fit on F^2 1.061

Final R indices [I>2sigma(I) = 17625 data] R1 = 0.0868, wR2 = 0.1783

R indices (all data, 0.80 Å)   R1 = 0.1147, wR2 = 0.1915

Largest diff. peak and hole   2.220 and -1.994 e.Å^{-3}

Table 4.19. Bond lengths [Å] and angles [°] for [K$_2$(18-c-6)$_3$]{[(R$_2$N)$_3$Nd]$_2$[μ-O]}.

Nd(1)-Nd(3)	0.7152(19)
Nd(1)-O(1)	2.142(7)
Nd(1)-N(2)	2.467(6)
Nd(1)-N(3)	2.498(6)
Nd(1)-N(1)	2.499(7)
Nd(2)-Nd(4)	0.679(2)
Nd(2)-O(1)	2.150(7)
Nd(2)-N(4)	2.465(6)
Nd(2)-N(6)	2.478(7)
Nd(2)-N(5)	2.499(6)
Nd(3)-N(1)	2.246(6)
Nd(3)-N(3)	2.304(6)
Nd(3)-N(2)	2.349(6)
Nd(3)-O(1)	2.854(7)
Nd(4)-N(5)	2.296(6)
Nd(4)-N(6)	2.301(7)
Nd(4)-N(4)	2.309(6)
Nd(4)-O(1)	2.828(7)
Nd(3)-Nd(1)-O(1)	173.9(2)
Nd(3)-Nd(1)-N(2)	72.2(2)
O(1)-Nd(1)-N(2)	113.2(2)
Nd(3)-Nd(1)-N(3)	66.2(2)
O(1)-Nd(1)-N(3)	113.6(2)
N(2)-Nd(1)-N(3)	106.5(2)
Nd(3)-Nd(1)-N(1)	61.4(2)

O(1)-Nd(1)-N(1)	113.6(2)
N(2)-Nd(1)-N(1)	103.4(2)
N(3)-Nd(1)-N(1)	105.5(2)
Nd(4)-Nd(2)-O(1)	176.6(2)
Nd(4)-Nd(2)-N(4)	68.9(2)
O(1)-Nd(2)-N(4)	112.8(2)
Nd(4)-Nd(2)-N(6)	67.2(2)
O(1)-Nd(2)-N(6)	114.7(2)
N(4)-Nd(2)-N(6)	103.2(2)
Nd(4)-Nd(2)-N(5)	65.0(2)
O(1)-Nd(2)-N(5)	111.6(2)
N(4)-Nd(2)-N(5)	106.6(2)
N(6)-Nd(2)-N(5)	107.3(2)
Nd(1)-Nd(3)-N(1)	102.4(3)
Nd(1)-Nd(3)-N(3)	97.3(2)
N(1)-Nd(3)-N(3)	122.0(2)
Nd(1)-Nd(3)-N(2)	91.0(2)
N(1)-Nd(3)-N(2)	116.1(2)
N(3)-Nd(3)-N(2)	117.6(2)
Nd(1)-Nd(3)-O(1)	4.58(17)
N(1)-Nd(3)-O(1)	98.7(2)
N(3)-Nd(3)-O(1)	97.2(2)
N(2)-Nd(3)-O(1)	95.0(2)
Nd(2)-Nd(4)-N(5)	99.5(3)
Nd(2)-Nd(4)-N(6)	97.1(3)
N(5)-Nd(4)-N(6)	121.3(2)
Nd(2)-Nd(4)-N(4)	95.1(3)
N(5)-Nd(4)-N(4)	119.6(2)
N(6)-Nd(4)-N(4)	114.3(2)
Nd(2)-Nd(4)-O(1)	2.56(19)
N(5)-Nd(4)-O(1)	96.9(2)
N(6)-Nd(4)-O(1)	98.5(2)
N(4)-Nd(4)-O(1)	96.5(2)
Nd(1)-O(1)-Nd(2)	178.2(3)
Nd(1)-O(1)-Nd(4)	178.4(2)
Nd(2)-O(1)-Nd(4)	0.81(6)

Nd(1)-O(1)-Nd(3)	1.53(6)
Nd(2)-O(1)-Nd(3)	177.7(2)
Nd(4)-O(1)-Nd(3)	177.3(2)
Nd(3)-N(2)-Nd(1)	16.85(6)
Nd(3)-N(3)-Nd(1)	16.50(7)
Nd(4)-N(4)-Nd(2)	15.92(6)
Nd(4)-N(5)-Nd(2)	15.54(7)
Nd(4)-N(6)-Nd(2)	15.77(7)

Table 4.20. Crystal data and structure refinement for **1-Nd(end-on)_80**

Identification code	abc49_80 (Amanda Chung)
Empirical formula	$C_{72} H_{180} K_2 N_8 Nd_2 O_{18} Si_{12} \bullet (C_4H_{10}O)$
Formula weight	2224.11
Temperature	193(2) K
Wavelength	0.71073 Å
Crystal system	Triclinic
Space group	$P\bar{1}$
Unit cell dimensions	a = 15.7266(10) Å α = 78.7269(11)°.
	b = 16.0690(10) Å β = 77.1419(11)°.
	c = 24.5326(16) Å γ = 84.2427(11)°.
Volume	5917.1(7) Å^3
Z	2
Density (calculated)	1.248 Mg/m^3
Absorption coefficient	1.115 mm^{-1}
F(000)	2360
Crystal color	green
Crystal size	0.670 x 0.453 x 0.372 mm^3
Theta range for data collection	1.330 to 30.508°
Index ranges	$-22 \leq h \leq 22, -22 \leq k \leq 22, -35 \leq l \leq 35$
Reflections collected	147620
Independent reflections	35739 [R(int) = 0.0889]
Completeness to theta = 25.242°	100.0 %
Absorption correction	Semi-empirical from equivalents
Max. and min. transmission	0.6445 and 0.5376

Refinement method	Full-matrix least-squares on F^2
Data / restraints / parameters	35739 / 16 / 1061
Goodness-of-fit on F^2	1.029
Final R indices [I>2sigma(I) = 26352 data]	R1 = 0.0537, wR2 = 0.1378
R indices (all data, 0.70 Å)	R1 = 0.0781, wR2 = 0.1560
Largest diff. peak and hole	1.413 and -1.280 e.$Å^{-3}$

Table 4.21. Bond lengths [Å] and angles [°] for **1-Nd(end-on)_80**

Nd(1)-N(1)	2.389(8)
Nd(1)-N(2B)	2.390(9)
Nd(1)-N(1B)	2.414(8)
Nd(1)-N(2)	2.415(8)
Nd(1)-N(3)	2.434(3)
Nd(1)-N(4)	2.443(3)
Nd(1)-N(5)	2.447(3)
Nd(2)-N(2B)	2.406(9)
Nd(2)-N(1B)	2.410(9)
Nd(2)-N(1)	2.422(8)
Nd(2)-N(2)	2.423(8)
Nd(2)-N(7)	2.425(3)
Nd(2)-N(8)	2.426(3)
Nd(2)-N(6)	2.452(3)
N(1)-N(2)	1.150(16)
N(1B)-N(2B)	1.087(19)
N(2B)-Nd(1)-N(1B)	26.1(4)
N(1)-Nd(1)-N(2)	27.7(4)
N(1)-Nd(1)-N(3)	106.6(7)
N(2B)-Nd(1)-N(3)	121.9(3)
N(1B)-Nd(1)-N(3)	96.0(2)
N(2)-Nd(1)-N(3)	110.7(7)
N(1)-Nd(1)-N(4)	123.2(4)
N(2B)-Nd(1)-N(4)	105.6(7)
N(1B)-Nd(1)-N(4)	114.7(7)

N(2)-Nd(1)-N(4)	97.1(3)
N(3)-Nd(1)-N(4)	107.54(10)
N(1)-Nd(1)-N(5)	98.2(4)
N(2B)-Nd(1)-N(5)	100.6(7)
N(1B)-Nd(1)-N(5)	116.5(7)
N(2)-Nd(1)-N(5)	119.5(5)
N(3)-Nd(1)-N(5)	110.39(10)
N(4)-Nd(1)-N(5)	110.43(10)
N(2B)-Nd(2)-N(1B)	26.1(4)
N(1)-Nd(2)-N(2)	27.5(4)
N(2B)-Nd(2)-N(7)	121.7(3)
N(1B)-Nd(2)-N(7)	95.6(3)
N(1)-Nd(2)-N(7)	108.7(7)
N(2)-Nd(2)-N(7)	107.9(7)
N(2B)-Nd(2)-N(8)	104.5(7)
N(1B)-Nd(2)-N(8)	115.2(8)
N(1)-Nd(2)-N(8)	98.1(3)
N(2)-Nd(2)-N(8)	122.8(4)
N(7)-Nd(2)-N(8)	107.40(10)
N(2B)-Nd(2)-N(6)	100.9(6)
N(1B)-Nd(2)-N(6)	115.2(6)
N(1)-Nd(2)-N(6)	119.3(5)
N(2)-Nd(2)-N(6)	96.2(4)
N(7)-Nd(2)-N(6)	110.96(10)
N(8)-Nd(2)-N(6)	111.13(11)
N(2)-N(1)-Nd(1)	77.4(6)
N(2)-N(1)-Nd(2)	76.3(6)
Nd(1)-N(1)-Nd(2)	153.7(5)
N(1)-N(2)-Nd(1)	74.9(6)
N(1)-N(2)-Nd(2)	76.2(6)
Nd(1)-N(2)-Nd(2)	151.1(4)
N(2B)-N(1B)-Nd(2)	76.7(6)
N(2B)-N(1B)-Nd(1)	75.7(7)
Nd(2)-N(1B)-Nd(1)	152.4(5)
N(1B)-N(2B)-Nd(1)	78.2(7)
N(1B)-N(2B)-Nd(2)	77.2(7)

Nd(1)-N(2B)-Nd(2)   155.4(5)

Table 4.22. Crystal data and structure refinement for **1-Nd(end-on)_90**

Identification code	abc49_90 (Amanda Chung)
Empirical formula	$C_{72} H_{180} K_2 N_8 Nd_2 O_{18} Si_{12} \cdot (C_4H_{10}O)$
Formula weight	2224.11
Temperature	183(2) K
Wavelength	0.71073 Å
Crystal system	Triclinic
Space group	$P\bar{1}$
Unit cell dimensions	a = 15.7137(9) Å α = 78.5879(10)°.
	b = 15.9635(9) Å β = 77.1516(10)°.
	c = 24.6115(14) Å γ = 83.3160(10)°.
Volume	5883.2(6) Å^3
Z	2
Density (calculated)	1.256 Mg/m^3
Absorption coefficient	1.121 mm^{-1}
F(000)	2360
Crystal color	green
Crystal size	0.670 x 0.453 x 0.372 mm^3
Theta range for data collection	1.333 to 28.283°
Index ranges	$-20 \leq h \leq 20, -21 \leq k \leq 21, -32 \leq l \leq 32$
Reflections collected	131771
Independent reflections	29182 [R(int) = 0.0833]
Completeness to theta = 25.242°	100.0 %
Absorption correction	Semi-empirical from equivalents
Max. and min. transmission	0.7461 and 0.6543
Refinement method	Full-matrix least-squares on F^2
Data / restraints / parameters	29182 / 7 / 1143
Goodness-of-fit on F^2	1.037
Final R indices [I>2sigma(I) = 22880 data]	R1 = 0.0497, wR2 = 0.1245
R indices (all data, 0.75 Å)	R1 = 0.0681, wR2 = 0.1381
Largest diff. peak and hole	1.999 and -1.359 e.Å^{-3}

Table 4.23. Bond lengths [Å] and angles [°] for **1-Nd(end-on)_90**

Nd(1)-N(1)	2.389(8)
Nd(1)-N(2B)	2.390(9)
Nd(1)-N(1B)	2.414(8)
Nd(1)-N(2)	2.415(8)
Nd(1)-N(3)	2.434(3)
Nd(1)-N(4)	2.443(3)
Nd(1)-N(5)	2.447(3)
Nd(2)-N(2B)	2.406(9)
Nd(2)-N(1B)	2.410(9)
Nd(2)-N(1)	2.422(8)
Nd(2)-N(2)	2.423(8)
Nd(2)-N(7)	2.425(3)
Nd(2)-N(8)	2.426(3)
Nd(2)-N(6)	2.452(3)
N(1)-N(2)	1.150(16)
N(1B)-N(2B)	1.087(19)

N(2B)-Nd(1)-N(1B)	26.1(4)
N(1)-Nd(1)-N(2)	27.7(4)
N(1)-Nd(1)-N(3)	106.6(7)
N(2B)-Nd(1)-N(3)	121.9(3)
N(1B)-Nd(1)-N(3)	96.0(2)
N(2)-Nd(1)-N(3)	110.7(7)
N(1)-Nd(1)-N(4)	123.2(4)
N(2B)-Nd(1)-N(4)	105.6(7)
N(1B)-Nd(1)-N(4)	114.7(7)
N(2)-Nd(1)-N(4)	97.1(3)
N(3)-Nd(1)-N(4)	107.54(10)
N(1)-Nd(1)-N(5)	98.2(4)
N(2B)-Nd(1)-N(5)	100.6(7)
N(1B)-Nd(1)-N(5)	116.5(7)

N(2)-Nd(1)-N(5)	119.5(5)
N(3)-Nd(1)-N(5)	110.39(10)
N(4)-Nd(1)-N(5)	110.43(10)
N(2B)-Nd(2)-N(1B)	26.1(4)
N(1)-Nd(2)-N(2)	27.5(4)
N(2B)-Nd(2)-N(7)	121.7(3)
N(1B)-Nd(2)-N(7)	95.6(3)
N(1)-Nd(2)-N(7)	108.7(7)
N(2)-Nd(2)-N(7)	107.9(7)
N(2B)-Nd(2)-N(8)	104.5(7)
N(1B)-Nd(2)-N(8)	115.2(8)
N(1)-Nd(2)-N(8)	98.1(3)
N(2)-Nd(2)-N(8)	122.8(4)
N(7)-Nd(2)-N(8)	107.40(10)
N(2B)-Nd(2)-N(6)	100.9(6)
N(1B)-Nd(2)-N(6)	115.2(6)
N(1)-Nd(2)-N(6)	119.3(5)
N(2)-Nd(2)-N(6)	96.2(4)
N(7)-Nd(2)-N(6)	110.96(10)
N(8)-Nd(2)-N(6)	111.13(11)
N(2)-N(1)-Nd(1)	77.4(6)
N(2)-N(1)-Nd(2)	76.3(6)
Nd(1)-N(1)-Nd(2)	153.7(5)
N(1)-N(2)-Nd(1)	74.9(6)
N(1)-N(2)-Nd(2)	76.2(6)
Nd(1)-N(2)-Nd(2)	151.1(4)
N(2B)-N(1B)-Nd(2)	76.7(6)
N(2B)-N(1B)-Nd(1)	75.7(7)
Nd(2)-N(1B)-Nd(1)	152.4(5)
N(1B)-N(2B)-Nd(1)	78.2(7)
N(1B)-N(2B)-Nd(2)	77.2(7)
Nd(1)-N(2B)-Nd(2)	155.4(5)

Table 4.24. Crystal data and structure refinement for **1-Nd(end-on)_100**

Identification code	abc49_100 (Amanda Chung)
Empirical formula	$C_{72} H_{180} K_2 N_8 Nd_2 O_{18} Si_{12} \bullet (C_4H_{10}O)$
Formula weight	2224.11
Temperature	173(2) K
Wavelength	0.71073 Å
Crystal system	Triclinic
Space group	$P\bar{1}$
Unit cell dimensions	a = 15.911(2) Å α = 80.064(2)°.
	b = 16.237(2) Å β = 76.8452(19)°.
	c = 24.300(3) Å γ = 82.923(2)°.
Volume	5998.4(15) $Å^3$
Z	2
Density (calculated)	1.231 Mg/m^3
Absorption coefficient	1.100 mm^{-1}
F(000)	2360
Crystal color	green
Crystal size	0.670 x 0.453 x 0.372 mm^3
Theta range for data collection	1.650 to 26.372°
Index ranges	$-19 \leq h \leq 19, -20 \leq k \leq 20, -30 \leq l \leq 30$
Reflections collected	69167
Independent reflections	24513 [R(int) = 0.0857]
Completeness to theta = 25.242°	99.9 %
Absorption correction	Semi-empirical from equivalents
Max. and min. transmission	0.7457 and 0.5219
Refinement method	Full-matrix least-squares on F^2
Data / restraints / parameters	24513 / 12 / 1121
Goodness-of-fit on F^2	1.014
Final R indices [I>2sigma(I) = 15142 data]	R1 = 0.0614, wR2 = 0.1335
R indices (all data, 0.80 Å)	R1 = 0.1140, wR2 = 0.1637
Largest diff. peak and hole	1.891 and -1.117 e.$Å^{-3}$

Table 4.25. Bond lengths [Å] and angles [°] for **1-Nd(end-on)_100**

_____

Nd(1)-N(1)	2.255(6)
Nd(1)-N(3)	2.402(5)
Nd(1)-N(5)	2.404(5)
Nd(1)-N(4)	2.408(4)
Nd(2)-N(2)	2.248(6)
Nd(2)-N(8)	2.394(5)
Nd(2)-N(7)	2.402(5)
Nd(2)-N(6)	2.410(5)
Nd(3)-N(1)	1.600(8)
Nd(3)-N(5)	2.566(8)
Nd(3)-N(3)	2.692(8)
Nd(3)-N(4)	2.723(8)
Nd(3)-N(2)	2.782(8)
Nd(4)-N(2)	1.613(9)
Nd(4)-N(8)	2.616(9)
Nd(4)-N(7)	2.625(9)
Nd(4)-N(6)	2.681(9)
Nd(4)-N(1)	2.797(9)
N(1)-N(2)	1.183(7)

N(1)-Nd(1)-N(3)	106.49(18)
N(1)-Nd(1)-N(5)	104.65(18)
N(3)-Nd(1)-N(5)	111.04(16)
N(1)-Nd(1)-N(4)	106.46(18)
N(3)-Nd(1)-N(4)	113.59(17)
N(5)-Nd(1)-N(4)	113.81(17)
N(2)-Nd(2)-N(8)	104.98(18)
N(2)-Nd(2)-N(7)	106.72(19)
N(8)-Nd(2)-N(7)	110.74(19)
N(2)-Nd(2)-N(6)	103.82(19)
N(8)-Nd(2)-N(6)	113.42(17)

N(7)-Nd(2)-N(6)	116.05(18)
N(1)-Nd(3)-N(5)	122.9(4)
N(1)-Nd(3)-N(3)	118.6(4)
N(5)-Nd(3)-N(3)	97.7(2)
N(1)-Nd(3)-N(4)	117.2(4)
N(5)-Nd(3)-N(4)	99.3(3)
N(3)-Nd(3)-N(4)	96.0(2)
N(1)-Nd(3)-N(2)	1.8(2)
N(5)-Nd(3)-N(2)	121.1(3)
N(3)-Nd(3)-N(2)	119.8(3)
N(4)-Nd(3)-N(2)	117.8(3)
N(2)-Nd(4)-N(8)	119.2(4)
N(2)-Nd(4)-N(7)	121.6(4)
N(8)-Nd(4)-N(7)	97.7(3)
N(2)-Nd(4)-N(6)	115.0(4)
N(8)-Nd(4)-N(6)	98.6(3)
N(7)-Nd(4)-N(6)	100.6(3)
N(2)-Nd(4)-N(1)	0.7(2)
N(8)-Nd(4)-N(1)	119.7(3)
N(7)-Nd(4)-N(1)	120.9(3)
N(6)-Nd(4)-N(1)	115.3(3)
N(2)-N(1)-Nd(3)	175.9(6)
N(2)-N(1)-Nd(1)	178.4(5)
N(2)-N(1)-Nd(4)	0.9(3)
Nd(3)-N(1)-Nd(4)	176.0(4)
N(1)-N(2)-Nd(4)	178.4(6)
N(1)-N(2)-Nd(2)	178.2(5)
N(1)-N(2)-Nd(3)	2.4(3)
Nd(4)-N(2)-Nd(3)	177.5(4)

_____

References

(1)   Ryan, A. J.; Balasubramani, S. ; Ziller, J. W.; Furche, F.; Evans, W. J. *J. Am. Chem. Soc.* **2020**, *142* (20), 9302–9313.

(2)   Woen, D. H.; Chen, G. P.; Ziller, J. W.; Boyle, T. J.; Furche, F.; Evans, W. J. *J. Am. Chem. Soc.* **2017**, *139*, 14861–14864.

(3)   Evans, W. J.; Lee, D. S.; Rego, D. B.; Perotti, J. M.; Kozimor, S. A.; Moore, E. K.; Ziller, J. W. *J. Am. Chem. Soc.* **2004**, *126* (44), 14574–14582.

(4)   Cramer, R. E.; Rimsza, J. M.; Boyle, T. J. *J. Mol. Struct.* **2021**, *1242*, 130661.

(5)   Steed, J. W.; Junk, P. C. *J. Chem. Soc. Dalt. Trans.* **1999**, 2141–2146.

(6)   Ando, I. *Coord. Chem. Rev.* **2004**, *248*, 185–203.

(7)   Desiraju, G. R. *Acc. Chem. Res.* **1996**, *29*, 441–449.

(8)   Demir, S.; Gonzalez, M. I.; Darago, L. E.; Evans, W. J.; Long, J. R. *Nat. Commun.* **2017**, *8*, 1–9.

(9)   Rinehart, D.; Fang, M.; Evans, W. J.; Long, R. *J. Am. Chem. Soc.* **2011**, *133*, 14236–14239.

(10)   Fang, M.; Lee, D. S.; Ziller, J. W.; Doedens, R. J.; Bates, J. E.; Furche, F.; Evans, W. J. *J. Am. Chem. Soc.* **2011**, *133* (11), 3784–3787.

(11)   Allen, F. H.; Kennard, O.; Watson, D. G.; Brammer, L.; Orpen, A. G.; Taylor, R. *J. Chem. Soc. Perkin Trans. 2* **1987**, 1–19.

(12)   Holland, P. L. *Dalt. Trans.* **2010**, *39* (23), 5415–5425.

(13)   Ryan, A. J. University of California, Irvine, 2020.

(14)   Fieser, M. E.; Woen, D. H.; Corbey, J. F.; Mueller, T. J.; Ziller, J. W.; Evans, W. J. *Dalt. Trans.* **2016**, *45* (37), 14634–14644.

(15)   Karraker, D. G. *Inorg. Chem.* **1968**, *7* (3), 473–479.

(16)   Staroverov, V. N.; Scuseria, G. E.; Tao, J.; Perdew, J. P. *J. Chem. Phys.* **2003**, *119* (23), 12129–12137.

(17)   Grimme, S.; Antony, J.; Ehrlich, S.; Krieg, H. *J. Chem. Phys.* **2010**, *132* (15), 154104.

(18)   Grimme, S.; Ehrlich, S.; Goerigk, L. *J. Comput. Chem.* **2012**, *32* (7), 1456–1465.

(19)   Weigend, F.; Ahlrichs, R. *Phys. Chem. Chem. Phys.* **2005**, *7* (18), 3297–3305.

(20)   Gulde, R.; Pollak, P.; Weigend, F. *J. Chem. Theory Comput.* **2012**, *8* (11), 4062–4068.

(21)   Eichkorn, K.; Treutler, O.; Öhm, H.; Häser, M.; Ahlrichs, R. *Chem. Phys. Lett.* **1995**, *240*, 283–290.

(22)   Bauernschmitt, R.; Häser, M.; Treutler, O.; Ahlrichs, R. *Chem. Phys. Lett.* **1997**, *264* (6), 573–578.

(23)   Dolg, M.; Preuss, H. *J. Chem. Phys.* **1989**, *90* (October 1988), 1730–1734.

(24)   Kashinski, D. O.; Chase, G. M.; Nelson, R. G.; Di Nallo, O. E.; Scales, A. N.; Vanderley, D. L.; Byrd, E. F. C. *J. Phys. Chem. A* **2017**, *121* (11), 2265–2273.

(25)   Reed, A. E.; Weinstock, R. B.; Weinhold, F. *J. Chem. Phys.* **1985**, *83* (2), 735–746.

(26)   Perdew, J. P.; Ernzerhof, M.; Burke, K. *J. Chem. Phys.* **1996**, *105* (22), 9982–9985.

(27)   Tamm, I. *J. Phys. USSR* **1991**, *9*, 449–460.

(28)   S.M. Dancoff. *Phys. Rev.* **1950**, *78* (4), 382–385.

(29)   Ryan, A. J.; Darago, L. E.; Balasubramani, G.; Chen, G. P.; Ziller, J. W.; Furche, F.; Long, J. R.; Evans, W. J. *Chem. Eur. J.* **2018**, No. 2, 7702–7709.

(30)   Woen, D. H.; Chen, G. P.; Ziller, J. W.; Boyle, T. J.; Furche, F.; Evans, W. J. *Angew. Chem. Int. Ed.* **2017**, *129*, 2082–2085.

(31)   Aspinall, H. C.; Bradley, D. C.; Hursthouse, M. B.; Sales, K. D.; Walker, N. P. C.; Hussain, B. *J. Chem. Soc. Dalt. Trans.* **1989**, No. 1, 623–626.

(32)   Klamt, A.; Schüürmann, G. *J. Chem. Soc. Perkin Trans. 2* **1993**, No. 5, 799–805.

(33)   Grimme, S. *Chem. Eur. J.* **2012**, *18*, 9955–9964.

(34)   Rappoport, D.; Furche, F. *J. Chem. Phys.* **2007**, *126* (20), 201104.

(35)   Bates, J. E.; Furche, F. *J. Chem. Phys.* **2012**, No. 137, 164105.

Appendix A

Reactivity of Dianionic Dinitrogen Complexes, $[(R_2N)_3Ln]_2[\mu\text{-}\eta^x{:}\eta^x\text{-}N_2]^{2-}$

$(R = SiMe_3; x = 1, 2)$

Introduction

This Appendix describes the examination of the reactivity of the dianionic end-on and

mixed end-on side-on bound dinitrogen complexes, $[(R_2N)_3Ln]_2[\mu\text{-}\eta^x{:}\eta^x\text{-}N_2]^{2-}$ (Ln = Y, Nd, Gd,

Dy; x = 1, 2) described in Chapter 4 with phenazine, Me_3SiN_3, and NO. This Chapter also

describes the reaction of the neutral side-on bound complexes, $[(THF)(R_2N)_2Ln]_2[\mu\text{-}\eta^2{:}\eta^2\text{-}N_2]$ (Ln

= Y, Gd) with 2,2-bipyridine. It was of interest to determine if the end-on, side-on, or mixed

dianionic dinitrogen complexes would have a difference in reactivity compared to the neutral side-

on bound complexes. The results in this Appendix are a start toward that goal.

Results

Phenazine. Under an atmosphere of N_2, an Et_2O solution of phenazine, chilled to to −35

°C, was added to a yellow solution of $[K_2(18\text{-}c\text{-}6)_3][(R_2N)_3Y]_2[\mu\text{-}\eta^1{:}\eta^1\text{-}N_2]$, dissolved in Et_2O and

chilled to −35 °C. The solution became dark purple and was placed in a −35 °C freezer. Purple

crystals were isolated after several days and were crystallographically characterized as [(18-c-

6)K$(\mu\text{-}\eta^2{:}\eta^2\text{-}C_{12}H_8N_2)Y(NR_2)_3]$, **1-Y,** eq A.1, Figure A.1. **1-Y** contains a phenazine monoanion

bound by both the Y and K. As shown in eq A.1, preliminary data suggests that the charge for the

phenazine monoanion is delocalized.

R = SiMe₃
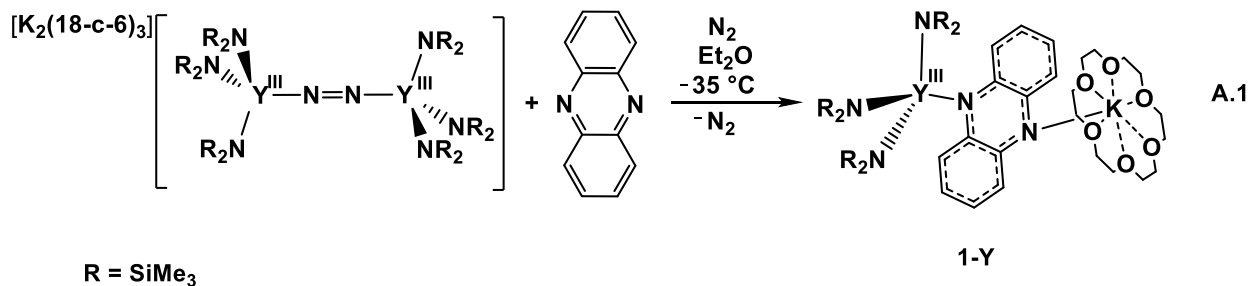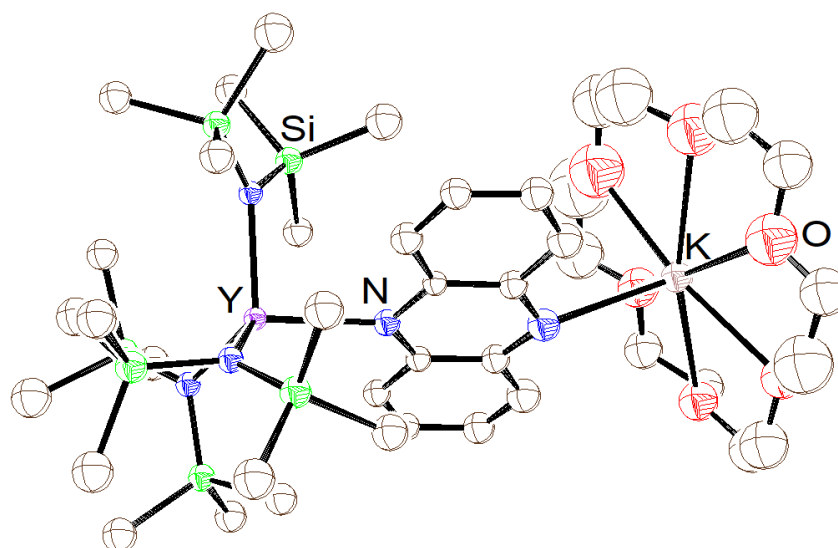
Figure A.1. Representation of [(18-c-6)K(μ-η^2:η^2-C$_{12}$H$_8$N$_2$)Y(NR$_2$)$_3$], **1-Y**, with atomic displacement parameters drawn at the 50% probability level. Hydrogen atoms are excluded for clarity.

The reaction analogous to eq A.1 was performed with [K$_2$(18-c-6)$_3$][(R$_2$N)$_3$Dy]$_2$[μ-η^x:η^x-N$_2$] (x = 1, 2), a complex in which the dinitrogen unit is mixed between end-on and side-on bonding modes. The solution turned from a dark orange to a dark red and red crystals were isolated and crystallographically characterized as [(18-c-6)K(μ-η^2:η^2-C$_{12}$H$_8$N$_2$)Y(NR$_2$)$_3$], **1-Dy**, Figure A.2. **1-Dy** is not isomorphous to **1-Y** as the coordination between the phenazine monoanion and the [K(18-c-6)]$^{1+}$ are different.
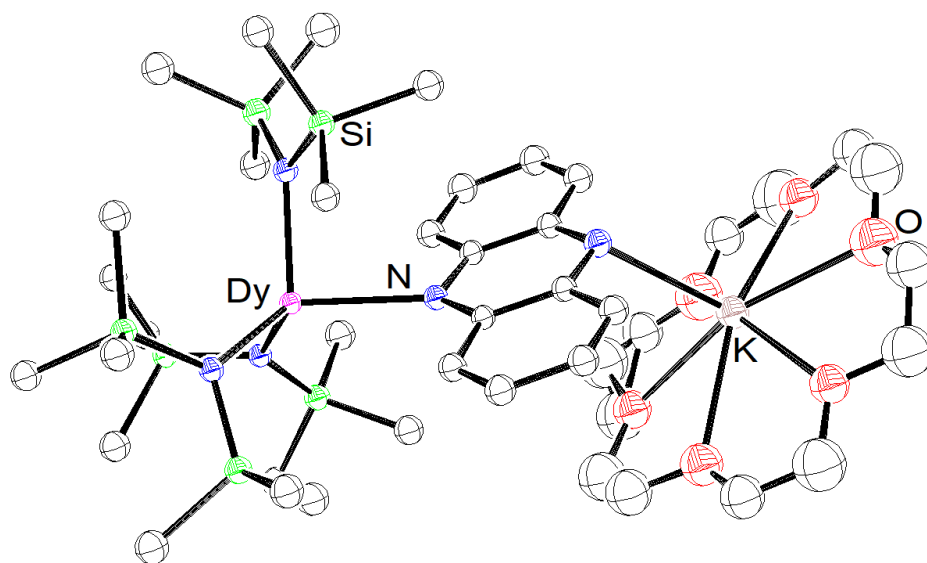
Figure A.2. Representation of [(18-c-6)K(μ-η^2:η^2-C$_{12}$H$_8$N$_2$)Dy(NR$_2$)$_3$], **1-Dy**, with atomic displacement parameters drawn at the 50% probability level. Hydrogen atoms are excluded for clarity.

The phenazine reduction reaction was probed further by examining the LnA$_3$/M reaction performed with Y(NR$_2$)$_3$ and KC$_8$ in the presence of 18-c-6 in Et$_2$O at −35 °C. Initially, a dark blue solution of Y(II) was generated and filtered. When an Et$_2$O solution of phenazine, chilled to −35 °C, was added, the solution turned dark purple. The dark purple solution was left in a −35 °C freezer and a few days later, purple crystals were isolated. These purple crystals were crystallographically characterized as, [K(18-c-6)$_2$]{[(NR$_2$)$_3$Y]$_2$(μ-η^2:η^2-C$_{12}$H$_8$N$_2$)}, **2-Y**, eq A.2, Figure A.3. The phenazine was reduced to a monoanion, but in this case it is bound through the N atoms by two Y(NR$_2$)$_3$ units.
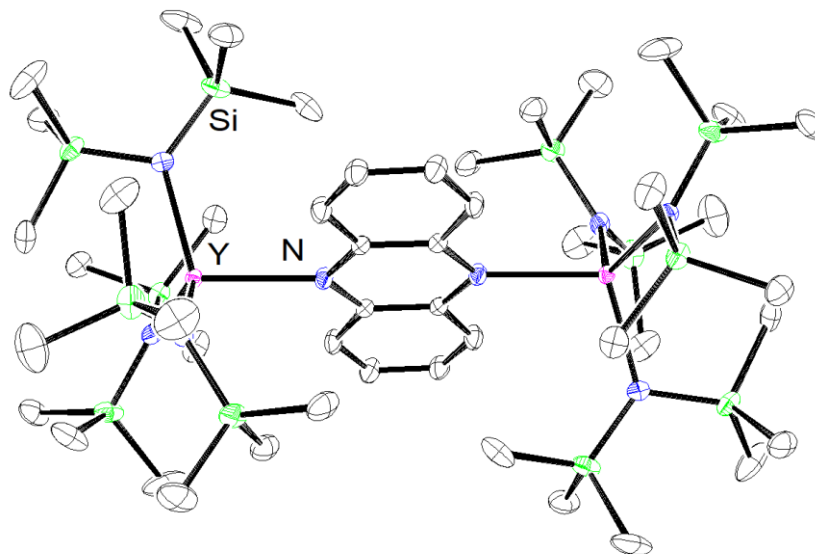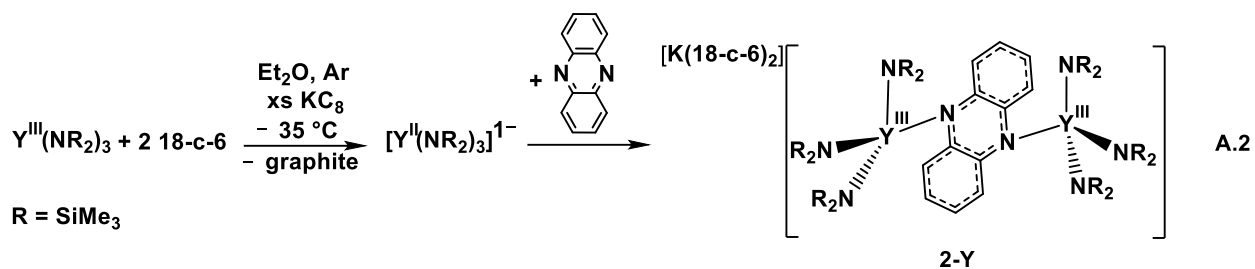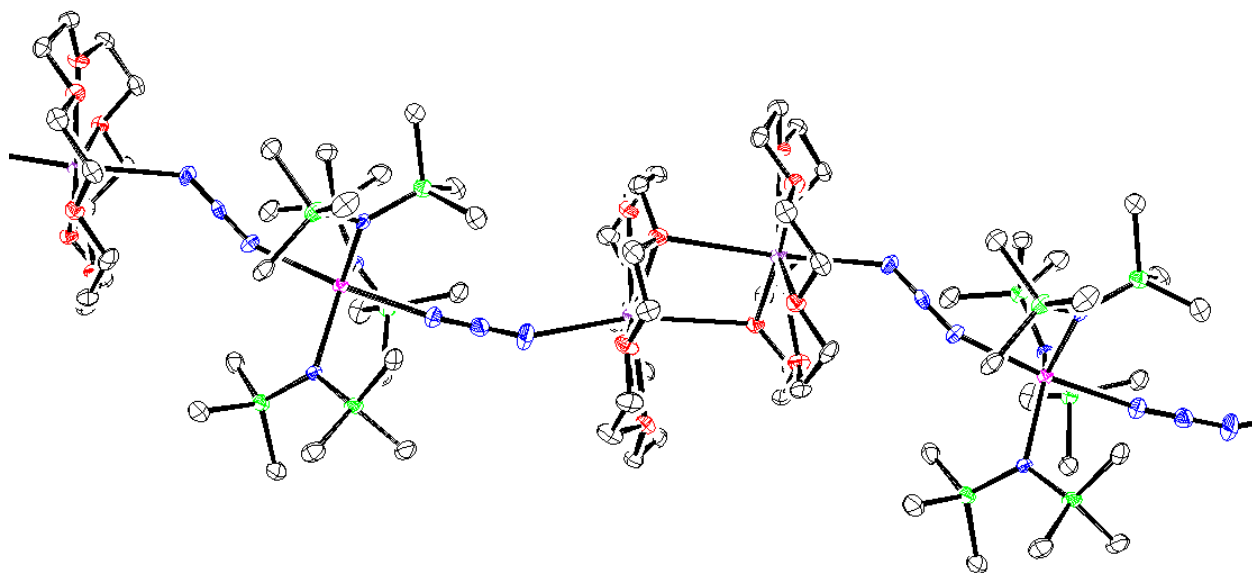
Figure A.3. Representation of $[K(18\text{-}c\text{-}6)_2]\{[(NR_2)_3Y]_2(\mu\text{-}\eta^2{:}\eta^2\text{-}C_{12}H_8N_2)\}$, **2-Y**, with atomic displacement parameters drawn at the 50% probability level. Hydrogen atoms, $[K(18\text{-}c\text{-}6\text{-})_2]^{1+}$, and one molecule of $[K(18\text{-}c\text{-}6)_2]\{[(NR_2)_3Y]_2(\mu\text{-}\eta^2{:}\eta^2\text{-}C_{12}H_8N_2)\}$ are excluded for clarity.

Me₃SiN₃. Under an atmosphere of N_2, Me_3SiN_3, chilled to $-35\ °C$ was added to a green solution of $[K_2(18\text{-}c\text{-}6)_3][(R_2N)_3Nd]_2[\mu\text{-}\eta^2{:}\eta^2\text{-}N_2]$ dissolved in Et_2O and chilled to $-35\ °C$. The solution became light green and opaque and was placed in a $-35\ °C$ freezer. Colorless crystals were isolated after several days and were crystallographically characterized as $[(18\text{-}c\text{-}6)K(\mu\text{-}\eta^2{:}\eta^2\text{-}N_3)Nd(NR_2)_3]_n$, **3-Nd,** eq A.3, Figure A.4. The N_3–$(SiMe_3)$ bond was cleaved leaving the $(N_3)^{1-}$ monoanion. The extended structure is shown in Figure A.5
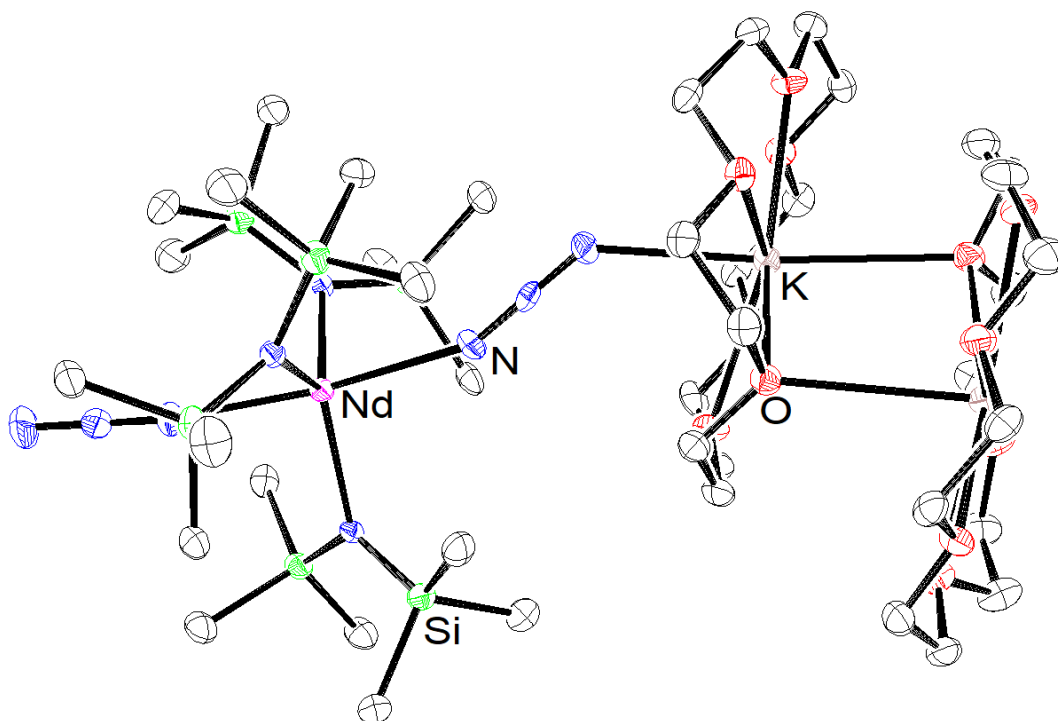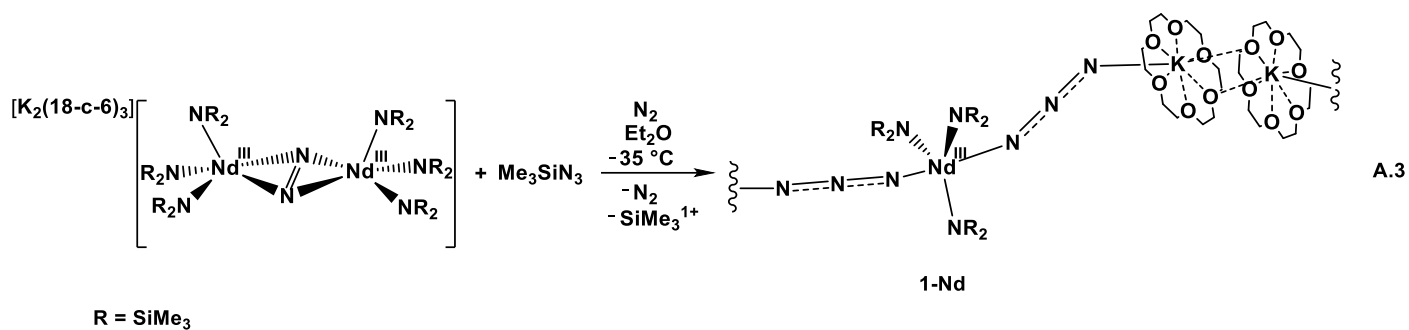
Figure A.4. Representation of [(18-c-6)K(μ-η^2:η^2-N$_3$)Nd(NR$_2$)$_3$]$_n$, **3-Nd**, with atomic displacement parameters drawn at the 50% probability level. The asymmetric unit it shown. Hydrogen atoms and an Et$_2$O molecule are excluded for clarity.
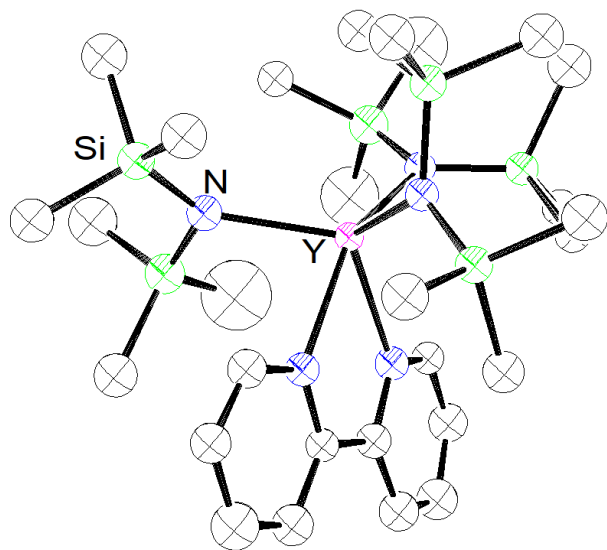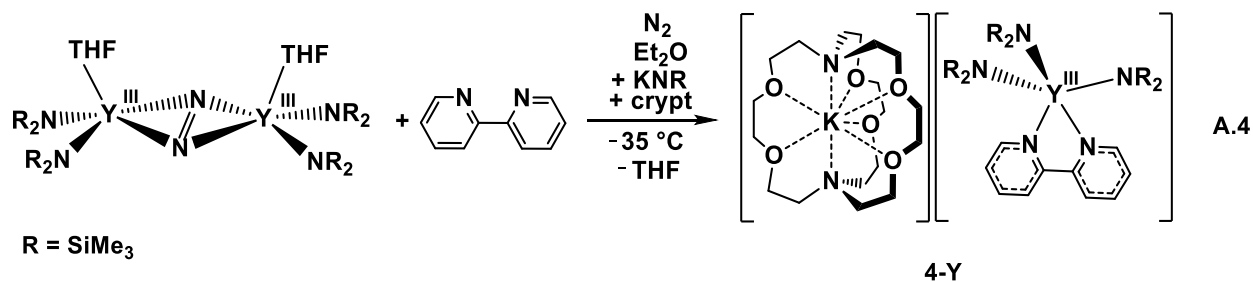
Figure A.5. Extended structure shown of [(18-c-6)K(μ-η^2:η^2-N$_3$)Nd(NR$_2$)$_3$]$_n$, **3-Nd**, with atomic displacement parameters drawn at the 50% probability level.

The reaction analogous to eq A.3 was performed with [K$_2$(18-c-6)$_3$][(R$_2$N)$_3$Gd]$_2$[μ-η^x:η^x-N$_2$] (x = 1, 2), a complex in which the dinitrogen unit is mixed between end-on and side-on bonding modes. The solution turned from a yellow to a white opaque solution and colorless crystals were isolated and crystallographically characterized as [(18-c-6)K(μ-η^2:η^2-N$_3$)Gd(NR$_2$)$_3$]$_n$, **3-Gd**. Complexes **3-Nd** and **3-Gd** are not isomorphous.

2,2-Bipyridine. Under an atmosphere of N$_2$, an Et$_2$O solution of 2,2-bipyridine, chilled to −35 °C was added to a yellow solution of [(THF)(R$_2$N)$_2$Y]$_2$[μ-η^2:η^2-N$_2$], dissolved in Et$_2$O and chilled to −35 °C. The solution became dark red and was placed in a −35 °C freezer. However, no crystalline materials formed from this reaction. An equivalent of 2.2.2-cryptand (crypt) was dissolved in Et$_2$O and chilled to −35 °C and added to the reaction mixture. The color did not change. Unable to isolate anything from the reaction, an equivalent of KNR$_2$ was added. Red

crystals were isolated after several days and were crystallographically characterized [K(crypt)][(R$_2$N)$_3$Y(C$_{10}$H$_8$N$_2$-κN, κN)], **4-Y,** eq A.4, Figure A.6. The 2,2-bipyridine ligand was reduced to a monoanion and is bound to the Y center through both N atoms.

Figure A.6. Representation of [K(crypt)][(R$_2$N)$_3$Y(C$_{10}$H$_8$N$_2$-κN, κN)], **4-Y**, with atomic displacement parameters drawn at the 50% probability level. The asymmetric unit it shown. Hydrogen atoms, an Et$_2$O molecule, and [K(crypt)]$^{+1}$ countercation are excluded for clarity.

The reaction analogous to eq A.4 was performed with [(THF)(R$_2$N)$_2$Gd]$_2$[μ-η^2:η^2-N$_2$] and red crystals were able to isolated and crystallographically characterized as [K(crypt)][(R$_2$N)$_3$Gd(C$_{10}$H$_8$N$_2$-κN, κN)], **4-Gd**. Complexes **4-Y** and **4-Gd** are not isomorphous.

NO. Reactions of $[K_2(18\text{-c-}6)_3][(R_2N)_3Nd]_2[\mu\text{-}\eta^2{:}\eta^2\text{-}N_2]$ and $[K_2(18\text{-c-}6)_3][(R_2N)_3Dy]_2[\mu\text{-}\eta^x{:}\eta^x\text{-}N_2]$ (x = 1, 2) with NO were also performed. Isolated $[K_2(18\text{-c-}6)_3][(R_2N)_3Ln]_2[\mu\text{-}\eta^x{:}\eta^x\text{-}N_2]$ was dissolved in Et_2O and placed in a Schlenk flask and exposed to NO. The reaction with Ln = Nd went from green to an opaque light green solution and the reaction with Ln = Dy went from a dark yellow to a light orange opaque solution. Both solutions were taken back into the glovebox and were placed in a −35 °C freezer to crystallize. Crystals were able to be isolated from these reactions, however, the data obtained could not be solved to identify the products.

Discussion

The reactivity of both end-on and mixed end-on and side-on dinitrogen complexes, $[K_2(18\text{-}c\text{-}6)_3][(R_2N)_3Ln]_2[\mu\text{-}\eta^x{:}\eta^x\text{-}N_2]$ (Ln = Y, x = 1; Ln = Dy, x = 1, 2), with phenazine results in mono-reduced phenazine complex, $[(18\text{-c-}6)K(\mu\text{-}\eta^2{:}\eta^2\text{-}C_{12}H_8N_2)Ln(NR_2)_3]$ (Ln = Y, Dy). This contrasts with the reaction of phenazine with the traditional Sm(II) complex which makes a dianionic phenazine ligand bound to two Sm(III) centers.[1] With Me_3SiN_3, the side-on and mixed end-on side-on complexes, $[K_2(18\text{-c-}6)_3][(R_2N)_3Ln]_2[\mu\text{-}\eta^x{:}\eta^x\text{-}N_2]$ (Ln = Nd, x = 2; Ln = Gd, x = 1, 2), give a similar reduction product to the phenazine results, an anionic $[XLn(NR_2)_3]^{1-}$ complex which in this case has X = N_3. These reactions show that the $(N=N)^{2-}$ complexes are potent reductants. This type of reactivity has been observed before.[2,3] Analogous reactivity studies with the neutral complexes, $[(THF)(R_2N)_2Ln]_2[\mu\text{-}\eta^2{:}\eta^2\text{-}N_2]$, remain to be done for comparison. However, these neutral complexes clearly cannot make analogous products since neither K nor chelate is present and there are only two $(NR_2)^{1-}$ ligands per metal. Interestingly, the reaction of $[(THF)(R_2N)_2Ln]_2[\mu\text{-}\eta^2{:}\eta^2\text{-}N_2]$ (Ln = Y, Gd) with 2,2-bipyridine did not give an isolable product until an additional equivalent of KNR_2 and crypt were added. This led to a $[XLn(NR_2)_3]^{1-}$ complex of the type isolated from the end-on and side-on complexes with phenazine and Me_3SiN_3. This

may demonstrate a good method to get crystallographically characterizable complexes in reduction reactions of amide-ligand rare earth complexes. However, more examples are needed to determine if this is a trend.

Experimental Details

All manipulations and syntheses described below were conducted with the rigorous exclusion of air and water using standard Schlenk line and glovebox techniques under an argon or dinitrogen atmosphere. Solvents were sparged with UHP argon and dried by passage through columns containing Q-5 and molecular sieves prior to use. 2.2.2-Cryptand (crypt, Merck) was placed under vacuum (10^{-4} torr) for 12 h before use. 18-Crown-6 (18-c-6, Alfa Aesar) was sublimed before use. KNR_2 (Sigma) was extracted into toluene, filtered, and dried before use. Phenazine (Sigma) was sublimed before use. Me_3SiN_3 (Sigma) were freeze-pump-thawed and stored over 3Å molecular sieves for one week before use. 2,2-Bipyridine (Sigma) was sublimed before use. $Y(NR_2)_3$ was synthetized according to literature procedures.[4] $[K_2(18\text{-c-}6)_3]\{[(NR_2)_3Ln]_2[\mu\text{-}\eta^x{:}\eta^x\text{-}N_2]\}$ (Ln = Nd, Gd, Dy, Y) syntheses can be found in Chapter 4 Experimental Details. $[(THF)(NR_2)_2Ln]_2[\mu\text{-}\eta^2{:}\eta^2\text{-}N_2]$ (Ln = Gd, Y) were synthesized according to literature procedures.[5]

$[(18\text{-c-}6)K(\mu\text{-}\eta^2{:}\eta^2\text{-}C_{12}H_8N_2)Y(NR_2)_3]$, 1-Y. In a dinitrogen filled glovebox, $[K_2(18\text{-c-}6)_3]\{[(NR_2)_3Y]_2[\mu\text{-}\eta^1{:}\eta^1\text{-}N_2]\}$ (25 mg, 0.010 mmol) was dissolved in -35 °C Et_2O (2 mL) and placed in a -35 °C freezer for one hour. Phenazine (2 mg, 0.01 mmol) was dissolved in -35 °C Et_2O (1 mL) and also placed in a -35 °C freezer for one hour. The phenazine solution was then dropwise added to the orange solution containing $[K_2(18\text{-c-}6)_3]\{[(NR_2)_3Y]_2[\mu\text{-}\eta^1{:}\eta^1\text{-}N_2]$. The orange solution was immediately turned purple and was placed in a -35 °C freezer. The resulting purple solution produced bright purple crystals of **1-Y** suitable for X-ray diffraction.

[(18-c-6)K(μ-η^2:η^2-C$_{12}$H$_8$N$_2$)Dy(NR$_2$)$_3$], 1-Dy. In a dinitrogen filled glovebox, [K$_2$(18-c-6)$_3$]{[(NR$_2$)$_3$Dy]$_2$[μ-η^x:η^x-N$_2$]} (x = 1, 2) (25 mg, 0.010 mmol) was dissolved in −35 °C Et$_2$O (2 mL) and placed in a −35 °C freezer for one hour. Phenazine (2 mg, 0.01 mmol) was dissolved in −35 °C Et$_2$O (1 mL) and also placed in a −35 °C freezer for one hour. The phenazine solution was then dropwise added to the dark orange solution containing [K$_2$(18-c-6)$_3$]{[(NR$_2$)$_3$Dy]$_2$[μ-η^x:η^x-N$_2$]. The orange solution was immediately turned dark red and was placed in a −35 °C freezer. The resulting dark red solution produced red crystals of **1-Dy** suitable for X-ray diffraction.

[K(18-c-6)$_2$]{[(NR$_2$)$_3$Y]$_2$(μ-η^2:η^2-C$_{12}$H$_8$N$_2$)}, 2-Y. In an argon filled glovebox, an Et$_2$O solution of Y(NR$_2$)$_3$ (50 mg, 0.090 mmol) and 18-c-6 (46 mg, 0.18 mmol) was cooled to −35 °C and was added to a −35 °C chilled vial of excess KC$_8$. The colorless solution went to dark blue and was immediately filtered. A solution of phenazine (16 mg, 0.090 mmol) dissolved in Et$_2$O (1 mL), chilled to −35 °C, was then added to the dark blue solution. The solution was swirled and immediately turned dark purple. The solution was layered into a −35 °C chilled vial of hexanes and placed in a −35 °C freezer to crystallize. Purple crystals were isolated and crystallographically characterized as **2-Y**.

[(18-c-6)K(μ-η^2:η^2-N$_3$)Nd(NR$_2$)$_3$]$_n$, 3-Nd. In a dinitrogen filled glovebox, [K$_2$(18-c-6)$_3$]{[(NR$_2$)$_3$Nd]$_2$[μ-η^2:η^2-N$_2$]} (25 mg, 0.010 mmol) was dissolved in −35 °C Et$_2$O (2 mL) and placed in a −35 °C freezer for one hour. Me$_3$SiN$_3$ (1 µL, 0.01 mmol) chilled to −35 °C was added the solution of [K$_2$(18-c-6)$_3$]{[(NR$_2$)$_3$Nd]$_2$[μ-η^2:η^2-N$_2$]}. The green solution was immediately turned a light opaque green and was placed in a −35 °C freezer. The resulting solution produced red crystals of **3-Nd** suitable for X-ray diffraction.

[(18-c-6)K(μ-η^2:η^2-N$_3$)Gd(NR$_2$)$_3$]$_n$, 3-Gd. In a dinitrogen filled glovebox, [K$_2$(18-c-6)$_3$]{[(NR$_2$)$_3$Gd]$_2$[μ-η^2:η^2-N$_2$]} (25 mg, 0.010 mmol) was dissolved in −35 °C Et$_2$O (2 mL) and

placed in a −35 °C freezer for one hour. Me$_3$SiN$_3$ (1 µL, 0.01 mmol) chilled to −35 °C was added the solution of [K$_2$(18-c-6)$_3$]{[(NR$_2$)$_3$Gd]$_2$[μ-η^2:η^2-N$_2$]}. The green solution was immediately turned a light opaque green and was placed in a −35 °C freezer. The resulting solution produced red crystals of **3-Gd** suitable for X-ray diffraction.

[K(crypt)][(R$_2$N)$_3$Y(C$_{10}$H$_8$N$_2$-κN, κN)], 4-Y. In a dinitrogen filled glovebox, [(THF)(NR$_2$)$_2$Y]$_2$[μ-η^2:η^2-N$_2$] (25 mg, 0.020 mmol) was dissolved in −35 °C Et$_2$O (2 mL) and placed in a -35 °C freezer for one hour. 2,2-bipyridine (3 mg, 0.02 mmol) was dissolved in −35 °C Et$_2$O (1 mL) and also placed in a −35 °C freezer for one hour. The 2,2-bipyridine solution was then dropwise added to the yellow solution containing [(THF)(NR$_2$)$_2$Y]$_2$[μ-η^2:η^2-N$_2$]. The yellow solution was immediately turned dark red and was placed in a −35 °C freezer. An Et$_2$O solution of KNR$_2$, (4 mg, 0.02 mmol) and crypt (7 mg, 0.02 mmol), chilled to −35 °C was added to the dark red solution. The resulting red solution produced red crystals of **4-Y** suitable for X-ray diffraction.

[K(crypt)][(R$_2$N)$_3$Gd(C$_{10}$H$_8$N$_2$-κN, κN)], 4-Gd. In a dinitrogen filled glovebox, [(THF)(NR$_2$)$_2$Gd]$_2$[μ-η^2:η^2-N$_2$] (25 mg, 0.020 mmol) was dissolved in −35 °C Et$_2$O (2 mL) and placed in a -35 °C freezer for one hour. 2,2-bipyridine (3 mg, 0.02 mmol) was dissolved in −35 °C Et$_2$O (1 mL) and also placed in a −35 °C freezer for one hour. The 2,2-bipyridine solution was then dropwise added to the yellow solution containing [(THF)(NR$_2$)$_2$Gd]$_2$[μ-η^2:η^2-N$_2$]. The yellow solution was immediately turned dark red and was placed in a −35 °C freezer. An Et$_2$O solution of KNR$_2$, (3 mg, 0.02 mmol) and crypt (6 mg, 0.02 mmol), chilled to −35 °C was added to the dark red solution. The resulting red solution produced red crystals of **4-Gd** suitable for X-ray diffraction.

References

(1)   Evans, W. J.; Gonzales, S. L.; Ziller, J. W. *J. Am. Chem. Soc.* **1994**, *116* (6), 2600–2608.

(2)   Lorenz, S. E.; Schmiege, B. M.; Lee, D. S.; Ziller, J. W.; Evans, W. J. *Inorg. Chem.* **2010**, *49*, 6655–6663.

(3)   Evans, W. J.; Lorenz, S. E.; Ziller, J. W. *Inorg. Chem.* **2009**, *48* (5), 2001–2009.

(4)   Aspinall, H. C.; Bradley, D. C.; Hursthouse, M. B.; Sales, K. D.; Walker, N. P. C.; Hussain, B. *J. Chem. Soc. Dalt. Trans.* **1989**, No. 1, 623–626.

(5)   Evans, W. J.; Lee, D. S.; Rego, D. B.; Perotti, J. M.; Kozimor, S. A.; Moore, E. K.; Ziller, J. W. *J. Am. Chem. Soc.* **2004**, *126* (44), 14574–14582.